Study on Seismic Behavior of Precast Drift-hardening Concrete Columns Confined by Bolted Circular Steel Tube

羅, 京

(Degree)
博士（工学）

(Date of Degree)
2024-03-25

(Date of Publication)
2025-03-01

(Resource Type)
doctoral thesis

(Report Number)
甲第8922号

(URL)
https://hdl.handle.net/20.500.14094/0100490147

Doctoral Dissertation

Study on Seismic Behavior of Precast Drift-hardening Concrete Columns Confined by Bolted Circular Steel Tube

（ボルト接合円形鋼板で拘束されたドリフト硬化型プレキャスト RC 柱の耐震性能及び評価方法）

January, 2024

Graduate School of Engineering

Kobe University

LUO JING

羅　京

Acknowledgements

I would like to express my sincere gratitude to all those who have contributed to the completion of this doctoral dissertation.

First and foremost, I extend my deep gratitude to my supervisor, Professor Sun Yuping. From the selection of the thesis topic to the research and writing process, all has been accomplished under Professor Sun's meticulous guidance. His profound theoretical knowledge, rich practical experience, and rigorous academic attitude have been invaluable to me. Without Professor Sun's patient guidance, constructive suggestions and unwavering support, completing this doctoral thesis would have been impossible. As graduation approaches, I extend my sincerest thanks and heartfelt blessings to the esteemed Professor Sun.

I must also express my profound appreciation to Professor Zhao Jun from Zhengzhou University, another of my esteemed supervisors. Professor Zhao not only granted me a valuable opportunity for overseas studies but also provided invaluable guidance and support throughout my academic research journey. Without his unwavering assistance, the smooth completion of my studies would not have been possible. As I approach graduation, I extend my genuine gratitude and deep blessings to Professor Zhao.

I extend my sincere appreciation to the members of dissertation committee, Professor Mukai Yoichi and Professor Fujinaga Takashi, for their valuable feedback and constructive criticism. Their collective expertise has significantly enriched the quality of this research.

I also would like to thank Associate Professor Takeuchi Takashi for his academic guidance and advices.

I am grateful to Mr. Kanao Masaru, technician of Kobe University, for his assistance in all the experimental works.

I express thanks to Associate Professor Zhang Xiangcheng from Zhengzhou University for his academic guidance and advices.

I am deeply appreciative of the scholarships offered by the China Scholarship Council (File No.201907040095) and Zhengzhou University (No. 20201009), which have supported my daily expenses and allowed me to focus on academic research. The experimental studies described in this dissertation were financially supported by JSPS KAKENHI, grant number 22H01642, for which I am also sincerely grateful.

I want to express sincere thanks to fellow postgraduate students from Sun laboratory of Kobe University – Ms. Zhang Chi, Mr. Che Jiayu, Mr. Yang Shoudi and Mr. Quan Ziran, in particular for Mr. Yuan Shiyu and Mr. Li Ganggang. Without their kind assistance, the experiments in this dissertation would not be conducted favorably.

I also want to give sincere thanks to my friends Dr. Zeng Lingxin, Dr. Shen Fuqiang, Dr. Yinlu, Dr. Si Chenzhe, Dr. Li Xiaopeng, Dr. Zhou Aixin, Ms. Jia Mian, Dr. Wei Chuxuan, Dr. Wei Chengjin for their kind support.

Thanks would also be expressed to Ms. Zhang Man, Mr. Ding Ruilin, Mr. Wang Siyuan from Beijing University of Technology for their kind assistance.

Last but not least, deepest gratitude goes to my parents, two sisters, and fiancée–Ms. Ding Juan. Their selfless dedication and undivided support have provided me with the greatest motivation.

The road ahead is still long, and no matter where this journey leads, I will tread it with a grateful heart, steadfastly forging my own future.

羅 京　LUO JING

January, 10, 2024

Contents

List of Figures

List of Tables

Abbreviations

USGS	: United States Geological Survey
IBC	: International Building Code
ASCE	: American Society of Civil Engineers
ACI	: American Concrete Institute
NBC	: National Building Code
NZS	: New Zealand Standard
RC	: Reinforced concrete
UPT	: Unbonded post-tensioning
FRP	: Fiber-reinforced polymer
GFRP	: Glass fiber reinforced polymer
CFRP	: Carbon fiber reinforced polymer
BFRP	: Basalt fiber reinforced polymer
WBUHS	: Weakly bonded ultra-high strength
GS	: Grouted sleeve
ED	: Energy dissipation
PSBCs	: Precast segmental bridge columns
NS	: Normal strength
FSE	: Finite spring element
DTs	: Displacement transducers
HS	: High-strength
PC	: Prestressed concrete
DH	: Drift-hardening

CHAPTER ONE

1. Introduction

1.1 Backgrounds

Earthquake disasters are among the most destructive forces in nature, often resulting in large-scale casualties, property losses, and even social chaos. According to statistics from the United States Geological Survey (USGS), there have been a staggering 1494 large-scale earthquakes worldwide with a magnitude exceeding 7.0 since 1900 [1.1]. In the period from 2000 to 2015 alone, there were 253 such earthquakes, as illustrated in Fig. 1-1 [1.1].

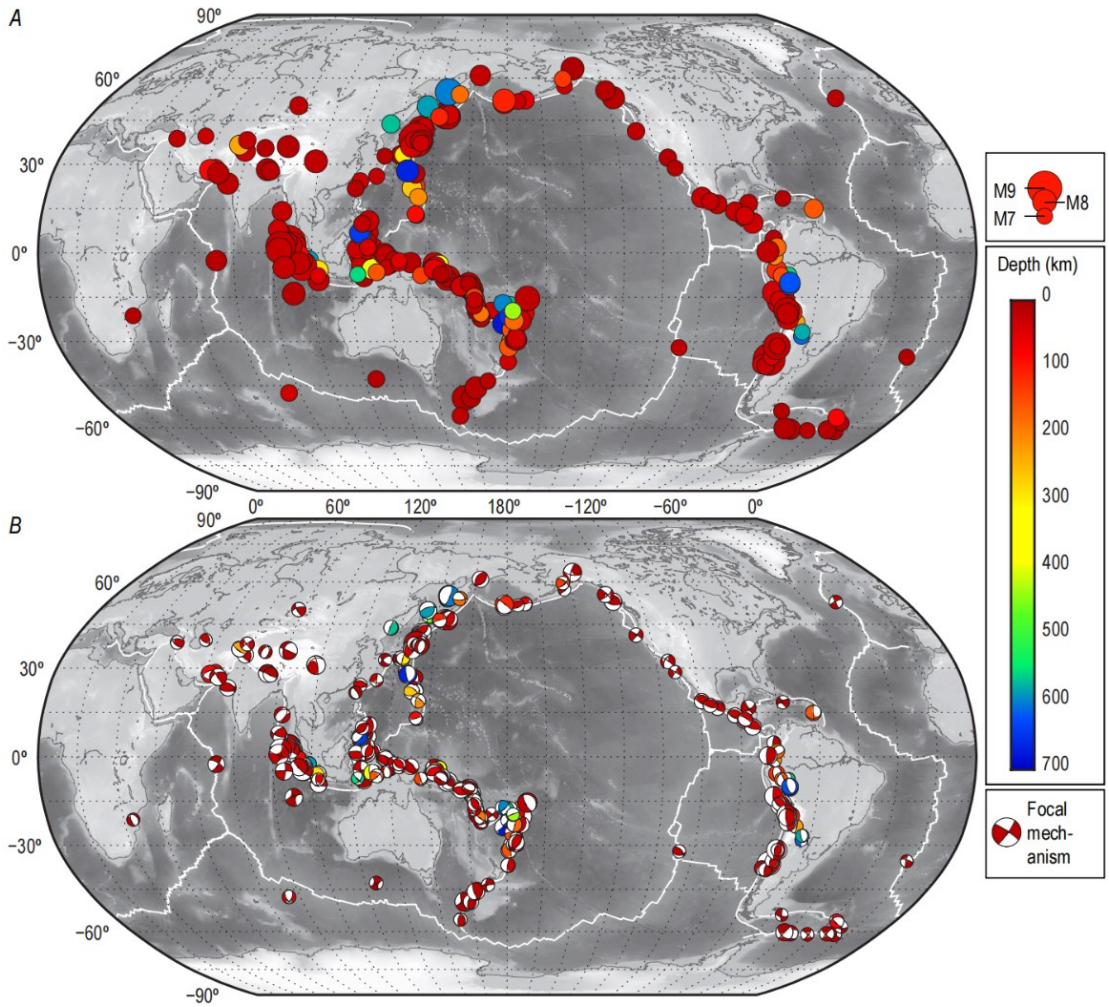

Fig. 1-1 The locations of earthquakes with a magnitude of 7 or greater, 2000–2015 [1.1]

Notable examples include the 1960 Great Chilean Earthquake with a magnitude of 9.5, remaining the most powerful earthquake ever recorded. It triggered widespread tsunamis, resulting in substantial casualties [1.2]. The 1976 Tangshan earthquake in China is infamous for its widespread destruction and high casualty toll [1.3]. The 1995 Great Hanshin Earthquake exposed vulnerabilities in urban infrastructure in Japan, particularly in Kobe [1.4]. The 2008 Wenchuan earthquake in China with a magnitude of 8.0 and the 2011 Great Tohoku Earthquake in Japan with a magnitude of 9.1, also stand as reminders of the profound impact that earthquakes can have on densely populated areas [1.5, 1.6]. And the 2023 Turkey–Syria earthquakes underscores the ongoing seismic risks faced by diverse regions globally [1.7]. These seismic events have left indelible marks on history, causing immense human suffering and altering the landscape of affected regions. In addition to the immediate and visible effects, earthquakes often have far-reaching consequences, affecting infrastructure, economies, and societal structures. Fig. 1-2 shows an example of damaged buildings by earthquakes.

(a) Buildings in Great Hanshin Earthquake (b) Buildings in Wenchuan Earthquake

Fig. 1-2 Damaged buildings suffering from earthquakes

A frequently repeated saying is, “earthquakes don’t kill people, but buildings do”. While it may be infeasible to prevent the occurrence of earthquake disasters in the communities where people reside and/or work, there exist alternative strategies for saving lives and reducing losses caused by a seismic event: the adoption and implementation of up-to-date construction standards and advanced technologies. It is imperative to recognize that the conceptual framework for structural design and the corresponding specification systems are to continually develop and to gradually upgrade to meet the evolving needs of social development. In earthquake-prone countries like China and Japan, seismic design codes have undergone several stages of

development and continuous refinement with the accumulation of disaster experience and the progress of science and technology. In the 1950s, China issued its first “Code for Seismic Design of Buildings”, and made a specification regarding the seismic theories and methods during the 1970s. However, the primary focus still remained on strength-based principles. Since the late 1990s, a shift towards displacement-based seismic design principles has been implemented, emphasizing the importance of deformation capacity and energy dissipation capacity in concrete structures. In 2001, the performance-based seismic design concept was first introduced into the building seismic design code, followed by further revisions in 2010, which mainly included the determination of performance objectives, the division of performance grades and the methods for performance evaluation [1.8].

In parallel, drawing from investigations into past seismic events, Japan enacted the “Building Standards Law” in 1950, which placed emphasis on the overall performance of structures and paid particular attention to the displacement and deformation control of structures during earthquakes, marking it a milestone in seismic design in Japan. In 1981, on the basis of continuous research in seismic-resistant engineering field and practical experience, as well as the summary and reflections on past codes [1.9], the Building Standard Law underwent modification and the New Anti-seismic Design Code became operative. This revision emphasized the imperative for buildings to maintain regular functionality during frequently encountered moderate earthquakes (magnitude 5~7) and to withstand rare and substantial earthquakes of magnitude 7 or higher without experiencing collapse. Also, the European and North American countries have established their own seismic design codes and guidelines to assure the structural safety in earthquake-prone zones. The representative codes include the International Building Code (IBC) [1.10], American Society of Civil Engineers (ASCE) code [1.11], American Concrete Institute (ACI) code [1.12], National Building Code (NBC) [1.13], Eurocode 8 [1.14], and New Zealand Standard (NZS) 1170.5 [1.15], etc.

To meet the aforementioned criteria for seismic design, building structures should possess two important seismic properties: one is the enough energy dissipation capacity to absorb and dissipate seismic energy, and the other is sufficient ductility to allow them to deform without undergoing catastrophic failure. In more recent decades, ductile reinforced concrete (RC) components, both walls and columns, are widely employed as the favored lateral force resisting system for mid-high rise buildings situated in seismically active regions owing to

their outstanding seismic properties, including high strength, deformability, and energy dissipation capacity. As suggested from the recently occurred catastrophic earthquakes such as the 2008 Wenchuan earthquake [1.16], the 2011 Great East Japan earthquake [1.17], and the 2023 Turkey–Syria earthquake [1.18], code-compliant ductile RC components have indeed played a crucial role in guaranteeing life safety during seismic hazards due to their excellent ductility and energy-dissipating capacity. Nevertheless, the sufficient ductility and dissipation of energy exhibited by the ductile RC components are often inevitably accompanied by the occurrence of severe damage and large residual deformation, easily resulting in substantial economic burden due to business downtime, repair or reconstruction, as shown in Fig. 1-2. Accordingly, how to guarantee people's life during an earthquake while promoting the societal recovery after the earthquake has emerged as an essential objective within the seismic research field.

In recent years, the concept of "resilient city" has gained increasing attention within structural engineering community because it puts emphasis on reducing the permanent post-earthquake deformation and swift restoration of essential building functions [1.19], as highlighted by Mileti in 1999 [1.20]: "*Local resiliency with regard to disasters means that a locale is able to withstand an extreme natural event without suffering devastating losses, damage, diminished productivity, or quality of life and without a large amount of assistance from outside the community*".

Sun et al. has introduced an innovative approach for enhancing the earthquake resilience of RC structures, in which two crucial structural features are highlighted: drift-hardening capacity as well as self-centering capacity [1.21]. The former refers to the ever-increasing lateral resistance along with lateral deformation, ensuring that structures can withstand large deformations without experiencing failure caused by strength degradation. While the latter refers to the reduced residual deformation after being greatly deformed by strong earthquake, contributing to the rapid recovery of structures. The concept of resilient structures provided by Sun et al. is depicted in Fig. 1-3, accompanied by a contrast to traditional ductile structures. This comparison emphasizes the distinct features of resilient structures, including both drift-hardening and self-centering capacities, showing their improved seismic performance to withstand and recover from seismic events more effectively than traditional ductile structures.

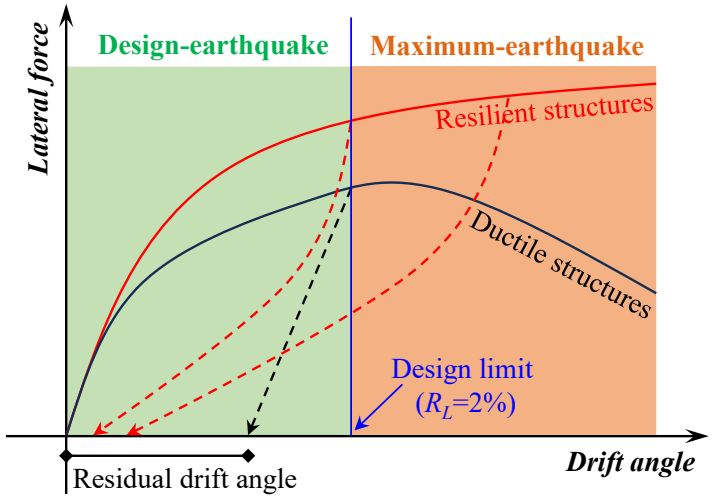

Fig. 1-3 Comparison between the ductile and the resilient structures

To materialize resilient concrete components with both drift-hardening and self-centering capacity, Professor Sun and his research team have carried out comprehensive experimental research and theoretic analysis in the past dozen years, making several significant achievements while simultaneously identifying some existing issues. Together with the prior efforts of other researchers, these achievements and issues will be succinctly reviewed in the following sections.

1.2 Previous Study on Resilient Concrete Columns

From the perspective of swiftly restoring social activities and reducing repair costs, numerous attempts have been made by earthquake researchers to develop self-centering concrete components. An early effort involved the usage of a well-known prestressing technique, in which unbonded post-tensioning (UPT) tendons were employed to provide a restoring effect [1.22, 1.23], and then this application of UPT was further extended by Priestley et al., Zatar et al. and Marriott et al. [1.24-1.26]. To facilitate construction and avoid the negative impact on seismic performance caused by the prestress loss, Yuan et al. [1.27], Liu et al. [1.28], and Ou et al. [1.29] introduced the utilization of unstressed steel strands as longitudinal reinforcement in RC components (both columns and walls), as shown in Fig. 1-4. The test results illustrated that employing unstressed steel strands in concrete columns to replace normal deformed rebars was a convenient and feasible means of effectively controlling residual deformation after unloading the lateral loads. While one point worth highlighting is that the unstressed steel strands in the compressive zone are prone to bulging under compression, thus resulting in a reduction in resilience of concrete members.

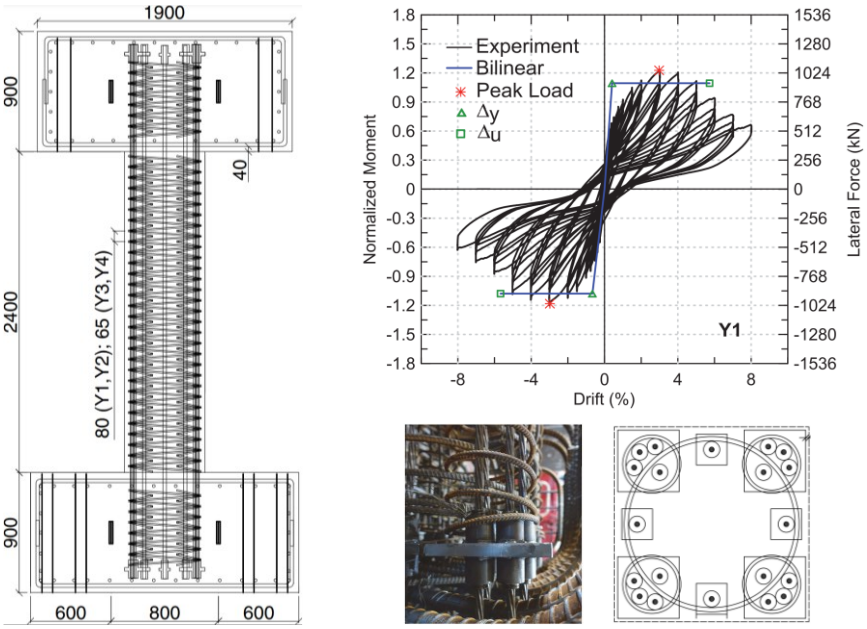

Fig. 1-4 Self-centering behavior of concrete columns reinforced by steel strands [1.29]

Fiber-reinforced polymer (FRP) materials, referring to a composite material made up of a polymer matrix reinforced with fibers, were initially employed for seismic strengthening of RC and masonry structures [1.30, 1.31], or to address the corrosion of ordinary steel bars [1.32]. Subsequently, FRP materials were processed into straight bars to develop self-centering concrete components owing to their high tensile strength and linear elasticity up to failure. Mohamed et al. [1.33] carried out an experimental study by substituting all longitudinal steel bars of concrete walls with glass fiber reinforced polymer (GFRP) bars, and the test results suggested that concrete walls reinforced by GFRP bars displayed stable flexural capacity without strength degradation and recoverable behavior up to allowable drift limits. Based on the study carried out by Zhao et al. [1.34] and Wang et al. [1.35], as compared with traditional ductile components, significant self-centering capacity could also be obtained in both RC walls and columns reinforced by carbon fiber reinforced polymer (CFRP) rebars or basalt fiber reinforced polymer (BFRP) rebars in addition to the enhanced lateral resistance, as illustrated in Fig. 1-5. However, compared to the tensile strength, FRP bars exhibits weaker compressive capacity and are prone to fracture under compression, especially when deformed to a large drift ratio after the spalling of cover concrete [1.36]. This phenomenon may reduce the lateral resistance and self-centering capacity of CFRP bar reinforced concrete components.

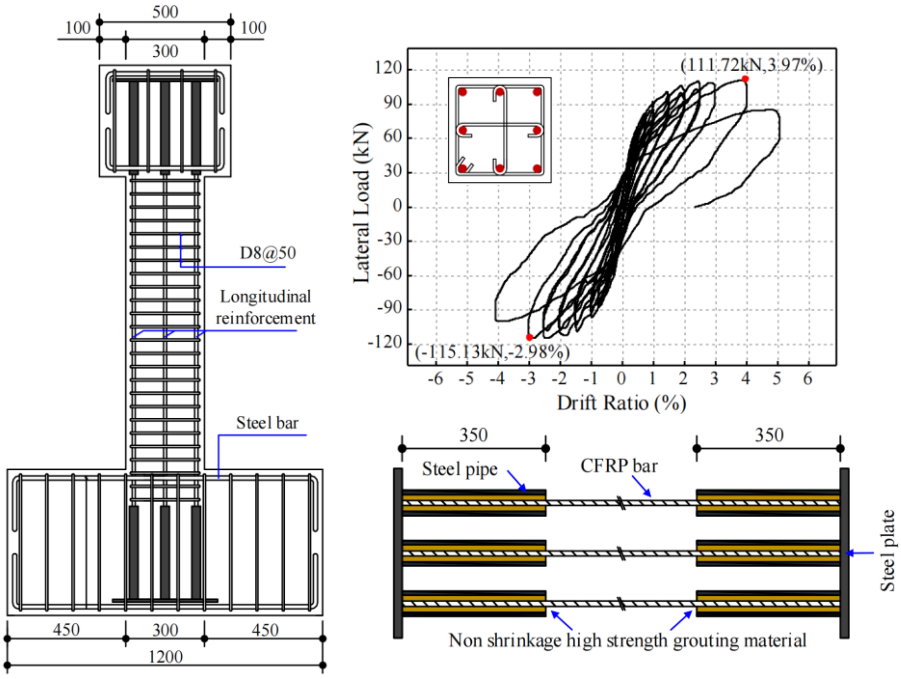

Fig. 1-5 Self-centering behavior of concrete columns reinforced by CFRP rebars [1.34]

Another innovative alternative to materialize resilient concrete components involves the usage of a kind of weakly bonded ultra-high strength (WBUHS) bars featuring spiral grooves on the surfaces, the key aspect of which lies in their high yield strength (1275 N/mm^2) as well as low bond strength (3.0–4.0 N/mm^2) [1.37]. The former provided the RC components with high lateral resistance, while the latter could delay the yielding of WBUHS rebars to endow both drift-hardening capacity and self-centering capacity. Sun et al. [1.38-1.40] have confirmed the feasibility of WBUHS rebars in providing drift-hardening capacity for both square and circular RC columns, regardless of whether they were subjected to high axial compression or deformed in double curvatures. However, the WBUHS rebars were still observed buckling at larger drifts than 5.0% and 3.0% because of spalling of cover concrete in columns and walls under relatively high axial compressive loads, respectively, and resulted in the degradation of both lateral resistance and resilience in these structural elements. In view of the excellent effect in enhancing both concrete strength and ductility, Sun et al. employed bolted steel tubes to confine the circular concrete columns reinforced with WBUHS rebars for the purpose of enhancing the resilience [1.41]. Their test results showed that more pronounced drift-hardening capacity can be expected when concrete columns are reinforced with WBUHS rebars and simultaneously confined by bolted thin steel tubes, especially for those with circular sections.

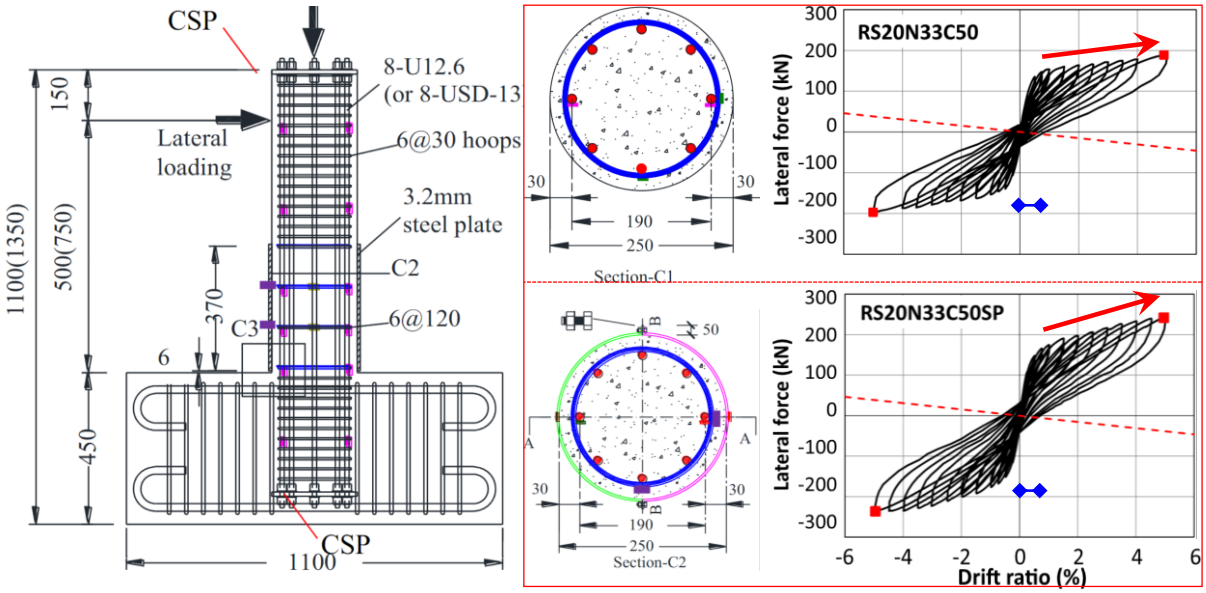

Fig. 1-6 Drift-hardening behavior of confined columns reinforced with WBUHS rebars [1.41]

1.3 Previous Study on Precast Concrete Columns

In the field of industrialization of construction, substantial attention was being paid to precast concrete structures in many countries and regions because it emerged in response to the need for efficient and cost-effective construction methods, driven by increased urbanization, demand for rapid infrastructure development, and the desire to overcome limitations associated with traditional on-site concrete construction. Precast construction offers benefits such as saving of construction time, reducing of labor requirements, enhancement of construction quality, and minimization of environmental impact, and hence contributing to the evolution of modern construction practices.

Precast concrete structures are broadly utilized in bridge engineering, industrial warehouse, residential buildings, and commercial malls across the globe [1.42]. It is widely recognized that the seismic performance of prefabricated building and bridge structures is deeply influenced by the properties of the connection joints, encompassing factors like stiffness, strength, and deformability.

Researchers have developed a multitude of techniques to promote the jointing of prefabricated concrete columns, inclusive of grouting-anchoring lap splices, mechanical

sleeve splices, shaped steel splices [1.43]. However, as for the jointing method of grouting-anchoring lap splices, it is inapplicable to the large-diameter steel bars because of the requirement for overlapping length. In the case of the usage of mechanical sleeve splices or shaped steel splices, while an additional option, the latter pouring concrete easily results in an increase in constructional complexity [1.44]. Currently, the grouted sleeve (GS) connection is widely employed in prefabricated reinforced concrete columns due to its reliability and high-efficiency constructability [1.45, 1.46]. The seismic performance of prefabricated columns with GS connections is contingent on critical factors such as grout strength, embedded length, and duct properties. As suggested based on the tensile tests on GSs, the failure modes were mainly reflected in three aspects: pullout of the rebars, fracture of rebars, and the fracture of GSs [1.47].

In the meantime, how to develop precast concrete columns with high resilience has become an urgent research topic, because they are prone to serious damage and permanent deformation in earthquake-prone areas, impeding the development of resilient city. Based on the effectiveness of the steel strands, FRP bars and WBUHS bars in improving self-centering and/or drift-hardening capacity as described in section 1.2, their application also played a critical role in the development of resilient precast concrete structures. The efficacy of employing prestressing tendons to provide self-centering capacity for precast concrete columns had been experimentally by many researchers [1.48-1.50], whereas the energy dissipation capacity would reduce compared with ductile precast columns. Therefore, many researchers proposed to develop resilient precast columns with acceptable energy dissipation capacity by combining the benefits of prestressing tendons with energy dissipation (ED) devices, in which prestressing tendons were utilized to provide a restoring effect, while ED devices were employed to add extra energy dissipation [1.51-1.53]. Fig. 1-7 exhibited an example of the self-centering behavior of precast columns with prestressing tendons.

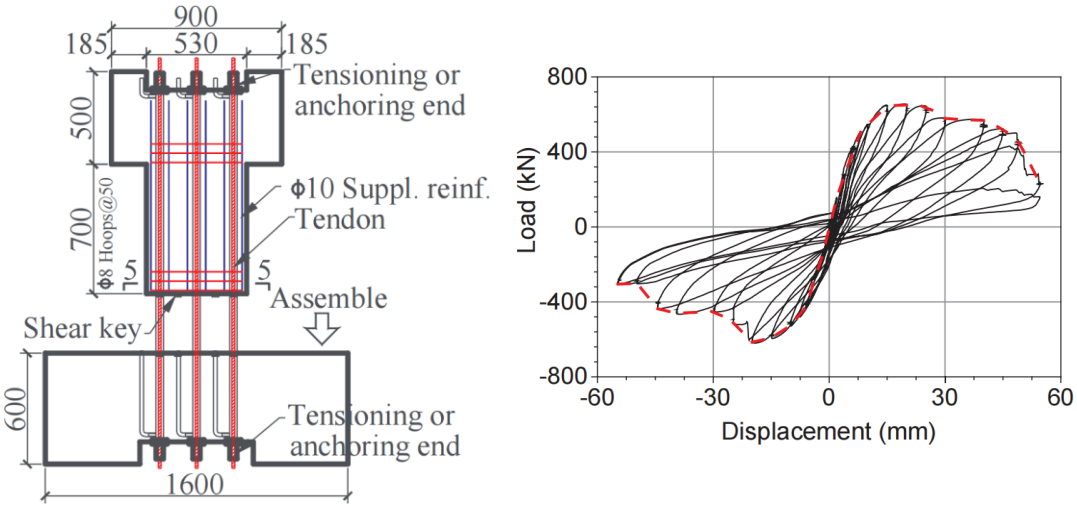

Fig. 1-7 Self-centering behavior of precast columns with prestressing tendons [1.51]

For the purpose of addressing the potential corrosion problem of the unbonded steel tendons, Li et al. [1.54] utilized CFRP tendons in precast concrete columns to replace steel tendons, and proposed to use replaceable energy dissipation rebars to achieve quick post-earthquake retrofitting. Based on the test results, they revealed that the proposed precast columns could be adopted in earthquake-prone regions to provide good restorability even when struck by strong earthquakes. Cai et al. [1.55] found that employing both FRP rebars and steel rebars as longitudinal reinforcements in precast segmental bridge columns (PSBCs) system could obtain increased post-yield stiffness ratio and reduced residual deformation, as well as comparable energy-dissipating capacities with the steel-reinforced counterparts. An example of self-centering behavior exhibited by precast columns reinforced with FRP bars was depicted in Fig. 1-8.

The utilization of WBUHS rebars have been experimentally and theoretically verified to be a simple and practical way to provide concrete members with excellent drift-hardening capacity in addition to self-centering capacity, whereas there are few studies on the resilience of precast columns reinforced with WBUHS rebars, only one conducted by Takeda et al. [1.56]. In the study conducted by Takeda et al., the lower end of the WBUHS bars was anchored using high-strength nuts and washers to simplify construction, while sheathing ducts and grouting material were used to joint the column and footing. The test results showed that embedment length of WBUHS bars had a great influence on both the failure mode and drift-hardening capacity, as shown in Fig. 1-9.

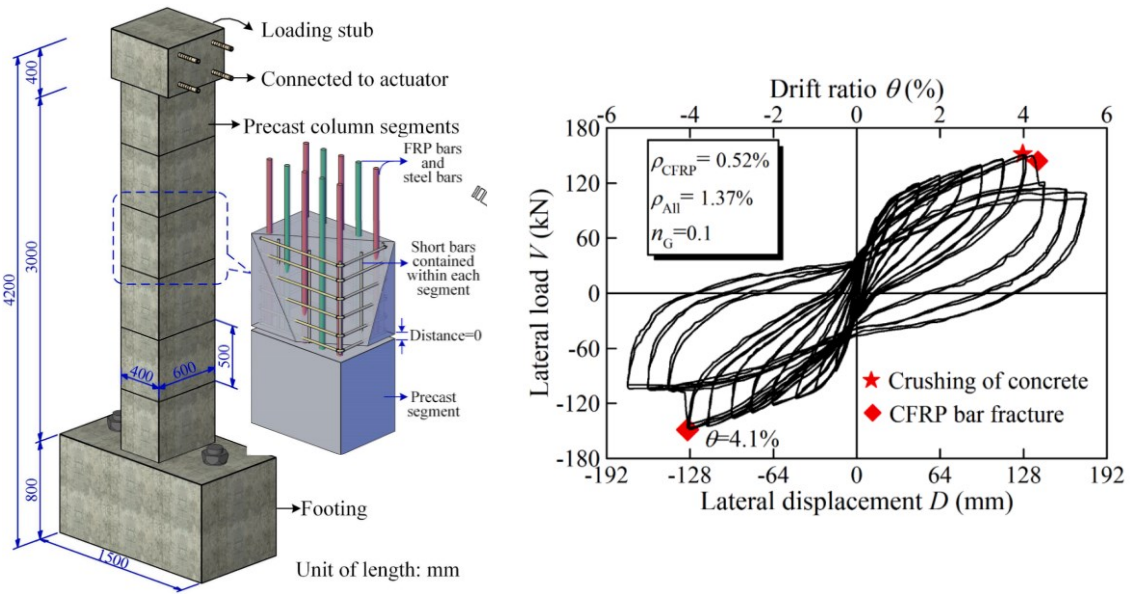

Fig. 1-8 Self-centering behavior of precast columns with FRP bars [1.55]

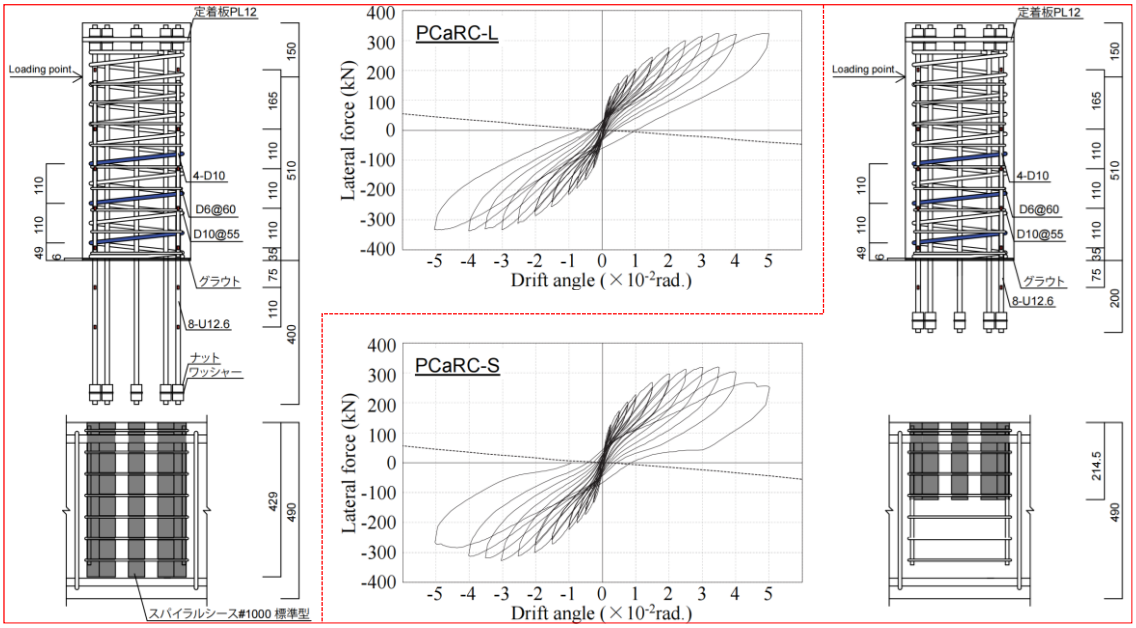

Fig. 1-9 Drift-hardening behavior of precast columns with WBUHS rebars [1.56]

1.4 Problems and Research Objectives

As implied in the above research background and literature review, when compared to other high-performance reinforcements such as steel strands and FRP bars, the utilization of WBUHS rebars indeed played a simple and effective role in developing resilient concrete columns with significant drift-hardening and self-centering capacity. However, the previous studies described above primarily concentrated on square concrete columns and rectangular walls, and there are few, if any, information regarding the seismic behavior of particularly precast circular columns, while they are also well used in buildings and bridge piers.

To enhance the resilience provided by WBUHS rebars and promote the application of precast circular drift-hardening columns in industry and civil construction, the following important issues need to be addressed:

1) Effective prevention of the buckling of WBUHS rebars: The buckling of WBUHS rebars is the main factor that leads to the decrease of lateral resistance and deformation capacity for resilient concrete members. WBUHS rebars tended to buckle at significant drift levels resulting from the crushing of cover concrete and lateral expand of core concrete especially when the confinement of concrete was insufficient. For the purpose of delaying the buckling and/or enhancing the post-buckling behavior of WBUHS rebars, more effective confinement measures is desirable.

2) Solution of the construction difficulty in the rectangular beam-circular column joints: Circular concrete columns reinforced with WBUHS rebars generally exhibited higher resilience than square and rectangular components because of the much higher confinement effect provided by circular spirals and/or hoops. However, circularly arranged longitudinal rebars in a circular column generally makes it difficult to anchor the longitudinal rebars in the horizontal beams, and increase complexities of the construction of beam-column joints.

3) Accumulation of information concerning the seismic behavior of precast circular concrete columns reinforced with WBUHS rebars: While there has been some information on seismic behavior of resilient cast-in-site circular concrete columns, literature related to that of precast circular concrete columns is very scarce.

As solutions of the above-mentioned problems, the paper proposes the confinement by bolted circular thin steel tubes as well as the square arrangement of longitudinal rebars in a precast circular concrete column. The objectives of this paper are listed below:

1) To experimentally verify effectiveness of the confinement by the bolted thin circular steel tubes in terms of delaying buckling of WBUHS rebars and to develop a simple and rational evaluation method for this type of confinement through concentric loading on short concrete columns.

2) To provide fundamental experimental data concerning the seismic performance of precast circular concrete columns reinforced by squarely-arranged WBUHS rebars and laterally confined by bolted thin steel tube with emphasis placed on the effects of the embedded length of WBUHS rebars, confinement of bolted thin steel tubes, as well as steel amount of WBUHS rebars.

3) To present a numerical analysis method that can reliably and accurately evaluate the hysteretic behavior of the precast circular concrete columns. This method can not only take into account the confinement effect of bolted circular steel tubes, but also consider the slippage of WBUHS rebars.

4) To propose a reliable and simple method for predicting the ultimate flexural capacity of circular concrete columns reinforced with squarely-arranged WBUHS rebars and confined by the bolted thin steel tube, and to verify its reliability and accuracy through a comparison between the experimental results with calculated values.

1.5 Format of This Thesis

To achieve the goals described above, this doctoral dissertation is comprised of seven chapters. Each chapter deals respective aforementioned issues except for chapter one and chapter seven. The main content of each chapter is outlined as follows:

Chapter one introduces the research background of this dissertation, reviews previous research efforts, identifies several existing issues and describes the research objectives.

Chapter two presents experimental research on the axial behavior of WBUHS rebars within short concrete columns confined by bolted thin steel tubes with emphasis placed on investigating the effects of the steel tubes in delaying WBUHS rebars' buckling and on the degree of concrete confinement. A total of twenty short concrete columns reinforced with normal strength (NS) rebars or WBUHS rebars were fabricated and tested under concentric compression. With hoop spacing, reinforcement type, confinement of steel tubes and section type as the main experimental variables, the test results were analyzed in terms of failure mode, load-strain curves, buckling strain of WBUHS rebars, strain ductility, and stress-strain behaviors of WBUHS rebars.

Chapter three discusses seismic performance of precast circular concrete columns reinforced with squarely-arranged WBUHS rebars and simultaneously confined by bolted circular thin steel tube. Taking construction methods, anchoring length of WBUHS rebar, axial load ratio, width-to-thickness ratio of the confining steel tubes, reinforcement type, and shear span ratio as main experimental variables, twelve 1/2.5-scale circular concrete columns were made and tested under reversed cyclic lateral loading and constant compression. The seismic behaviors with respect to the failure mode, lateral force-drift angle curves, residual deformation, energy dissipation capacity, reinforcement strain, and average axial strain were described and discussed based on the experimental results.

Chapter four extends the experimental study of the seismic performance of precast circular concrete columns reinforced by large-diameter WBUHS rebars to study the influence of the steel amount of WBUHS rebars and steel tube confinement. With main variables including longitudinal steel ratio, construction methods, axial load ratio, and confinement method, six

1/2.5-scale circular concrete columns were fabricated and tested under reversed cyclic lateral loading. The seismic behavior of the test columns was analyzed in terms of the failure mode, lateral force-drift angle curves, residual deformation, energy dissipation capacity, reinforcement strain, and average axial strain.

Chapter five is intended to numerically analyze the hysteretic performance of the circular concrete columns confined by bolted circular steel tubes. A finite spring element (FSE) method, which could take into account both the bond-slip relationship of WBUHS rebars and the confinement effect of hoops and/or steel tubes on concrete, was presented to assess the hysteresis performance of the proposed concrete columns. Validity and accuracy of this method will be confirmed through a comparison between the calculated lateral force-drift angle curves, reinforcement strain and energy dissipation capacity with the measured ones.

Chapter six proposes a simplified method to evaluate the ultimate flexural capacity of the resilient precast circular concrete columns developed in this study. First, the computed values based on the plane-remain-plane assumption are examined. And then, a method that can take into consideration of the bond-slip behavior of WBUHS rebars is proposed. Finally, the accuracy of the calculated ultimate bearing capacity was verified by comparing with experimental results.

Chapter seven summarizes the main conclusions obtained from chapters two through six, and presents several future issues regarding the drift-hardening concrete columns confined by bolted circular steel tube.

References

[1.1] https://www.usgs.gov/search?keywords=earthquake

[1.2] Cifuentes I.L. The 1960 chilean earthquakes. Journal of Geophysical Research: Solid Earth, 1989, 94(B1): 665-680.

[1.3] Wan Y.G., Wan Y.K., Jin Z.T., et al. Rupture distribution of the 1976 Tangshan earthquake sequence inverted from geodetic data. Chinese Journal of Geophysics, 2017, 60(6): 583-601.

[1.4] Sawada Y., Shimizutani S. How do people cope with natural disasters? Evidence from the Great Hanshin-Awaji (Kobe) earthquake in 1995. Journal of Money, Credit and Banking, 2008, 40(2-3): 463-488.

[1.5] Yin A. A special issue on the great 12 May 2008 Wenchuan earthquake (Mw7. 9): Observations and unanswered questions. Tectonophysics, 2010, 491(1-4): 1-9.

[1.6] Ritsema J, Lay T, Kanamori H. The 2011 tohoku earthquake. Elements, 2012, 8(3): 183-188.

[1.7] Dal Zilio L, Ampuero J P. Earthquake doublet in Turkey and Syria. Communications Earth & Environment, 2023, 4(1): 71.

[1.8] Code for seismic design of buildings: GB 50011-2010. China Architecture & Building Press (in Chinese)

[1.9] The building standard law of Japan: June 2004. Building Center of Japan, 2004. www.bcj.or.jp/en/03/01_03.html

[1.10] "2021 International Building Code (IBC)," International Code Council, Washington, DC, 2020.

[1.11] American Society of Civil Engineering, "ASCE 7-05 Minimum Design Loads for Buildings and Other Structures", 2006.

[1.12] ACI Committee, American Concrete Institute, & International Organization for Standardization. (2011). Building code requirements for structural concrete (ACI 31811) and commentary. American Concrete Institute.

[1.13] National Research Council of Canada, National Building Code of Canada 2020, Ottawa, 2022.

[1.14] Eurocode 8: design of structures for earthquake resistance - Part 1: general rules, seismic actions and rules for buildings. European Committee for Standardization. 2004.

[1.15] Standards New Zealand. “NZS 1170.5: Structural Design Actions Part 5: Earthquake actions–New Zealand”. Wellington, New Zealand, 2004.

[1.16] Wang Z. A preliminary report on the Great Wenchuan Earthquake. Earthquake Engineering and Engineering Vibration, 2008, 7: 225-234.

[1.17] Mimura N., Yasuhara K., Kawagoe S., et al. Damage from the Great East Japan Earthquake and Tsunami-a quick report. Mitigation and Adaptation Strategies for Global Change, 2011, 16: 803-818.

[1.18] D'Ayala D. Commentary: Reflections on the Turkey–Syria earthquakes of 6 February 2023. Proceedings of the Institution of Civil Engineers-Structures and Buildings, 2023, 176(6): 478-481.

[1.19] Godschalk D.R. Urban hazard mitigation: Creating resilient cities. Natural Hazards Review, 2003, 4: 136-143.

[1.20] Mileti, D. Disasters by design: A reassessment of natural hazards in the United States, Joseph Henry Press, Washington, D.C., 1999.

[1.21] Sun Y.P., Cai G.C., Takeuchi T. Seismic behavior and performance-based design of resilient concrete columns. Applied Mechanics and Materials, 2013, 438: 1453-1460.

[1.22] Priestley M.J.N., Tao J.R. Seismic response of precast prestressed concrete frames with partially debonded tendons. PCI journal, 1993, 38(1): 58-69.

[1.23] El-Sheikh M.T., Sause R., Pessiki S., et al. Seismic behavior and design of unbonded post-tensioned precast concrete frames. PCI journal, 1999, 44(3): 54-71.

[1.24] Priestley M.J.N., Sritharan S., Conley J.R., et al. Preliminary results and conclusions from the PRESSS five-story precast concrete test building. PCI journal, 1999, 44(6): 42-67.

[1.25] Zatar W.A., Mutsuyoshi H. Residual displacements of concrete bridge piers subjected to near field earthquakes. Structural Journal, 2002, 99(6): 740-749.

[1.26] Marriott D., Pampanin S., Palermo A. Quasi-static and pseudo-dynamic testing of unbonded post-tensioned rocking bridge piers with external replaceable dissipaters. Earthquake engineering & structural dynamics, 2009, 38(3): 331-354.

[1.27] Yuan W.G., Zhao J., Sun Y.P., et al. Experimental study on seismic behavior of concrete walls reinforced by PC strands. Engineering Structures, 2018, 175: 577-590.

[1.28] Liu Z.H., Zhao H., Sun Y.P., et al. Seismic performance of circular concrete columns reinforced by PC strands. Journal of Advanced Concrete Technology, 2020, 18(5): 256-271.

[1.29] Ou Y.C., Joju J., Liu Y.C. Cyclic Behavior of Reinforced Concrete Columns with Unstressed Steel Strands as Longitudinal Reinforcement. Journal of Structural Engineering, 2022, 148(9): 04022125.

[1.30] Liu J., Sheikh S.A. Fiber-Reinforced Polymer-Confined Circular Columns under Simulated Seismic Loads. ACI structural journal, 2013, 110(6).

[1.31] Ercan E., Arisoy B., Ertem O.B. Experimental assessment of RC beam-column connections with internal and external strengthening techniques. Advances in Civil Engineering, 2019.

[1.32] Choo C.C., Harik I.E., Gesund H. Strength of rectangular concrete columns reinforced with fiber-reinforced polymer bars. ACI Materials Journal, 2006, 103(3): 452.

[1.33] Mohamed N., Farghaly A.S, Benmokrane B., et al. Experimental investigation of concrete shear walls reinforced with glass fiber–reinforced bars under lateral cyclic loading. Journal of Composites for Construction, 2014, 18(3): A4014001.

[1.34] Zhao J., Si C.Z., R W.B., et al. Experimental and numerical studies on seismic performance of rectangular concrete columns reinforced by CFRP bars with different ratios and positions. Structures, 2021, 32: 237-253.

[1.35] Wang Z., Cai Z.. Analysis of post-tensioned precast segmental bridge piers reinforced with steel and FRP bars. Proc 8th Int Conf Fibre-Reinforced Polym Compos Civ Eng CICE. 2016: 754-759.

[1.36] Sun Z., Wu G., Zhang J., et al. Experimental study on concrete columns reinforced by hybrid steel-fiber reinforced polymer (FRP) bars under horizontal cyclic loading. Construction and Building Materials, 2017, 130: 202-211.

[1.37] Funato Y.; Sun Y.P. Modeling and application of bond behavior of ultra-high strength bars with spiraled grooves on the surface. Proceedings of the Japan Concrete Institute, 2012, 34, 157–62. (in Japanese)

[1.38] Zhang J., Liu X., Liu J., et al. Seismic performance and reparability assessment of recycled aggregate concrete columns with ultra-high-strength steel bars. Engineering Structures, 2023, 277: 115426.

[1.39] Takeuchi T., Sun Y.P., Tani M., et al. Seismic performance of concrete columns reinforced with weakly bonded ultrahigh-strength longitudinal bars. Journal of Structural Engineering, 2021, 147(1): 04020290.

[1.40] Wang J.H., Sun Y.P., Takeuchi T. Seismic fragility and post-earthquake reparability of circular reinforced concrete bridge columns with low-bond high-strength

reinforcements. Structures, 2021, 34: 840-855.

[1.41] Sun Y.P., Cai G.C. Seismic Behavior of Circular Concrete Columns Reinforced by Low Bond Ultrahigh Strength Rebars. Journal of Structural Engineering, 2023, 149(9): 04023126.

[1.42] Liu H., Wang Z., Xu C., et al. Influence of axial compression ratio on the seismic performance of precast columns with grouted sleeve connections. Journal of Structural Engineering, 2021, 147(12): 04021194.

[1.43] Xu L., Pan J., Cai J. Seismic performance of precast RC and RC/ECC composite columns with grouted sleeve connections. Engineering Structures, 2019, 188: 104-110.

[1.44] Chen J., Xiao Y. Experimental study on seismic behavior of precast concrete column with longitudinal reinforcement grouting-anchoring connections. China Civil Engineering Journal, 2016;49(5):63–73. (in Chinese)

[1.45] Popa V., Papurcu A., Cotofana D., et al. Experimental testing on emulative connections for precast columns using grouted corrugated steel sleeves. Bulletin of Earthquake Engineering, 2015, 13: 2429-2447.

[1.46] Belleri A., Riva P. Seismic performance and retrofit of precast concrete grouted sleeve connections. PCI journal, 2012, 57.

[1.47] Jansson P. O. Evaluation of grout-filled mechanical splices for precast concrete construction, 2008.

[1.48] Yoon W., Hamahara M., Motooka J. Experimental study on restoring force characteristics of precast prestressed concrete columns. Journal of Structural and Construction Engineering, 480: 151-160. (in Japanese)

[1.49] Guerrini G., Restrepo J., Schoettler M. Self-centering, low-damage, precast post-tensioned columns for accelerated bridge construction in seismic regions. World Conference on Earthquake Engineering, Oakland, CA: Earthquake Engineering Research Institute. 2017.

[1.50] Wang Z, Wang J, Zhao G, et al. Design criterion for the self-centering capacity of precast segmental UHPC bridge columns with unbonded post-tensioning tendons. Engineering Structures, 2019, 200: 109706.

[1.51] Li T., Qu H., Wang Z., et al. Seismic performance of precast concrete bridge columns with quasi-static cyclic shear test for high seismic zones. Engineering Structures, 2018, 166: 441-453.

[1.52] Han Q., Jia Z., Xu K., et al. Hysteretic behavior investigation of self-centering

double-column rocking piers for seismic resilience. Engineering Structures, 2019, 188: 218-232.

[1.53] Guerrini G., Restrepo J.I., Massari M., et al. Seismic behavior of posttensioned self-centering precast concrete dual-shell steel columns. Journal of structural engineering, 2015, 141(4): 04014115.

[1.54] Li C., Xiang Y., Cai C. Performance of a seismic-resilient precast segmental column with UHPC segments and CFRP tendon. Engineering Structures, 2023, 282: 115833.

[1.55] Cai Z.K, Yuan W., Wang Z., et al. Seismic behavior of precast segmental bridge columns reinforced with hybrid FRP-steel bars. Engineering Structures, 2021, 228: 111484.

[1.56] Takeda Y., Kimura K., Takeuchi T., Sun Y.P. Seismic behavior of square precast concrete columns reinforced by circularly-arranged WBUHS rebars, Proceedings of the Japan Concrete Institute, 2019, 41(2): 91-96.

CHAPTER TWO

2 Axial Behavior of Short Concrete Columns Confined by Bolted Steel Tubes

2.1 Introduction

Sargsyan et al. [2.1] and Zhang et al. [2.2] have experimentally verified that concrete columns and walls reinforced by WBUHS rebars could behave in a resilient manner and exhibited satisfactory drift-hardening capability up to large drift. Meanwhile, because of the crushing of concrete and local buckling of WBUHS rebars, the lateral resistance of concrete walls tends to degrade at the drift level of 3% [2.3].

To address the local buckling of the WBUHS rebars in resilient concrete components, Zhou et al. [2.4] have conducted axial compression tests of concrete columns with WBUHS rebars and studied the influence of stirrup spacing, section shape, and concrete strength on the axial behavior of the columns as well as the buckling strain. The test results have revealed that the WBUHS rebars with smaller hoop spacing exhibited relatively higher buckling strain. Nevertheless, even when the slenderness ratio (s/D ratio) was as small as 4, the premature buckling of WBUHS rebars was also observed before yielding. The axial strain corresponding to the peak stress did not exceed 0.8% and less than the yield strain of WBUHS rebars, and the columns' load-carrying ability after the peak load degraded significantly, implying less ductility and deformability.

Considering that lateral confinement by steel tubes is superior to that of conventional hoops and/or spirals in enhancing both concrete strength and ductility, the usage of steel tubes can be expected to limit the circumferential expansion of concrete, thus to effectively delay the premature buckling and improve the post-buckling capacity of WBUHS rebars. This chapter is intended to verify the effectiveness of confinement by bolted steel tubes in enhancing the buckling-resistance of WBUHS bars.

2.2 Experimental Program

2.2.1 Description of Test Specimens

To accomplish the above-mentioned objectives of this chapter, twenty concrete columns were made and tested under concentric loading with hoop spacing (25, 50, 75 or 100 mm), reinforcement type (NS rebar or WBUHS rebar), confinement of steel tubes, and section type (square or circular) as main experimental variables. Of them, four concrete columns were reinforced with NS rebars and confined by both hoops and steel tubes, eight concrete columns were reinforced with WBUHS rebars and confined by only hoops as reference specimens, and the other eight were reinforced with WBUHS rebars and confined by bolted steel tubes to verify the confinement effect by bolted steel tubes.

The details and outlines of test columns are shown in Fig. 2-1 and Table 2-1. As shown in Fig. 2-1 and Table 2-1, twelve specimens are square columns and eight specimens are circular columns with width or diameter of 150mm. The longitudinal reinforcement in each specimen consisted of four NS rebars or WBUHS rebars, while the transverse steel (hoop) was composed of D6 deformed bars (SD295). Test region was the middle portion (146mm in length) of the columns with hoop spacing of 50, 75, 100 and 150mm, to give the volumetric ratio of 2.4%, 1.6%, 1.2% and 0.8%, respectively. Outside the test region, besides reducing hoop spacing to 25mm, two pairs of 6mm-thick steel jackets were adopted to confine both end regions of each specimen to protect the end regions from premature failure.

The upper and lower end plates were used to facilitate the formation of reinforcement cage, and small threaded nails were inserted into the interstice between the end plates and longitudinal rebars to ensure that the position of the end plates remained unchanged when casting concrete. To prevent the steel jackets at both ends and the middle thin steel tubes from directly sustaining axial stress, clearances of 3mm and 6mm was provided between the steel jackets and the specimen’s ends, and the middle steel tubes, respectively. The bolted steel tubes, with a thickness of 1.6mm and volumetric ratio of 4.1%, were formed by connecting two pieces of semi-squarely or semi-circularly fabricated steel plates using high strength bolts and nuts. The number of bolts was determined based on the criteria that the hoop tensile force of steel tubes remained below the yield force of the high-strength bolts.

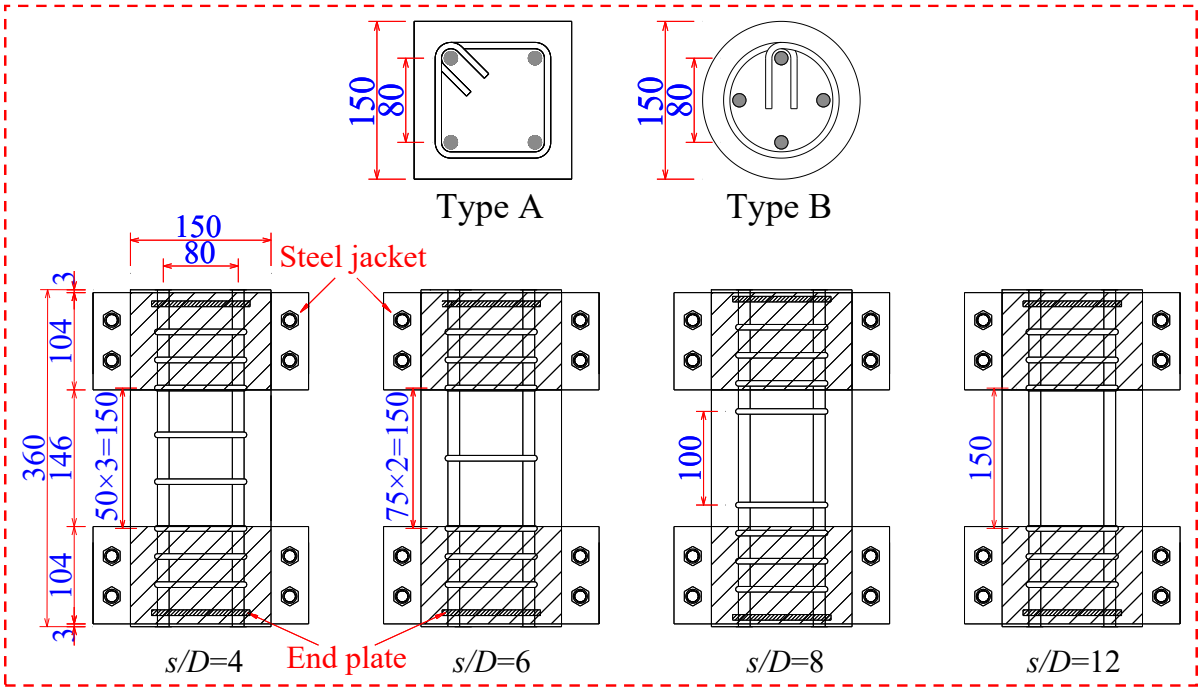

(a) Specimens confined by hoops only

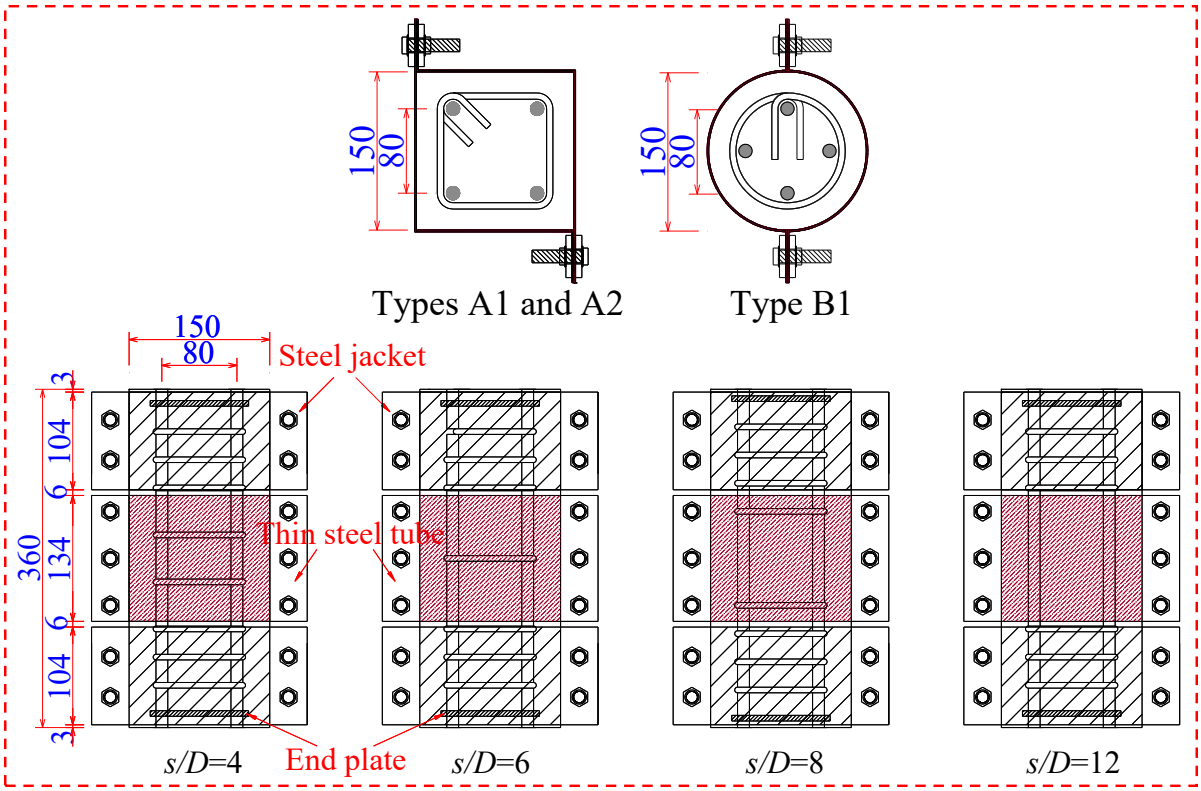

(b) Specimens confined by hoops and bolted steel tubes

Fig. 2-1 Dimensions and reinforcement details (unit: mm)

Table 2-1 Summary of the test specimens

Section details	Specimen	Section type	Transverse confinement	Longitudinal rebar	D (mm)	s (mm)	s/D	f_c' (N/mm^2)
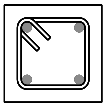	SA-4	A	D6	WBUHS rebar	12.6	50	4	35.8
	SA-6					75	6	35.8
	SA-8					100	8	35.8
	SA-12					150	12	35.8
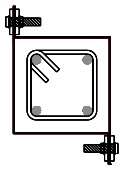	SA1-4	A1	D6+PL1.6	WBUHS rebar	12.6	50	4	36.2
	SA1-6					75	6	36.2
	SA1-8					100	8	33.0
	SA1-12					150	12	33.0
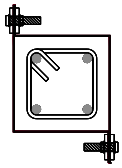	SA2-4	A2	D6+PL1.6	NS rebar	12.7	50	4	33.2
	SA2-6					75	6	36.1
	SA2-8					100	8	36.1
	SA2-12					150	12	36.2
	CB-4	B	D6	WBUHS rebar	12.6	50	4	36.9
	CB-6					75	6	36.9
	CB-8					100	8	36.9
	CB-12					150	12	35.8
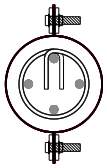	CB1-4	B1	D6+PL1.6	WBUHS rebar	12.6	50	4	33.2
	CB1-6					75	6	33.2
	CB1-8					100	8	36.1
	CB1-12					150	12	36.2

Note: D6: the hoop with a nominal diameter of 6.35mm, PL1.6: the bolted steel tube with a thickness of 1.6mm, D: nominal diameter of longitudinal rebar; s: hoop spacing; s/D: slenderness ratio; f_c': concrete compression strength at the testing.

2.2.2 Material Properties

Ready-mixed concrete, which was made of common Portland cement and regular coarse aggregates having a maximum particle size of 20mm, was used to fabricate the test columns. On the basis of the test results of three cylinders (100mm in diameter and 200mm in height) at 28 days after casting, the average values of splitting tensile strength, Young's modulus, and

peak strain were 3.1MPa, 29.1GPa, 0.2%, respectively. The concrete compression strength at 28 days and the time of testing was 29.3MPa and 35.3MPa, respectively. The mechanical properties and stress-strain relationships of the used materials are presented in Table 2-2 and Fig. 2-2, respectively.

Table 2-2 Mechanical properties of the used materials

Material	*D or T* (mm)	E_s (kN/mm^2)	f_y (N/mm^2)	ε_y (%)	f_u (N/mm^2)
WBUHS rebar (U12.6)	12.6	196.1	1392*	0.91*	1465
NS rebar (D13)	12.7	177.1	365	0.25	541
Hoop (D6)	6.35	194.6	412	0.25	548
Steel tube (PL1.6)	1.6	195.2	404	0.21	429

Note: D: diameter of reinforcements, T: thickness of bolted thin steel tube, E_s: Young's modulus, f_y: yield stress, ε_y: yield strain, f_u: tensile stress, *: the value based on 0.2% offset method.

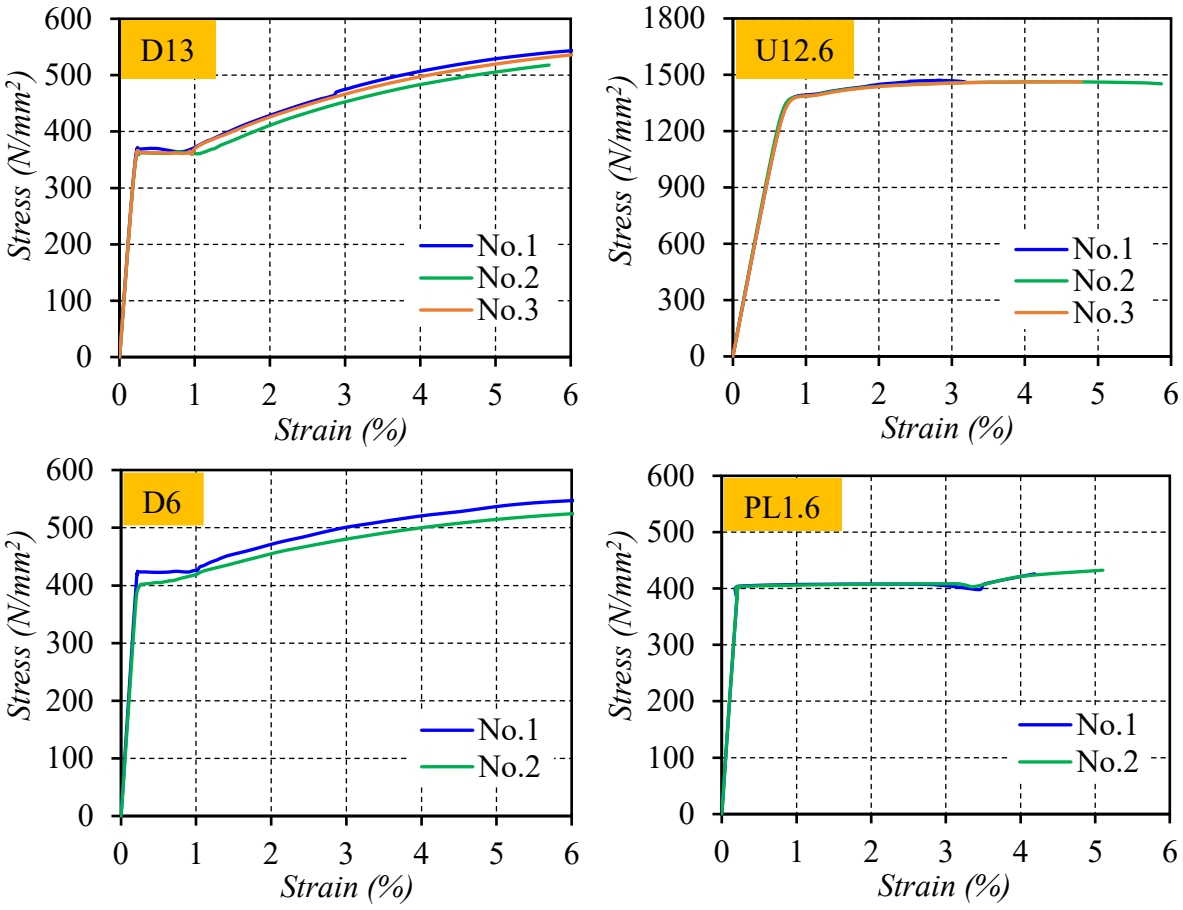

Fig. 2-2 Stress-strain curves of the used materials

2.2.3 Loading Apparatus and Measurements

Monotonic axial compressive loading was applied to the test columns via a universal testing machine with maximum capacity of 2000kN, as shown in Fig. 2-3.

Two 40mm-thick steel plates were placed on the top and bottom of the test columns to facilitate the uniform application of axial compression into columns and the installation of displacement transducers (DTs). The average axial deformation was measured by four DTs installed between the top steel plate and the platform of testing machine. Strain gages were attached on longitudinal rebars, hoops and steel tubes to measure their mechanical behavior, as depicted in Fig. 2-4. Especially, four strain gages (marked with S1−S4) were pasted on the opposite sides of two reinforcement rebars aiming to study the buckling behavior of SD345 and WBUHS rebars.

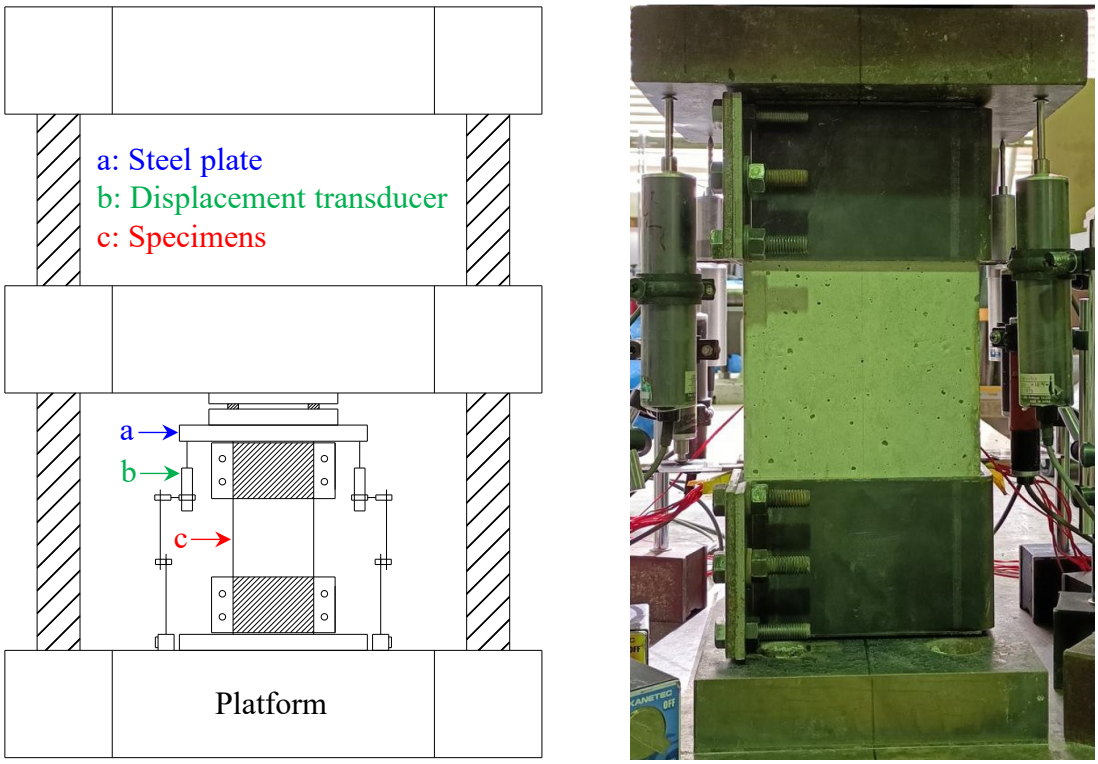

Fig. 2-3 Schematic view of test apparatus

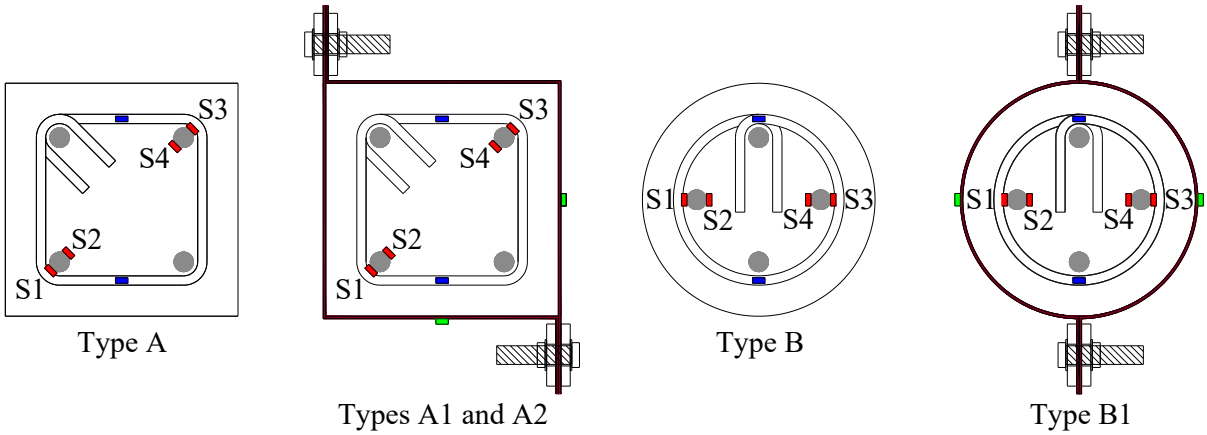

Fig. 2-4 The distribution of strain gauges

2.3 Test Results and Observations

2.3.1 Observations of Test Specimens

The ultimate failure modes of all test columns after removing the steel tubes and crushing concrete were presented in Fig. 2-5. As expected, the major deformation and damage of the test specimens concentrated within the middle test region (146mm in length). As can be seen from Fig. 2-5, the damage degree of group SA and CB specimens was serious with significant crushing of concrete and buckling of WBUHS rebars. For the group CB1 specimens, the damage degree seemed to be more severe than those of groups SA1 and SA2 specimens due to the fracture observed along the bent edge of bolted circular tubes at large strain. Fig. 2-5 also indicated that the confinement of bolted thin steel tubes could alleviate the extent of concrete damage and improve the buckling resistance of WBUHS rebars.

(a) Group SA

(b) Group SA1

(c) Group SA2

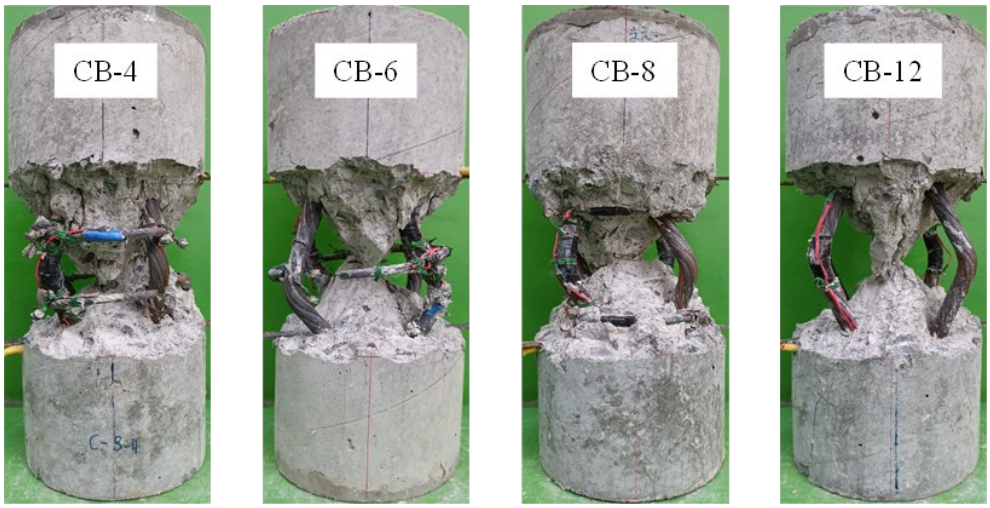

(d) Group CB

Fig. 2-5 Failure mode of test columns

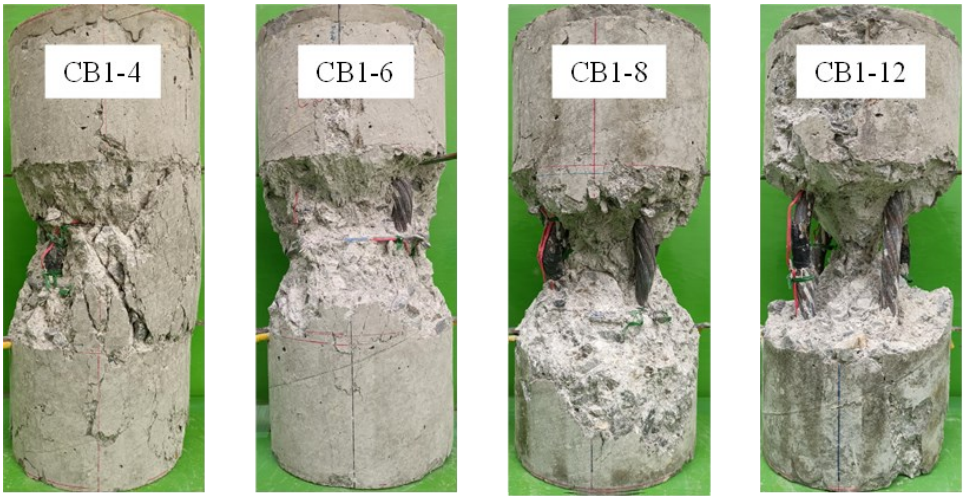

(e) Group CB1

Fig. 2-5 Continued

2.3.2 Lateral Load-strain Curves

The axial load versus axial strain relationships are displayed in Fig. 2-6. While failure seemed to concentrate within the middle portion of specimens with length of 146mm, the lateral dilation of 6mm-thick steel jackets at both ends was also observed. Therefore, the axial strain was obtained by dividing the axial displacement measured by four DTs with the overall height of specimens. In the axial load-strain curves of specimens confined by bolted steel tubes, the circle mark represents the onset of contact between steel jacket and steel tube, and the triangular mark expresses the fracture of steel tube. It should be mentioned that there are some circular holes on the bottom steel plate with the same diameter as the WBUHS rebar. Along with the increase of axial load, WBUHS rebars in specimen SA1-4 and CB1-6 slipped a little through the bottom plate of the test specimen into the holes, resulting in a certain degree of reduction in load-carrying capacity.

In general, the specimens with smaller hoop spacing possessed relatively higher loading capacity and more ductile post-peak behavior, because smaller hoop spacing meant stronger confinements to core concrete. As compared with the specimens of group SA, the specimens of group SA1 showed a little higher peak load but significant enhancement in the post-peak behavior, because of the confinement of square bolted steel tubes. More significant improvement on peak load and ductility can be observed by comparing the measured axial load-strain curves of specimens of groups CB and CB1, which implies that the load-bearing capability and ductility of concrete columns with WBUHS rebars can be greatly enhanced by the confinement of bolted circular steel tubes. The main reason was that the uniform confinement of circular steel tubes provided larger strength and ductility enhancement to concrete than square steel tubes.

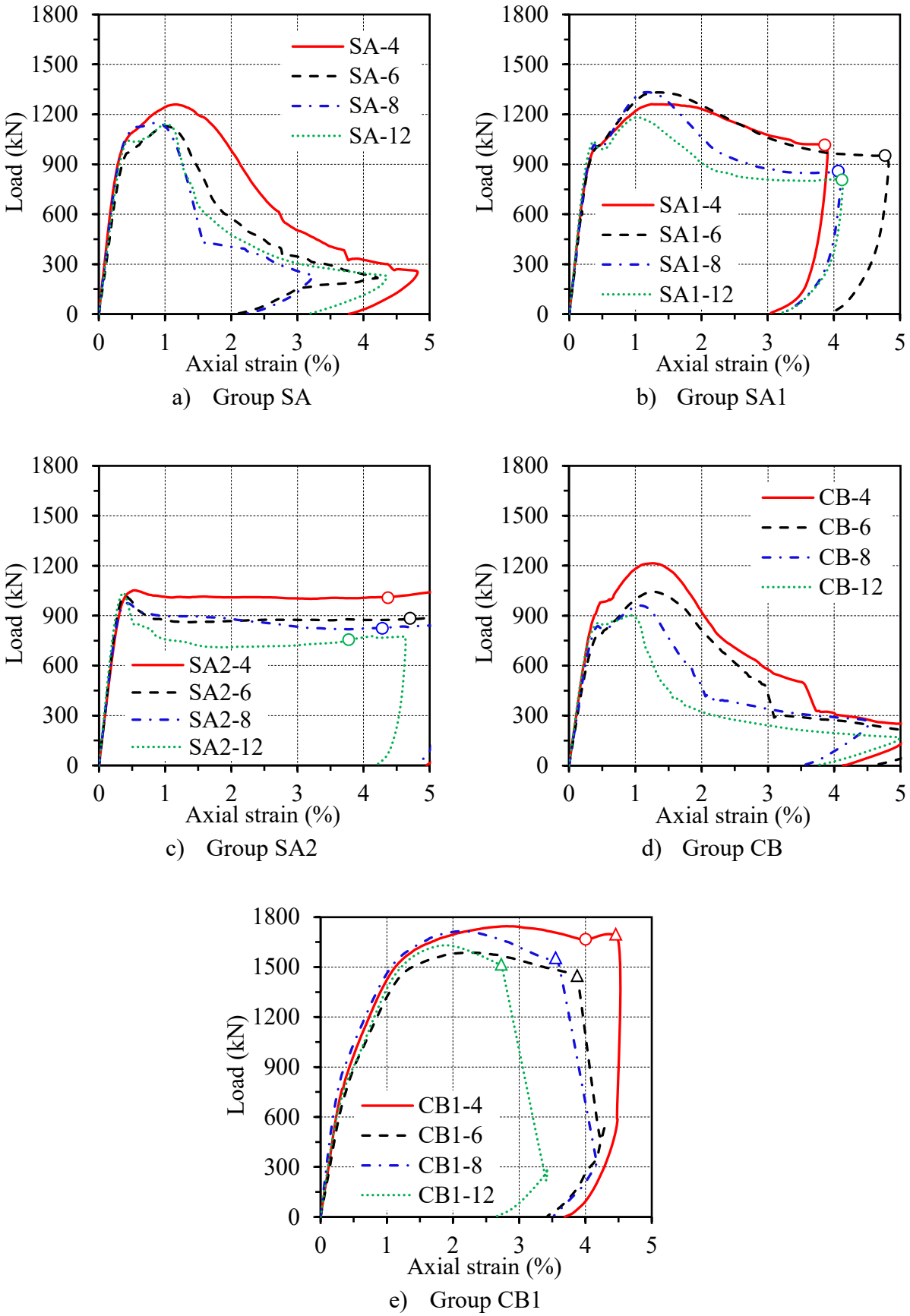

Fig. 2-6 Measured axial load-strain relationships

Table 2-3 listed the axial strains measured at the peak load. As obvious from Table 2-3, the axial strains at the peak load of specimens with slenderness ratio (s/D) of 4 and 6 exhibited larger values than that of specimens with s/D of 8 and 12. In addition, the axial strains at the peak load could be increased by 12.7% and 87.8% on average by the confinement of square and circular thin steel tubes, respectively. This observation indicated that more significant confinement effect can be expected in the WBUHS rebar-reinforced columns when confined by circular steel tubes.

To better find out the influence of experimental parameters on the post-yield load capacity of test columns, the axial load corresponding to axial strains of 1%, 2% and 3%, and their ratios to the peak load were summarized in Table 2-3. It can be found that the group SA2 specimens displayed good post-yield load capacity with only 5%~14% (31% for specimen SA2-12) induction in strength degradation. As can be seen for group SA and CB specimens, the decline of load-carrying capacity became obvious along with axial strain, and the larger the s/D ratio, the more pronounced the decline. For group SA1 and CB1 specimens, the axial load (except for specimen SA1-12) could maintain more than 80% of the peak load till axial strain of 2.0%. Even at the axial strain of 3.0%, the axial resistance of CB1 specimens could still maintain 95%~99.7% (62% for specimen CB1-12) of their peak loads. This observation clarified the effectiveness of confinement by the bolted steel tubes in enhancing the post-peak load capacity of concrete columns with WBUHS rebars.

Table 2-3 Summary of the test results

Specimen	ε_b (%)			ε_b*	ε_p	N_{exp}	$N_{1\%}$	$N_{2\%}$	$N_{3\%}$	$\frac{N_{1\%}}{N_{exp}}$	$\frac{N_{2\%}}{N_{exp}}$	$\frac{N_{3\%}}{N_{exp}}$
	ε_{b1}	ε_{b2}	avg	(%)	(%)	(kN)	(kN)	(kN)	(kN)			
SA-4	0.69	0.38	0.54	0.86	1.18	1259.3	1243.6	983.8	504.8	0.99	0.78	0.40
SA-6	0.20	0.58	0.39	0.57	0.99	1129.0	1129.0	578.2	344.6	1.00	0.51	0.31
SA-8	0.26	0.28	0.27	0.47	0.86	1149.6	1127.2	404.3	258.6	0.98	0.35	0.23
SA-12	0.24	0.25	0.25	0.47	1.02	1141.2	1140.0	479.8	305.8	1.00	0.42	0.27
SA1-4	0.67	0.27	0.47	0.81	1.26	1261.0	1219.0	1228.7	1077.4	0.97	0.97	0.85
SA1-6	0.39	0.29	0.34	0.49	1.26	1331.8	1277.0	1249.7	1063.0	0.96	0.94	0.80
SA1-8	0.24	0.20	0.22	0.41	1.07	1332.8	1302.4	1065.8	873.5	0.98	0.80	0.66
SA1-12	0.23	0.26	0.25	0.43	0.94	1180.9	1180.6	909.5	808.0	1.00	0.77	0.68
SA2-4	1.04	0.60	0.82	0.53	0.54	1052.0	1019.8	1010.0	1004.2	0.97	0.96	0.95
SA2-6	0.24	0.25	0.25	0.34	0.39	1018.9	879.9	866.5	875.3	0.86	0.85	0.86
SA2-8	0.26	0.22	0.24	0.37	0.42	974.5	901.8	885.6	838.5	0.93	0.91	0.86
SA2-12	0.23	0.24	0.24	0.41	0.36	1037.4	774.6	710.6	718.4	0.75	0.68	0.69
CB-4	0.59	0.87	0.73	0.99	1.25	1214.4	1182.4	921.3	581.2	0.97	0.76	0.48
CB-6	0.73	0.52	0.63	0.83	1.33	1044.4	996.5	814.8	475.0	0.95	0.78	0.46
CB-8	0.23	0.20	0.22	0.47	1.18	960.5	956.4	461.1	341.9	1.00	0.48	0.36
CB-12	0.25	0.20	0.23	0.40	1.06	901.6	888.8	321.6	242.4	0.99	0.36	0.27
CB1-4	0.86	0.68	0.77	1.21	2.81	1745.5	1422.3	1694.7	1740.6	0.82	0.97	1.00
CB1-6	0.80	0.38	0.59	0.81	2.24	1587.2	1316.8	1580.3	1542.4	0.83	1.00	0.97
CB1-8	0.48	0.50	0.49	0.84	2.12	1715.1	1458.8	1711.2	1620.5	0.85	1.00	0.95
CB1-12	0.34	0.23	0.29	0.62	1.89	1630.2	1372.9	1626.1	1002.2	0.84	1.00	0.62

Note: ε_{b1}: buckling strain based on S1 and S2 gauges; ε_{b2}: buckling strain based on S3 and S4 gauges; avg: average of ε_{b1} and ε_{b2}; ε_{b*}: average of axial strain corresponding to ε_{b1} and ε_{b2}; ε_p: axial strain at peak load; N_{exp}: experimental peak load; $N_{1\%}$, $N_{2\%}$, and $N_{3\%}$: the load at 1%, 2%, and 3% axial strain, respectively; μ: the calculated strain ductility.

2.3.3 Buckling Strains of Longitudinal reinforcements

Along with the axial strain, the cover concrete will spall off and crush gradually, while the core concrete will expand laterally, both of which can promote the local buckling of WBUHS rebar. Because it is difficult to accurately identify the onset of the buckling, to evaluate the buckling strain of WBUHS rebars, the definition of the onset of local buckling proposed by Rodriguez et al. [2.5] is adopted. According to reference [2.5], the onset buckling strain could be defined as the strain when the measured strain difference between the two sides of each WBUHS rebar reached 20%. Fig. 2-7 shows an example of strains measured on both sides of a WBUHS rebar (specimen SA-4) with blue diamond mark to represent the onset of buckling.

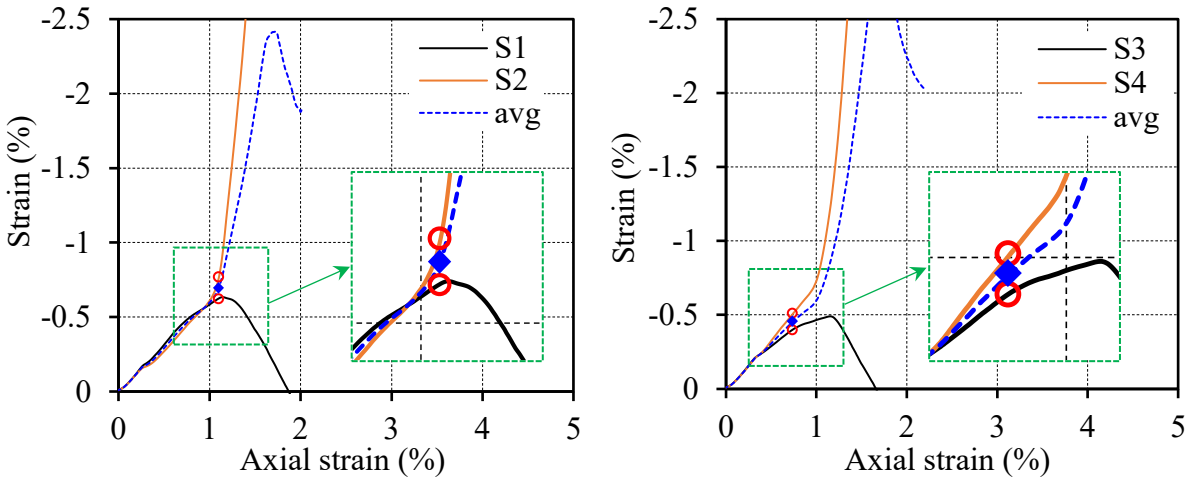

Fig. 2-7 Example of axial strains of WBUHS rebar

The buckling strains such obtained are listed in Table 2-3. As one can see from Table 2-3, reducing the hoop spacing so that s/D ratio is less than 6.0 was beneficial to delay the buckling of WBUHS rebar which was consistent with Zhou's conclusion [2.6]. However, judging from the buckling strains measured by strain gauges, the confinement by bolted steel tubes had little effect on the improvement of buckling strain. This might be attributed to that the definition of the onset of buckling is not necessarily proper. In fact, by comparing the buckling strains obtained following the definition of Rodriguez et al. [2.5] with the measured strains at the peak loads, one can see that the axial strains corresponding to the onset of buckling of WBUHS rebars are much less than the peak strains, as compared in Table 2-3. Since the buckling of rebars generally results in a reduction in the axial resistance of concrete members, the definition for onset of the local buckling in reference 2.5 needs to be revised to more accurately evaluate buckling strains of rebars.

2.3.4 Strain Ductility

Strain ductility is a crucial index to evaluate the deformability of concrete members under axial compression without significant strength degradation after entering an inelastic stage, and usually can be defined as the ratio of ultimate strain in which 85% of the peak load is maintained after peak to the yield strain [2.7], as given in Eq. (2.1) and shown in Fig. 2-8. Since there are several definitions of the yield strain [2.8], the ductility may change if different definition is taken. To avoid confusion and conduct absolute evaluation of the strain ductility, this paper proposes using the peak strain of unconfined concrete as the yield strain, in which the peak strain of unconfined concrete will be obtained by Eq. (2.2) [2.9].

$$\mu = \frac{\varepsilon_u}{\varepsilon_y} \tag{2.1}$$

$$\varepsilon_0 = 0.94 \cdot f_c^{0.25} \cdot 10^{-3} \tag{2.2}$$

Where, μ represents the strain ductility, ε_u is the ultimate strain where 85% of the peak load is maintained after peak, ε_y represents the yield strain, which is presumed to be the peak strain of unconfined concrete ε_0.

The measured strain ductility is compared in Fig. 2-9. As obvious from Fig. 2-9, the smaller the hoop spacing, the higher the strain ductility. The NS rebar-reinforced columns with a hoop spacing of 25mm and 50mm presented the largest strain ductility owing to the confinement of square steel tubes, but the increase of hoop spacing would lead to a significant reduction in strain ductility. Furthermore, the effectiveness of steel tube confinement in enhancing ductility of columns with WBUHS rebars can be clearly observed from Fig. 2-9. As compared with hoop-confined columns, confinement by square steel tubes increased the strain ductility by 36%−89%, while confinement by circular steel tubes could increase the strain ductility by 112−153%, exhibiting a more prominent enhancement effect.

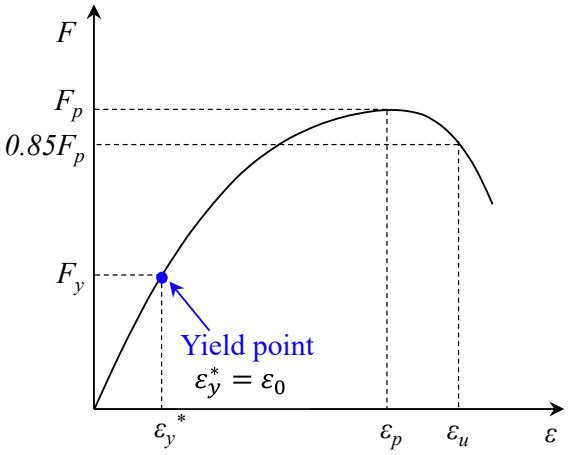

Fig. 2-8 Definition of yield point

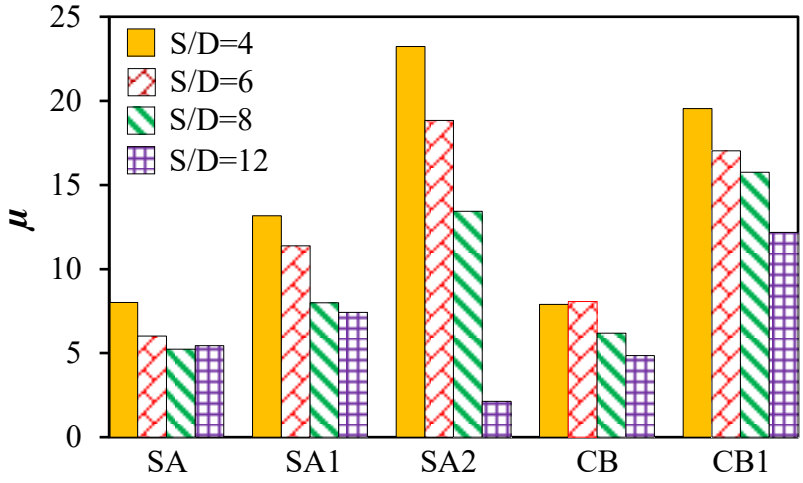

Fig. 2-9 Comparison of strain ductility

2.3.5 Stress-Strain Behavior of WBUHS Rebars

Although the previous sections have demonstrated the effectiveness of steel tubes in improving the bearing capacity, both the peak and post-peak, and ductility of concrete columns, it is essential to extract the stress-strain behavior of longitudinal reinforcements aiming to more intuitively understand the effect of steel tubes on the buckling behavior of the longitudinal reinforcements. The axial load borne by WBUHS rebars can be determined by extracting the contribution of the concrete from the measured axial load of tested columns. Then, the stress of WBUHS rebars can be calculated by Eq. (2.3).

$$\sigma_s = \frac{N - N_{cov} - N_{cor}}{A_s} \tag{2.3}$$

In which, σ_s and A_s represent the stress and area of WBUHS rebars, N is the axial load of test specimens, N_{cov} and N_s represent the load borne by cove concrete and core concrete, respectively.

Whereas for the concrete, a constitutive model that can trace the stress-strain relationship accurately is urgently needed, because it will directly affect the accuracy of the calculation results. Sun et al. [2.9] proposed a complete stress-strain model for confined concrete that can consider the confinement effects of both hoops and steel tubes (called Sakino-Sun model hereafter), and its reliability has been verified by similar studies conducted by Zhou et al. [2.10]. Therefore, the Sakino-Sun model was adopted in this paper to calculate the contribution of confined concrete, which can be mathematically expressed in Eqs. (2.4)−(2.13).

$$f_c = K \cdot f_p \cdot \frac{AX + (D-1)X^2}{1 + (A-2)X + DX^2} \tag{2.4}$$

Where, f_c is the stress of concrete; f_p represents the ultimate compressive strength of plain concrete according to the test performed on three cylinders (100 mm in diameter and 200 mm in height); K represents the strength-raising coefficient of confined concrete, and the double confinement effects provided by both thin steel tubes and common hoops are considered for group SA1 and CB1 specimens.

$$A = \frac{E_c \varepsilon_{co}}{f_{co}} \tag{2.5}$$

$$D = 1.5 - 0.017 f_p + \gamma_D \sqrt{(K-1)\, f_p / 23} \tag{2.6}$$

$$X = \frac{\varepsilon_c}{\varepsilon_{co}} \tag{2.7}$$

Where, E_c denotes elasticity modulus of plain concrete; f_{co} represents the ultimate compressive strength of confined concrete; ε_c represents the strain of confined concrete; ε_{co} represents the strain of confined concrete when reaching its ultimate compressive strength.

$$E_c = \left(0.69 + 0.33\sqrt{f_p}\right) \times 10^4 \tag{2.8}$$

$$\varepsilon_{co} = \varepsilon_o \cdot \begin{cases} [1 + 4.7(K-1)] & K \le 1.5 \\ 3.35 + 20(K - 1.5) & K > 1.5 \end{cases} \tag{2.9}$$

$$\varepsilon_o = 0.94 \cdot f_p^{0.25} \times 10^{-3} \tag{2.10}$$

$$\gamma_D = \begin{cases} 1.6 & for\ hoop \\ 2.4 & for\ steel\ tube \end{cases} \tag{2.11}$$

$$K = \frac{f_{co}}{f_p} = \begin{cases} 1 + 2.05\left(1 - \frac{s}{2D_c}\right)^2 \cdot \frac{\rho_h \cdot f_{yh}}{f_p} & for\ circular\ hoop \\ 1 + 11.5\left(\frac{d}{C}\right)\left(1 - \frac{s}{2D_c}\right) \cdot \frac{\rho_h \cdot f_{yh}}{f_p} & for\ rectilinear\ hoop \end{cases} \tag{2.12}$$

$$K = \frac{f_{co}}{f_p} = \begin{cases} 1 + 4.1\left(\frac{2}{D'/t-2}\right) \cdot \frac{f_{yt}}{f_p} & for\ welded\ circular\ steel\ tube \\ 1 + 46\frac{f_{yt} \cdot (B'/t-1)}{f_p \cdot (B'/t-2)^3} & for\ welded\ rectilinear\ steel\ tube \end{cases} \tag{2.13}$$

Where, ε_o represents the strain of plain concrete when reaching its maximum compressive strength; s is the hoop spacing; D_c denotes the side length or diameter of the centerline of common hoops (see Fig. 2-10); ρ_h represents the volumetric ratio of common hoops; f_{yh} represents the yield stress of common hoops; d denotes the nominal diameter of the common hoop; C represents the center-to-center spacing between the longitudinal rebars within a square cross-section (see Fig. 2-10); D' denotes the outer diameter of thin steel tubes; t represents the thickness of bolted thin steel tubes (see Fig. 2-10); f_{yt} represents the yield stress of thin steel tubes; B' denotes the center-to-center spacing between the square steel tubes (see Fig. 2-10).

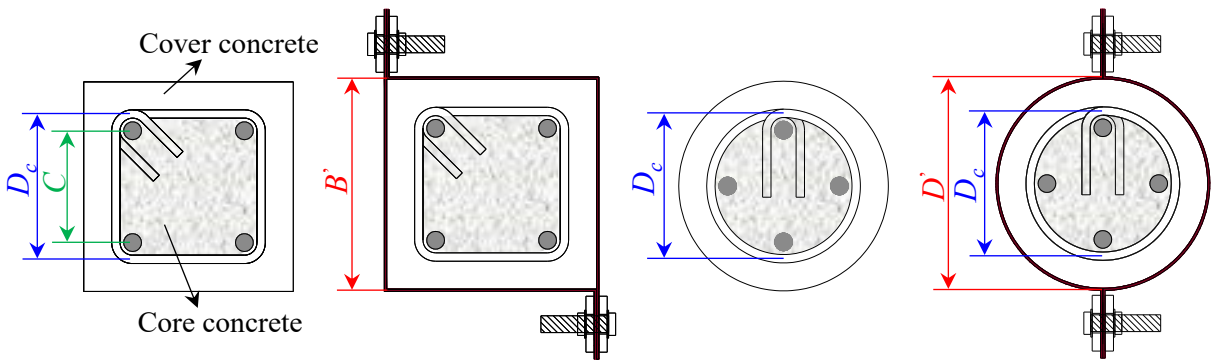

Fig. 2-10 Definition of the cover concrete and confined concrete

It is worth highlighting that the calculated values based on the Sakino-Sun model (derived from welded steel tubes) might potentially lead to an overestimation of the strength-raising coefficient (K) especially for concrete confined by bolted circular steel tubes because of the discontinuity, as listed in Table 2-4. As a result, 0.49 and 0.33 times the calculated K values based on the Sakino-Sun model were adopted in the above calculation formula for bolted circular steel tube and square steel tube respectively, as indicated by the axial compression test results of short concrete columns confined by steel tubes formed by the same joining method, as given in Table 2-4.

Table 2-4 Comparison of experimental and calculated strength-raising coefficient (K)

Name	Diameter (mm)	Yield strength (N/mm^2)	Plain concrete strength (N/mm^2)	Confined concrete strength (N/mm^2)	K_{exp}	K_{cal}
Bolted circular steel tube (PL1.6)	1.6	404	34.4	51.1	1.49	2.01
Bolted rectilinear steel tube (PL1.6)	1.6	404	36.1	36.9	1.02	1.06

Note: K_{exp} and K_{cal} represent the experimental and calculated value (derived from Sakino-Sun model) of the strength-raising coefficient, respectively.

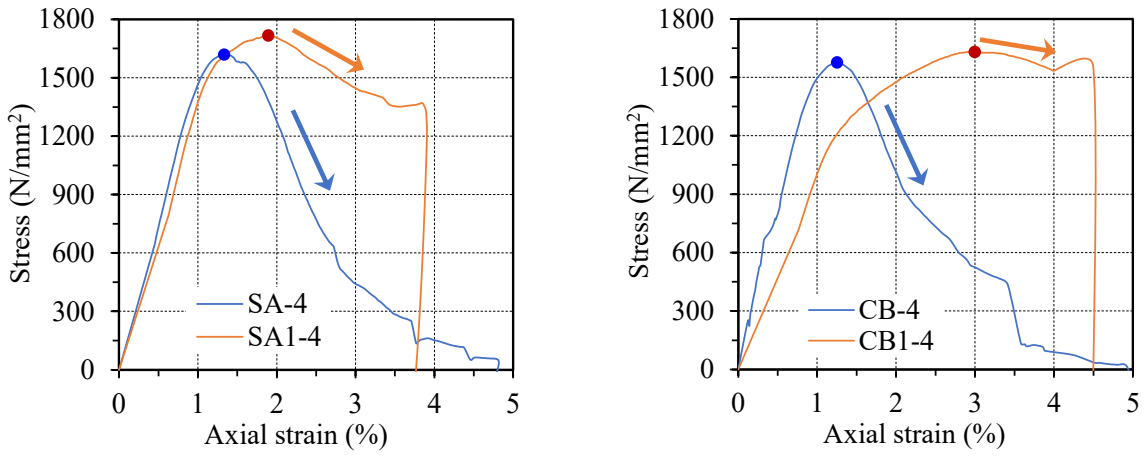

(a) s/D=4

Fig. 2-11 Stress-strain behavior of WBUHS rebars

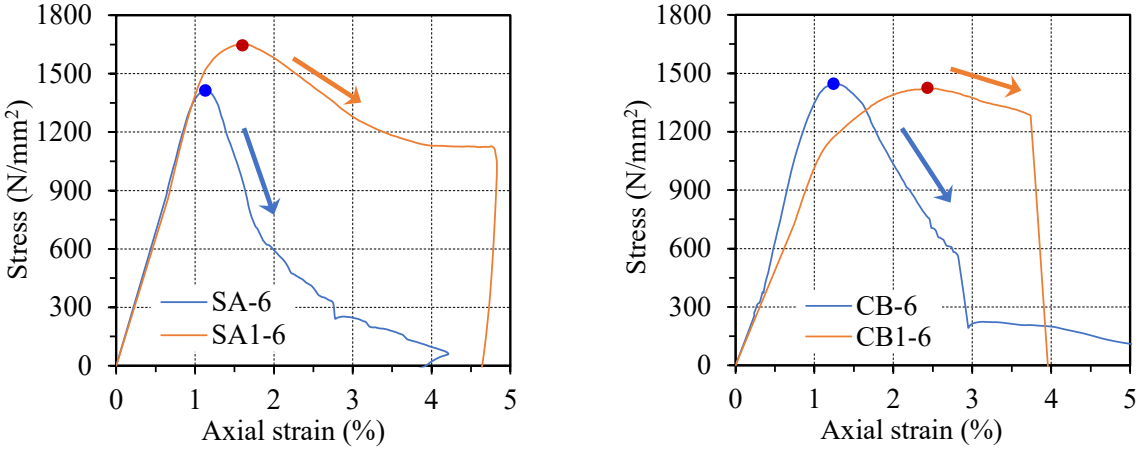

(b) s/D=6

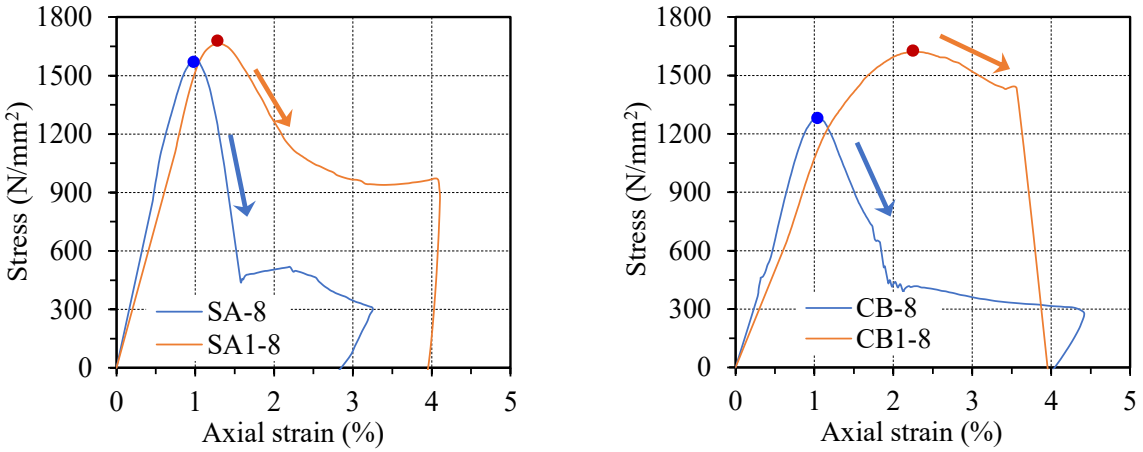

(c) s/D=8

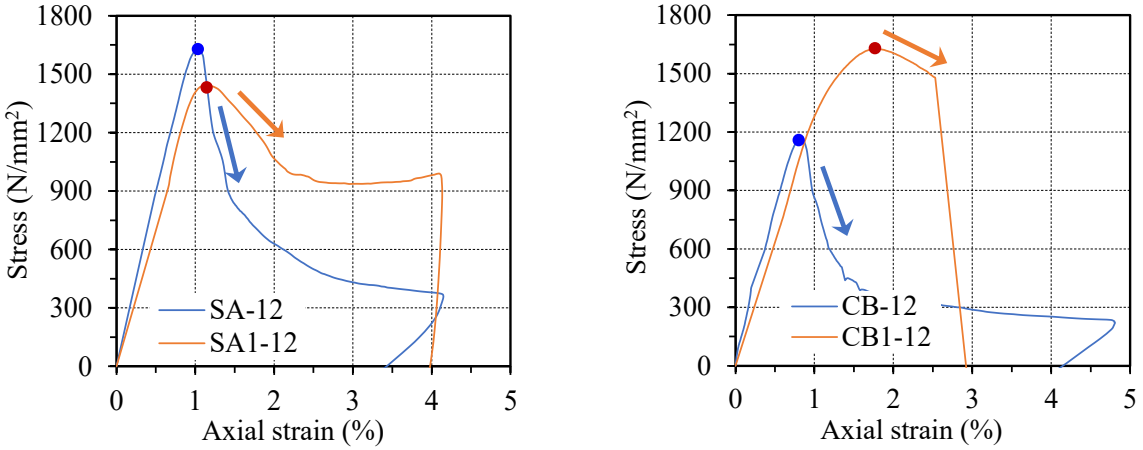

(d) s/D=12

Fig. 2-11 Continued

The stress-strain relationships of WBUHS bars were extracted according to the aforementioned calculation method, and a comparison is presented in Fig. 2-11. The axial load sustained by the WBUHS bar is obtained by the difference between the axial load of test specimens and the axial load borne only by concrete. As long as the strain at the peak load of concrete remains below the peak strain of test specimens, the strain at the peak stress of the WBUHS rebar (buckling strain) will be not less than the peak strain of test specimens. According to this point, reducing the hoop spacing and employing bolted steel tubes can effectively delay the buckling of WBUHS rebars and enhance its post-buckling behavior. Notably, as compared with bolted rectangular steel tube, the usage of bolted circular steel tube can more significantly delay the premature buckling of WBUHS rebar and mitigate the reduction in stress after buckling owing to the uniform confinement effect.

2.4 Conclusions

Twenty concrete columns with NS rebars or WBUHS rebars were made and tested under monotonic concentric loading with the aim of investigating the effect of hoop spacing and confinement by the bolted thin steel tubes on the axial behavior with emphasis placed on the enhancement of ductility and delaying the buckling of WBUHS rebars. According to the test results and discussions presented in this chapter, the main conclusions are made as follows:

(1) Confinement by bolted thin steel tubes could reduce concrete damage and simultaneously enhance the strain at peak load of concrete columns with WBUHS rebars significantly. In particular, the bolted circular steel tube could also upgrade the concrete strength, while the confinement effect on concrete strength by square steel tubes was little.

(2) The strain ductility of test specimens confined by square and circular steel tubes were 36 % − 89 % and 112 % − 152.9% higher than those of concrete columns confined only by hoops, respectively.

(3) The current definition of the onset of local buckling of rebars may not be necessarily accurate and needs to be revised because buckling of the reinforcements should lead to a decrease in bearing capacity. From this point and on the basis of the extracted stress-strain behavior of WBUHS rebars, the buckling strain and post-buckling behavior of WBUHS rebars could also be improved by confining the columns with bolted steel tubes. Confinement by bolted square thin steel tube could increase the peak strain beyond 1.0%, which is larger than the yield strain of WBUHS rebar, while the bolted circular steel tube with the same thickness as square tube enhanced the peak strain close to and/or beyond 2.0% even the slenderness ratio was as large as 12, due to its uniform confinement effect.

References

[2.1] Sargsyan S., Tanaka Y., Takeuchi T., et al. Seismic behavior andassessment of circular concrete columns reinforced by ultra-high strength rebars. 16th WCEE, No.664, 2017.

[2.2] Zhang J., Liu X., Liu J., et al. Seismic performance and reparability assessment of recycled aggregate concrete columns with ultra-high-strength steel bars. Eng. Struct. 2023, 277, 115426.

[2.3] Wei C., Sun Y., Takeuchi T., et al. Seismic behaviors and evaluation of reinforced concrete walls reinforced by SBPDN rebars. JCI, Vol. 43, Jul. 2021, pp. 175-180.

[2.4] Zhou A., Sun Y., Takeuchi T., et. al. Experimental study on axial behavior of concrete columns reinforced by SBPDN rebars. JCI, Vol. 42, Jul. 2020, pp. 43-48.

[2.5] Rodriguez, M., Botero, J. and Villa, J. Cyclic stress-strain behavior of reinforcing steel including effect of buckling. J Struct Eng, ASCE, Vol. 125, Jun. 1999, pp. 605-612.

[2.6] Zhou A., Sun Y., Takeuchi T., et. al. Experiment on buckling behavior of ultra-high strength rebars in RC column. JCI, Vol. 41, 2019, pp. 37-42.

[2.7] Duan L, Cooper T.R. Displacement ductility capacity of reinforced concrete columns. Concrete International, 1995, 17(11): 61-65.

[2.8] Park R. Ductility evaluation from laboratory and analytical testing. Proceedings of the 9th world conference on earthquake engineering. Tokyo-Kyoto Japan, 1988, 8: 605-616.

[2.9] Sun, Y. and Sakino, K. Ultimate Strength of RC Columns Retrofitted by Circular Steel Tubes. JCI, Vol. 20, Jun. 1998, pp. 1117-1122. (In Japanese)

[2.10] Zhou A., Sun Y., Takeuchi T., et al. Monotonically compressive stress-strain model of ultra-high-strength rebar considering buckling. 17th WCEE, 2020.

CHAPTER THREE

3 Seismic Behavior of Concrete Columns Confined by Bolted Circular Steel Tube

3.1 Introduction

Sun et al [3.1] have developed a new kind of resilient concrete components by utilizing weakly bonded ultra-high strength (WBUHS) rebar with helical surface as longitudinal tensile steel. The key point in the new resilient concrete components is that the weak bond strength (about 3 N/mm^2) promotes stress transfer along the entire length of the rebar, thereby delaying the strain concentration in the plastic hinge zone (Sun et al. [3.1], Funato et al. [3.2]). Previous experimental study has confirmed the validity and practicability of this approach in developing resilience, even when concrete members are subjected to higher axial forces or deformed with double curvature (Wang et al. [3.3]; Takeuchi et al. [3.4]). Notably, more pronounced resilience could be observed particularly in circular columns reinforced by WBUHS rebars and simultaneously confined by steel tubes owing to the strong confinement effect of steel tubes on concrete (Sun and Cai [3.5]). Concrete columns with a circular cross-section present a compelling blend of structural efficiency, aesthetic allure, and strength uniformity, making them a highly favored choice across various architectural and engineering domains. However, it is important to note that the longitudinally rebars arranged in a circular configuration in conventional circular columns may potentially lead to a reduction in the available spacing between the reinforcement from adjacent beams in the horizontal direction, and increasing complexities during the construction of beam-column joints. As one of solutions for these problems, this paper proposes squarely arranging longitudinal WBUHS rebars for circular columns from the viewpoint of facilitating the construction of beam-column connections.

In the meantime, there is a growing trend towards increased adoption of prefabricated and modular buildings, primarily motivated by the desire to enhance construction quality and reduce construction timelines. Consequently, it is of great significance to materialize the

prefabrication of resilient concrete components reinforced with WBUHS rebars. Moreover, previous research has emphasized that achieving the optimal mechanical properties of UHS rebars (steel strands, FRP bars and WBUHS rebars) requires secure anchoring with sufficient anchoring length at the ends [3.6-3.8]. For the purpose of promoting the application of WBUHS rebars in precast concrete construction, it is crucial to assess the difference in seismic performance between precast and cast-in-place components and to determine the required embedment length for WBUHS rebars to achieve optimal performance of the resilient precast concrete components.

The primary objectives of this chapter are: 1) to provide experimental information on the seismic performance of circular concrete columns reinforced with squarely-arranged WBUHS rebars and confined by bolted circular steel tubes; 2) to find the necessary embedment length for WBUHS rebars to achieve the optimal performance; and 3) to verify if there is difference in seismic performance between precast and cast-in-place construction.

3.2 Experimental Program

3.2.1 Description of Test Specimens

A total of twelve 1/2.5-scale concrete columns were designed and each of them was composed of a loading stub of 400×350×350mm, a circular column with an outer diameter of 300 mm, and a footing of 1000×540×400mm (or 1000×500×400mm for the columns with a shear span ratio of 2.5). Among the twelve test columns, two were reinforced with normal strength (NS) rebars featuring hooked ends as reference specimens and the other ten were reinforced with WBUHS rebars. The main experimental parameters are reinforcement type (NS rebar, WBUHS rebar), shear span ratio (1.7, 2.5), diameter-thickness ratio of the bolted circular steel tubes to confine concrete (96, 132), axial load ratio (0.20, 0.33), embedment length of reinforcement (20d, 30d) and construction method (cast-in-place, precast).

The parameters of test columns are listed in Table 3-1 and the reinforcement details are depicted as Fig. 3-1. Both NS rebars and WBUHS rebars were squarely arranged and transversely confined by D6 deformed rebars with a hoop spacing of 100 mm, meeting the requirements of the hoop reinforcement ratio specified in the AIJ code [3.9]. For NS rebars, the ends were bent at a 90-degree angle or 180-degree angle to meet anchoring requirements. As for WBUHS rebars, the upper end was secured by high-strength (HS) nuts and a steel plate to ensure the reinforcement position and the lower end was anchored using HS nuts and washers (with outer diameter of 32 mm) to facilitate prefabricated construction. For the purpose of preventing the early crushing of cover concrete and pursuing the resilience up to a large drift, all the test columns were externally confined by steel tubes with diameter-thickness ratios of 132 or 96, to give a volumetric ratio of 3.1% or 4.3%. The steel tubes were fabricated by joining two pre-manufactured semi-circular plates through high-strength bolts and nuts, and steel plates with 9 mm thickness (PL9) were added for preventing the local buckling of the flange. Aiming at hindering the steel tubes from directly withstanding axial stress, a 6mm clearance was maintained between the bolted steel tubes and the loading stub (or the footing). For precast columns, the column and footing were manufactured and poured separately. After one week of pouring, concrete strength could meet the requirements of removing the formwork and lifting operation. Then, WBUHS rebars protruding from the column were inserted into sheathing ducts pre-embedded in the footing and jointed using high-strength and no-shrinkage grouting material. The jointing process of precast columns was described in Fig. 3-2.

Table 3-1 Parameters and primary test results of the test columns

Specimen	Longitudinal rebar	*a/D*	Construction method	l_e (mm)	*n*	Transverse confinement	f_c' (MPa)	Q_{exp} (kN)	R_{exp} (×0.01rad.)
C17N20STU	8-U12.6 (ρ_g=1.41%)	1.7	Cast-in-place	20d	0.20	D6+PL2.3	38.1	309.7	4.9
C17N20LTU				30d			37.9	305.7	6.0
PC17N20STU			Precast	20d			38.5	306.0	5.9
PC17N20LTU				30d			37.5	314.8	6.0
PC17N33STU				20d	0.33		38.4	309.7	5.8
PC17N33LTU				30d			38.0	330.2	5.9
PC17N33STTU				20d		D6+PL3.2	38.5	319.0	6.0
PC17N33LTTU				30d			38.3	329.3	6.0
PC25N33LTU		2.5		30d		D6+PL2.3	41.3	190.1	6.0
C25N33LTU			Cast-in-place				40.6	199.1	5.0
C17N20STD	8-D13 (ρ_g=1.41%)	1.7		20d	0.20		41.7	193.6	3.6
C17N33STD					0.33		42.8	254.5	2.2

Note: ρ_g: longitudinal rebar ratio, *a/D*: shear span ratio, l_e: embedment length of longitudinal rebar, *d*: diameter of WBUHS rebar, *n*: axial load ratio, ρ_w: volumetric ratio of the common hoop, ρ_t: volumetric ratio of the bolted circular steel tube, f_c': the measured standard cylindrical concrete compressive strength, Q_{exp}: average value of measured peak loads in both positive and negative drift ratios, R_{exp}: drift ratio at peak load.

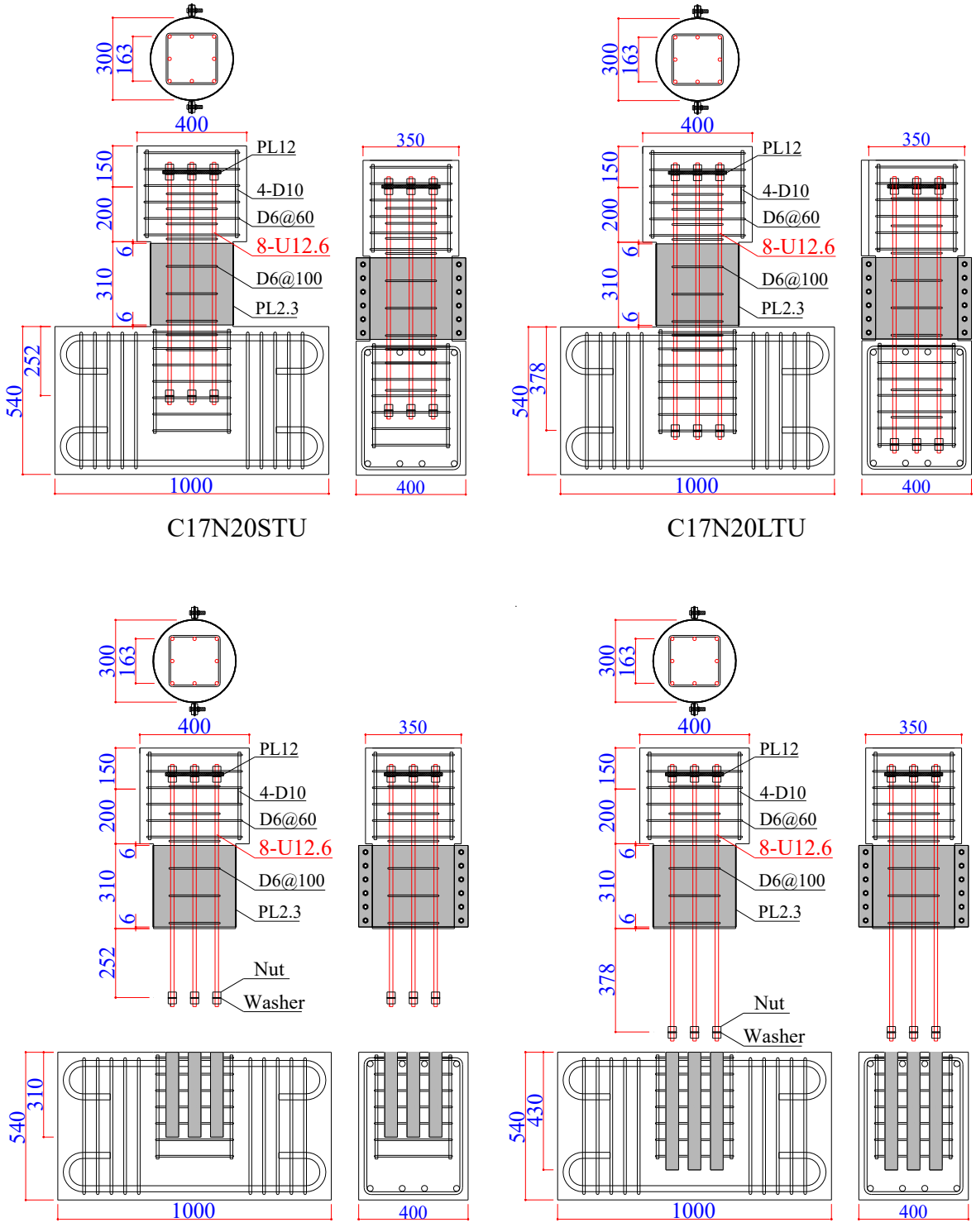

Fig. 3-1 Reinforcement details of test columns

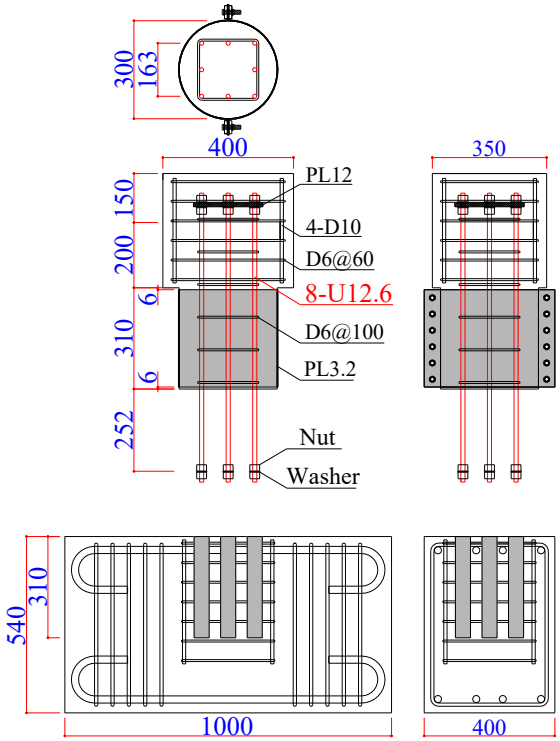

PC17N33STTU

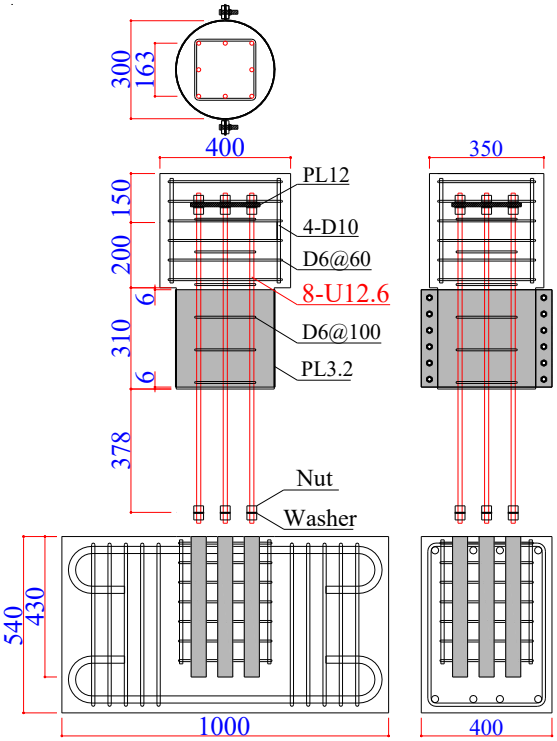

PC17N33LTTU

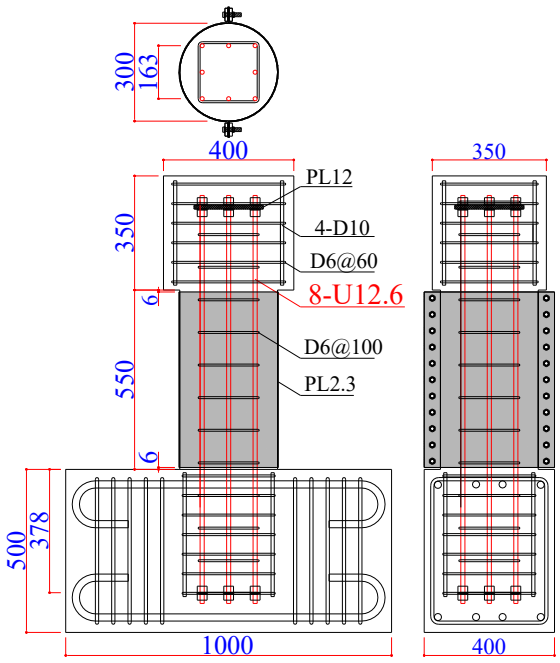

C25N33LTU

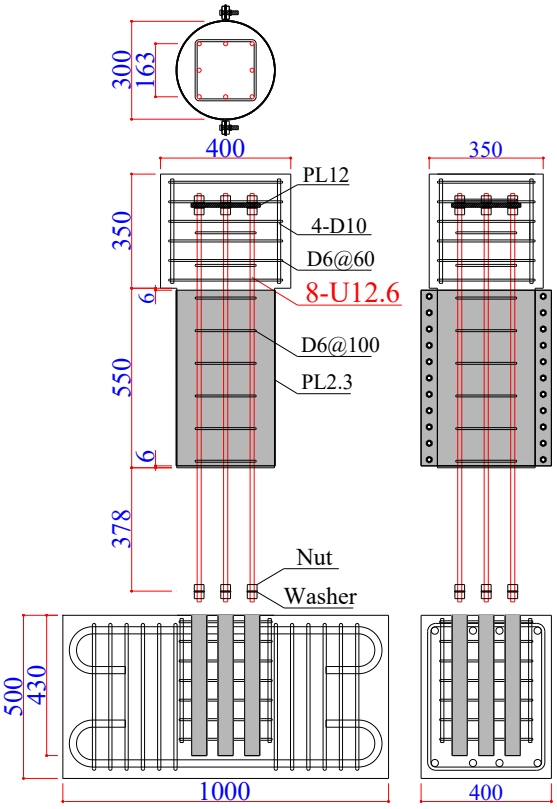

PC25N33LTU

Fig. 3-1 Continued

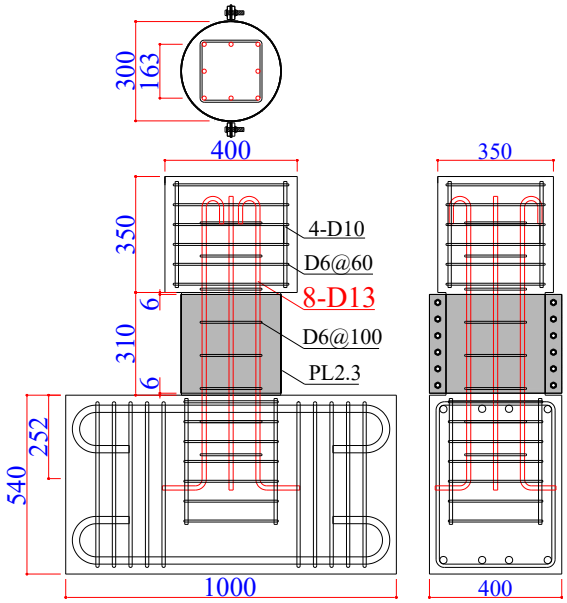

C17N20STD and C17N33STD

Fig. 3-1 Continued

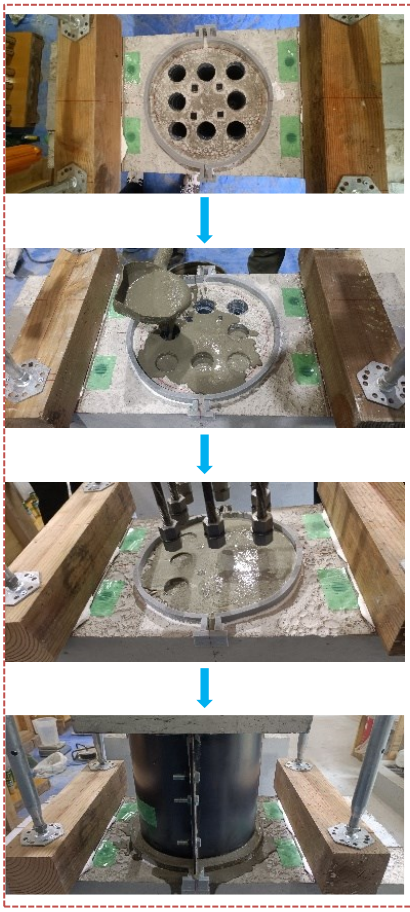

Step 1:
Clean the surface (joint surface) of the foundation beam and draw the center line in four directions on the surface of the column and the footing.

Step 2:
Adjust the height of the support rod to the target value and inject high-strength grouting material into each sheathing duct.

Step 3:
Lift the column to the joint position and determine the orientation of the front side of the column.

Step 4:
Insert the WBUHS bars extending from the column into the embedded sheathing duct, and confirm the final position of the column.

Fig. 3-2 Jointing process of precast concrete columns

3.2.2 Material Properties

Ready-mixed concrete made of common Portland cement and regular coarse aggregates having maximum particle size of 20mm, which was widely employed when constructing the main supporting members, was used for the fabrication of the test columns. According to the test results from three cylinders (100mm in diameter and 200mm in height), the compressive strength (f_c') of concrete for each loading day was summarized in Table 3-1. The mechanical properties and stress-strain relationships for the used steel materials are presented in Table 3-2 and Fig. 3-3, respectively.

Table 3-2 Mechanical properties of the used materials

Material	*D or T* (mm)	E_s (kN/mm^2)	f_y (N/mm^2)	f_u (N/mm^2)	ε_y (%)
WBUHS rebar (U12.6)	12.6	212	1401*	1478	0.86*
SD345 rebar (D13)	12.7	200	403	600	0.22
Hoop (D6)	6.35	197	400	525	0.22
Steel tube (PL2.3)	2.3	201	391	465	0.20
Steel tube (PL2.3)	3.2	200	395	467	0.20

Note: D: diameter of reinforcements, T: thickness of bolted circular steel tubes, E_s: Young's modulus, f_y: yield stress, f_u: tensile stress, ε_y: yield strain, *: the value based on 0.2% offset method.

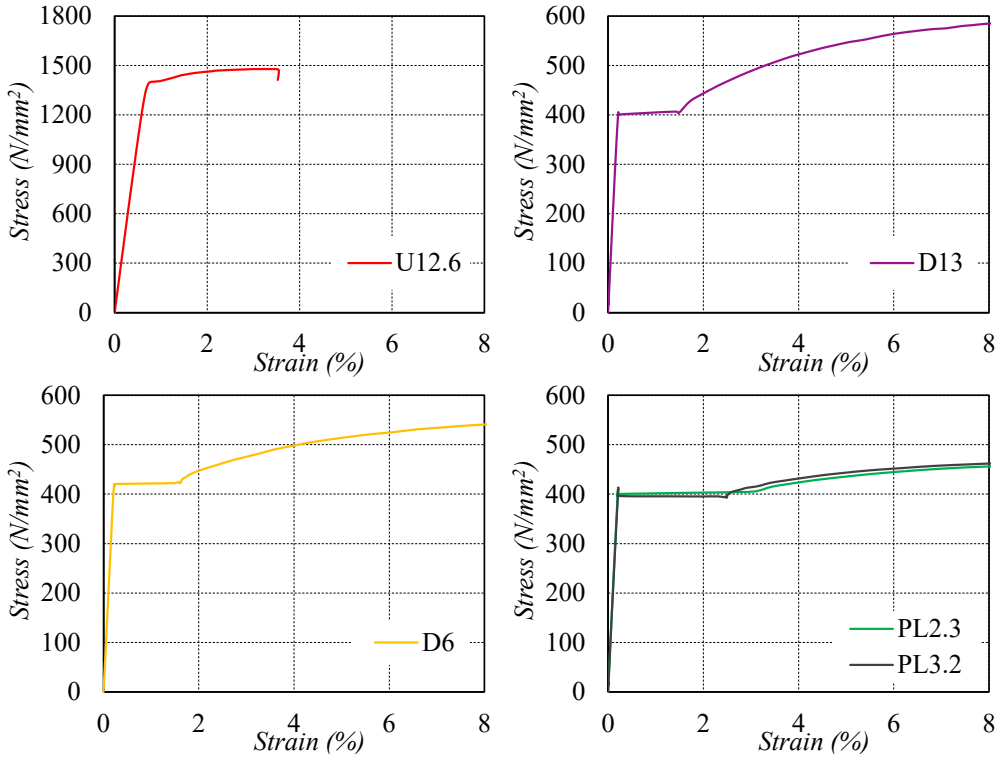

Fig. 3-3 Stress-strain curves of the used steels

3.2.3 Test Setup and Loading Program

The test setup and loading program of test columns were illustrated in Fig. 3-4 and Fig. 3-5, respectively. First, the footing was firmly secured to the strong floor using 8 high-strength steel bars with a diameter of 21mm. Next, a constant axial force (calculated according to the axial compression ratio) was applied at the top surface of the loading stub via a vertical jack with 1000kN capacity, and the linear rolling guide between the slide track and hydraulic jack could assure both axial load stability and loading position synchronization. Finally, cyclic lateral loading was imposed using two lateral jacks with 500kN capacity and controlled by the drift angle R, which can be obtained by dividing the lateral displacement (Δ) at the loading point by the shear span (a). Two complete cycles were applied within 0.02rad. drift angle, and one cycle was applied at subsequent drift levels of 0.025rad., 0.03 rad., 0.035 rad., 0.04 rad., 0.05 rad. and 0.06 rad., as shown in Fig. 3-5.

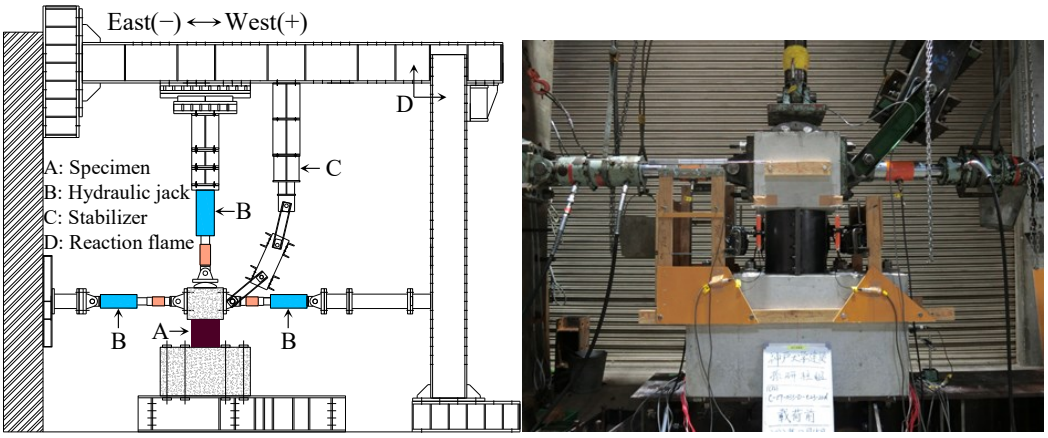

(a) For the columns with a/D=1.7

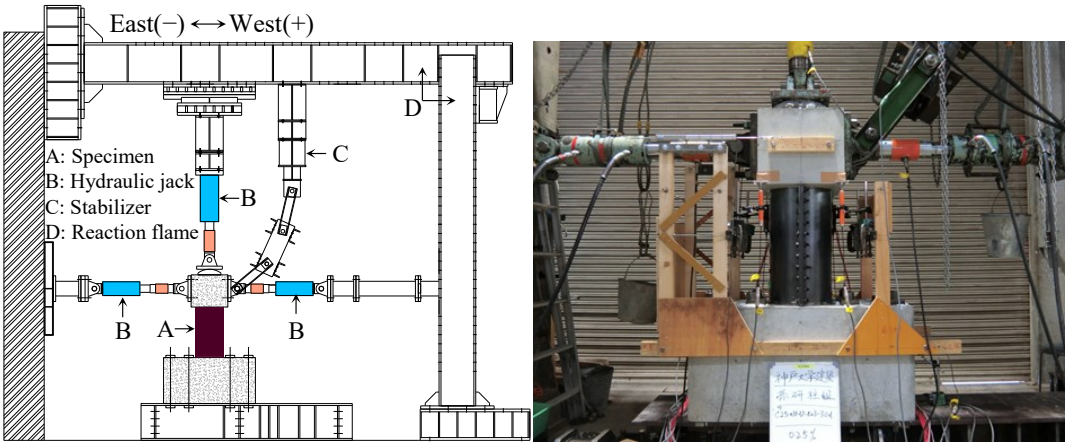

(b) For the columns with a/D=2.5

Fig. 3-4 The test setup of test columns

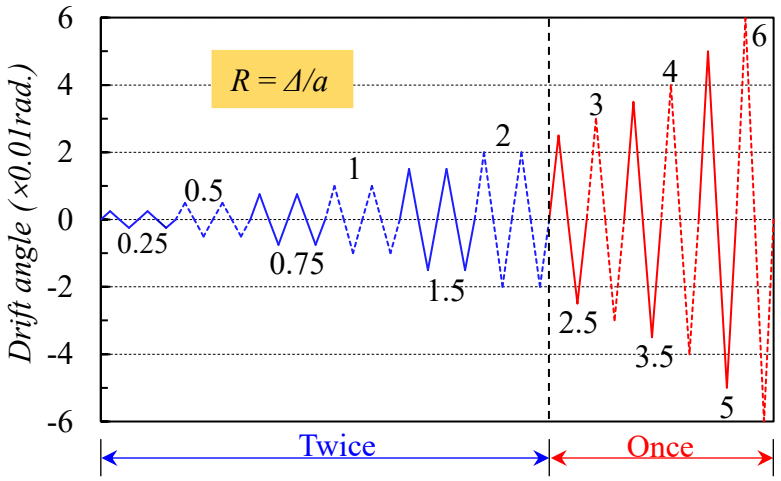

Fig. 3-5 Loading program

3.2.4 Instrumentation and Measurement

Two lateral displacement transducers (DTs) were installed in the loading stub for the measurement of lateral displacement (Δ) at loading point and four vertical DTs were placed for the measurement of axial deformation between the loading stub and footing. Besides, strain gages were attached to longitudinal rebars, transverse hoops and bolted steel tubes to serve the subsequent analysis of their mechanical properties. The location of DTs and strain gages were displayed as Fig. 3-6 and Fig. 3-7.

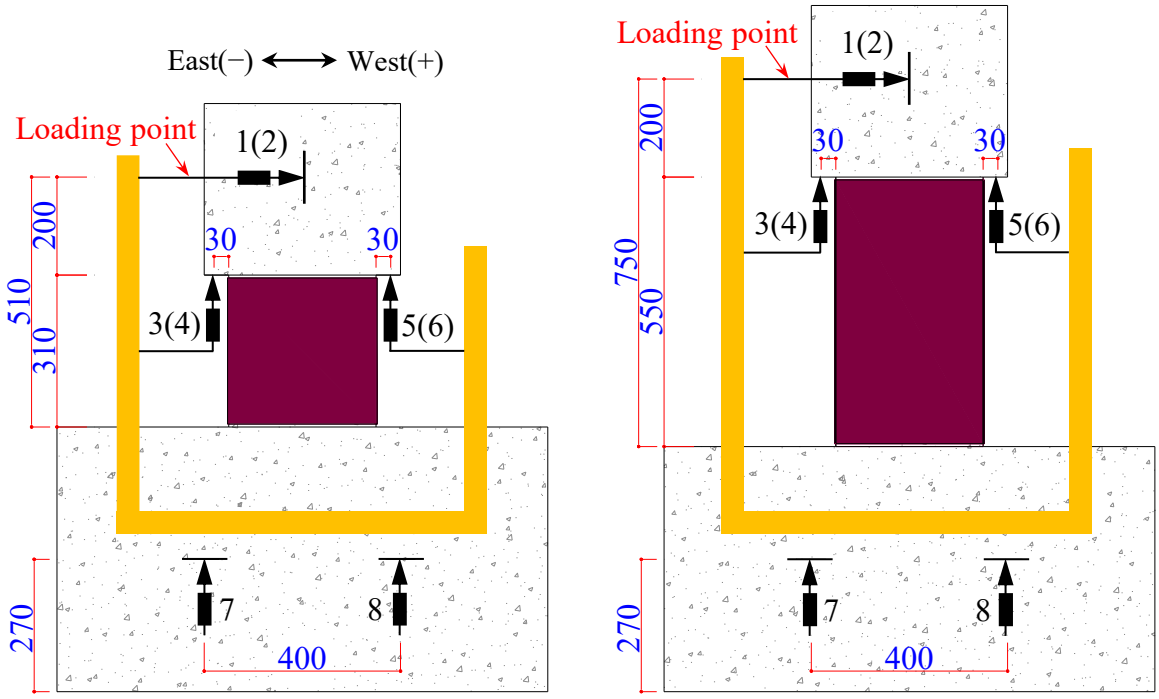

Fig. 3-6 Locations of displacement transducers

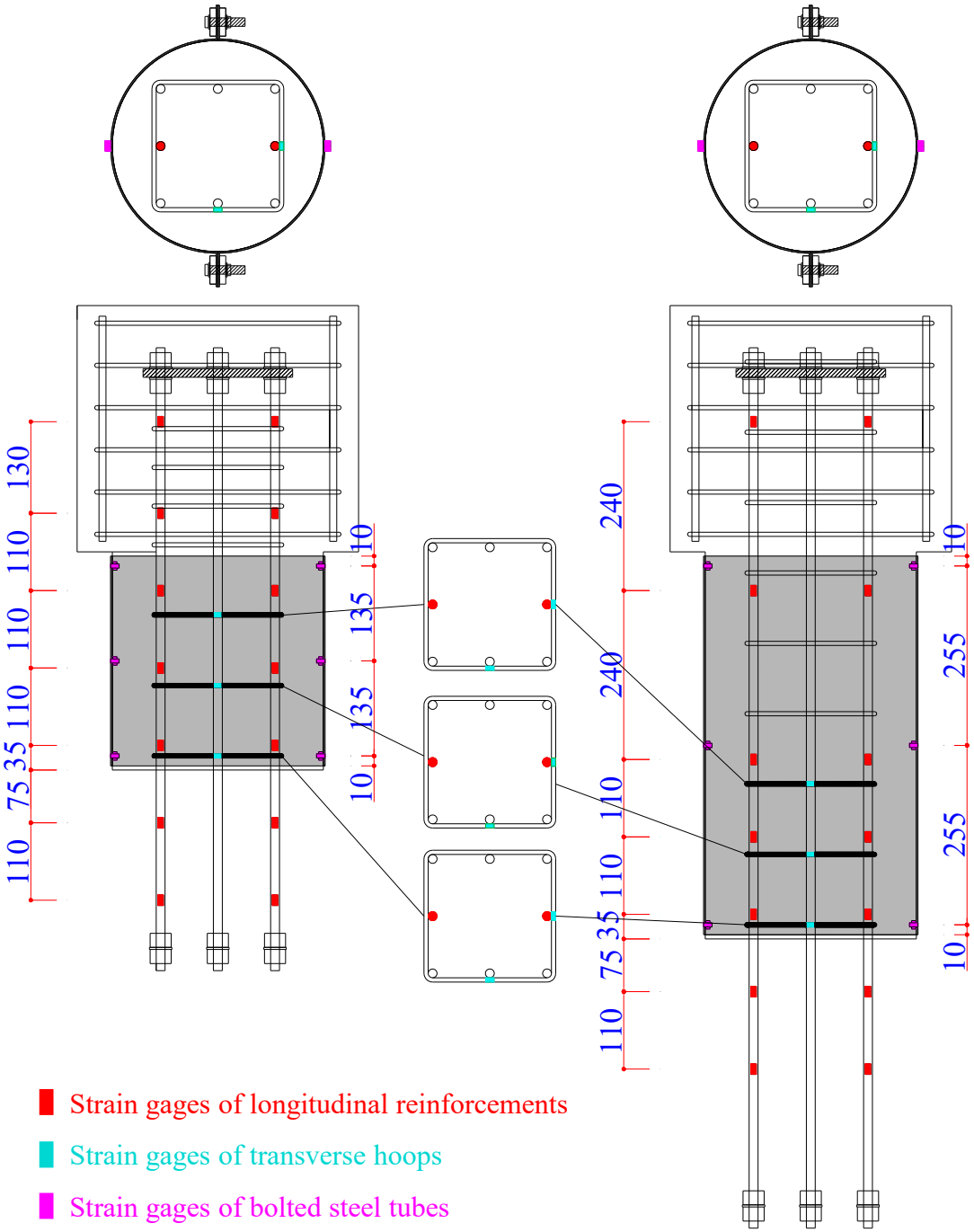

Fig. 3-7 Locations of strain gages

3.3 Test Results and Observations

3.3.1 Observations of Test Specimens

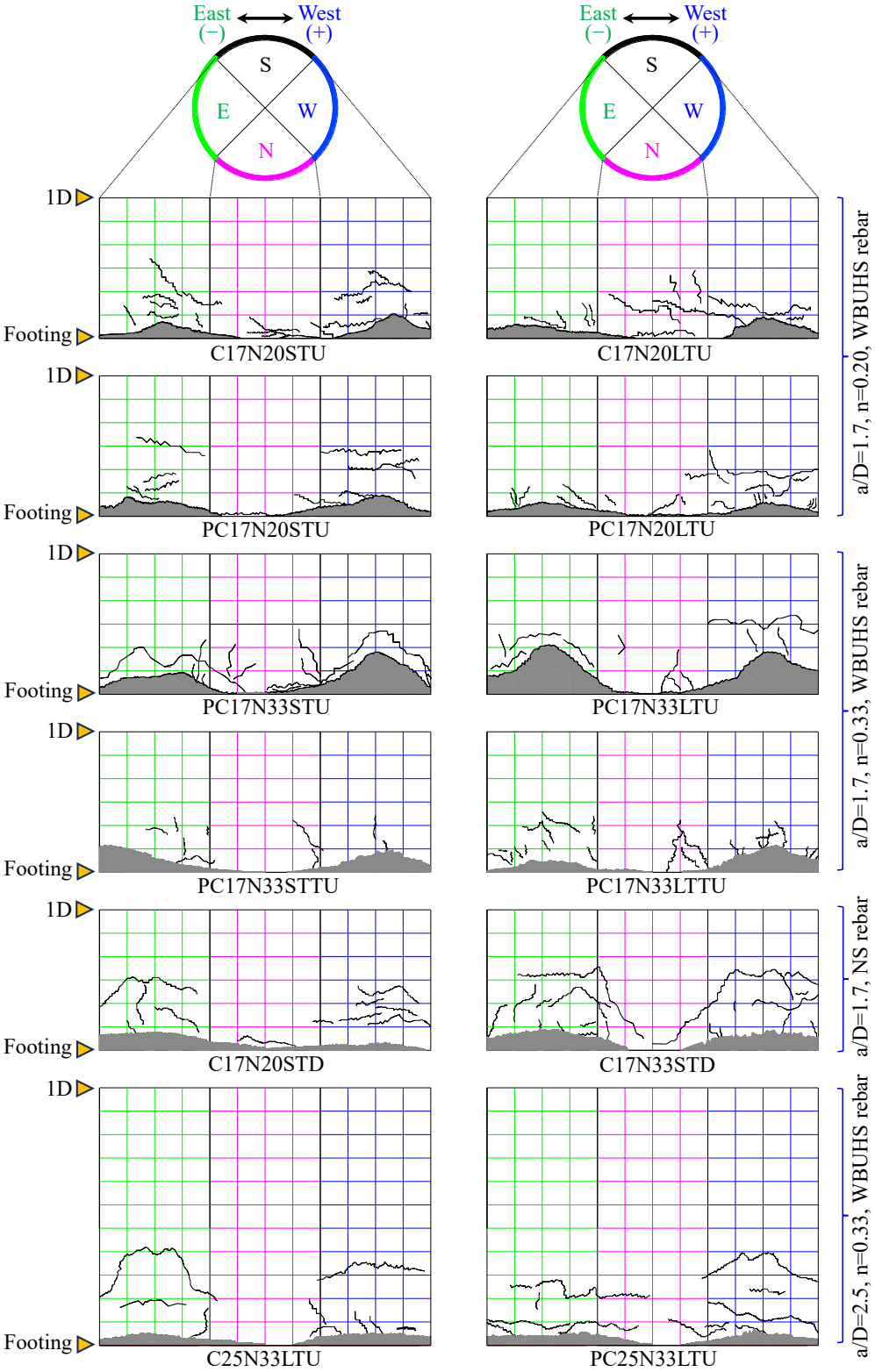

Fig. 3-8 Failure condition of specimens

Due to the confinement of steel tubes, it was challenging to observe the damage state of the specimens during the loading process. Fig. 3-8 illustrated the damage state of test specimens after removing the steel tubes subsequent to the testing, with the gray shaded areas representing crushed concrete. The yielding of steel tube was monitored prior to the maximum lateral load. Pullout of the WBUHS rebars or pre-embedded sheathing ducts was not observed, indicating the reliability of the anchoring technique for the reinforcements and the jointing method for the precast columns. In addition, concrete damage in all specimens was predominantly concentrated at the bottom of the columns on the eastern and western sides with no obvious diagonal cracks occurred, which was indicative of the characteristic of flexural failure. As the axial compression level increased, the damage to concrete on the compression side of test columns with a/D=1.7 became pronounced and the corresponding range also expanded. Because a larger axial load ratio results in higher stress level for the concrete in compressive side [3.10, 3.11].

3.3.2 Lateral Force Versus Drift Angle Relationship

The measured lateral force versus drift angle curves of test columns is illustrated in Fig. 3-9, in which the blue blocks, red dots and red dotted line represent the lateral load when steel tubes (PL2.3 or PL3.2) is yielding in the transverse direction, maximum lateral load and strength decline caused by P-Δ effect, respectively. It should be noted that drift angles in the two ductile columns (C17N20STD and C17N33STD) are not completely consistent with the scheduled loading program depicted in Fig. 3-5.

The specimens reinforced with WBUHS rebars performed ever-increasing lateral resistance without strength degradation but slow-growing residual deformation even up to a so large drift of 5%, showing significant drift hardening capacity. While the two ductile columns reinforced with NS rebars displayed traditional “fat” hysteresis loops, and the lateral force began to decrease slowly with the concrete damage and P-Δ effect. Owing to the confinement of steel tubes, the lateral force could be kept 93% (85% for C17N33STD) of their maximum lateral load even when deformed to such a large drift of 6%, demonstrating favorable load-holding capacity. Additionally, it can be inferred that the stable response without deterioration in lateral resistance after yielding of steel tubes mainly depends on the WBUHS rebars since the yielding of thin steel tubes usually signify the maximum confinement effect on concrete.

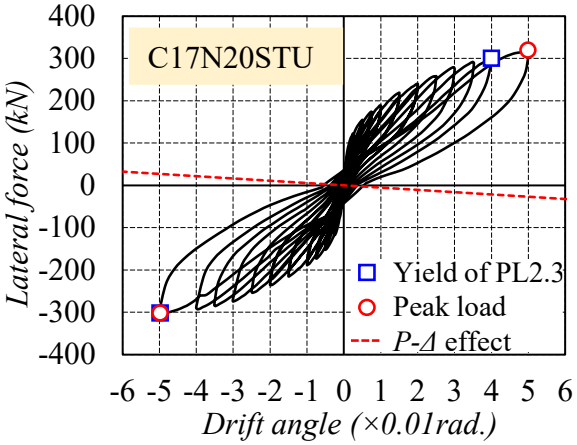

1) C17N20STU

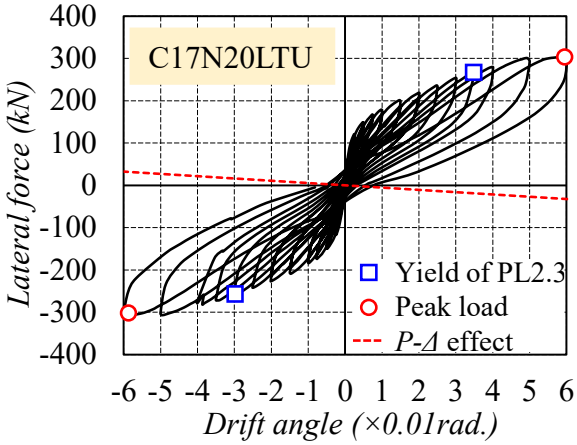

2) C17N20LTU

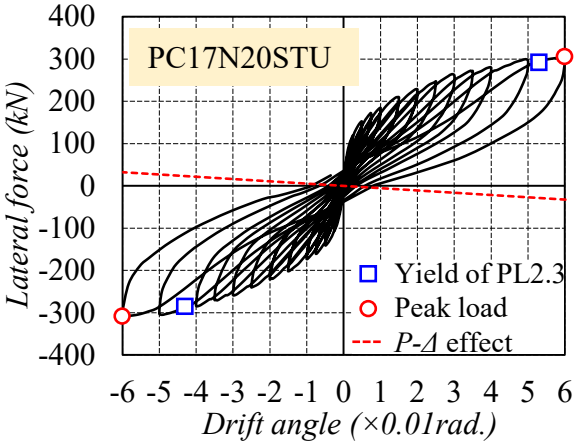

3) PC17N20STU

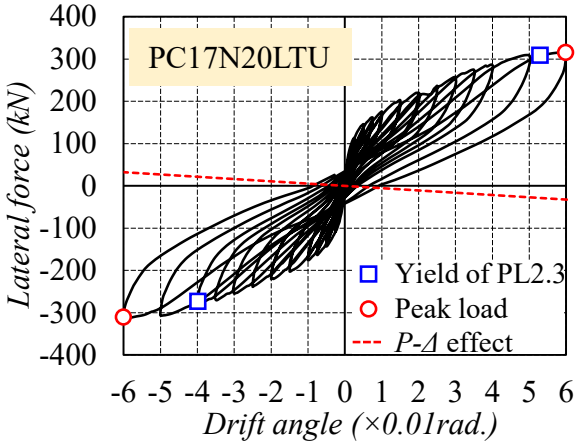

4) PC17N20LTU

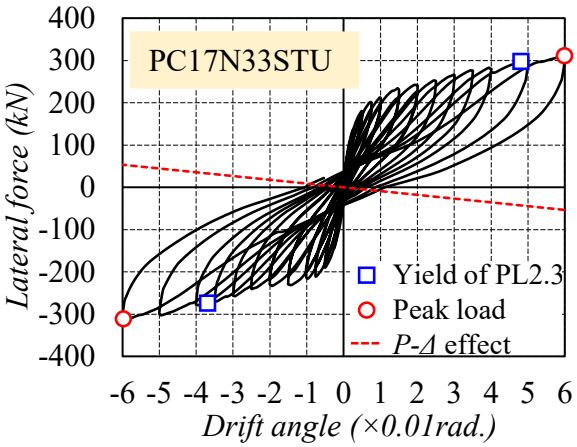

5) PC17N33STU

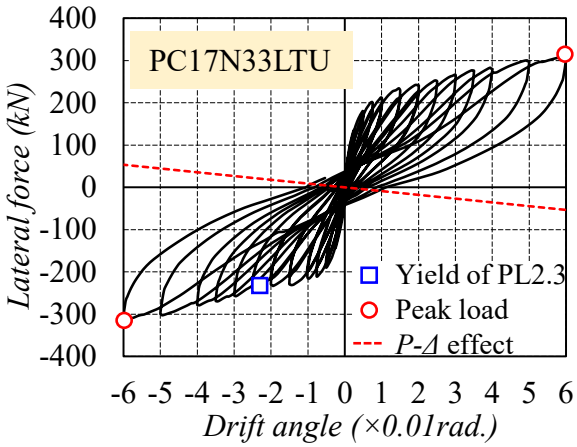

6) PC17N33LTU

Fig. 3-9 Lateral force versus drift angle relationships

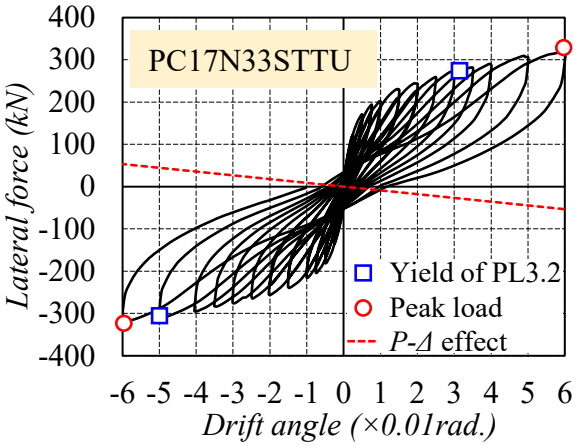

7) PC17N33STTU

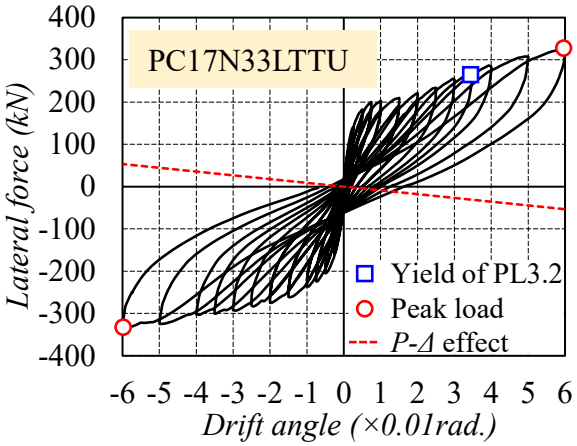

8) PC17N33LTTU

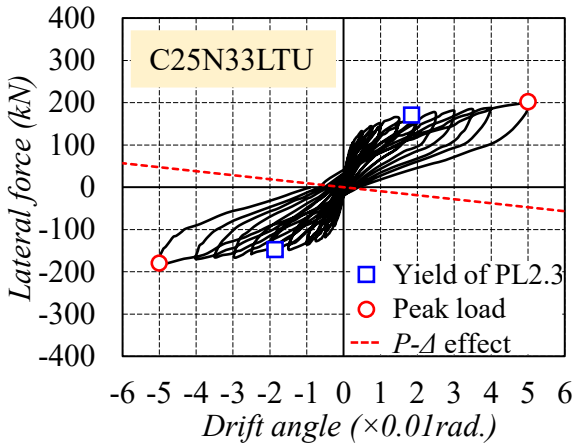

9) C25N33LTU

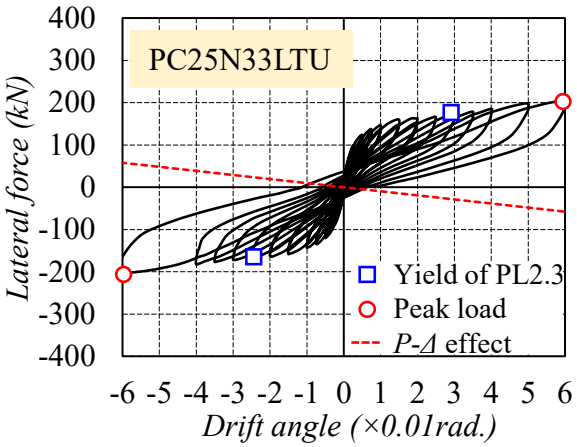

10) PC25N33LTU

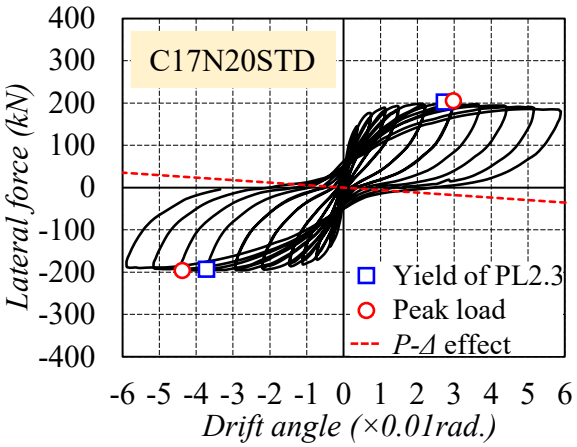

11) C17N20STD

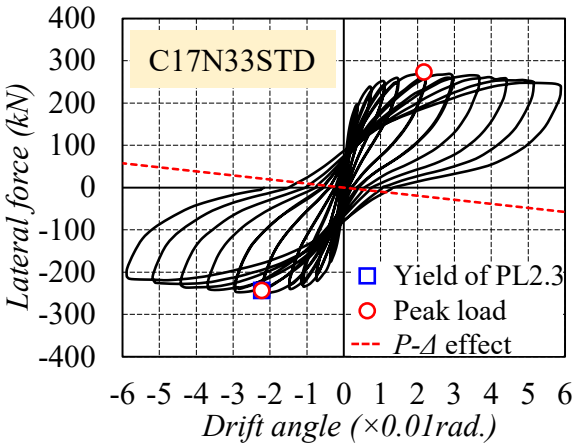

12) C17N33STD

Fig. 3-9 Continued

Fig. 3-10 compared the envelopes of lateral force-drift angle relationships and moment-drift angle relationships. As is obvious from Figs. 3-10 (a) and (d), both the utilization of WBUHS rebars and the increasing of axial load ratio could significantly enhance the lateral force and moment resistance. Because the ultra-high strength could augment the force and/or moment borne by longitudinal rebars, while increasing the axial load ratio always led to greater neutral axis depth, thus increasing the bending moment borne by the concrete. In addition, it seemed that the experimental variables of construction method and embedment length of longitudinal rebar had no obvious influence on the moment resistance, indicating that providing an embedment length of 20 times its diameter for WBUHS rebar could make the precast concrete columns perform almost the same excellent lateral response as the cast-in-place ones.

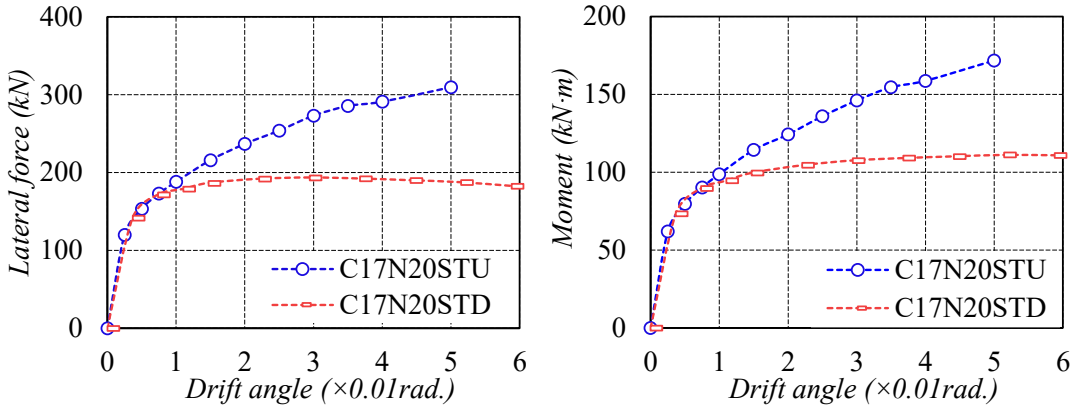

(a) The effect of reinforcement type (WBUHS rebar, NS rebar)

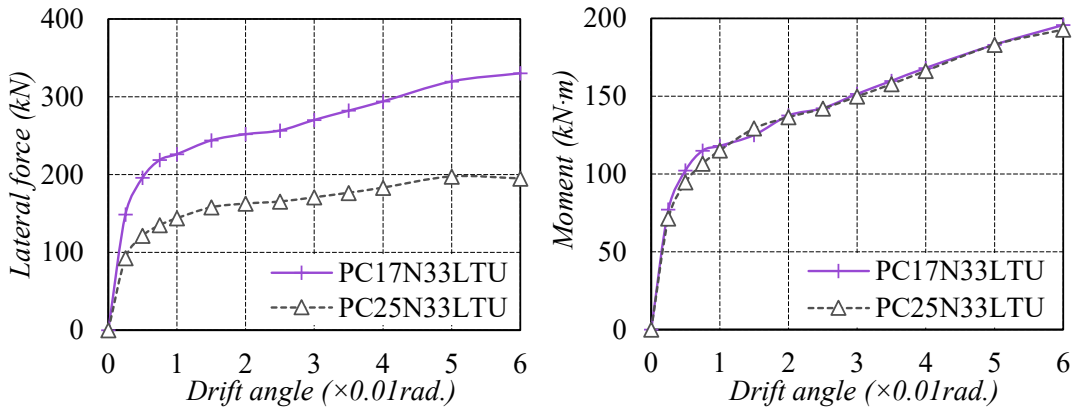

(b) The effect of shear span ratio (1.7, 2.5)

Fig. 3-10 Influence of experimental variables on lateral force and moment

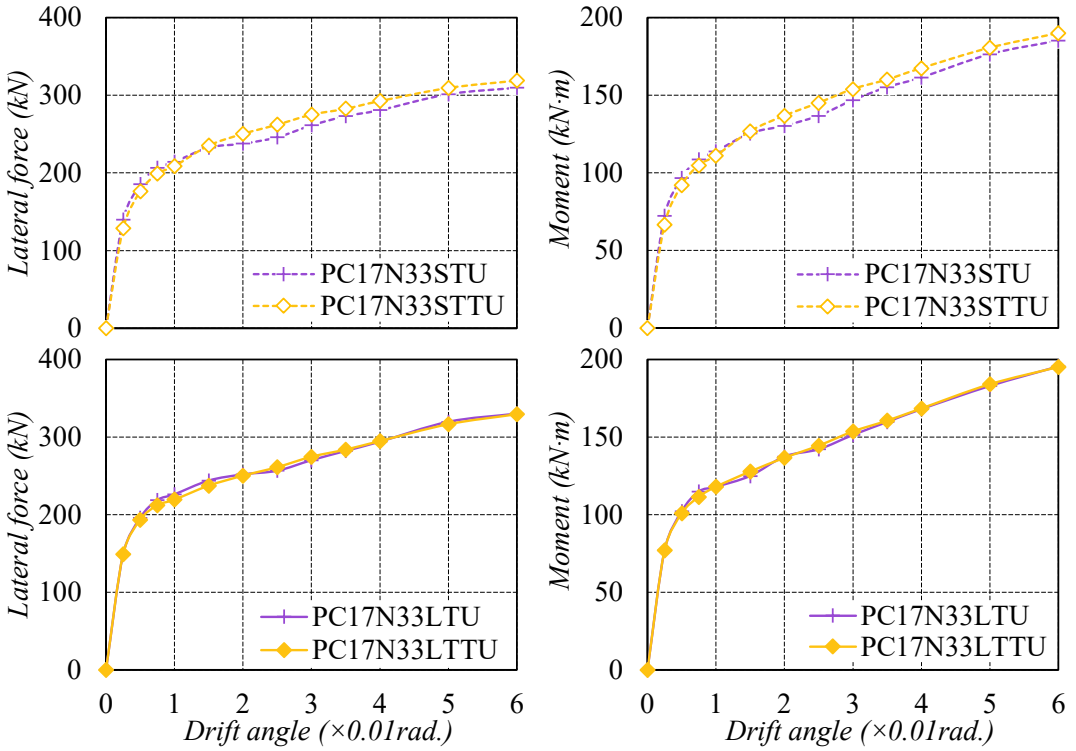

(c) The effect of diameter-to-thickness ratio (96, 132)

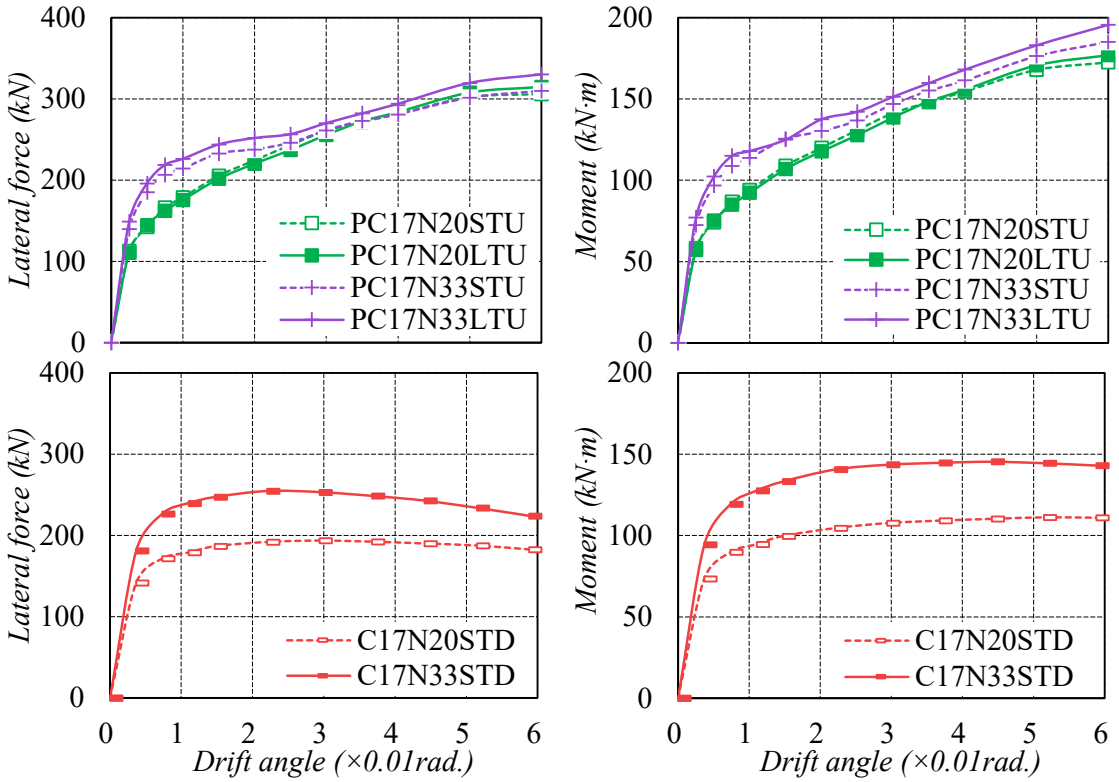

(d) The effect of axial load ratio (0.20, 0.33)

Fig. 3-10 Continued

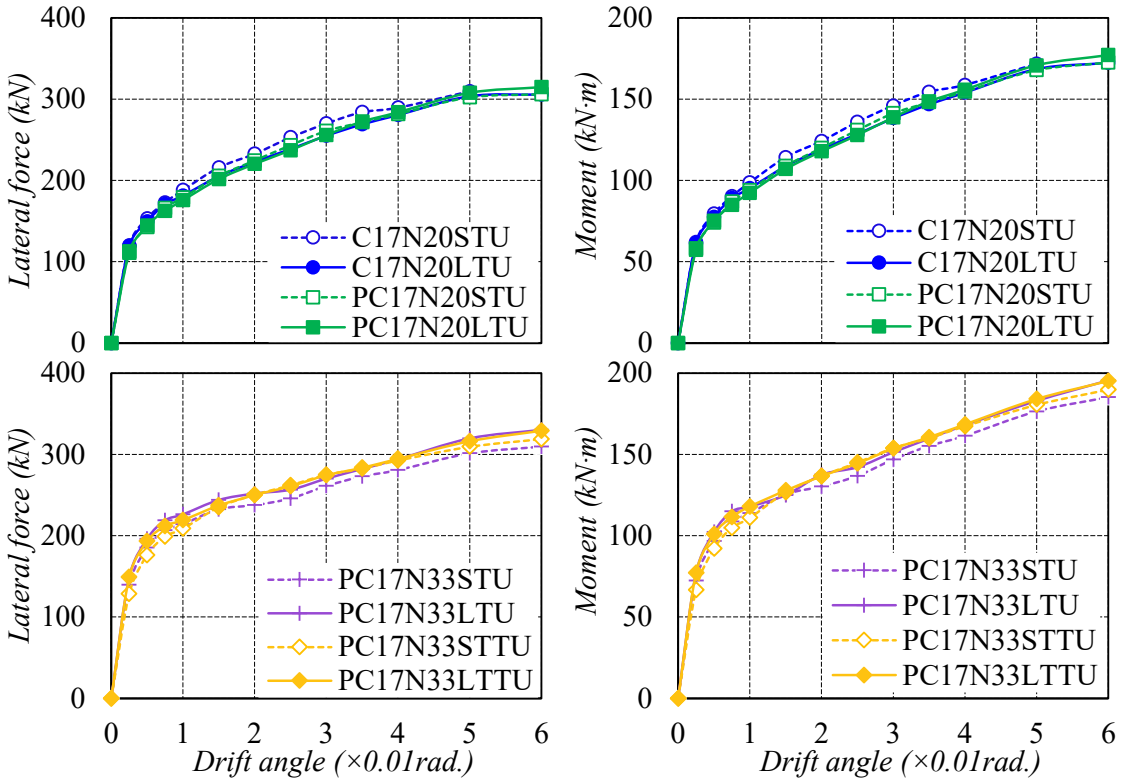

(e) The effect of embedment length of reinforcement (20d, 30d)

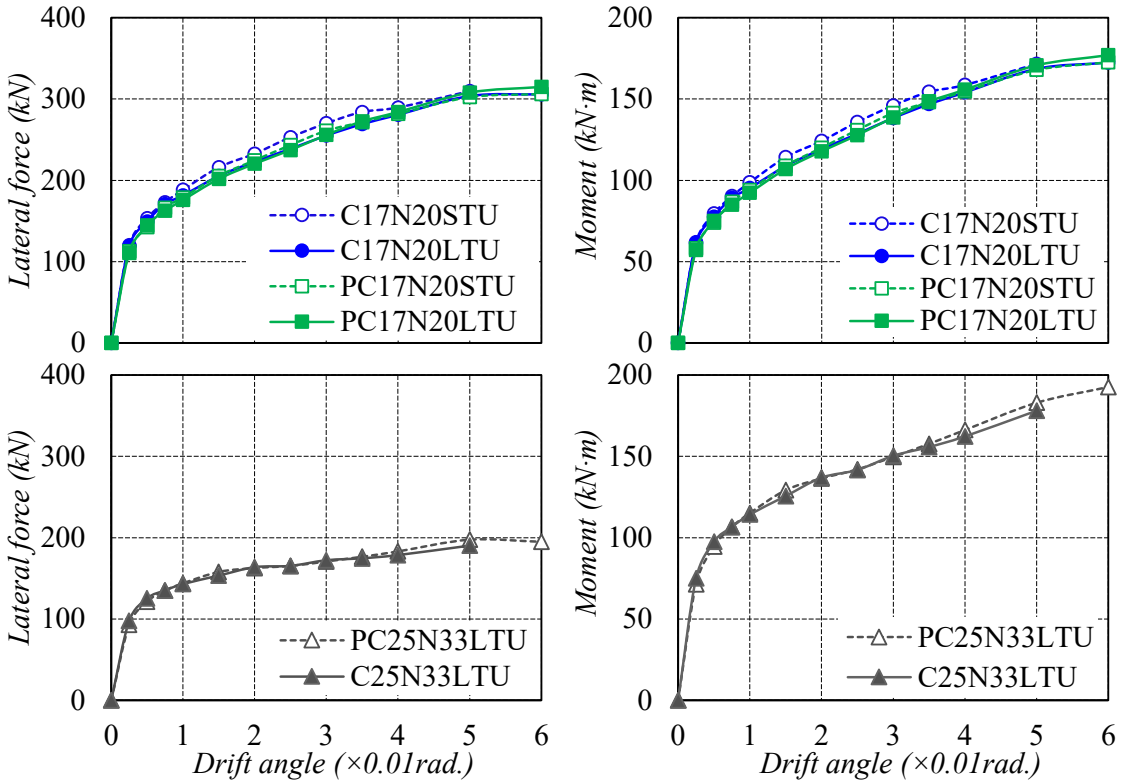

(f) The effect of construction method (cast-in-place, precast)

Fig. 3-10 Continued

3.3.3 Strain of Reinforcements

The performance of concrete columns is closely related to the mechanical behavior of longitudinal reinforcement, which can be evaluated by analyzing the strain of reinforcements. Fig. 3-11 compared the measured strains of the outermost longitudinal NS rebars and WBUHS rebars on the eastern side at a height of 35mm from the top of the footing. The horizontal black and red dotted lines respectively denote the yielding of NS rebars and WBUHS rebars. As the drift angle increased to 0.0075rad., the NS rebars in column C17N20STD reached the yield strain and then increased at a rapid rate. While the WBUHS rebars in specimen C17N20STU increased at a slow rate and did not yield even at a drift angle of 0.05rad, as illustrated in Fig. 3-11 (a). It can be found from Figs. 3-11 (b) that the WBUHS rebar strain in specimen with a/D=2.5 is lower than that of the specimen with a/D=1.7, which is the reason for the low lateral resistance of the specimen with a/D=2.5. As is obvious in Fig. 3-11 (d) that the higher the applied axial load level, the smaller the strain of WBUHS rebars was. This was because that the higher axial compression led to a larger depth of compression zone, which in turn, retarded the development of strain. In addition, the diameter-to-thickness ratio, embedment length of reinforcement and construction method have little influence on the strain development of WBUHS rebar with the drift angle of 0.04rad., as illustrated in Figs 3-11 (c), (e) and (f).

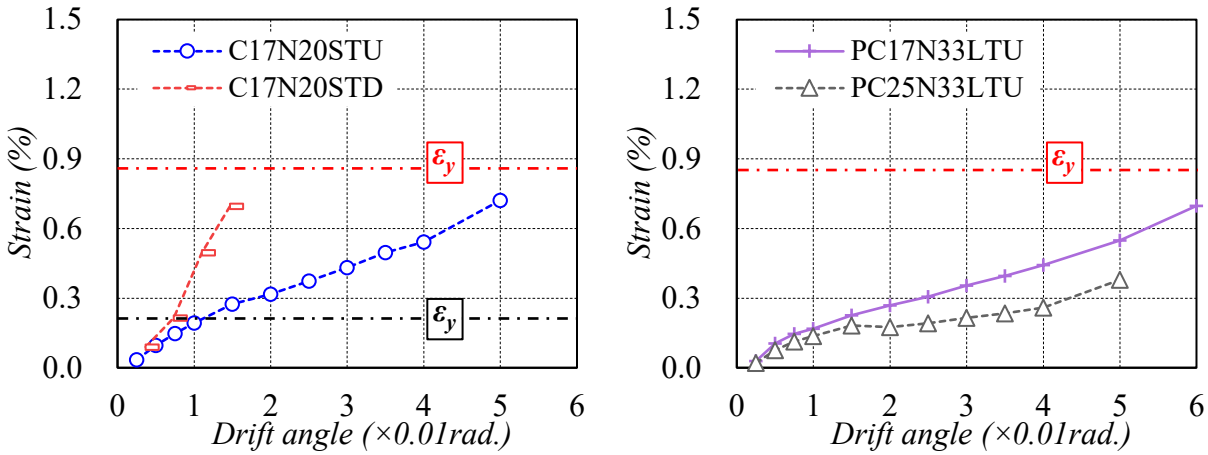

(a) The effect of reinforcement type (WBUHS rebar, NS rebar)

(b) The effect of shear span ratio (1.7, 2.5)

Fig. 3-11 Strain of Reinforcements

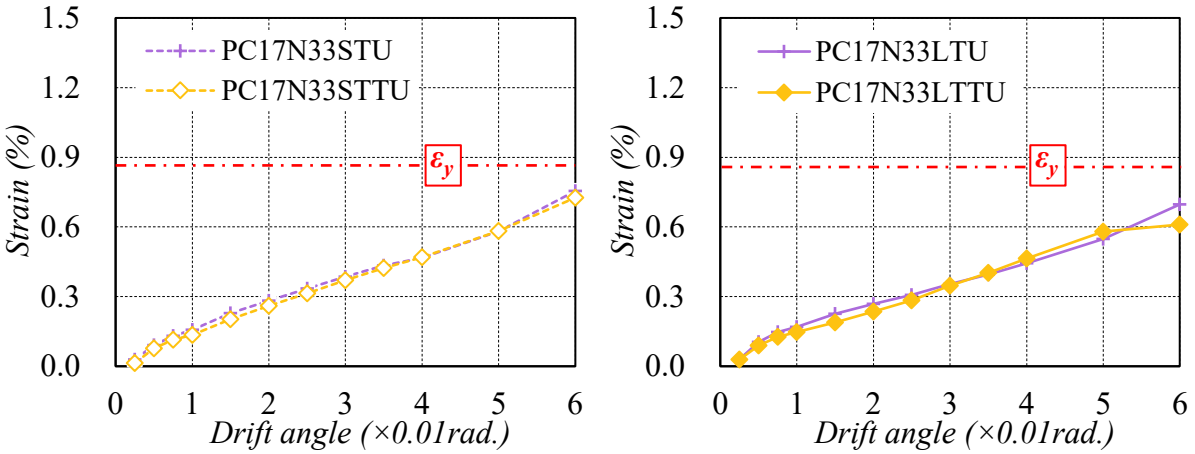

(c) The effect of diameter-to-thickness ratio (132, 96)

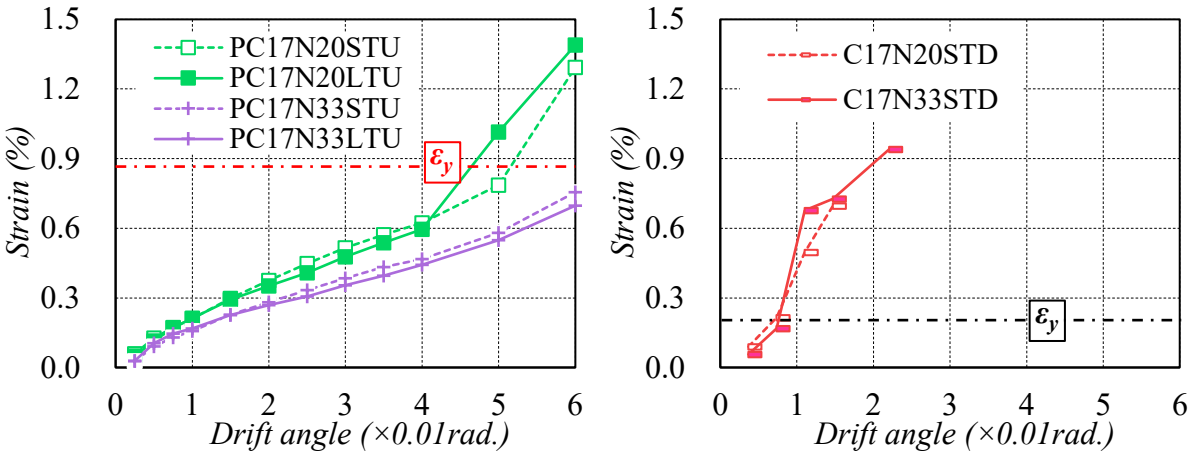

(d) The effect of axial load ratio (0.20, 0.33)

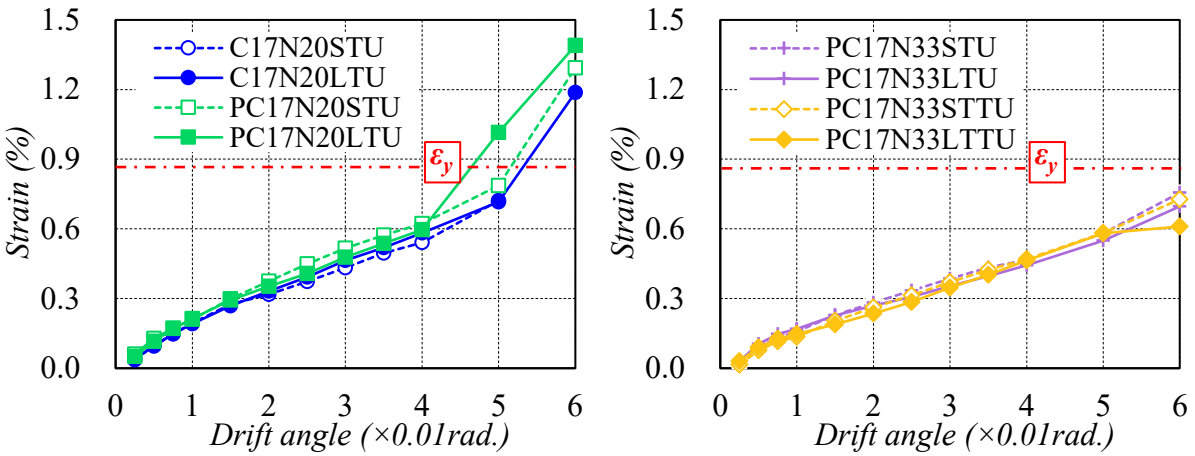

(e) The effect of embedment length of reinforcement (20d, 30d)

Fig. 3-11 Continued

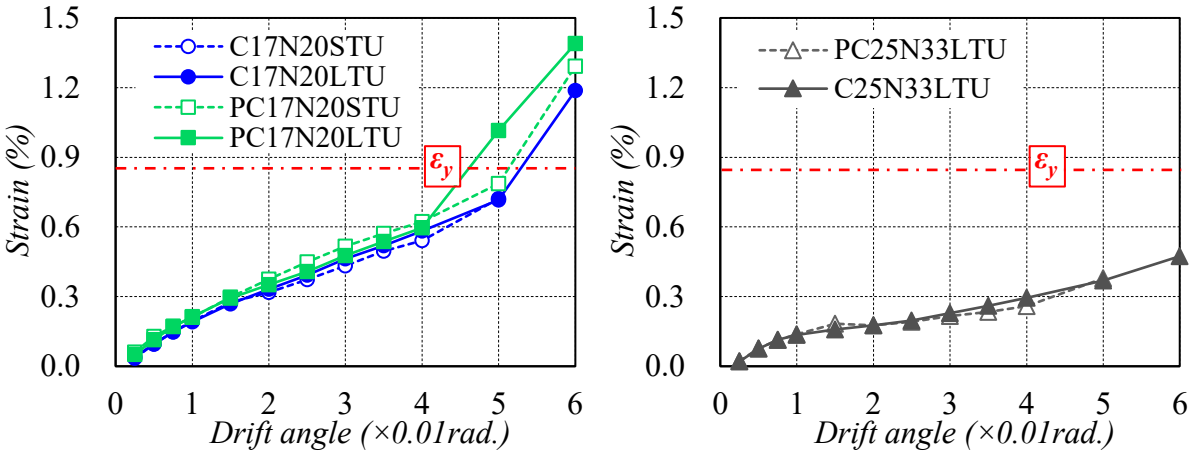

(f) The effect of construction method (cast-in-place, precast)

Fig. 3-11 Continued

The strain distribution of longitudinal reinforcements in two representative specimens (C17N20STD and C17N20STU) with a typical developing tendency is presented in Fig. 3-12. As drawn in Fig. 3-12, the NS rebar in C17N20STD reached its yield strain at 0.0075 rad. drift angle, followed by a sharp increase in strain observed near the critical section (35mm from the top of the footing). In contrast, the WBUHS rebar along the column height in C17N20STU displayed a very small strain gradient. This phenomenon is attributed to the lower bond strength of WBUHS rebars, which facilitates strain penetration along the column height toward the anchorage positions, thereby mitigating strain concentration in the potential plastic hinge region.

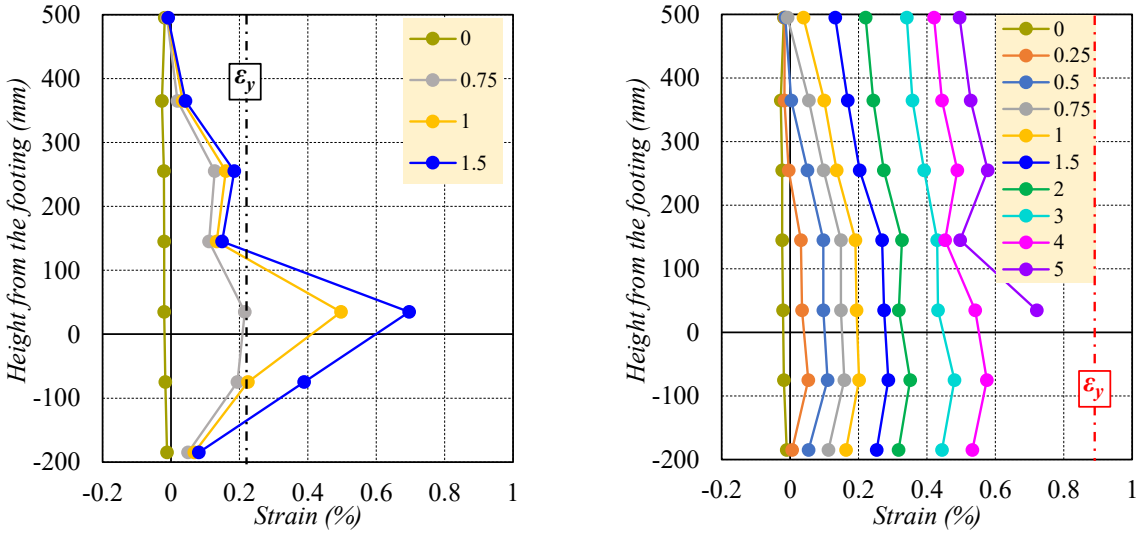

(a) Specimen C17N20STD (b) Specimen C17N20STU

Fig. 3-12 Representative example of strain distribution of longitudinal rebars

3.3.4 Residual Deformation

As a critical indicator for assessing the recoverability of concrete components, the self-centering capacity is commonly evaluated through the residual deformation when the lateral forces induced by an earthquake are removed. Fig. 3-13 illustrated the residual drift angle at each specified drift angle, which was determined by taking the average of the measurements in both positive and negative loading directions.

It can be found that reinforcement type and axial load ratio are two critical factors that influence residual deformation. One can be seen from Fig. 3-13(a) that the ductile column (C17N20STD) performed a significantly increased residual deformation from the drift angle of 0.015rad on, and the residual deformation has exceeded 0.025rad. when deformed to 0.06rad. drift angle. The reasons for this phenomenon can be explained as the fact that: When the NS rebars reached their yield strength, they undergone plastic deformation. Unlike elastic deformation, plastic deformation was permanent, and the steel does not return to its original shape even after the removal of lateral force. This plastic deformation contributed to residual deformations in the ductile column reinforced with NS rebars. Comparatively, as drift angle increases, the residual deformation in columns reinforced with WBUHS rebars is significantly lower compared to that in ductile columns. Even when the lateral deformation reaches a drift angle of 5%, the residual deformation can be controlled at approximately 0.5%, demonstrating excellent self-centering capacity and an economically viable range for repair (see Fig. 3-13 (a)). This phenomenon can be attributed to that weak bond strength (3 N/mm^2) delays the strain concentration in the plastic hinge zone and premature yielding of WBUHS rebars, thereby providing a restoring force to reduce the residual deformation, as described in section 3.3.3. In the case of concrete columns reinforced by WBUHS rebars, the increase of axial compression leads to slight increase of residual deformation, because a higher axial compression results in more serious concrete damage and a more obvious P-Δ effect, indicating greater plastic damage and permanent deformation. Moreover, it seems that the influence of other experimental parameters including embedded length of reinforcements, construction method, diameter-thickness ratio on residual deformation is almost negligible and increasing the shear span ratio can bring about lower residual deformation when the concrete column was deformed to a large drift angle (see Figs. 3-13 (b), (c), (e) and (f)).

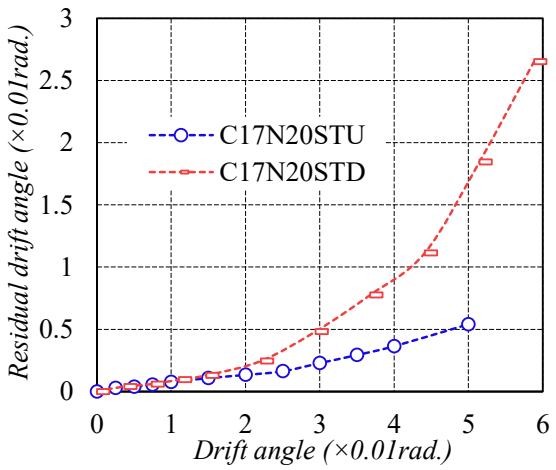

(a) The effect of reinforcement type (WBUHS rebar, NS rebar)

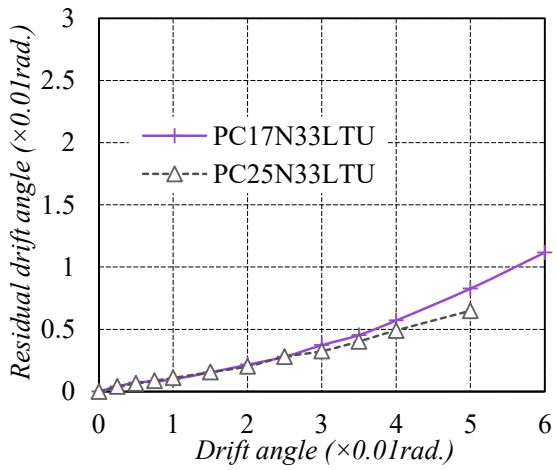

(b) The effect of shear span ratio (1.7, 2.5)

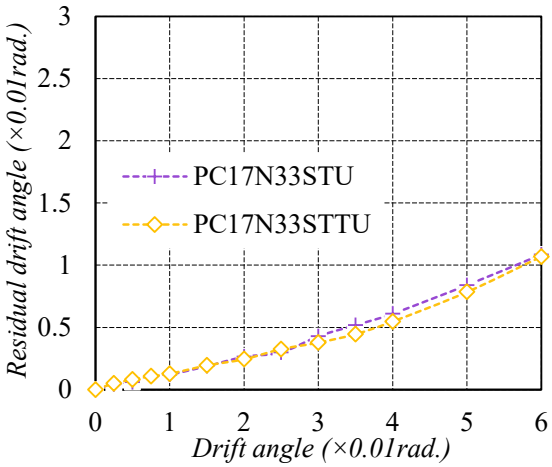

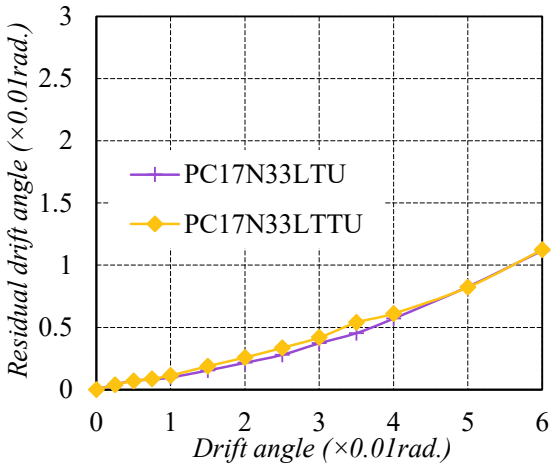

(c) The effect of diameter-to-thickness ratio (132, 96)

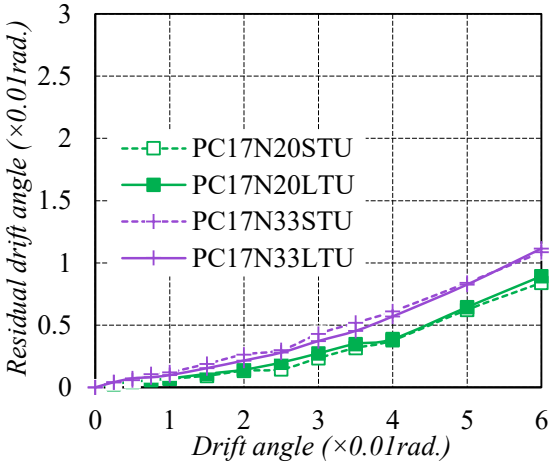

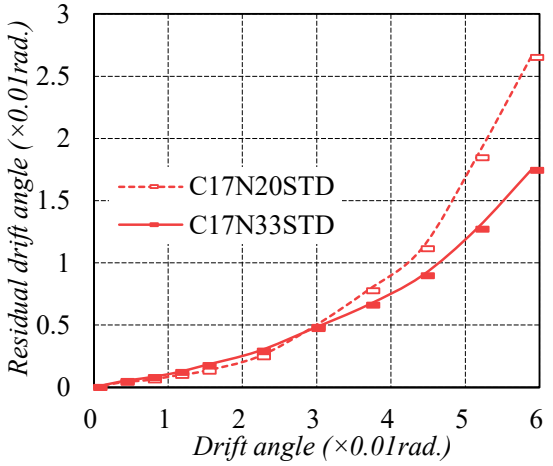

(d) The effect of axial load ratio (0.20, 0.33)

Fig. 3-13 Residual drift angle of specimens

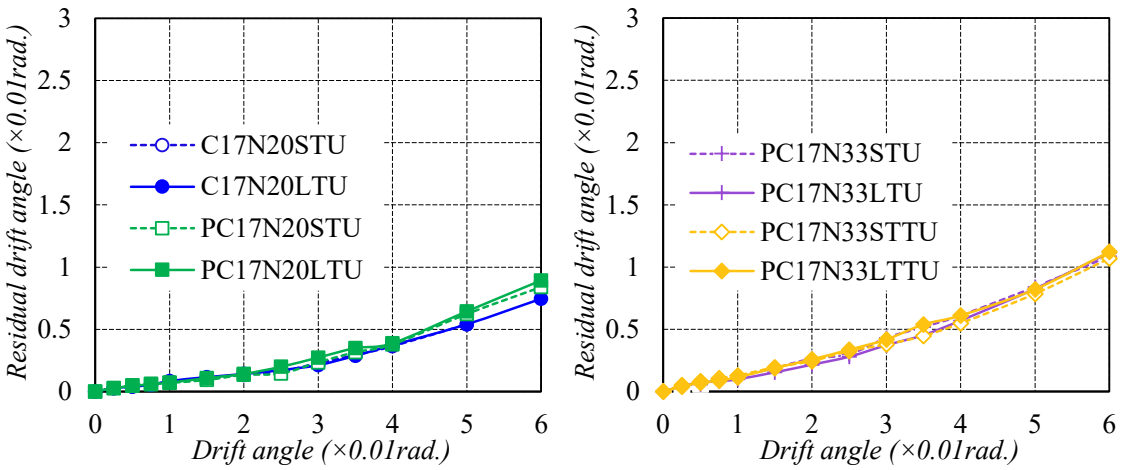

(e) The effect of embedment length of reinforcement (20d, 30d)

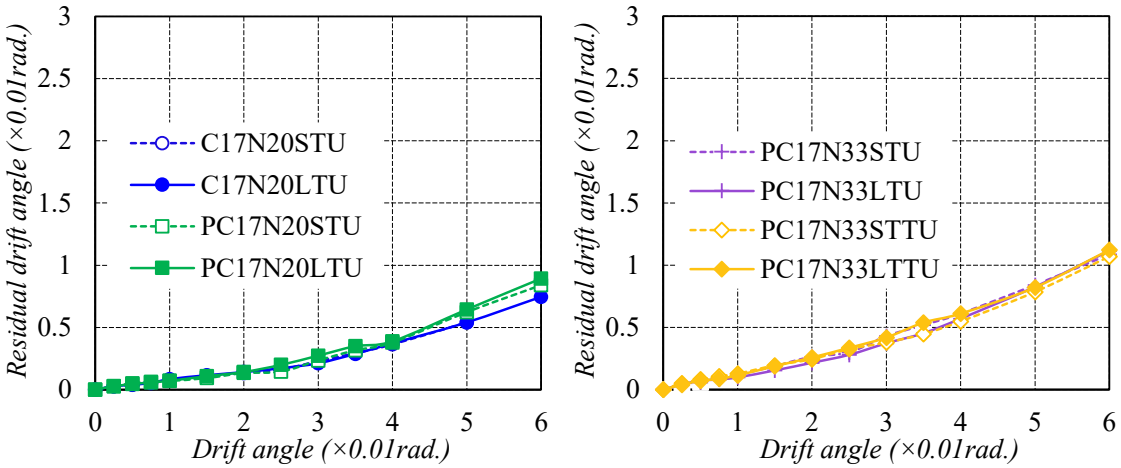

(f) The effect of construction method (cast-in-place, precast)

Fig. 3-13 Continued

3.3.5 Energy Dissipation Capacity

The equivalent viscous damping coefficient (h_{eq}) is frequently utilized as a crucial parameter for assessing the energy-dissipating capacity of seismic components. The schematic diagram was depicted in Fig. 3-14 and the calculation result was compared in Fig. 3-15.

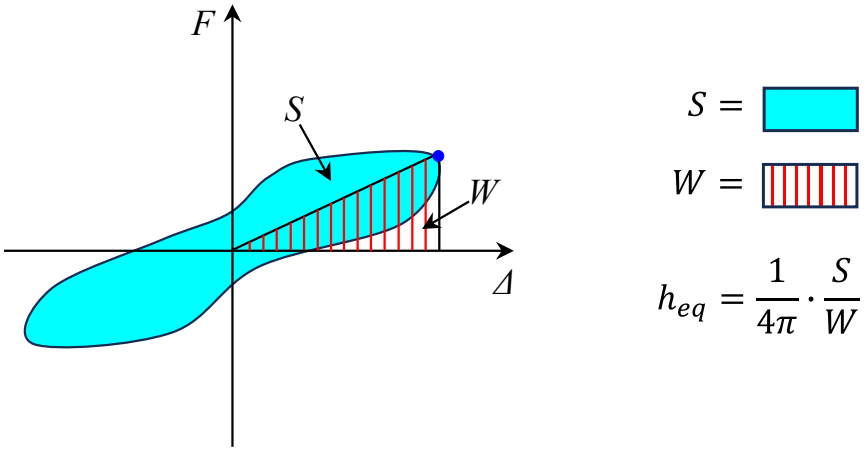

Fig. 3-14 Calculation diagram of h_{eq}

As is obvious in Fig. 3-15a and Fig. 3-15d, the h_{eq} in the two ductile columns increased rapidly owing to the inelastic deformation after yielding of NS rebars, and the increase of axial compression could result in a reduction of h_{eq} from the drift angle of 3%. However, in the case of the resilient columns reinforced with WBUHS rebars, only changes in axial load ratio could lead to a slight enhance in h_{eq} by comparing Fig. 3-15 (d) with Figs. 3-15 (b), (c), (e), and (f), and the h_{eq} tended to approach a constant value with the increasing of the drift, which agrees well with the findings in the study conducted by Liu et al. [3.12]. This suggests that the specimens reinforced by WBUHS rebars displayed nonlinear elastic behavior even when deformed to a large drift.

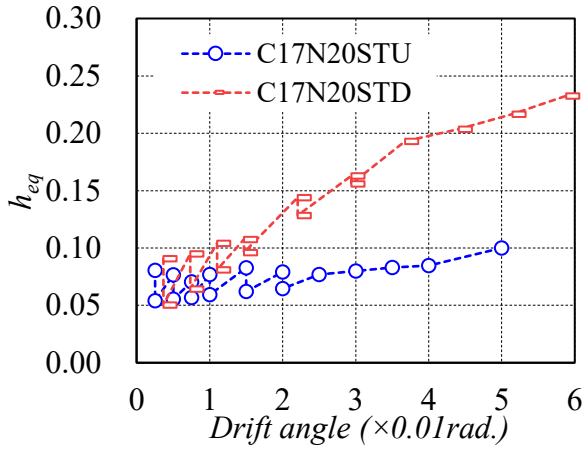

(a) The effect of reinforcement type (WBUHS rebar, NS rebar)

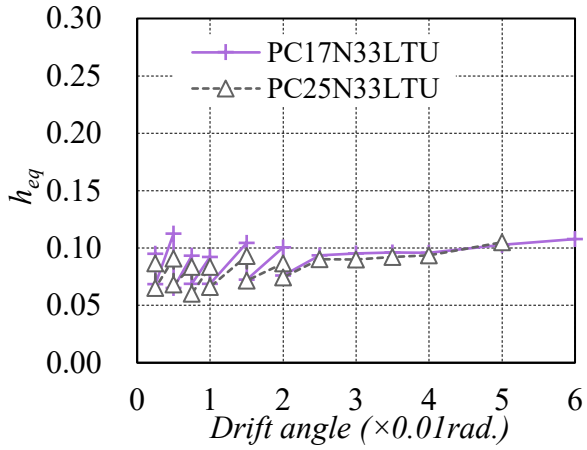

(b) The effect of shear span ratio (1.7, 2.5)

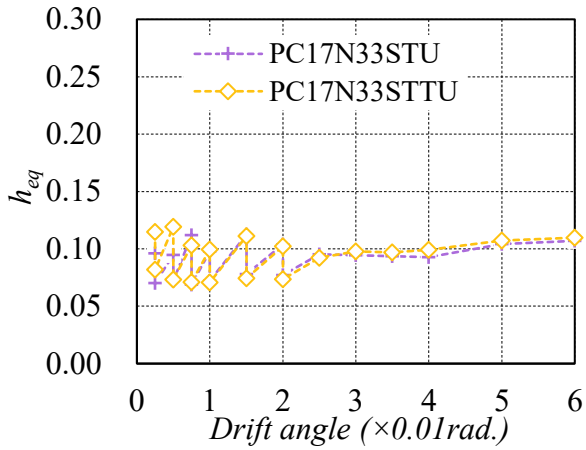

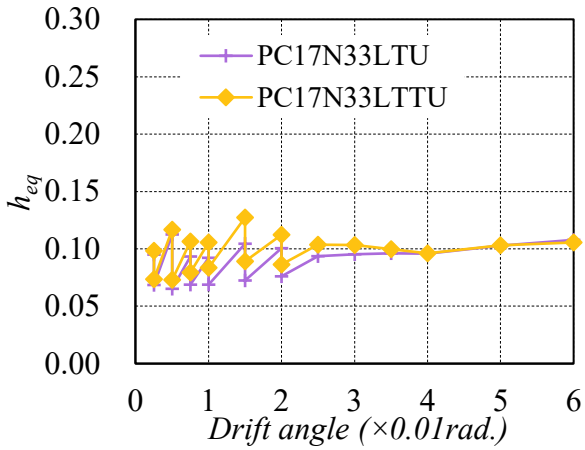

(c) The effect of diameter-to-thickness ratio (96, 132)

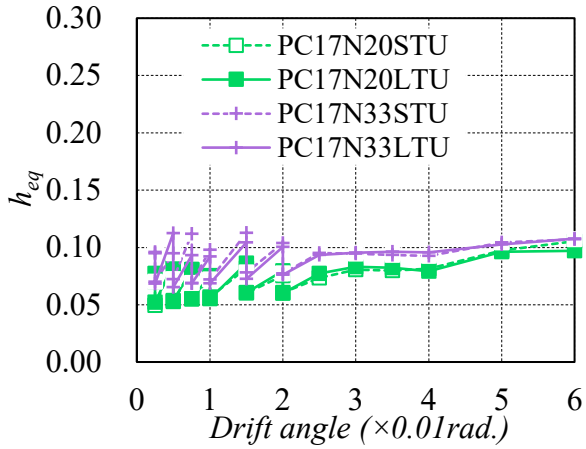

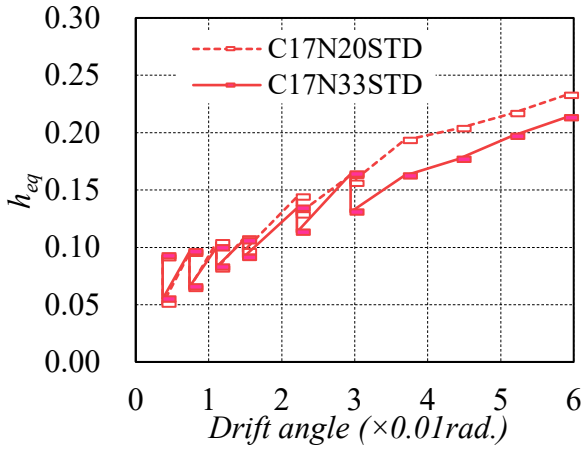

(d) The effect of axial load ratio (0.20, 0.33)

Fig. 3-15 The comparison of equivalent viscous damping coefficient (h_{eq})

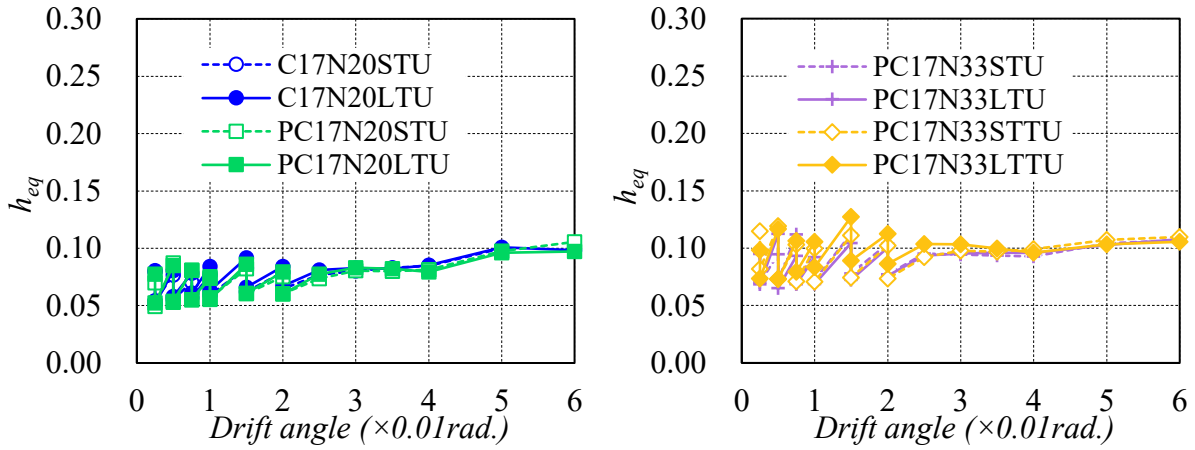

(e) The effect of embedment length of reinforcement (20d, 30d)

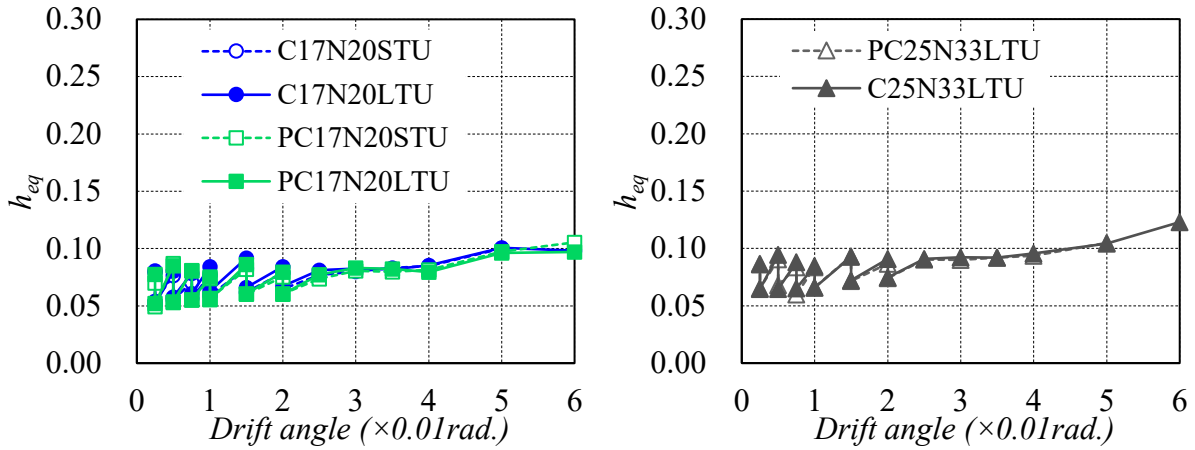

(f) The effect of construction method (cast-in-place, precast)

Fig. 3-15 Continued

3.3.6 Axial Strain

Axial deformations, which refer to changes in the length of the concrete members along their longitudinal axis, are crucial indicators of structural behavior under various loading conditions. When the axial strain of a concrete member increases at an alarming rate and approaches the ultimate compressive capacity of concrete, it indicates potential structural instability and damage.

The axial deformation between the footing and loading stub was measured via the average of the readings from four vertical DTs (3-6) (see Fig. 3-6) when each cycle was unloaded to the drift angle of 0 rad., and the corresponding axial strain was described in Fig. 3-16, obtained by calculating the ratio of measured axial deformation to the distance (310mm or 550mm)

between the footing and loading stub. As is apparent from the comparison in Fig. 3-16, the axial strain for columns with n=0.20 generally leveled off as drift increased. The columns with n=0.33 showed increasing axial strain because the increase of axial compression will impose more compressive stresses on the column cross-section. However, the maximum axial strain was restricted to within 0.3% even when deformed to a drift angle of 0.04rad., far below the peak strain of confined concrete. This suggests that the confinement effect provided by the bolted circular steel tubes can offer the resilient concrete columns good axial stability even at large drifts.

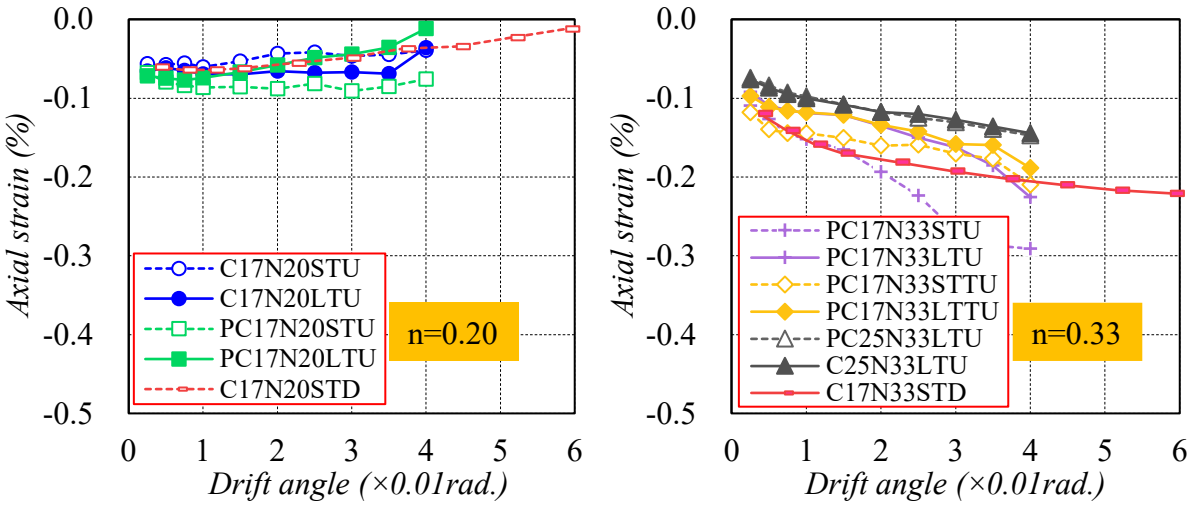

Fig. 3-16 Comparison of axial strain between the footing and loading stub

3.4 Conclusions

Taking reinforcement type (NS rebar, WBUHS rebar), shear span ratio (1.7, 2.5), diameter-to-thickness ratio (132, 96), axial load ratio (0.20, 0.33), embedment length of reinforcement (20d, 30d) and construction method (cast-in-place, precast) as main experimental variables, in this chapter, twelve specimens were made and tested under reversed cyclic lateral loading while simultaneously subjected to constant axial compression for the purpose of studying the seismic behavior of circular columns reinforced by squarely-arranged WBUHS rebars and confined by bolted circular steel tubes. Based on the test results discussed in this chapter, the main conclusions are drawn as follows:

1) When compared to traditional ductile concrete columns, all of the test columns reinforced by WBUHS rebars exhibited significant drift-hardening capacity as well as satisfactory self-centering capacity up to a large drift. Providing an embedment length of 20 times its diameter for WBUHS rebar could make the precast concrete columns perform almost the same excellent seismic behavior as the cast-in-site ones up to a drift ratio of at least 0.05 rad.

2) The strain gradient of WBUHS rebar along the column height remained small even when the columns were deformed to a significant drift ratio of 0.05 rad. when compared to NS rebars. This was beneficial for allowing the WBUHS rebars to remain in the elastic region for an extended time period, thus contributing to the remarkable drift hardening capacity and self-centering capacity.

3) The specimens under higher axial load level displayed slightly serious concrete damage and comparatively larger residual deformation but larger moment resistance as well as energy dissipation capacity.

4) For relatively short specimens with a/D=1.7, the axial strain consistently maintains at a low level as the drift angle increases, remaining below 0.1%. Even for the specimens subjected to higher axial compression, the axial strain gradually increases with the increase in drift angle, but remains below 0.3%. This strain level is much less than the ultimate compressive strain of confined concrete, revealing the favorable axial stability of the proposed precast concrete columns confined by bolted thin steel tubes.

References

[3.1] Sun Y.P., Cai G.C., Takeuchi T. Seismic behavior and performance-based design of resilient concrete columns. Applied Mechanics and Materials, 2013, 438: 1453-1460.

[3.2] Funato Y., Sun Y. Modeling and application of bond behavior of ultra-high strength bars with spiraled grooves on the surface. Proceedings of the Japan Concrete Institute, 2012, 34, 157–62. (in Japanese)

[3.3] Takeuchi, T., Sun, Y., Tani, M., Shing, P.S.B. Seismic performance of concrete columns reinforced with weakly bonded ultrahigh-strength longitudinal bars. J Struct Eng, 2021, 147, 04020290.

[3.4] Wang, J.H.; Sun, Y.P., Takeuchi, T. Seismic fragility and post-earthquake reparability of circular reinforced concrete bridge columns with low-bond high-strength reinforcements. Structures, 2021, 34, 840-855.

[3.5] Sun Y.P., Cai G.C. Seismic Behavior of Circular Concrete Columns Reinforced by Low Bond Ultrahigh Strength Rebars. Journal of Structural Engineering, 2023, 149: 04023126.

[3.6] Wei C.X., Sun Y.P. Takeuchi, T.; Che, J.Y. Influence of anchorage detailing on seismic behavior of precast concrete walls reinforced with SBPDN rebars. Journal of Structural Engineering B, 2022, 68, 75-86.

[3.7] Wang J.H., Cai G.C, Si Larbi A. Lateral behavior of rectangular concrete columns reinforced by partially debonded high-strength reinforcements based on a proposed equivalent stress block. Bulletin of Earthquake Engineering, 2021, 19, 1901-1930.

[3.8] Zhao J., Luo J., Zhang X.C., et al. Experimental study on seismic behavior of concrete walls with external magnetorheological dampers. Smart Mater Struct, 2023, 32, 065005.

[3.9] Architectural Institute of Japan (AIJ). Standard for structural calculation of reinforced concrete structures. Japan: Maruzen Co. Ltd, 2010.

[3.10] Abdallah, A.E.; El-Salakawy, E.F. Seismic performance of GFRP-RC circular columns with different aspect ratios and concrete strengths. Eng. Struct., 2022, 257, 114092.

[3.11] Abdallah, A.E; El-Salakawy, E.F. Seismic behavior of high-strength concrete circular columns reinforced with glass fiber-reinforced polymer bars. ACI Struct J, 2021, 118, 221-234.

[3.12] Liu Z., Zhao H., Sun Y., et al. Seismic performance of circular concrete columns reinforced by PC strands. J. Adv. Concr. Technol., 2020, 18(5): 256-271.

CHAPTER FOUR

4 Effect of Steel Amount and Confinement Method on Seismic Behavior of Circular Concrete Columns

4.1 Introduction

The essential information about the influence of different experimental parameters on the seismic performance of circular concrete columns reinforced by squarely-arranged WBUHS rebars, both cast-in place and precast, has been obtained according to the study conducted in chapter three. To promote the application of WBUHS rebars to concrete construction and widen applicability of the precast resilient circular concrete columns, effects of the steel amount of WBUHS rebars and confinement of bolted thin steel tubes on the seismic performance needs to be clarified.

In particular, while previous studies [4.1, 4.2] and the study described in chapter three have experimentally verified that the utilization of bolted circular thin steel tubes could effectively mitigate concrete damage and enhance the drift-hardening capacity of cast-in-site and precast circular concrete components up to drift of 0.05rad, it is not clear to what extent the confinement by the bolted thin steel tubes may enhance seismic property of the circular concrete columns with WBUHS rebars.

The objectives of this chapter are: 1) to study the influence of steel amount of WBUHS rebar through comparison of the experimental results of circular columns reinforced by larger-diameter WBUHS rebars with those of test columns described in chapter three; and 2) to quantitatively verify the influence of confinement of the bolted thin steel tubes on the seismic performance of circular concrete columns, cast-in-place and prefabricated, and confined by conventional hoops and bolted thin steel tube.

4.2 Experimental Program

4.2.1 Description of Test Specimens

A total of six 1/2.5-scale circular concrete columns were fabricated with identical geometric dimensions. Each specimen consisted of a loading stub of 400×350×350mm, a circular column with an outer diameter of 300 mm, and a footing of 1000×540×400mm as shown in Fig. 4-1. Among them, two were reinforced by eight large-diameter WBUHS rebars (U15) and transversely confined only by D6 deformed bars as reference specimens, and the other four were reinforced by U15 WBUHS rebars and transversely confined by bolted steel tubes to further enhance the resilience and to serve as quantitative analysis of the contribution of confinement by the bolted thin steel tubes to seismic behavior. The effective height of test columns was 510mm, which was measured from the top of the footing to loading point, to give a span ratio of 1.7. The main experimental variables are the longitudinal steel ratio, construction methods (cast-in-place, prefabrication), axial load ratio (0.20, 0.33), and confinement method (bolted tube, hoop). The steel ratio of WBUHS rebars in the six specimens was 1.92%, which is about 36.2% higher than that (1.41%) of the columns presented in chapter three. The outlines of test specimens are summarized in Table 4-1.

The reinforcement details in each concrete column are depicted in Fig. 4-1. Since providing 20d embedment length for WBUHS rebars could ensure that the precast concrete columns exhibited the same excellent seismic performance as the cast-in-place ones, the embedment length of larger diameter WBUHS rebars used in this chapter was set to be 20d. In each specimen, the longitudinal tensile reinforcement consisted of eight WBUHS rebars arranged in a square configuration. Similar to chapter three, the upper end of each WBUHS bar is firmly anchored by one steel plate and high-strength nuts to facilitate the construction and positioning of the steel cage, while the lower end was secured using two high-strength nuts to clamp a washer with an outer diameter of 40mm to simplify the construction. For specimens C20STU15, C33STU15, PC20STU15 and PC30STU15, the transverse confinement consisted of D6 circular hoops with a spacing of 100mm and bolted circular steel tubes with thickness of 2.3mm. The D6 circular hoops were used in these four specimens only as auxiliary steel to keep the alignment of WBUHS rebars. For specimens C33SU15 and PC33SU15, the transverse confinement consisted of D6 circular hoops with a spacing of 30mm.

The steel tubes were fabricated by joining two premanufactured semicircular plates through high-strength (HS) bolts and nuts. Furthermore, steel plates with 9 mm thickness (PL9) were added to prevent the local buckling of the flange. In order to prevent the bolted steel tubes from directly carrying axial load, a 6mm clearance was maintained between bolted steel tubes and the loading stub (or the footing). In the case of precast specimens, the column and footing were manufactured and poured separately. After one week of pouring, the concrete strength could meet the requirements of removing the formwork and lifting operation. Then, WBUHS rebars protruding from the column were inserted into sheathing ducts pre-embedded in the footing and jointed using high-strength and no-shrinkage grouting material. The jointing process of precast columns was the same as that in chapter three, as shown in Fig. 4-2.

Table 4-1 Parameters and primary test results of the test columns

Specimen	Longitudinal rebar	*a/D*	l_e (mm)	Construction method	*n*	Transverse confinement	f_c' (MPa)	Q_{exp} (kN)	R_{exp} (×0.01rad.)
C20STU15	8-U15 (ρ_g=1.92%)	1.7	20d	Cast-in-place	0.20	D6@100+PL2.3	39.8	358.3	6.0
C33STU15					0.33		42.4	375.0	6.0
C33SU15						D6@30	42.2	254.1	4.0
PC20STU15				Precast	0.20	D6@100+PL2.3	40.7	363.6	6.0
PC33STU15					0.33		43.1	382.8	6.0
PC33SU15						D6@30	40.9	250.6	5.0

Note: ρ_g: longitudinal rebar ratio, *a/D*: shear span ratio, l_e: embedment length of longitudinal rebar, *d*: the diameter of WBUHS rebar, *n*: axial load ratio, ρ_w: volumetric ratio of hoop, ρ_t: volumetric ratio of bolted steel tube, f_c': the measured standard cylindrical concrete compressive strength, Q_{exp}: average value of measured peak loads in both positive and negative drift ratios, R_{exp}: drift angle at peak load.

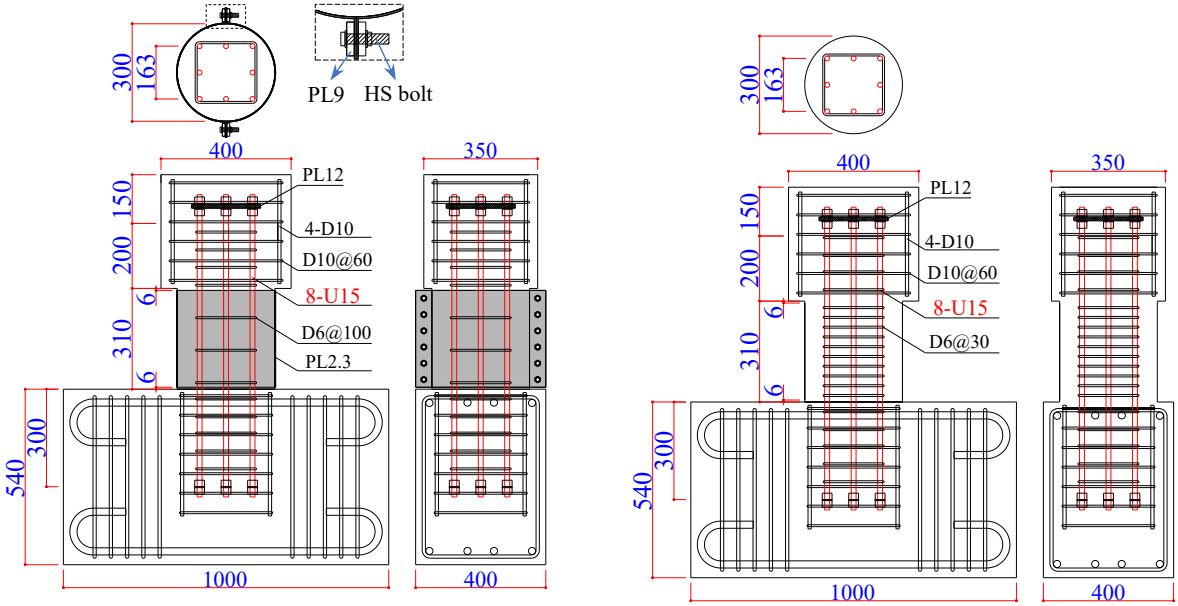

C20STU15, C33STU15 C33SU15

(a) Cast-in-place specimens

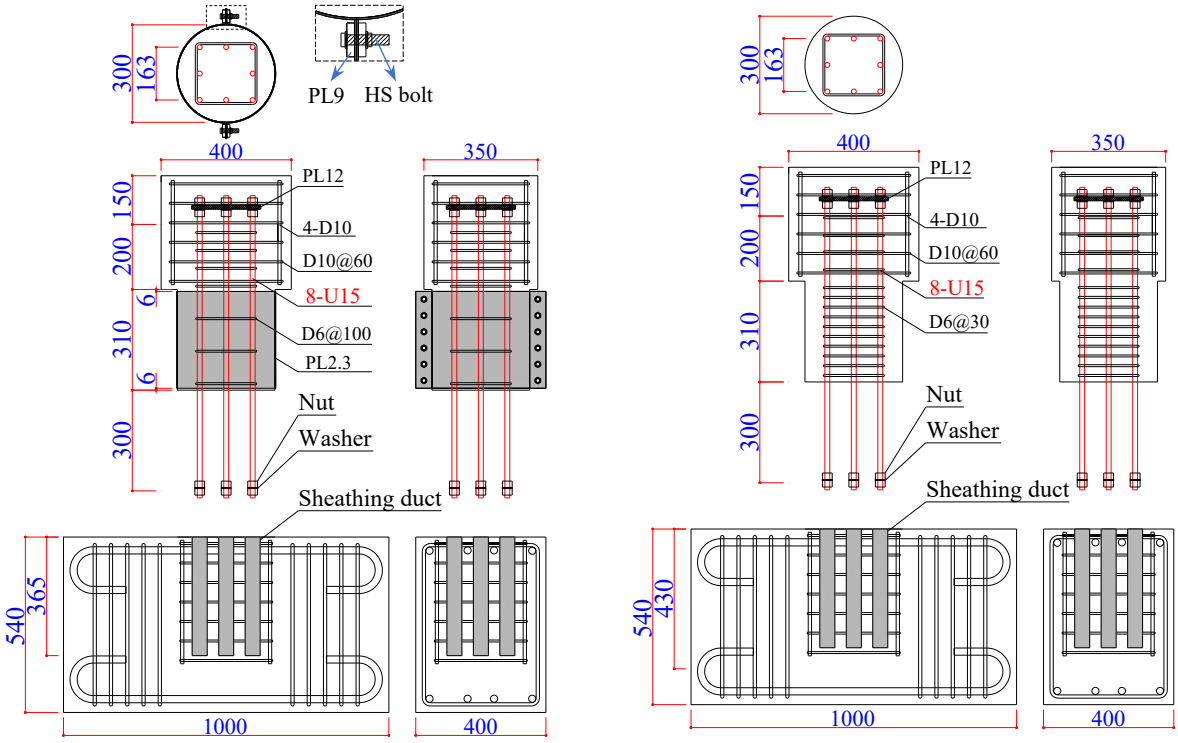

PC20STU15, PC33STU15 PC33SU15

(b) Precast specimens

Fig. 4-1 Reinforcement details of test columns

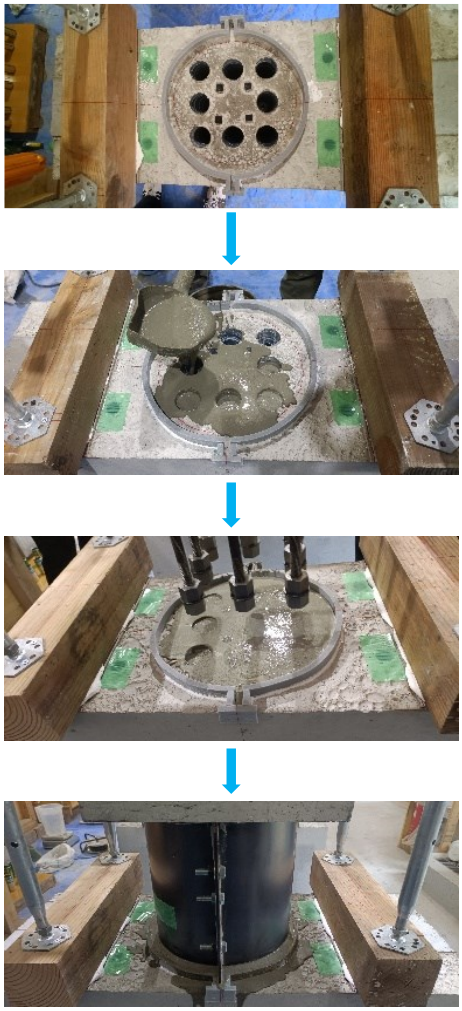

Step 1:
Clean the surface (joint surface) of the foundation beam and draw the center line in four directions on the surface of the column and the footing.

Step 2:
Adjust the height of the support rod to the target value and inject high-strength grouting material into each sheathing duct.

Step 3:
Lift the column to the joint position and determine the orientation of the front side of the column.

Step 4:
Insert the WBUHS bars extending from the column into the embedded sheathing duct, and confirm the final position of the column.

Fig. 4-2 Jointing process of precast concrete columns

4.2.2 Material Properties

Ready-mixed concrete which was made of common Portland cement and regular normal coarse aggregates having a maximum diameter of 20 mm was utilized to fabricate test columns. According to the test results of three concrete cylinders (with dimensions of 100 mm in diameter and 200 mm in height) cured under the same condition as the test specimens, the measured concrete compression strength during testing is presented in Table 4-1.

The mechanical properties and stress-strain relationships for the used steel materials are presented in Table 4-2 and Fig. 4-3, respectively. The yield stress of the WBUHS rebar is defined as the 0.2% offset yielding strength.

Table 4-2 Mechanical properties of the steels used

Material	*D or T* (mm)	E_s (kN/mm^2)	f_y (N/mm^2)	f_u (N/mm^2)	ε_y (%)
WBUHS rebar (U15)	12.6	202	1356*	1452	0.88*
Hoop (D6)	6.35	202	434	568	0.24
Steel tube (PL2.3)	2.3	199	348	435	0.18

Note: D: diameter of WBUHS rebar, T: thickness of steel tube, E_s: Young's modulus, f_y: yield stress, ε_y: yield strain, f_u: tensile stress, *: the value based on 0.2% offset method.

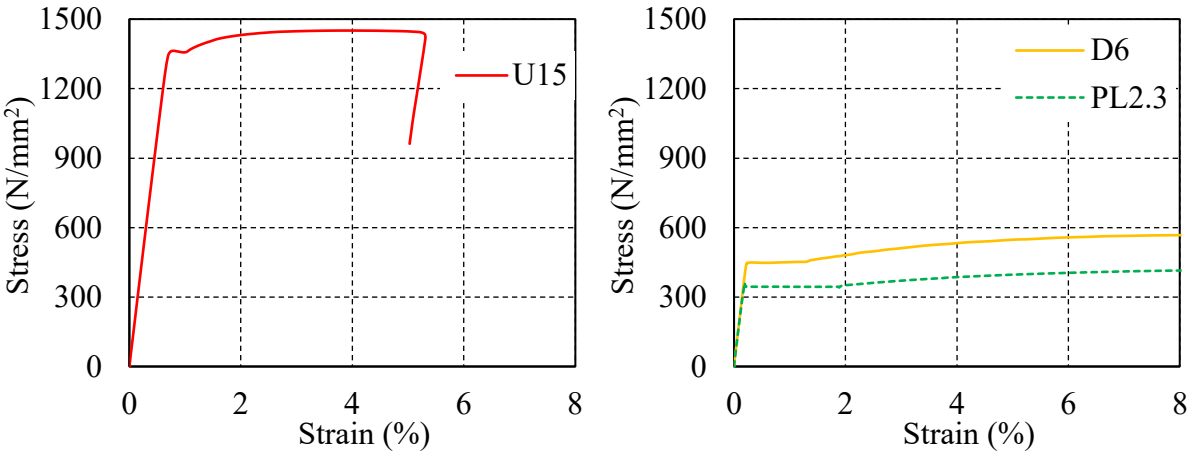

Fig. 4-3 Stress-strain curves of the used materials

4.2.3 Test Setup

The specimens were tested under reversed cyclic lateral loading while simultaneously subjected to constant axial compression with axial load ratios of 0.20 or 0.33. As illustrated in Fig. 4-4, The footing beam is securely fixed to the rigid beam using 8 high-strength steel rebars with a diameter of 21mm. In addition, a stabilizer was attached to the loading beam to prevent potential out-of-plane deformation. After applying the axial compression loads using a hydraulic jack with a 1000-kN capacity, two hydraulic jacks were employed jointly to impose the reversed cyclic lateral loads, which were controlled by the drift angle (R). The R was defined as the ratio of lateral displacement (Δ) at the loading point to the shear span (a). The test columns were cycled twice at each target drift angle within 0.02 rad., and were cycled once at subsequent drift angles, as shown in Fig. 4-5.

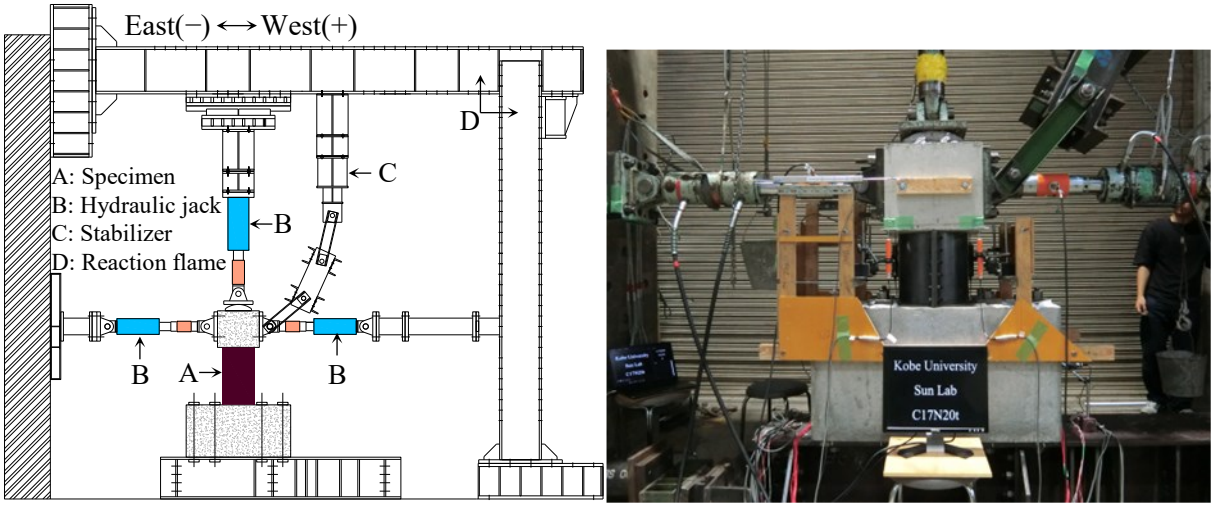

Fig. 4-4 The test setup of test columns

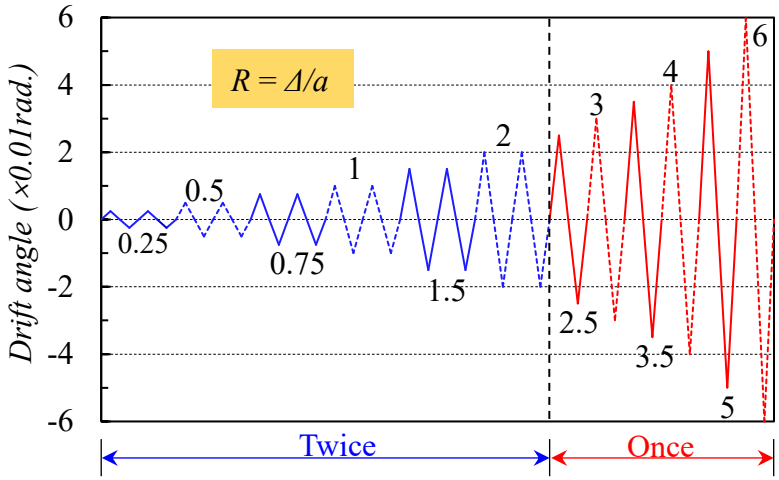

Fig. 4-5 Loading program

4.2.4 Instrumentation and Measurement

Two lateral displacement transducers (DTs) were installed in the loading stub for the measurement of lateral displacement (Δ) at loading point and four vertical DTs were placed for the measurement of axial deformation between the loading stub and footing. Besides, strain gages were attached to longitudinal rebars, transverse hoops and bolted steel tubes to serve the subsequent analysis of their mechanical properties. The location of DTs and strain gages were respectively displayed as Fig. 4-6 and Fig. 4-7.

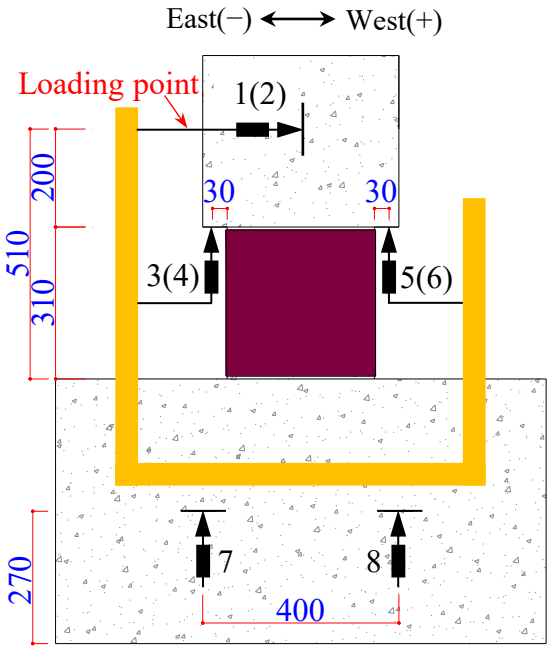

Fig. 4-6 Locations of displacement transducers (DTs)

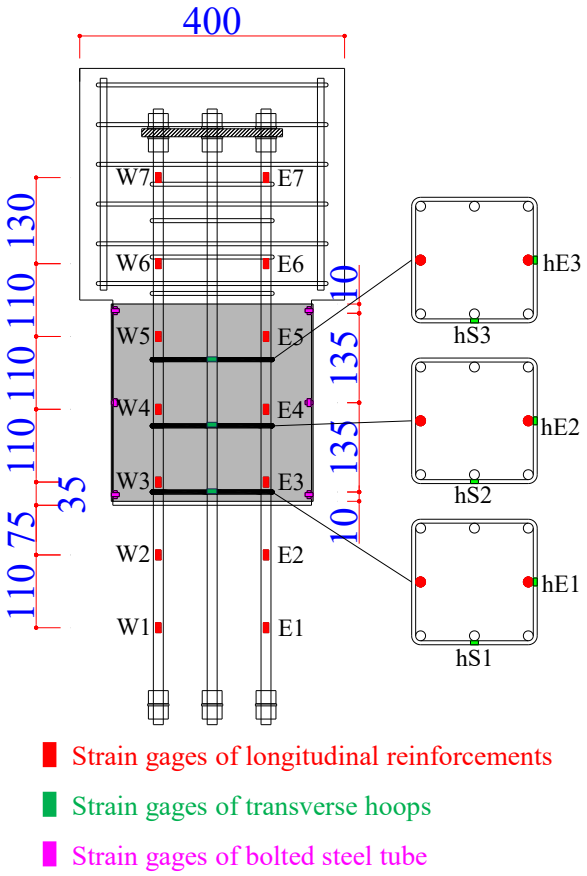

(a) For specimens transversely confined by bolted tubes

Fig. 4-7 Locations of strain gages

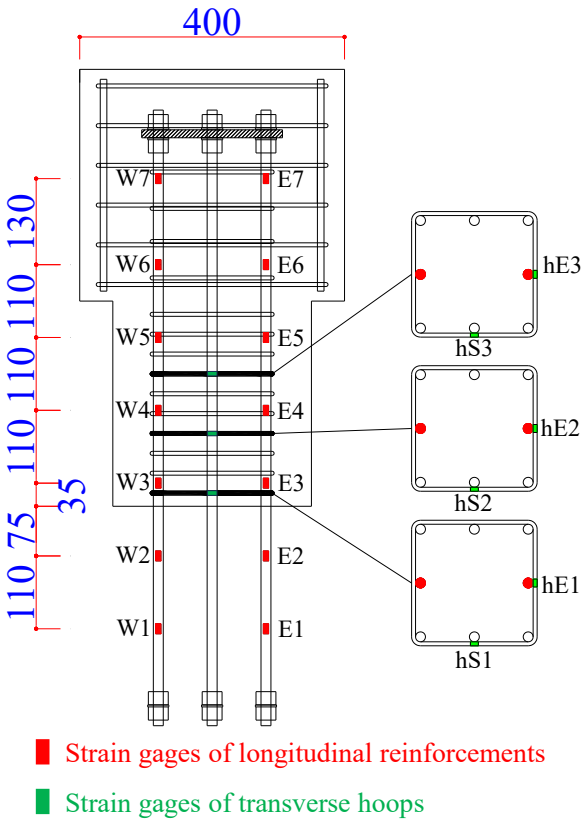

(b) For specimens transversely confined by only hoops

Fig. 4-7 Continued

4.3 Observed Behavior and Test Results

4.3.1 Observed Behavior of Test Specimens

During the loading process of R=0.0025rad., the occurrence of first crack was confirmed. For the test columns with n=0.20, the cracking loads ranged from 65 to 95 kN, and for the columns with n=0.33, the cracking loads were slightly larger, ranging from 80 to 100 kN. As the drift angle increased to 0.005rad., the measured maximum crack width was not exceeding 0.3mm, and complete crack closing was observed after unloading the lateral force to 0kN. With the continuous loading up to the drift angle of 0.01rad., the maximum crack width noticeably increased, but the residual crack width remained within 0.30mm. When the drift angle reached 0.02rad., the residual crack width of precast concrete columns was comparatively larger than that of the cast-in-place ones, with the maximum observed residual crack width being 1.5 mm. In subsequent loading levels, the measurement of residual crack width became difficult because of the spalling of cover concrete. For the test specimens confined by steel tubes, after cyclic loading to the drift angle of 0.06rad., a monotonic pushover was performed until reaching the movable limit of the test apparatus, with the maximum load leveling off but not decreasing during this period. As for the concrete columns transversely confined only by hoops, the load-bearing capacity decreased significantly at 0.05 rad. (0.06rad. for specimen PC33SU15) due to severe concrete damage, and then the test was terminated. It's worth noting that both the WBUHS bars and the embedded sheathing duct were firmly anchored in the footing beam without the occurrence of pull-out failure during the entire loading process.

Following the completion of loading, Fig. 4-8 illustrated the final damage condition of the test columns after the removal of steel tubes and crushed concrete. Under reversed cyclic lateral loading, the concrete columns displayed a combination of vertical and horizontal cracks, forming distinctive patterns. The severity of concrete damage was notably pronounced in specific localized areas. To be specific, the test columns confined by bolted thin steel tubes and subjected to lager axial compression (n=0.33) exhibited a relatively wide area of crushed concrete, but primarily concentrated within 30 mm of the column foot. By comparison, both cast-in-place and precast specimens confined only by hoops showed extensive concrete crushing with damage extending over 200 mm in height, and the crack distribution nearly occupied the entire column. Overall, the failure of the specimens was

primarily dominated by bending, and the utilization of steel tubes was significantly advantageous in mitigating the damage to concrete.

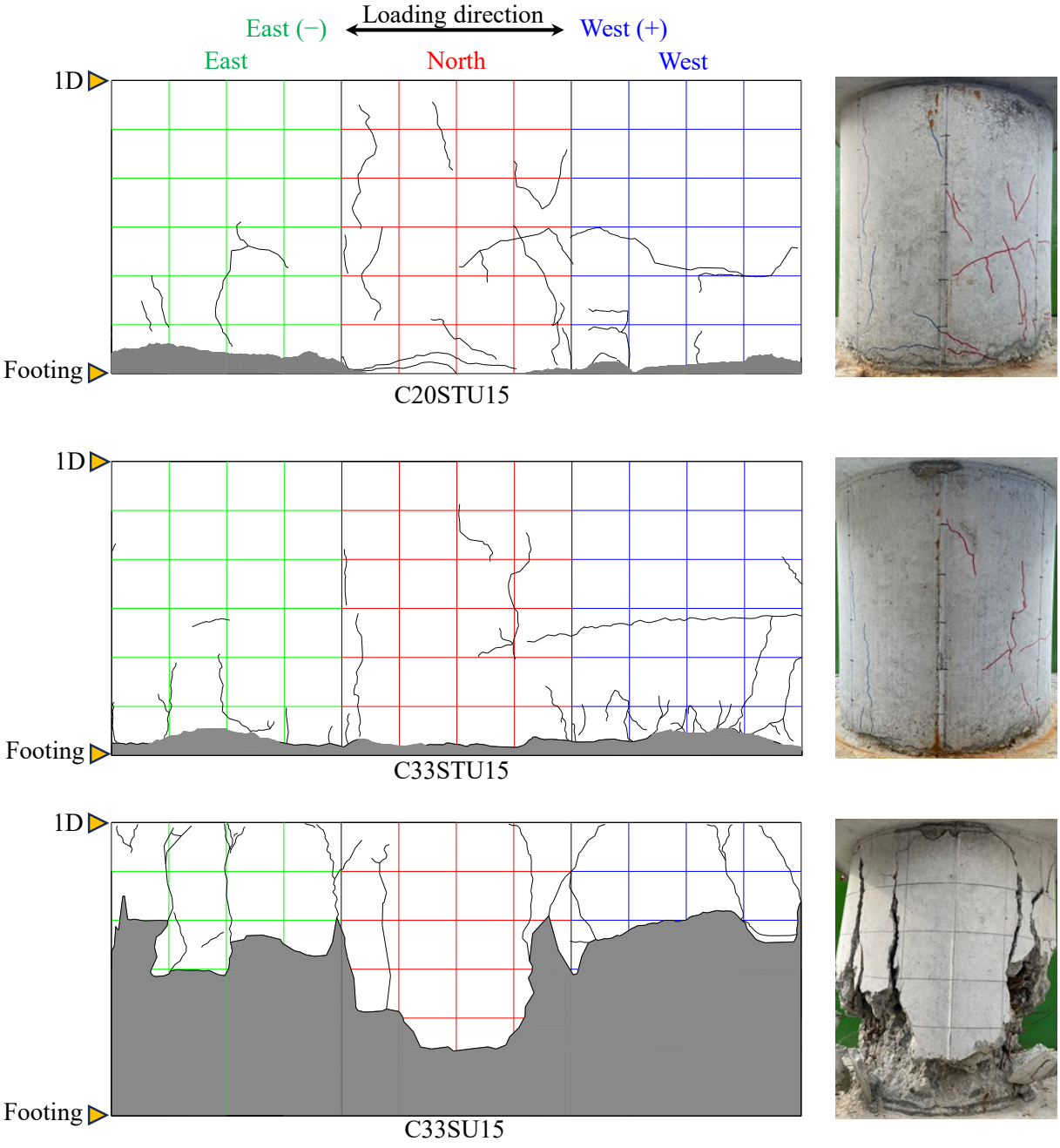

(a) Cast-in place specimens

Fig. 4-8 Damage state of specimens

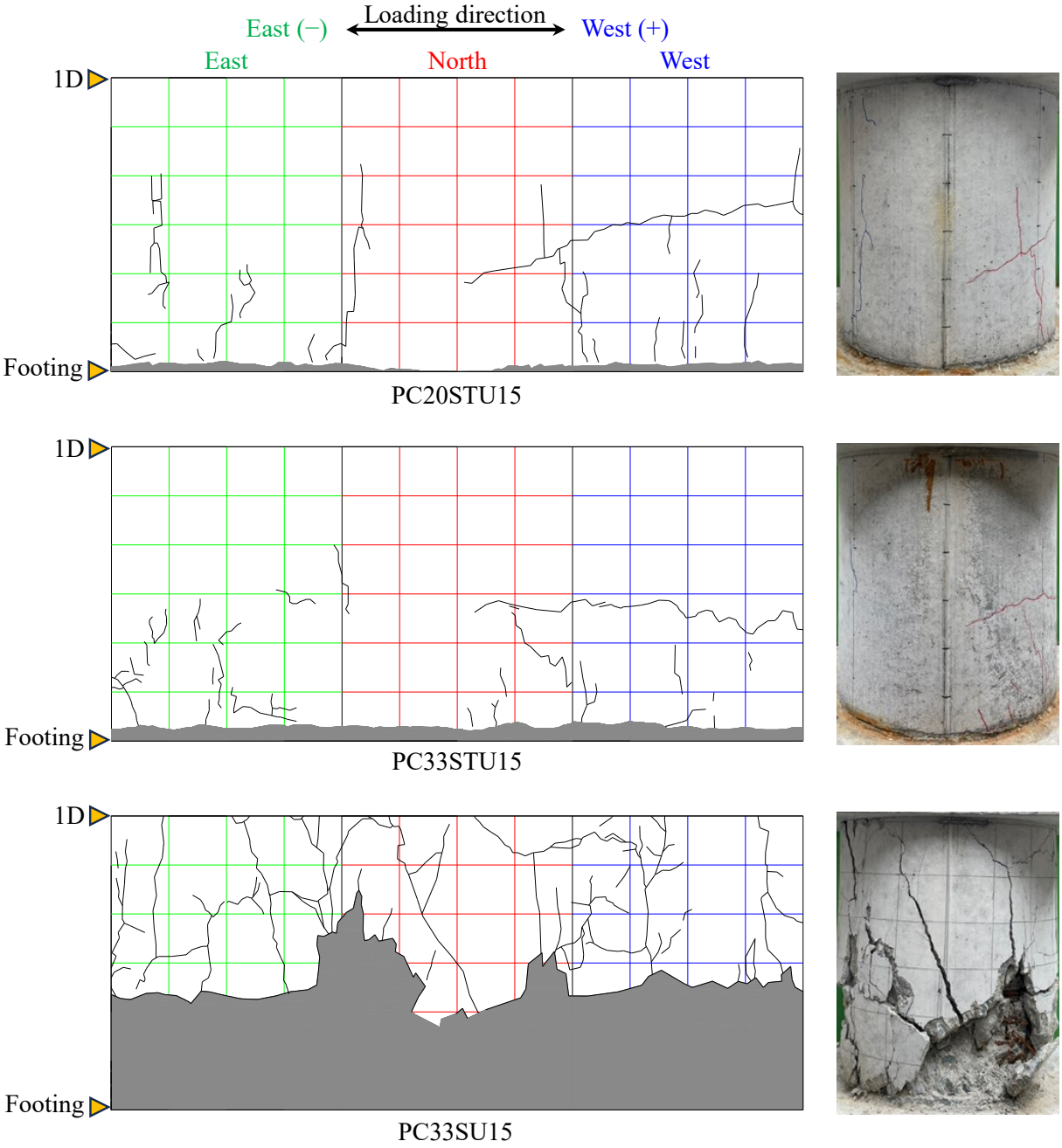

(b) Precast specimens

Fig. 4-8 Continued

4.3.2 Lateral Force Versus Drift Angle Relationship

The measured lateral force-drift angle curves for the test columns are depicted in Fig. 4-9, in which square and circular symbols respectively signify the yield of steel tubes and the peak load of test columns, while the red dashed line denotes the strength decline caused by P-Δ effect. As is apparent from Fig. 4-9, the test columns confined only by D6 hoops exhibited good drift hardening capacity without strength degradation until a drift angle of 0.04 rad., but after that drift angle, the lateral resistance begin to decrease due to severe concrete damage. In contrast, the concrete columns transversely confined by the bolted thin steel tubes, whether subjected to different axial load ratio (0.20 or 0.33) or fabricated according to different construction method (cast-in-place or prefabrication), exhibited very significant drift hardening capacity even when deformed to a drift angle as large as 0.06 rad. In addition, all bolted steel tubes yielded in the transverse direction before the test columns reached their peak loads, which indicated that the steel tubes fully exerted their confinement effect [4.3].

For the purpose of better understanding the influence of various experimental parameters on the seismic behavior of test specimens, the envelopes of both lateral force-drift angle relationships and moment-drift angle relationships are compared in Fig. 4-10. The experimental moment represents that measured at the column bottom section, and includes moment by the lateral force and P-delta effect. The following observations can be made from Fig. 4-10.

a) The effect of longitudinal steel ratio: By comparing with the test specimens in chapter three, it is evident that increasing the steel content of WBUHS rebars significantly enhances both lateral force and moment resistance, as depicted in Fig. 4-10 (a). When substituting U12.6 rebars with U15 rebars in the test columns subjected to a low axial compression (n=0.20), there is a notable increase of 17.9% in lateral force and 16.7% in moment resistance. In the specimens under higher axial compression (n=0.33), this enhancement becomes even more pronounced, reaching 23.3% for lateral force and 21.9% for moment resistance, respectively.

b) The effect of confinement method: Owing to the uniform confinement effect by bolted circular steel tubes, the lateral force and moment resistance of the test specimens, both cast-in place and precast, can be significantly improved. The improvement effect

becomes more obvious with the increasing of drift angle. Compared to the hooped cast-in-site column, the enhancement ratio of lateral forces and moment resistances of the cast-in-site column confined by bolted thin steel tube varied by 6.1−38.7% and 5.9−33.5% up to R=0.04rad., respectively, as the drift increased up to 0.04 rad (see Fig. 4-11). In the case of precast specimen, confinement by bolted steel tube could increase the lateral force and moment resistance by 4.1−48.1% and 3.9−40.5% up to R=0.05rad, respectively. Moreover, the confinement of steel tube can also significantly improve the deformation capacity.

c) The effect of construction method: Regardless of whether they were externally confined by steel tubes, the precast concrete columns exhibited nearly identical or even superior load-bearing capacity and/or moment resistance than the cast-in-place ones. Combining these findings with those obtained in Chapter 3, the effectiveness and wide applicability of the construction method (including the embedment depth of WBUHS rebar and jointing process) for precast concrete columns proposed in this paper has been confirmed once again, and this effectiveness is not affected by the axial load level, confinement method and even the steel amount of WBUHS rebar.

d) The effect of axial load ratio: The test columns under an axial load ratio of 0.33 exhibited significantly higher lateral force and moment resistance, reaching up to 1.35 times that of the specimens with an axial load ratio of 0.20. This is because that an increase in the axial load ratio tends to result in a larger neutral axis depth within the column, thus increasing the resistance provided by concrete, which was effectively confined by bolted steel tubes.

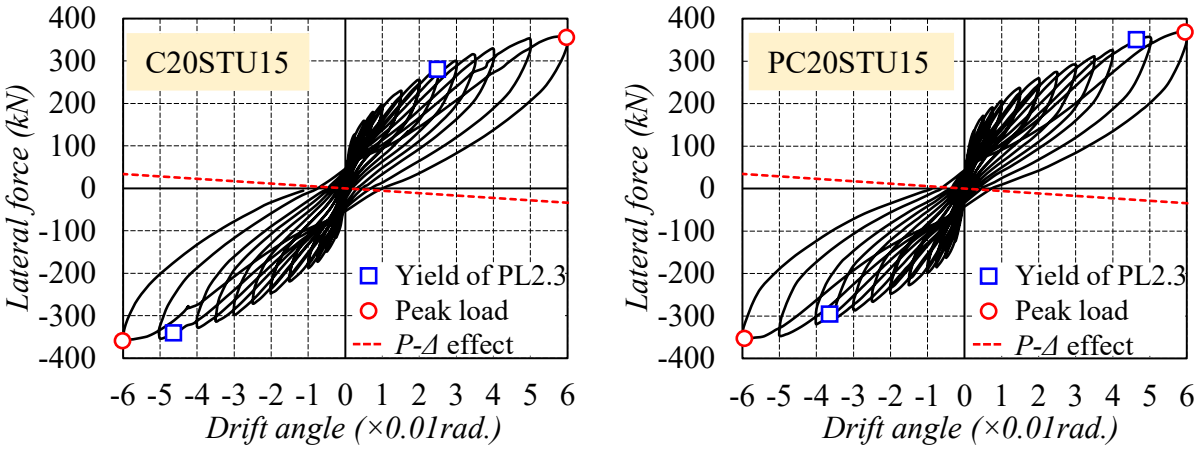

(n=0.20, confinement by bolted tube)

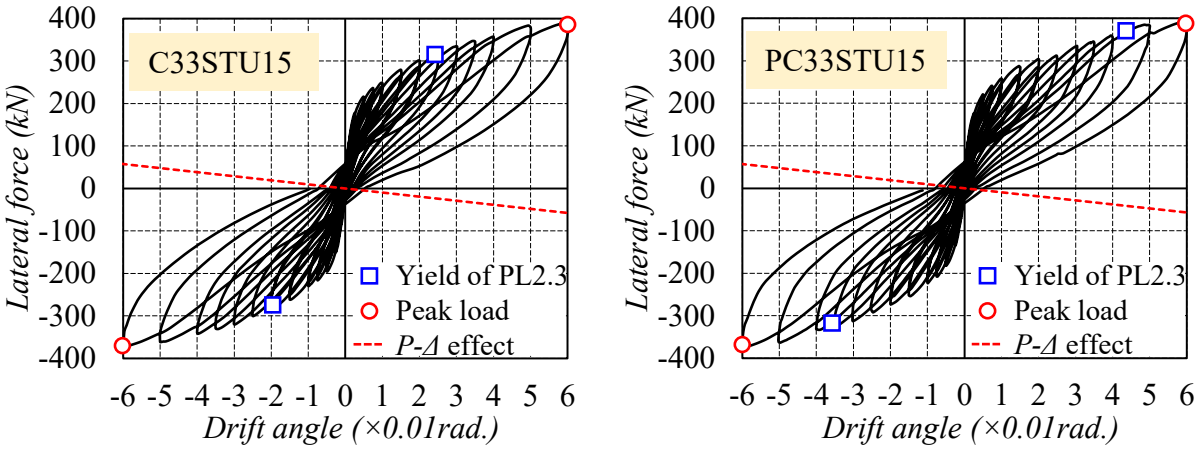

(n=0.33, confinement by bolted tube)

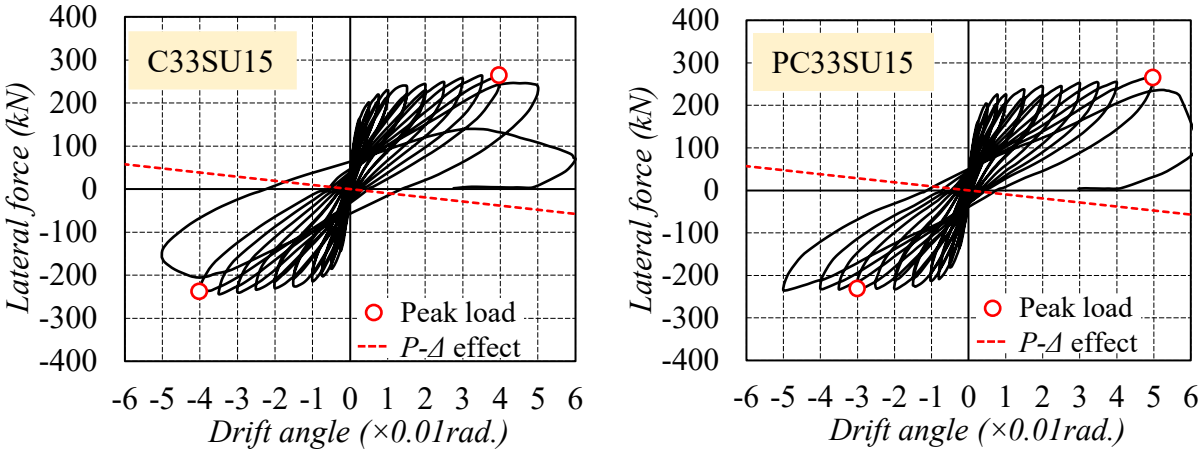

(n=0.33, confinement by D6 hoops)

Fig. 4-9 Lateral force versus drift angle relationships

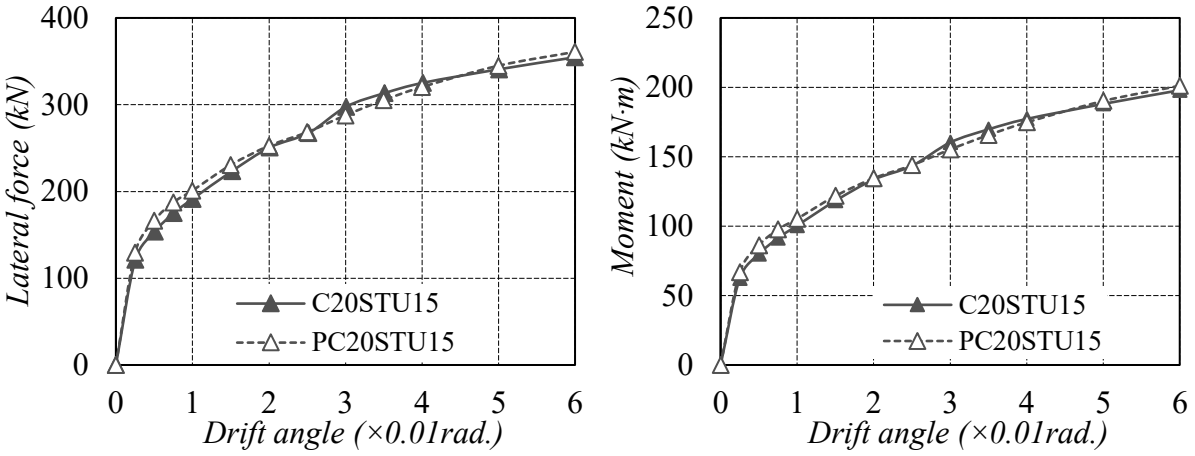

(n=0.20, confinement by bolted tube)

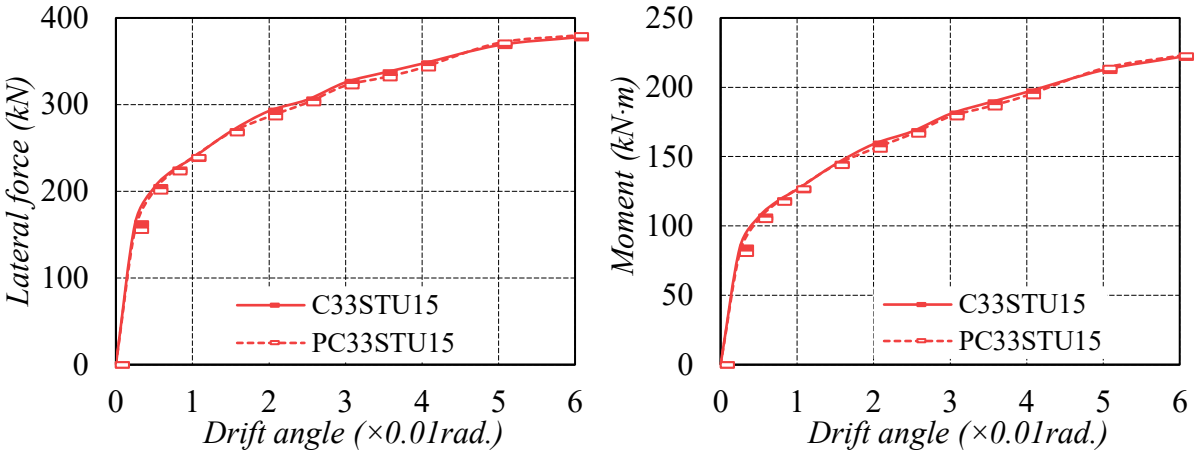

(n=0.33, confinement by bolted tube)

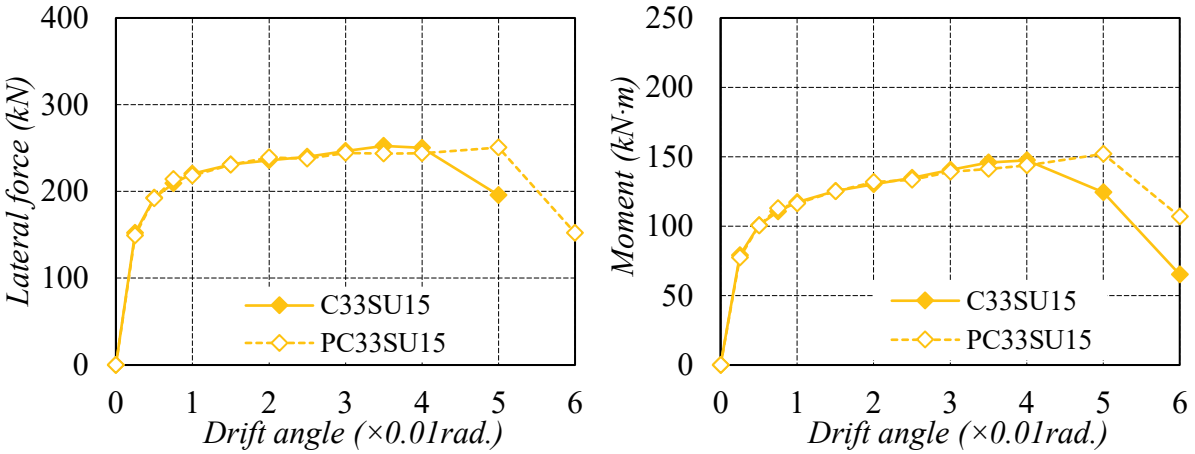

(n=0.33, confinement by D6 hoops)

(a) The effect of construction method (cast-in-place, prefabrication)

Fig. 4-10 Effects of experimental variables on lateral force and moment

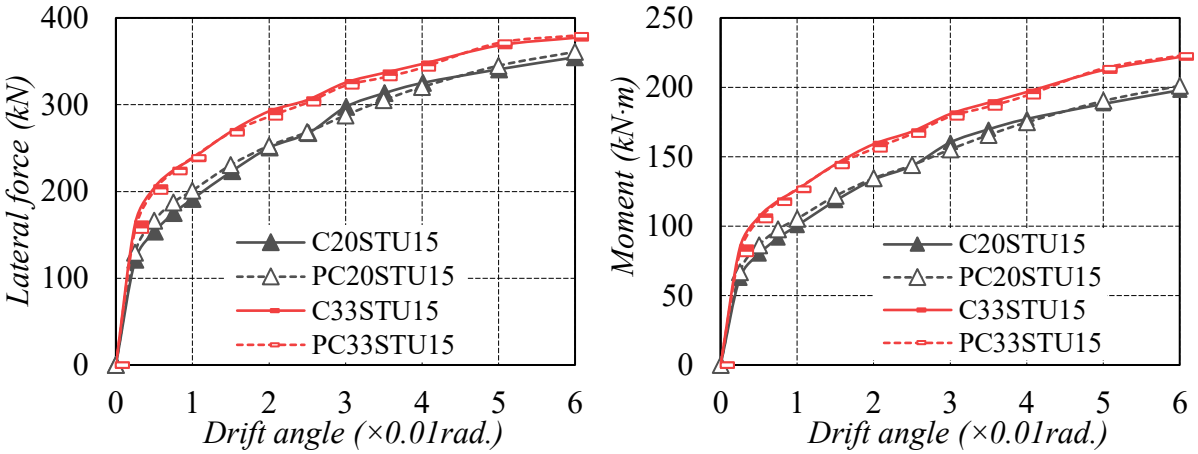

(b) The effect of axial load ratio (0.20, 0.33)

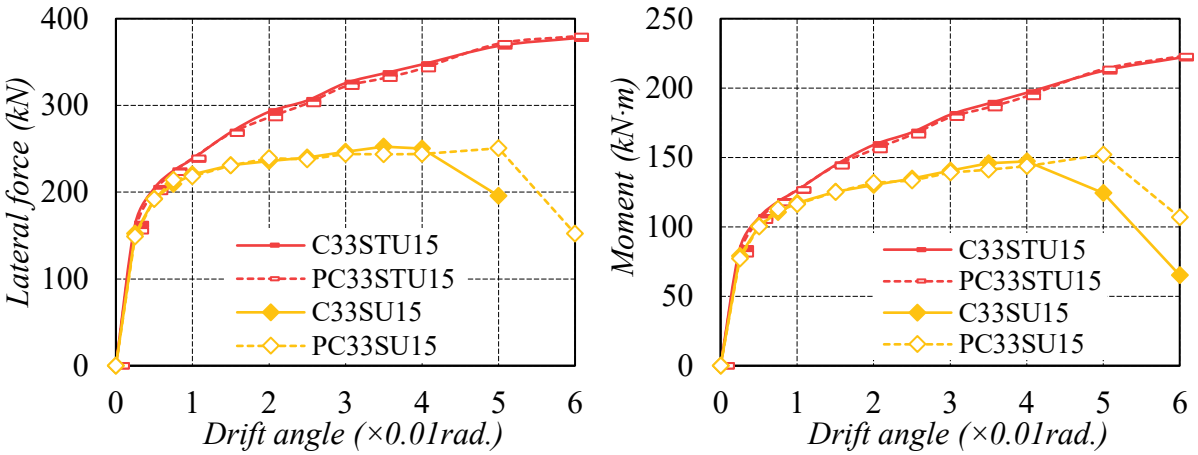

(c) The effect of confinement method (bolted tube, D6 hoops)

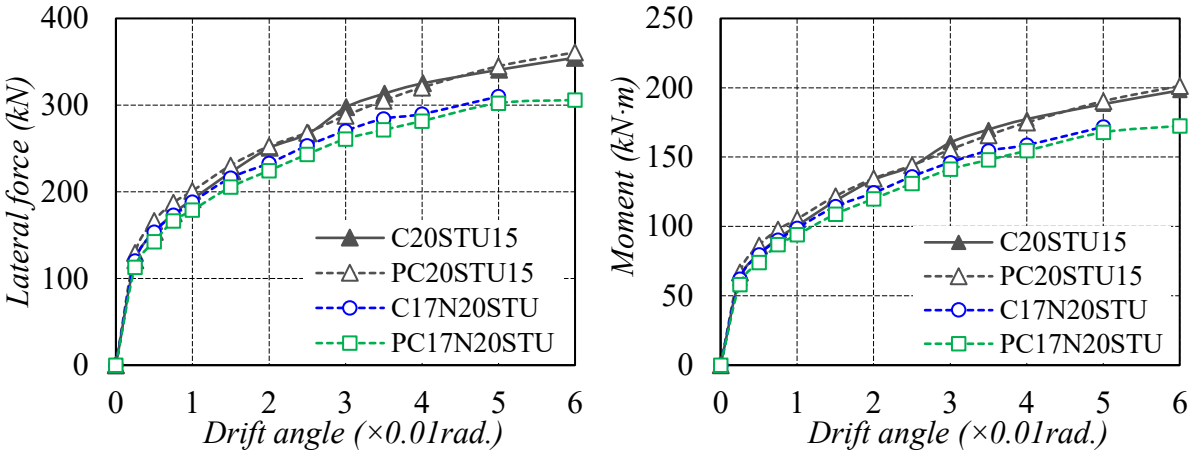

(n=0.20)

(d) The effect of steel amount of WBUHS rebars (1.41%, 1.92%)

Fig. 4-10 Continued

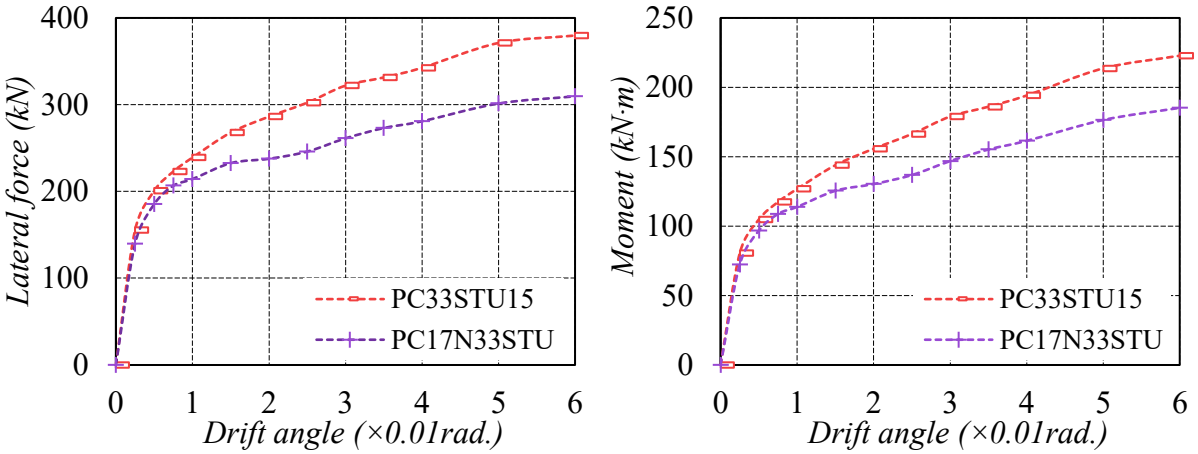

(n=0.33)

(d) Continued

Fig. 4-10 Continued

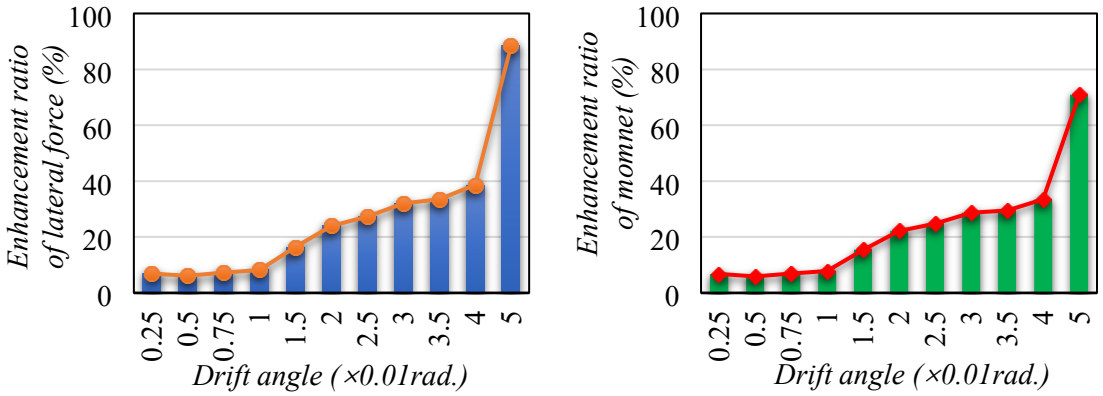

a) For cast-in-place specimen

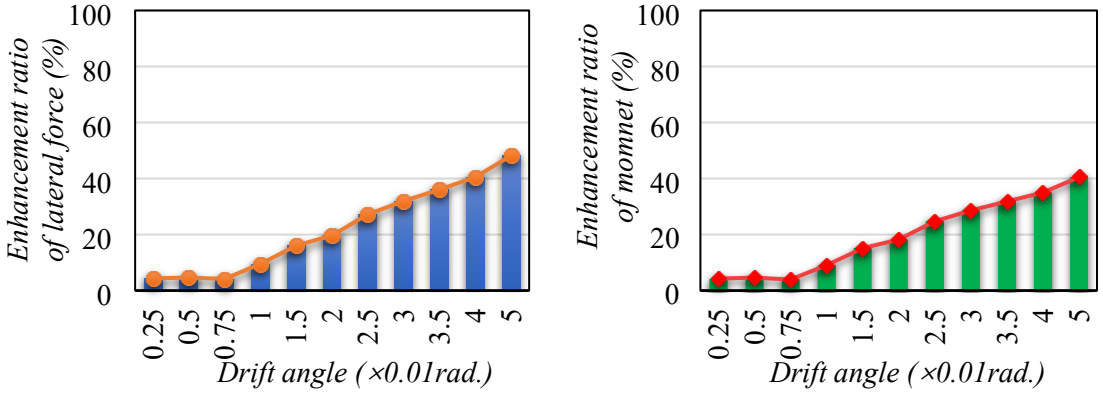

b) For precast specimen

Fig. 4-11 Enhancement ratio of the lateral force and moment resistance by confinement of bolted steel tube

4.3.3 Strain of WBUHS Rebars

Fig. 4-12 compared the variation trend of the strain of WBUHS rebars measured at the position 35mm away from the top surface of the footing at various loading levels. From Fig. 4-12, several important observations are made as follows.

a) The influence of longitudinal steel ratio: Regardless of the differences in the applied axial compression level and construction method, an increase in the steel amount of WBUHS rebars resulted in a decrease in their strain. This phenomenon arises from the large longitudinal steel ratio increasing the depth of the compression zone to balance the axial tensile force by more WBUHS rebars, consequently bringing about a relatively low strain level of WBUHS rebars in tensile region.

b) The influence of confinement method: In the cycles up to 0.035 rad drift angle, the WBUHS rebar strain was less affected by the confinement method. From the drift angle of 0.04 rad onward, the growth rate of WBUHS rebar strain in specimens transversely confined only by hoops decelerated significantly or even exhibited a decline. In contrast, WBUHS rebar strain in the columns confined by bolted thin steel tubes continued to demonstrate a steady upward trend.

c) The influence of construction method: The strain of WBUHS bars in the precast concrete columns was nearly identical to that in the cast-in-place ones. This was reasonable, considering their comparable lateral resistance, as detailed in Section 4.3.2.

d) The influence of axial load ratio: The tensile strain of WBUHS rebar in test specimens with higher axial load ratios was smaller, consistent with the findings presented in chapter three. This observation could be attributed to the fact that the higher axial compression led to a larger depth of compression zone, which in turn, retarded the development of strain in tension.

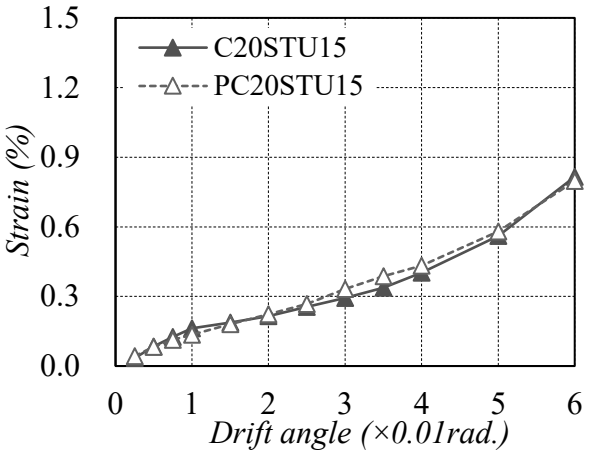

(n=0.20, confinement by bolted tube)

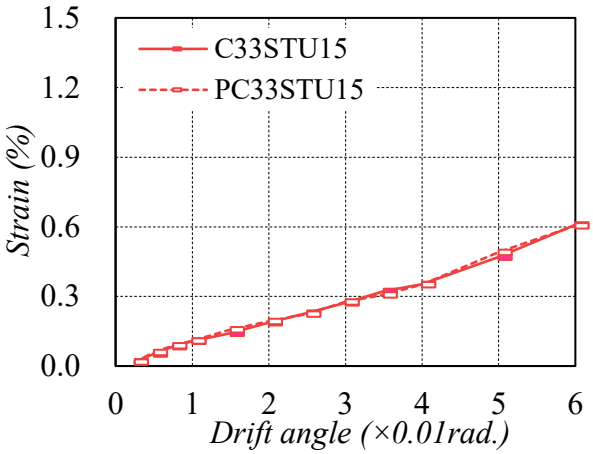

(n=0.33, confinement by bolted tube)

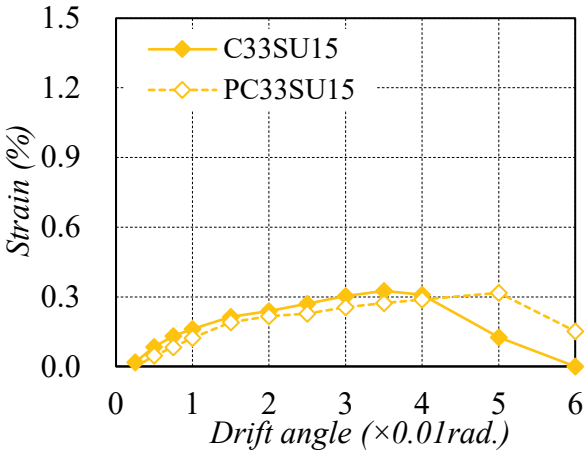

(n=0.33, confinement by D6 hoops)

(a) The effect of construction method (cast-in-place, prefabrication),

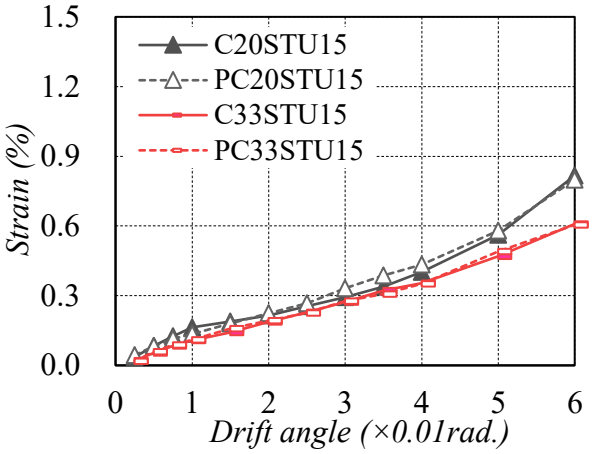

(b) The effect of axial load ratio (0.20, 0.33)

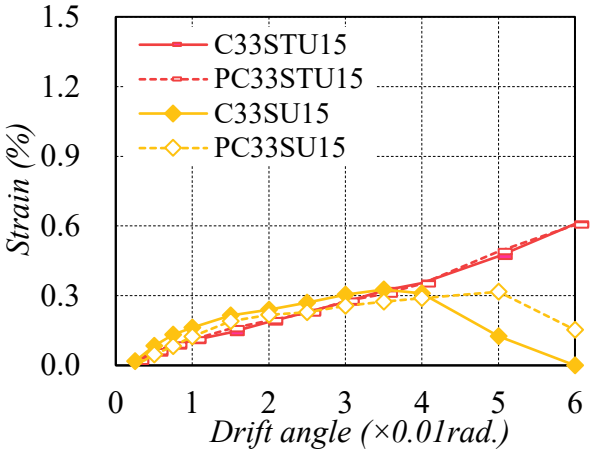

(c) The effect of confinement method (bolted tube, D6 hoops)

Fig. 4-12 Strain of WBUHS rebar

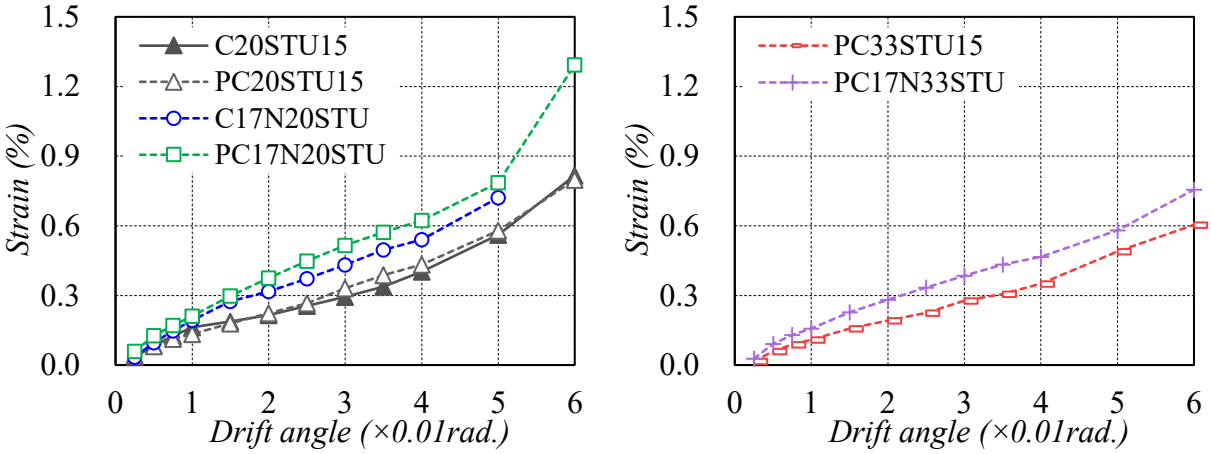

(d) The effect of steel amount of WBUHS rebar (1.41%, 1.92%)

Fig. 4-12 Continued

The measured strain distribution of WBUHS rebar along the column height was drawn in Fig. 4-13. It is obvious that the strain gradient remained small even when the columns were deformed to a significant drift angle of as large as 0.05 rad. This was beneficial for allowing the WBUHS rebars to remain in the elastic region for an extended time period, thus contributing to the remarkable drift-hardening and self-centering capacity.

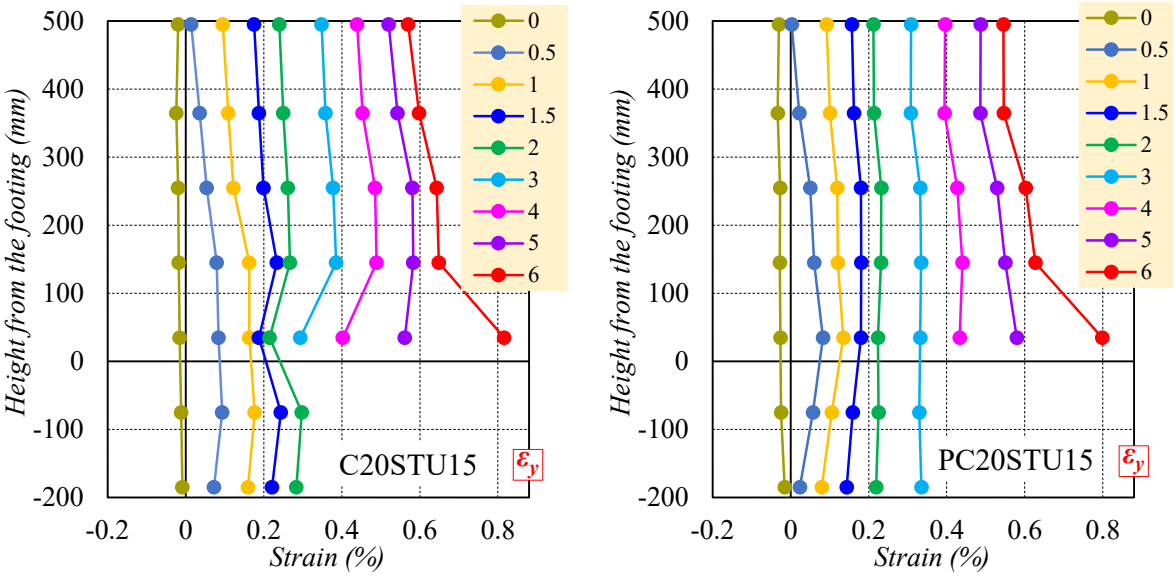

(n=0.20, confinement by bolted tube)

Fig. 4-13 Strain distribution of WBUHS rebar

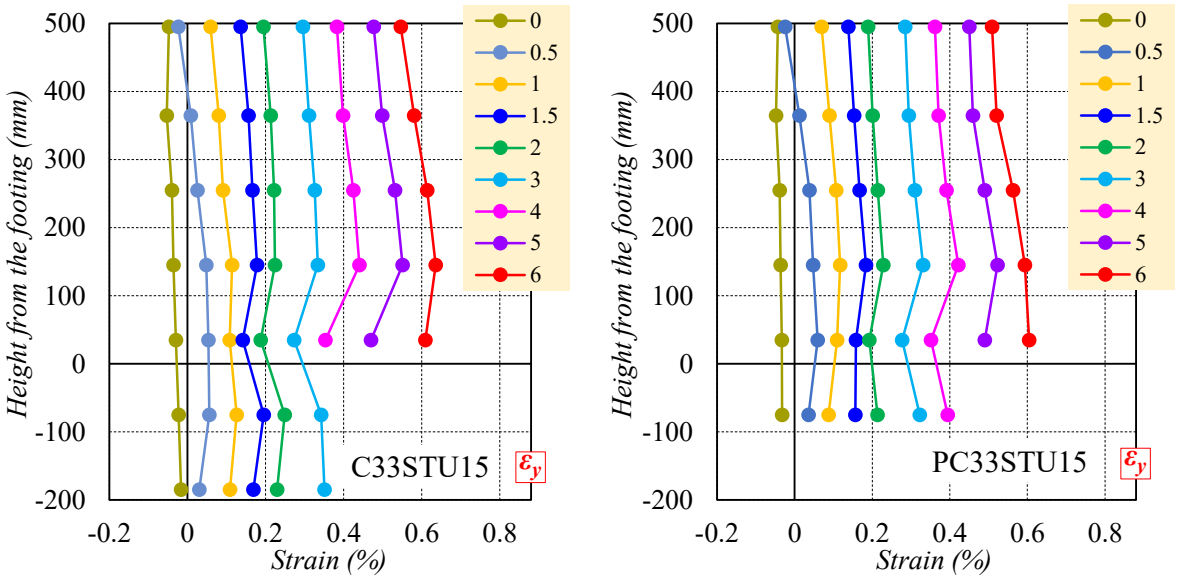

(n=0.33, confinement by bolted tube)

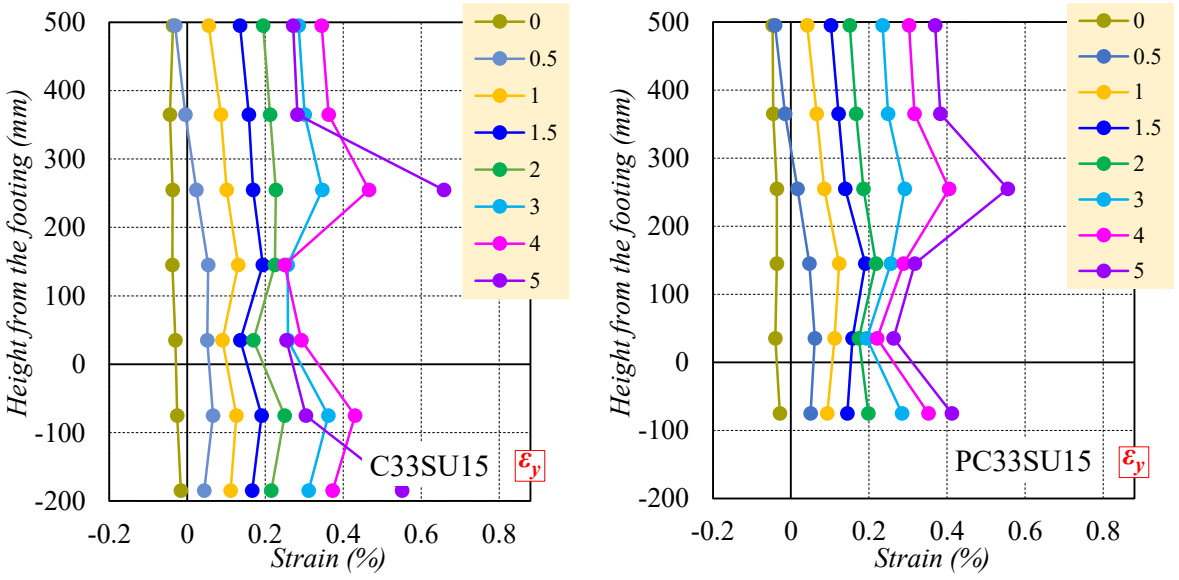

(n=0.33, confinement by D6 hoops)

Fig. 4-13 Continued

4.3.4 Residual Deformation

When the lateral force was unloaded to 0kN, the measured average value of residual deformation in positive and negative loading directions was illustrated in Fig. 4-14. Notably, the test specimens confined only by hoops exhibited significantly larger residual deformation than those confined by steel tubes from a drift angle of 0.02 rad onward. This difference may be attributed to the fact that the confinement of bolted circular steel tubes effectively reduced the permanent plastic deformation caused by concrete damage. Moreover, for columns with large-diameter WBUHS rebars, it is apparent that the residual deformation was constrained under a lower level when subjected to a higher axial compression. The similar phenomenon could also be observed from the study carried out by Li et al. [4.4], in which the same type of WBUHS rebars were utilized to reinforce the square concrete columns. In addition, the influence of the steel amount of WBUHS rebars on the residual deformation is complex. Under the axial load ratio of 0.20, the residual deformation of test columns with large steel amount of WBUHS rebars is slightly larger, while for those under the axial load ratio of 0.33, the increase of steel amount of WBUHS rebars shows an opposite trend.

On the whole, the residual deformation of specimens reinforced by WBUHS rebars increased slowly along with further loading, and could be kept under 0.005rad., 1/12−1/8 of the transient drift angle until the drift angle of 0.04rad., indicative of good self-centering capacity and high reparability [4.5]. Furthermore, employing bolted circular steel tubes is conducive to further enhancing the self-centering capacity of resilient columns, especially when deformed to large drift angle.

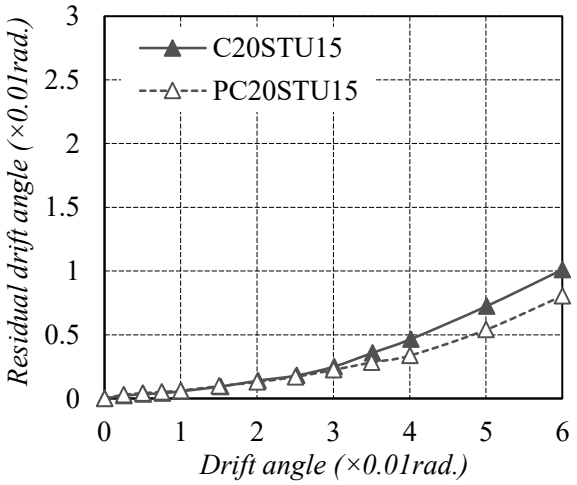

(n=0.20, confinement by bolted tube)

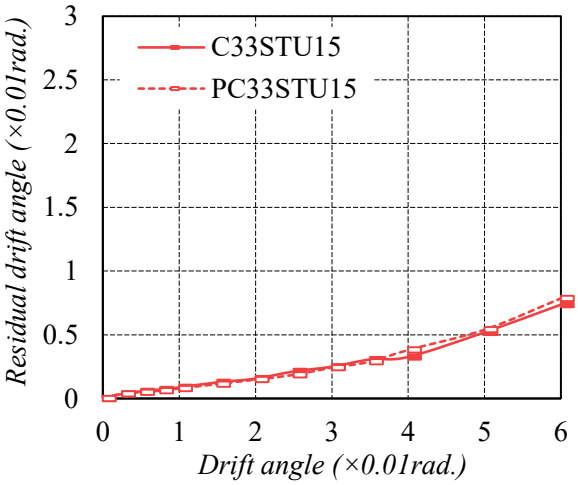

(n=0.33, confinement by bolted tube)

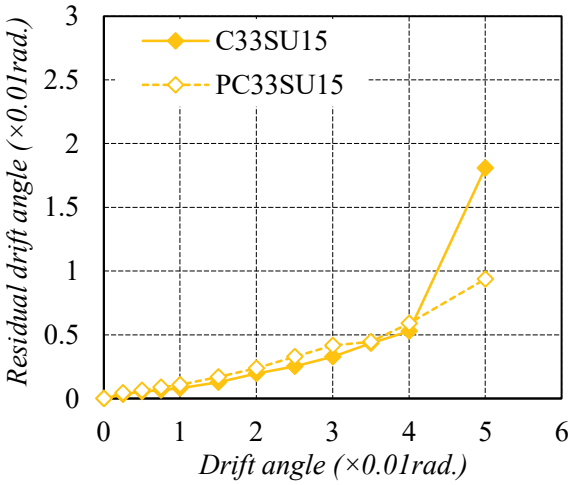

(n=0.33, confinement by D6 hoops)

(a) The effect of construction method (cast-in-place, prefabrication)

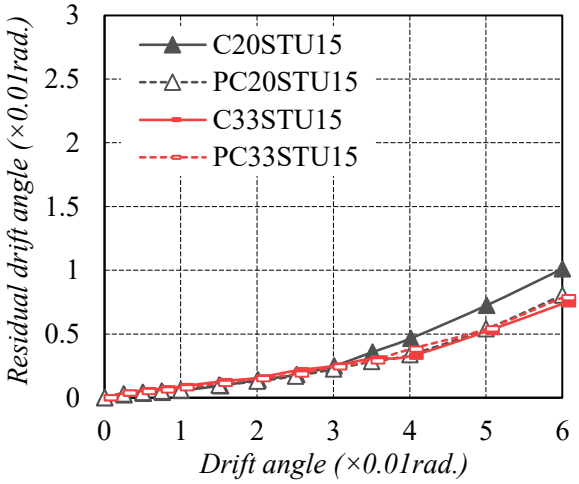

(b) The effect of axial load ratio (0.20, 0.33)

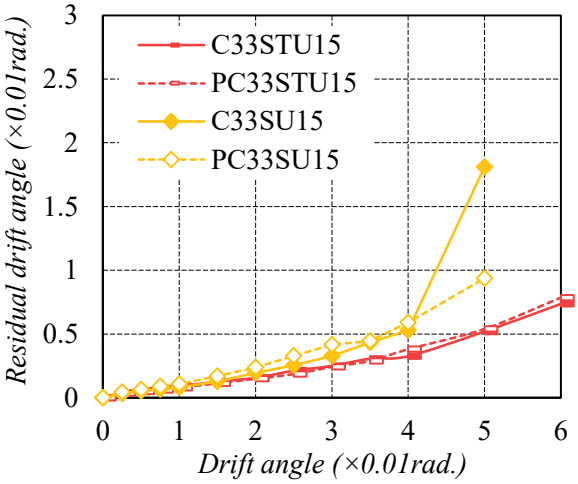

(c) The effect of confinement method (bolted tube, D6 hoops)

Fig. 4-14 Comparison of residual drift angle

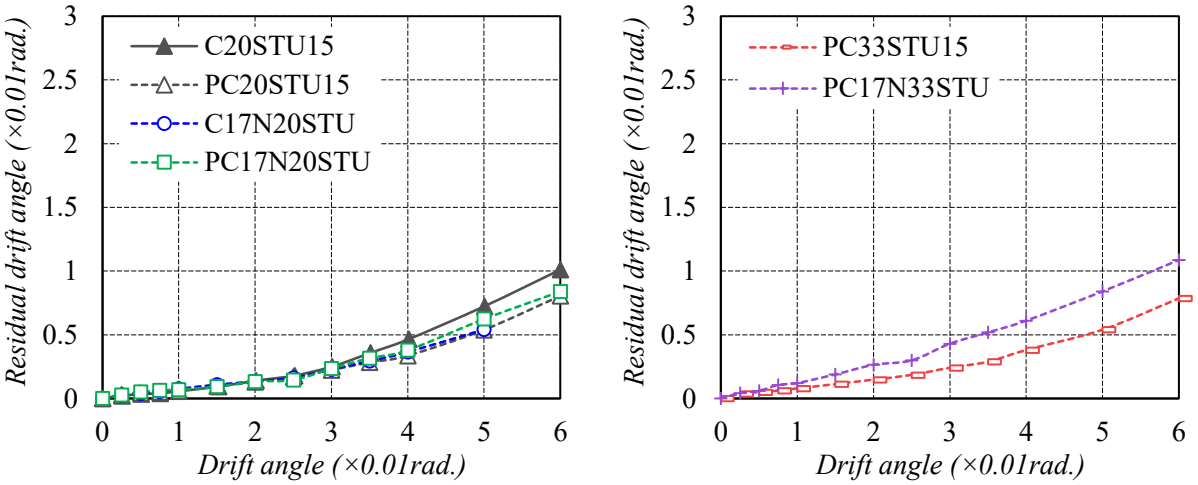

(n=0.20) (n=0.33)

(d) The effect of steel amount of WBUHS rebar (1.41%, 1.92%)

Fig. 4-14 Continued

4.3.5 Energy Dissipation Capacity

According to the calculation method proposed by Chopra [4.6], the obtained equivalent viscous damping coefficient (h_{eq}) was compared in Fig. 4-15. It can be found from Fig. 4-15 that the influence of the construction method or the steel amount of WBUHS rebar on the equivalent viscous damping coefficient appears to be negligible. Although there is a slight rise in the equivalent viscous damping coefficient owing to a higher axial compression, the improvement effect is limited. In contrast, the equivalent viscous damping coefficient of the specimens confined only by hoops is slightly higher, and increases significantly from 0.04 rad drift angle onward, showing better energy dissipation capacity but at the expense of severe concrete damage and substantial plastic deformation. Overall, the development trend of the equivalent viscous damping coefficient remains stable and approaches a constant value. This observation suggests that concrete columns reinforced with WBUHS rebar exhibit nonlinear elastic behavior.

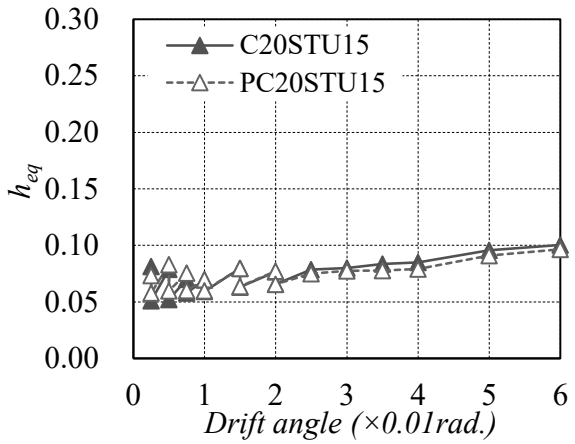

(n=0.20, confinement by bolted tube)

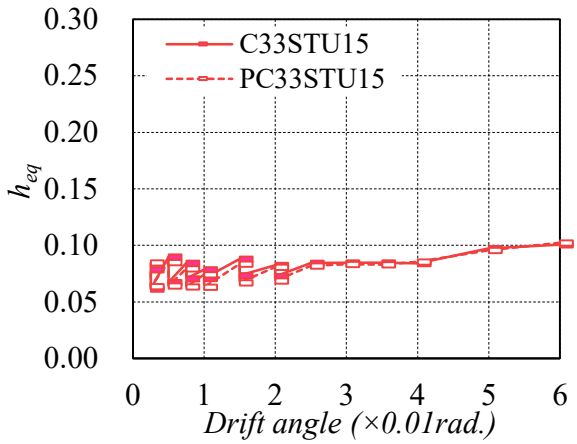

(n=0.33, confinement by bolted tube)

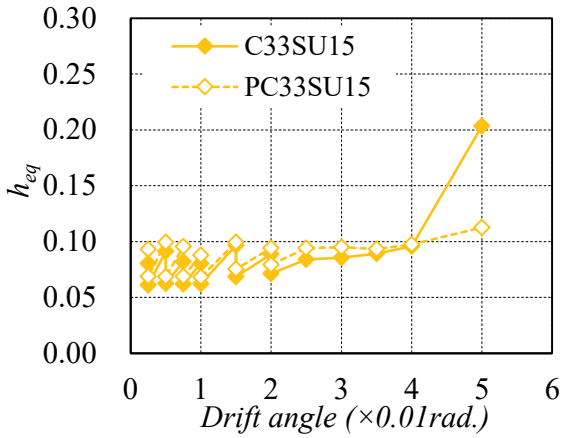

(n=0.33, confinement by D6 hoops)

(a) The effect of construction method (cast-in-place, prefabrication)

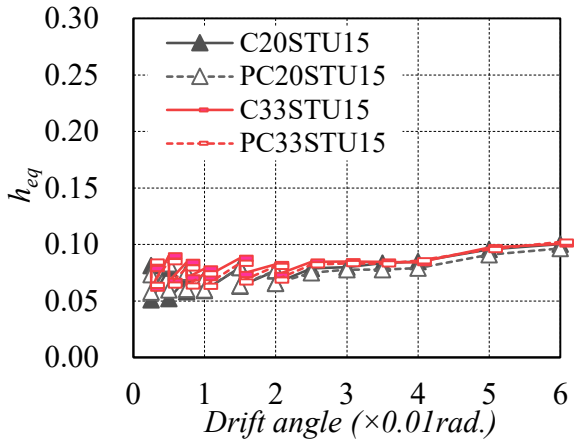

(b) The effect of axial load ratio (0.20, 0.33)

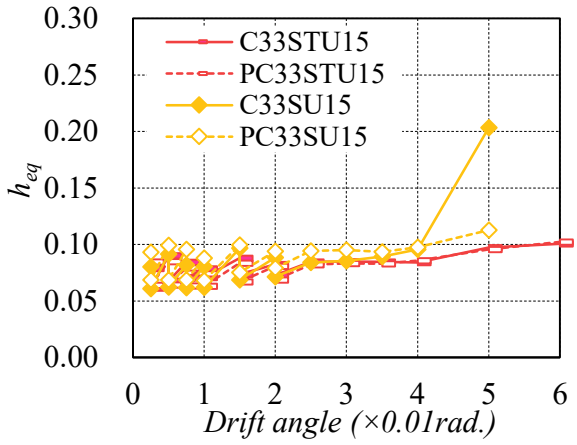

(c) The effect of confinement method (bolted tube, D6 hoops)

Fig. 4-15 Comparison of equivalent viscous damping coefficient (h_{eq})

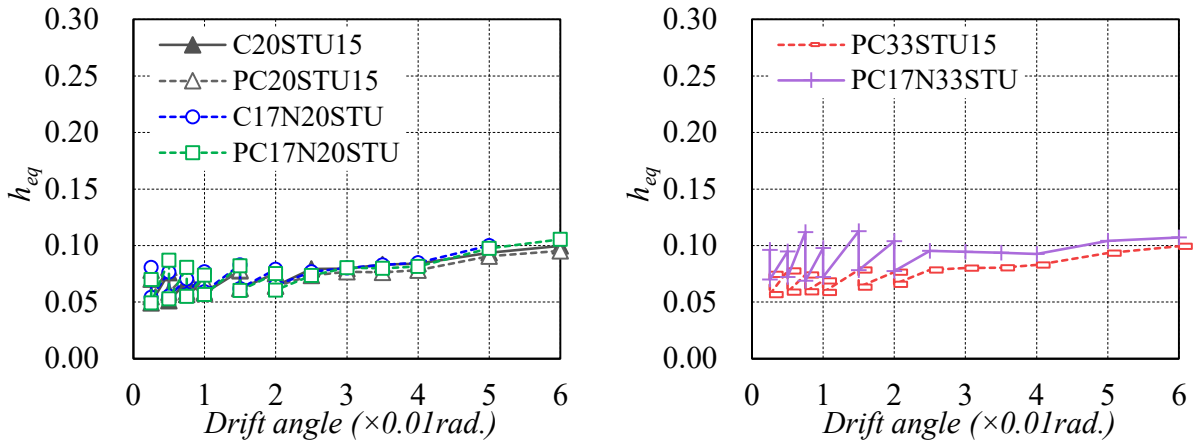

(d) The effect of steel amount of WBUHS rebar (1.41%, 1.92%)

Fig. 4-15 Continued

4.3.6 Axial Strain

The axial deformation between the footing and loading stub was measured by averaging the readings from four vertical DTs (3-6) (see Fig. 4-5), as shown in Fig. 4-16. When each cycle was unloaded to the drift angle of 0 rad., the corresponding axial strain was depicted in Fig. 4-17, obtained by calculating the ratio of measured axial deformation to the distance (310mm) between the footing and loading stub.

On the one hand, the axial deformation of the test specimens under a low axial compression level (n=0.20) remained a very low level and did not diverge as the drift angle increased. For up to a drift angle of 0.04rad., the maximum value of axial deformation could be kept below 0.32mm, to give an axial strain of only 0.1%. Although the test columns subjected to higher axial compression (n=0.33) performed increasing axial deformation along with lateral deformation because of the slightly larger depth of compression zone and concrete damage, the maximum axial deformation and the corresponding axial strain were respectively controlled within 0.68mm and 0.22% − far below the peak strain and ultimate strain of confined concrete [4.7]. On the other hand, as compared with specimens confined by bolted circular steel tube, a noticeable increase in axial deformation was observed in specimen PC33SU15, which was confined by hoops only. As the drift angle increased to 0.04 rad., the axial deformation reached 1.16mm, to give an axial strain of 0.36%. In the case of specimen C33SU15, the axial deformation did not exceed 0.63mm, but then, showed a significant increasing trend and reached 0.83mm at 0.04 rad. drift angle, to give an axial strain of 0.27%. For the test columns

without confinement of steel tube, the larger axial deformation was caused by serious concrete damage. When deformed to the drift angle of as large as 0.04rad., the average axial strain was close to the ultimate compressive capacity of plain concrete, which foreshadowed the degradation of lateral resistant capacity in subsequent loading.

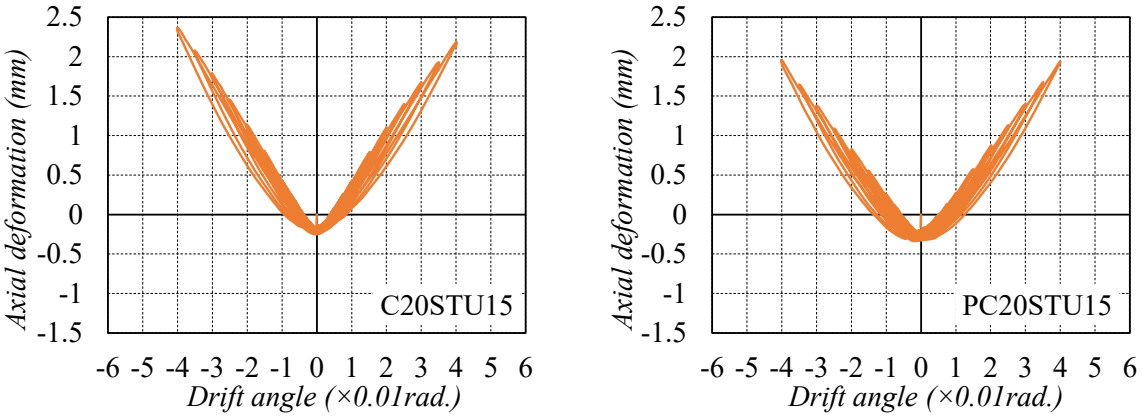

(n=0.20, confinement by bolted tube)

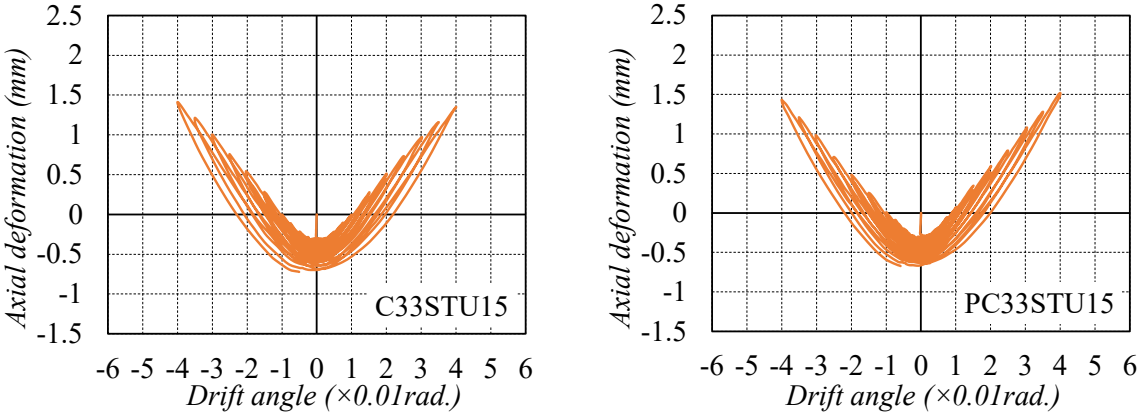

(n=0.33, confinement by bolted tube)

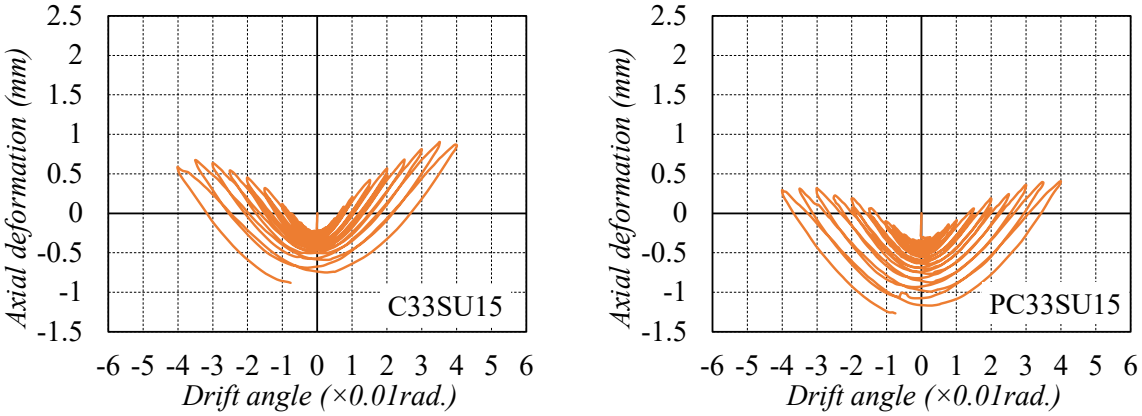

(n=0.33, confinement by D6 hoops)

Fig. 4-16 Measured axial deformation

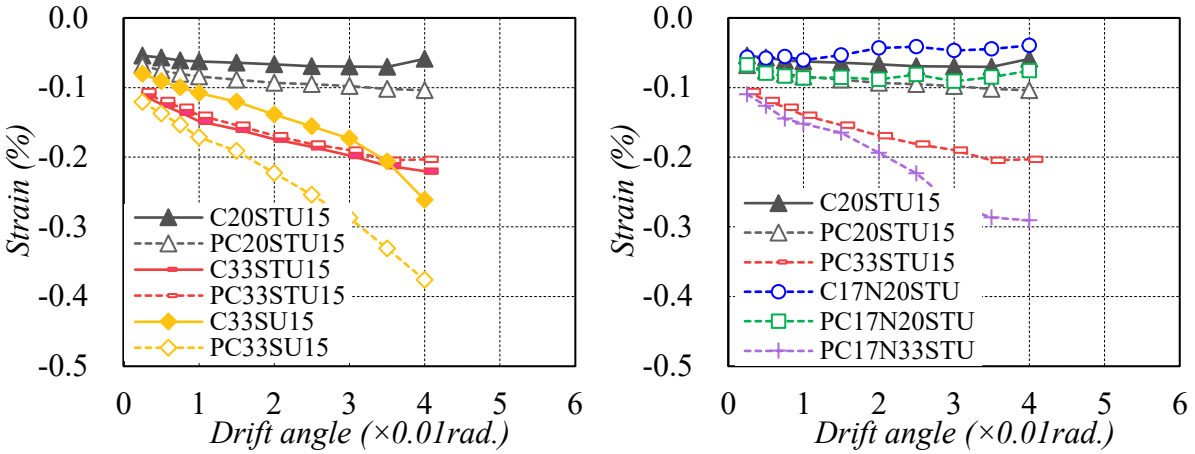

Fig. 4-17 Comparison of axial strain

4.4 Conclusions

To quantitatively analyze the influence of steel ratio of WBUHS rebar and confinement of bolted circular steel tube on the seismic performance of WBUHS rebar-reinforced circular concrete columns, both cast-in-place and precast, six concrete columns reinforced with large-diameter WBUHS rebars, including four specimens confined by bolted steel tubes and two specimens confined only by circular hoops, were made and tested under reversed cyclic lateral loading while subjected to constant axial compression. Based on the test results discussed in this chapter, the main conclusions are made as follows:

1) Squarely-arranged WBUHS rebars could provide high drift-hardening capacity for circular concrete columns confined by hoops until a drift level of 0.04 rad. However, after that drift angles, the lateral resisting capacity of hooped circular columns started to decrease due to serious concrete damage. On the other hand, the use of bolted circular steel tubes to confine the column could not only effectively reduce concrete damage but also significantly enhance the drift-hardening capacity of circular columns up to the drift angle of at least 0.06 rad., implying high confinement efficiency of the bolted steel tubes.

2) Providing a 20d anchorage length even for large-diameter WBUHS bars allowed the precast circular columns to demonstrate nearly the same excellent seismic performance as the cast-in-place ones in terms of drift-hardening capability and self-centering capacity. It is particularly noteworthy that increase the steel amount of WBUHS rebars could enhance the lateral resistance of the circular concrete columns without reducing their deformation capacity.

3) Increasing the axial compression level, the steel amount of WBUHS rebar, or utilizing steel tube confinement could effectively improve the lateral bearing capacity. In particular, confinement by bolted thin steel tubes showed the most significant improvement effect, with lateral force and bending moment resistance increased by up to 48.1% and 40.5% for drift angles within 0.05rad, respectively.

4) The residual deformation increased gradually along with the lateral deformation, but could be restrained below 0.005rad. (1/12−1/8 of the transient drift angle) when deformed to a drift angle of 0.04 rad., suggesting that the proposed circular columns have good reparability. Besides, the usage of bolted steel tube was also beneficial to reduce the residual deformation due to the strong confinement of the steel tubes.

References

[4.1] Sargsyan G., Cai G., Takeuchi T., et al. Seismic behavior and assessment of drift-hardening concrete columns. 16th World Conference on Earthquake Engineering, 2017.

[4.2] Wang J., Takeuchi T., Koyama T., et al. Seismic behavior of circular fly ash concrete columns reinforced by ultra high strength rebar and steel plates. Proceedings of the Japan Concrete Institute, 2014, 36(2): 115-120.

[4.3] Luo J., Yuan S., Zhao J., et al. Seismic Behavior of Concrete Columns Reinforced with Weakly Bonded Ultra-High Strength Rebars and Confined by Steel Tubes. Materials. 2023, 16(21):6868.

[4.4] Li G., Kanao M., Sun Y. Seismic Behavior of Square Spiral-confined Concrete Columns with Circularly Arranged SBPDN Bars (Part 2 Results and Discussions). AIJ, 2023, 123-124.

[4.5] Zhang J., Liu X., Liu J., et al. Seismic performance and reparability assessment of recycled aggregate concrete columns with ultra-high-strength steel bars, Engineering Structures, 277:115426, 2023.

[4.6] Chopra, A.K. Dynamics of Structure: Theory and Applications to Earthquake Engineering; Prentice-Hall: Upper Saddle River, NJ, USA, 1995.

[4.7] Sun, Y.P.; Sakino, K. Simplified design method for ultimate capacities of circularly confined high-strength concrete columns. ACI Spec. Publ, 193, 571–586, 2000.

CHAPTER FIVE

5 Analytical Method to Evaluate Hysteretic Behavior of Concrete Columns Confined by Bolted Circular Steel Tube

5.1 Introduction

The low bond strength (about 3 N/mm^2) of WBUHS rebar makes it easy to slip between the concrete and the reinforcements [5.1]. This slippage is conducive to the strain transfer of WBUHS rebar along column height and the avoidance of strain concentration in plastic hinge zone, so that the concrete column reinforced with WBUHS rebars can exhibit significant drift-hardening capacity and self-centering capacity [5.2-5.4]. The experimental results presented in chapters three and four confirmed that the strain distribution of WBUHS rebar along column height was relatively dispersed when compared to NS rebar. Moreover, even as the drift angle increased to as large as 0.04 rad., the strain in WBUHS rebar in the resilient concrete columns developed in this study were hard or even failed to yield. Consequently, the traditional analysis methods ignoring the slippage of longitudinal rebars will probably not give accurate prediction of the hysteresis performance of resilient concrete members reinforced by WBUHS rebars and a reliable and feasible analysis method appropriate for resilient columns reinforced with WBUHS rebar is urgently needed.

To this end, this paper adopted a finite spring element (FSE) method originally proposed by Sun et al. [5.5] to assess the hysteretic behavior of WBUHS rebar-reinforced concrete columns, in which both the slippage of WBUHS rebars and the confinement effect of hoops or/and bolted steel tubes on concrete can be taken into account. The main objectives of this chapter are: 1) to evaluate the hysteretic performance of the circular concrete columns reinforced by squarely-arranged WBUHS rebars and externally confined by bolted circular steel tubes by the FSE method, where the influence of the discontinuity of the bolted tube on confinement effect will be considered, and 2) to validate the applicability and accuracy of the FSE method by comparing analytical and experimental results in terms of hysteresis loop, strain of longitudinal rebar and equivalent viscous damping coefficient.

5.2 Stress-strain Models of the Used Materials and Analytical Method

The selection of appropriate material models is crucial for analysis methods as they provide reliable and precise descriptions of the behavior of engineering structures. By choosing suitable material models, the response of structures under various experiment parameter can be more precisely predicted, which is essential for ensuring the safety, stability, and reliability of structures and helping to better understand and optimize the structural performance. In this paper, three models are highlighted and used for numerical analysis.

5.2.1 Stress-strain Model for Confined Concrete

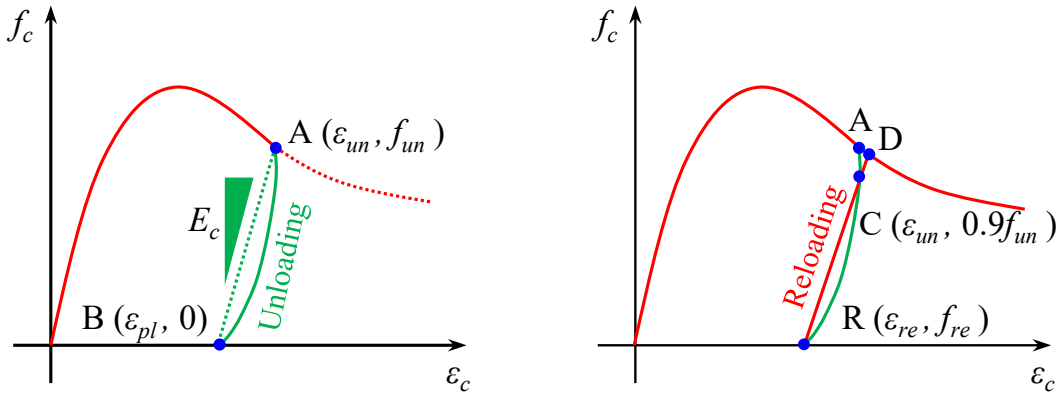

Fig. 5-1 Complete stress-strain curve of the confined concrete under compression

The cyclic rules (both unloading and reloading) outlined in the stress-strain model proposed by Sun et al. [5.6] were adopted to serve the subsequent numerical analysis, as shown in Fig. 5-1. During the unloading phase at point A (ε_{un}, f_{un}), it is presumed that the curve follows a parabolic path, reaching its apex at point B (ε_{pl}, 0) in which the tangential stiffness becomes zero. The reloading phrase in the curves is considered as a linear connection between the reloading point R (ε_{re}, f_{re}) and point C (ε_{un}, 0.9f_{un}) (see Fig. 5-1).

The unloading and reloading model described above is characterized by its simplicity and effectiveness in capturing the cyclic behavior of confined concrete. At point A, where unloading initiates, the parabolic shape of the unloading curve provides a realistic representation of the stress-strain response, taking into account the peak point B and subsequent reloading phase. The reloading curve, represented by a straight line, establishes a

connection between the reloading points R and C, intuitively and effectively simulating the reloading process.

With these assumptions, the unloading process (AB curve) and reloading process (BD curve) can be precisely delineated using Eqs. (5.1)–(5.2).

$$f_c = \begin{cases} f_{un} \cdot \left(\frac{\varepsilon_c - \varepsilon_{pl}}{\varepsilon_{un} - \varepsilon_{pl}}\right)^2 & unloading \\ f_{re} + \left(\frac{0.9f_{un} - f_{re}}{\varepsilon_{un} - \varepsilon_{re}}\right)(\varepsilon_c - \varepsilon_{re}) & reloading \end{cases} \quad (5.1)$$

$$\varepsilon_{pl} = \varepsilon_{un} - \frac{f_{un}}{E_c} \quad (5.2)$$

Where, ε_{pl} represents the plastic residual strain after unloading, and can be defined as the abscissa at the point where a straight line with a slope of E_c intersects the strain axis from point A, and its value can be determined based on the Eq. (5.2).

5.2.2 Stress-strain Model of WBUHS Rebar

Given the absence of a significant yield plateau in the stress-strain relations of WBUHS rebars, the stress-strain model developed by Fukuhara et al. [5.7] is chosen for the following analysis to describe the envelope of the stress-strain relations of WBUHS rebars. The stress-strain model is derived from the renowned Menegotto-Pinto model [5.8] and has been modified based on the test results of WBUHS bars to enhance the accuracy and reliability of the stress-strain predictions for the WBUHS rebars. Fig. 5-2 visually illustrates the distinctive features of the envelope curves, capturing the material's response with the initial elastic modulus, the tangent at the peak point, and the asymptotic behavior beyond. This ensures that the stress-strain model aligns closely with the observed behavior of WBUHS rebars, providing a robust foundation for subsequent analyses.

Notably, this curve exhibits two asymptotic linear trends, specifically showcasing an initial elastic modulus E_s and a tangential line at peak point characterized by a slope $E_t = Q \cdot E_s$. The mathematical formulation governing the curves can be expressed by Eqs. (5.3)−(5.6).

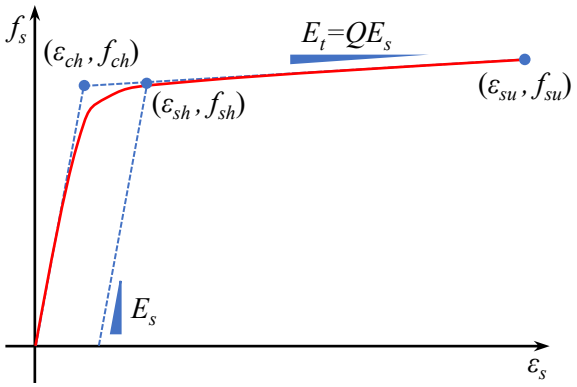

Fig. 5-2 Outline of envelope curve for the stress-strain model of WBUHS rebars

$$f_s = E_s \cdot \varepsilon_s \cdot \left\{ Q + \frac{1-Q}{[1+(\varepsilon_s/\varepsilon_{ch})^N]^{1/N}} \right\} \tag{5.3}$$

$$Q = 0.1(\varepsilon_{su})^{-2.5} \tag{5.4}$$

$$\varepsilon_{ch} = \frac{f_u - Q \cdot E_s \cdot \varepsilon_{su}}{E_s \cdot (1-Q)} \tag{5.5}$$

$$N = 3 \tag{5.6}$$

Where, f_s and ε_s denote the stress and strain of WBUHS rebars; f_{su} and ε_{su} represent the ultimate stress and strain of WBUHS rebars; E_s and E_t are the elasticity modulus and tangential stiffness, respectively; ε_{ch} denotes the characteristic strain (see Fig. 5-3); N represents the curvature coefficient; Q signifies the ratio between the tangential stiffness and initial stiffness.

There are three cases involving the unloading and/or reloading, as depicted in Fig. 5-3 and as described below.

(1) In the case of unloading or reloading at point A on the envelope of stress-strain curve: the target point C is positioned on the reversed envelope curves with the origin at point (ε_{mo},0). Assuming that the absolute strain ε_{ss} at point C is the same as the maximum strain experienced in the initial direction.
(2) In the case of reloading from point D at the unloading curve: point A is considered as a target point, serving as a starting point for the preceding unloading curve.
(3) In the case of unloading from point E on the reloading curve: the starting point D on the preceding reloading curve is regarded to be the target point.

This approach allows for a detailed analysis of the mechanical behavior of WBUHS rebars under different loading conditions, facilitating a comprehensive understanding of the cyclic characteristics and aiding in the accurate prediction of stress and strain levels throughout the loading history. The defined rules for unloading and reloading ensure consistency and reliability in the modeling of the material's response in various situations.

Once the strains of both the starting point and the target point are determined, the unloading and/or reloading curves can be precisely defined using the Menegotto-Pinto function. This function effectively captures the cyclic behavior of the material during unloading and reloading processes, providing a comprehensive representation of the stress-strain response in each scenario, as specified in Eqs. (5.7)–(5.8).

$$\frac{f_s - f_0}{\varepsilon_s - \varepsilon_0} = E_s \cdot \left\{ Q_1 + \frac{1 - Q_1}{\left[1 + \left(\frac{\varepsilon_s - \varepsilon_0}{\varepsilon_{ch1} - \varepsilon_0}\right)^{N_1}\right]^{1/N_1}} \right\} \tag{5.7}$$

$$N_1 = \begin{cases} 3.0 & \varepsilon_b < 0 \\ 3.0 - 18\varepsilon_b & \varepsilon_b \geq 0 \end{cases} \tag{5.8}$$

Where, Q_1 represents the ratio of tangent stiffness at ending point to the tangential stiffness at starting point (equivalent to the initial elastic modulus); ε_b denotes the strain at the endpoint, and can be defined as positive during a tensile situation; N_1 is the curvature coefficient, which can be calculated from the empirical formula developed by Fukuhara and Sun [5.9].

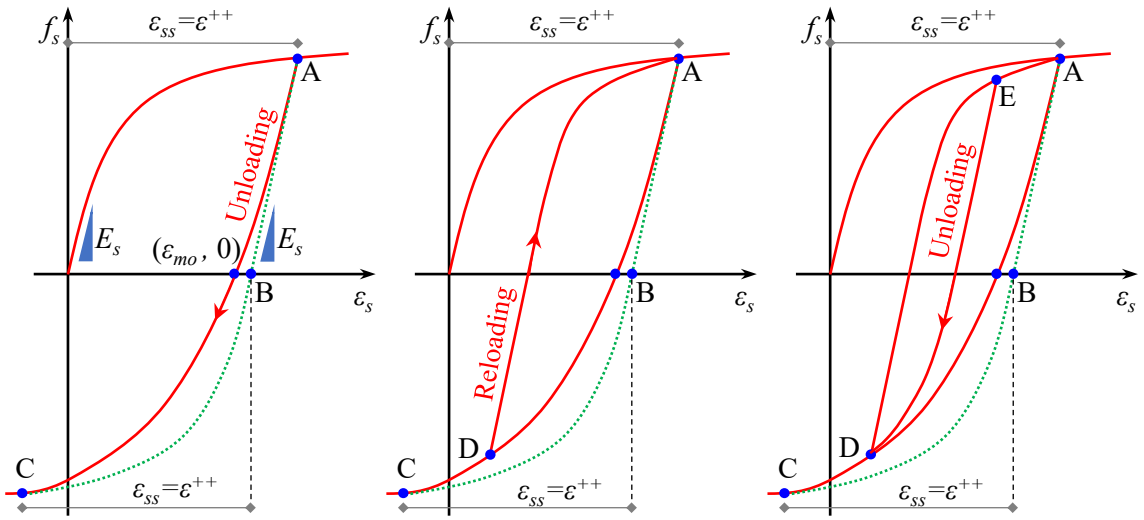

Fig. 5-3 Unloading and reloading rules for stress-strain curve of WBUHS rebars

5.2.3 Bond-slip Model of WBUHS Rebar

As for the WBUHS rebar utilized in this study, its surface feature−spiral groove, endows it with lower bond strength (approximately 3 kN/mm^2 for the unconfined concrete with compression strength of 40 kN/mm^2), implying that the WBUHS rebar is prone to relative slippage with concrete. Therefore, establishing a suitable bond slip model for the WBUHS rebar becomes essential for accurately evaluating the hysteretic behavior of resilient concrete columns reinforced by WBUHS rebars.

According to the tests conducted on the bond performance between concrete and WBUHS rebars, Funato et al. [5.1] proposed a model to capture the slippage of WBUHS rebars, hereafter referred to as the Funato model. The accuracy of this model has been verified through comparing with the experimental results, serving as a valuable tool in understanding and predicting the bond-slip behavior of WBUHS rebars. By incorporating experimental data, it offers a practical and reliable representation of the bond characteristics specific to WBUHS rebars. The presented envelope curve and rules for unloading and reloading contribute to the comprehensive modeling of the bond-slip response, ensuring a more accurate assessment of the overall behavior of resilient concrete columns reinforced by WBUHS rebars. The envelope curve of Funato model is illustrated in Fig. 5-4, highlighting the coordinates of key points. Additionally, the cyclic rules of bond stress–slip behavior of WBUHS rebar are presented in Fig. 5-5.

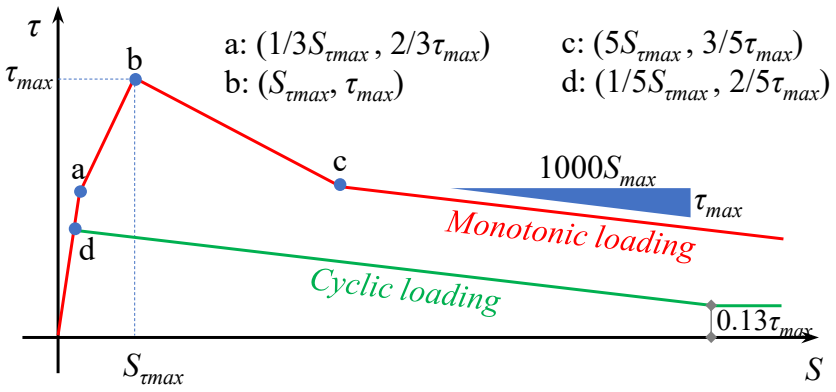

Fig. 5-4 The envelope curves of bond stress-slip relationship of WBUHS rebar

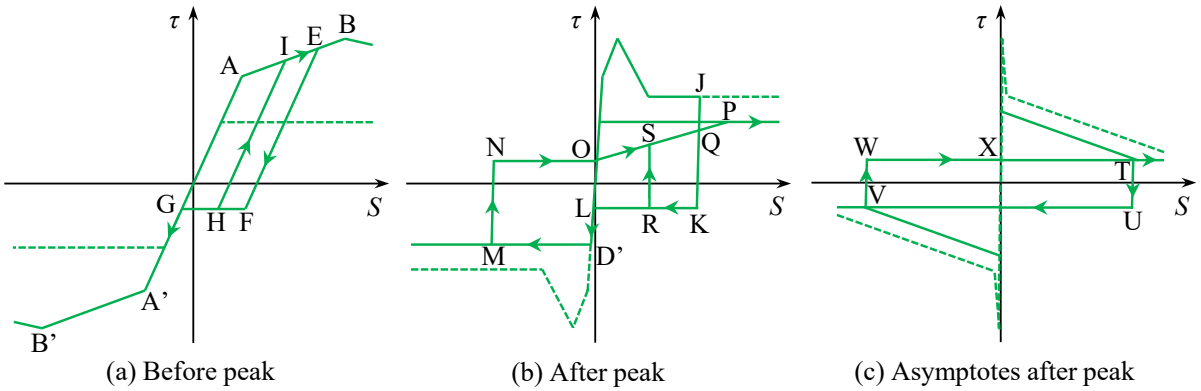

(a) Before peak (b) After peak (c) Asymptotes after peak

Fig. 5-5 Unloading and/or reloading bond stress – slip curves of WBUHS rebar

5.2.4 Analytical Assumptions and Procedures

In the FSE method, the basic assumptions can be made as follows:

1) Only WBUHS rebars withstand tensile stress in the tensile area;
2) Only the concrete part of the section maintains plane after bending;
3) The constitutive laws for WBUHS rebars conform to modified Menegotto and Pinto model [5.8];
4) The constitutive laws of confined concrete follow the Sakino-Sun model [5.6]. According to the experimental results discussed in chapter two of this thesis, when applying Sakino-Sun model, the strength enhancement ratio K for concrete confined by the bolted circular steel tubes is taken as 0.49 times the K value calculated in the original model, which is to take into account of effect of the discontinuity of bolted thin steel tubes;
5) The bond-slip relationship of WBUHS rebar conforms to the Funato model [5.1];
6) The lateral deformation of the test columns concentrates in the plastic hinge region with a length of 1.0D (D denotes the diameter of section), within which the strain and stress of WBUHS rebars are distributed uniformly.

The schematic diagram of section division and strain distribution are illustrated in Fig. 5-6 and Fig. 5-7, respectively. The detailed flow chart of the FSE method is presented in Fig. 5-8, and the analysis procedure is summarized in the following steps.

1) Divide the column into three regions and discretize the joint and rocking region equally into tiny segments (see Fig. 5-6).

2) Give an initial concrete strain ε_o at section's center, then obtain the strain distribution of concrete ε_c along the depth of section (see Fig. 5-8) based on Eq. (5.9).

$$\varphi = \frac{R}{l_h \cdot (1 - l_h/2a)} \tag{5.9}$$

where φ is the sectional curvature in the hinge region; R denotes the drift ratio; l_h represents the height of the hinge region; a is the shear span.

3) Give an initial slip S_0 (=S_J) of the WBUHS rebar in the first segment of the joint region. According to the relationships between the stress (f_{k+1}) and slip (S_{k+1}) listed by Eqs. (5.10)–(5.11), it is necessary to judge whether the boundary condition (see Eq. (5.12)) is satisfied, if not, regive a f_0 and S_0 and repeat this process until S_{n+1}=0 is satisfied. Then the strain of WBUHS rebar ε_s can be obtained from the constitutive law.

$$f_{k+1} = f_k - \tau_k \cdot \frac{4l}{d} \tag{5.10}$$

$$S_{k+1} = S_k - \varepsilon_{k+1} \cdot l \tag{5.11}$$

$$S_{n+1} = 0 \tag{5.12}$$

where f_k and f_{k+1} represent the stress of WBUHS rebar in the *k-th* segment and *k+1-th* segment, respectively; S_k, S_{k+1} and S_{n+1} represent the slip of WBUHS rebar in the *k-th*, *k+1-th* and *n+1-th* segment, respectively; τ_k is the bond stress in the *k-th* segment; l represents the length of each segment; d is the diameter of WBUHS rebar.

4) Calculate the slip S_0 (=S_R) of the WBUHS rebar in the first segment of the rocking region based on Eq. (5.13). And the stress f_0 (=f_R) of the rebar in the first segment of the rocking region can be computed by the same procedure shown in step (3).

$$S_R = (\varepsilon_c - \varepsilon_s) \cdot l_h - S_J \tag{5.13}$$

where S_R and S_J represent the slip of the WBUHS rebar in the rocking and jointing region, respectively; ε_s and ε_c represent the strain of WBUHS rebar and concrete in the hinge region, respectively.

5) Obtain the target value of strain and stress of the WBUHS rebar assumed in step (3) by repeating steps (3)–(4) until f_J=f_R was satisfied.

6) Calculate the force F_c and F_s borne by concrete and WBUHS rebar.

7) Verify whether $N=F_c+F_s$ was satisfied. If not, re-assign a new center strain ε_o and repeat the processes from step (2).
8) Calculate lateral force V based on Eqs. (5.14)–(5.15).

$$M = \sum f_s \cdot A_s \cdot h_s + \sum f_c \cdot A_c \cdot h_c \tag{5.14}$$

$$V = \frac{M}{a} - N \cdot R \tag{5.15}$$

where f_s and f_c represent the stress of WBUHS rebar and concrete, respectively; A_s and A_c represent the area of WBUHS rebar and concrete, respectively; h_s and h_c represent the distance from the acting point of force borne by WBUHS rebar and concrete to the neutral axis, respectively; N represents the applied axial force.

9) Repeat the above steps until the target R.

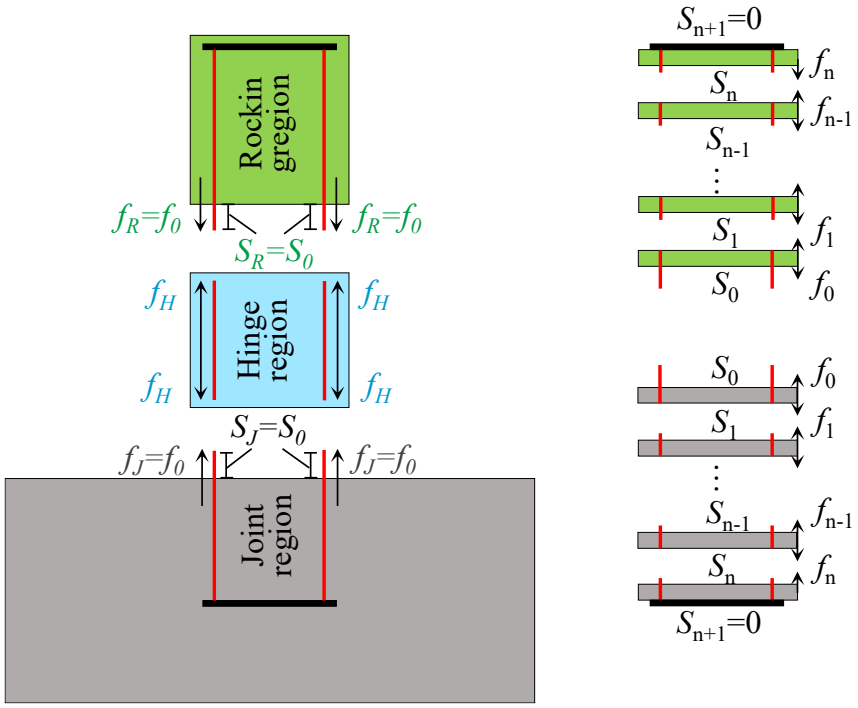

Fig. 5-6 The schematic diagram of section division

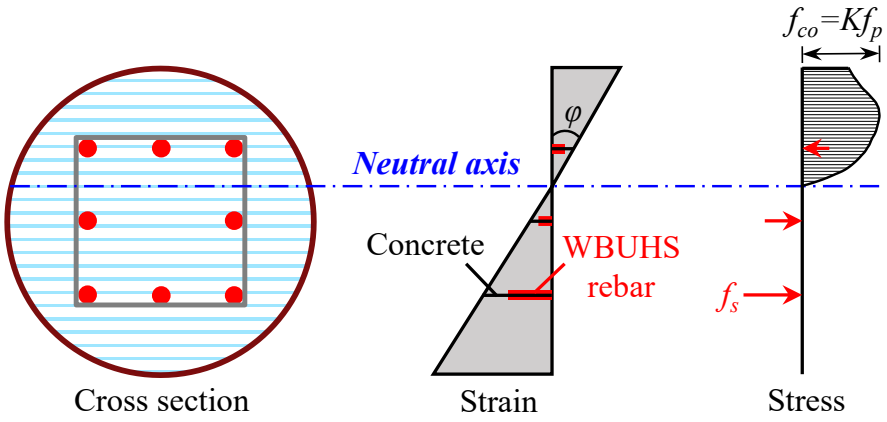

Fig. 5-7 Schematic diagram of strain and stress distribution

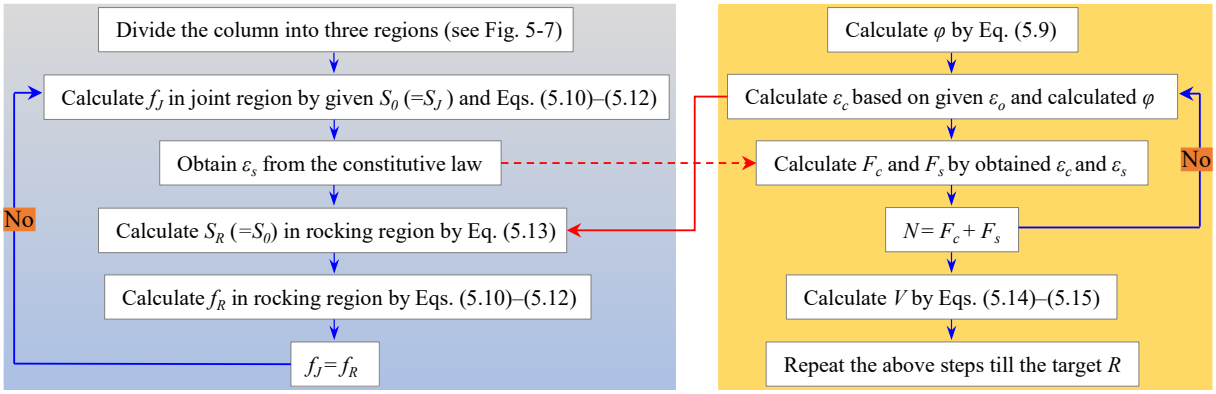

Fig. 5-8 Detailed flow chart of the FSE method

5.3 Comparison Between the Analytical and Experimental results

To verify the applicability and reliability of the FSE method in assessing the seismic behavior of the developed resilient circular columns, analytical results were compared with the experimental findings presented in chapters three and four. The discussion will focus on three aspects: 1) the hysteresis loop, 2) strain of longitudinal rebars, and 3) equivalent viscous damping coefficients. The experimental results were represented by solid black line, denoted as "*Exp.*", and the analytical results include two cases: one with consideration of the slippage of WBUHS rebar, represented by red dashed line and denoted as "*Anal. (with slip)*" and one without, represented by green dash dot line and denoted as "*Anal. (no slip)*".

5.3.1 Hysteresis Loop

Fig. 5-9 presents the comparison of hysteresis loops between the experimental and analytical results. The hysteresis characteristics between the two analytical results "*Anal. (no slip)*" and "*Anal. (with slip)*" exhibit notable differences. In the analytical result based on the former ("*Anal. (no slip)*"), the lateral force initially increases and then gradually decreases with the increase of the drift angle, displaying plump hysteresis loops and significantly increased residual deformation. This behavior is very similar to that of the traditional ductile concrete columns, so it aligns well with the experimental results of the NS rebar reinforced specimens (C17N20STD and C17N33STD), as shown in Fig. 5-9(d). However, it is contrary to the hysteretic characteristic of the resilient concrete columns reinforced by WBUHS rebars. To be specific, it not only seems to overestimate the residual deformation and energy dissipating capacity but also leads to a substantial overestimation of the lateral resistance of the concrete

columns reinforced with WBUHS rebars by 26.9% − 37.3%, when deformed to the same drift angle.

Comparatively, it is obvious that the analysis result with consideration for the slippage of reinforcements ("*Anal. (with slip)*") is competent to capture the hysteretic behavior of the test specimens reinforced with WBUHS rebars fairly well, characterized by both remarkable drift-hardening capacity and an evident pinching effect. When compared to the experimental results, the maximum load-bearing capacity obtained by considering the bond-slip behavior of WBUHS rebar ("*Anal. (with slip)*") is slightly lower, about 11.4% on average, suggesting that the analysis results, taking into account the bond slip of WBUHS rebar, can safely evaluate the bearing capacity of the drift-hardening specimens reinforced with WBUHS rebar and confined by steel tube.

Additionally, for specimens (C33SU15 and PC33SU15) confined only by transverse hoops, the analytical results (*"Anal. (with slip)"*) gave much more conservative prediction on the lateral resistance as compared to the measured experimental results (*"Exp."*). This discrepancy can be attributed to the neglect of the confinement effect of hoops on the core concrete in the analytical model.

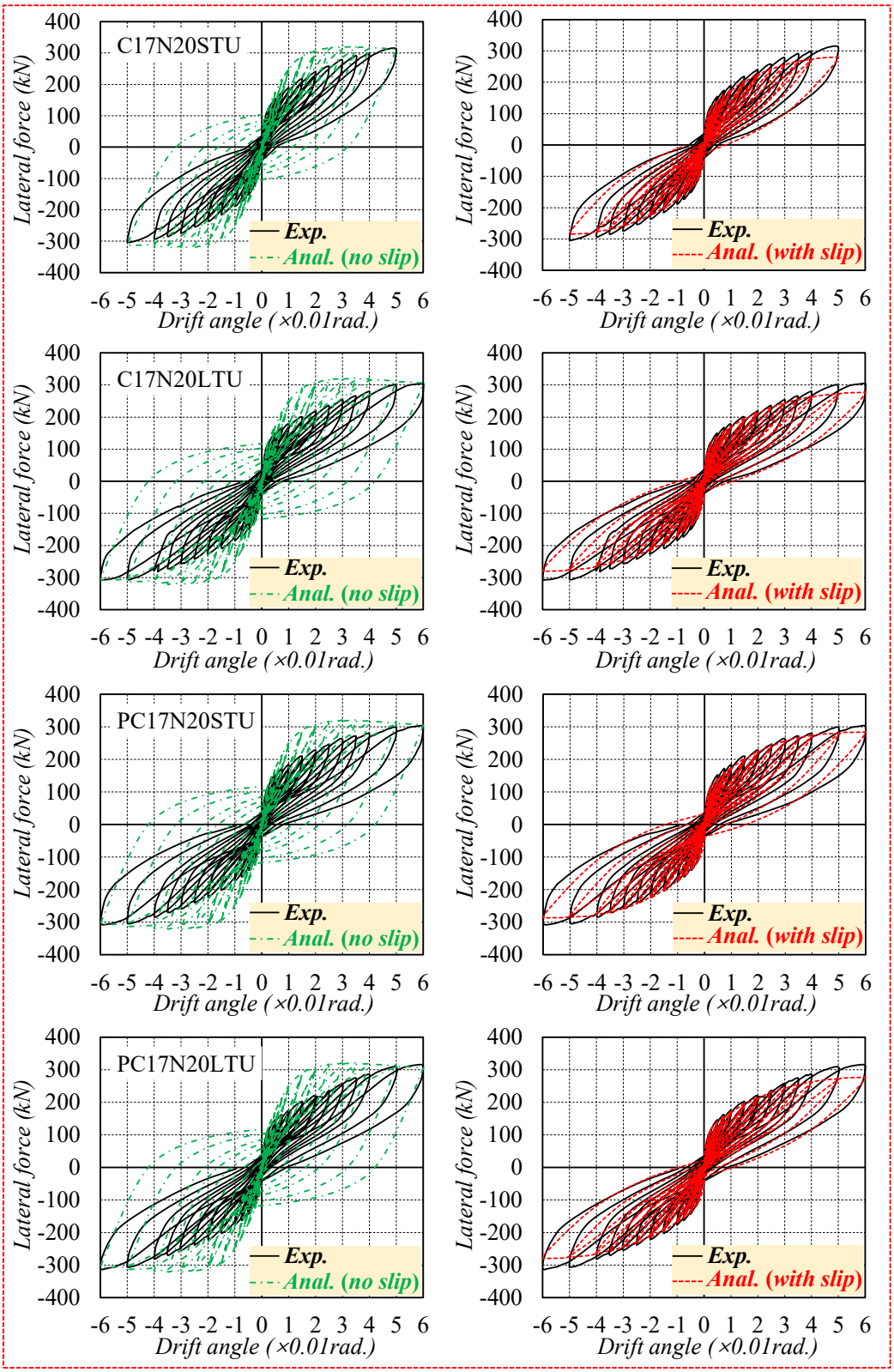

(a) Tubed specimens with a/D=1.7, n=0.20, U12.6 WBUHS rebar

Fig. 5-9 Comparison of the hysteretic loops

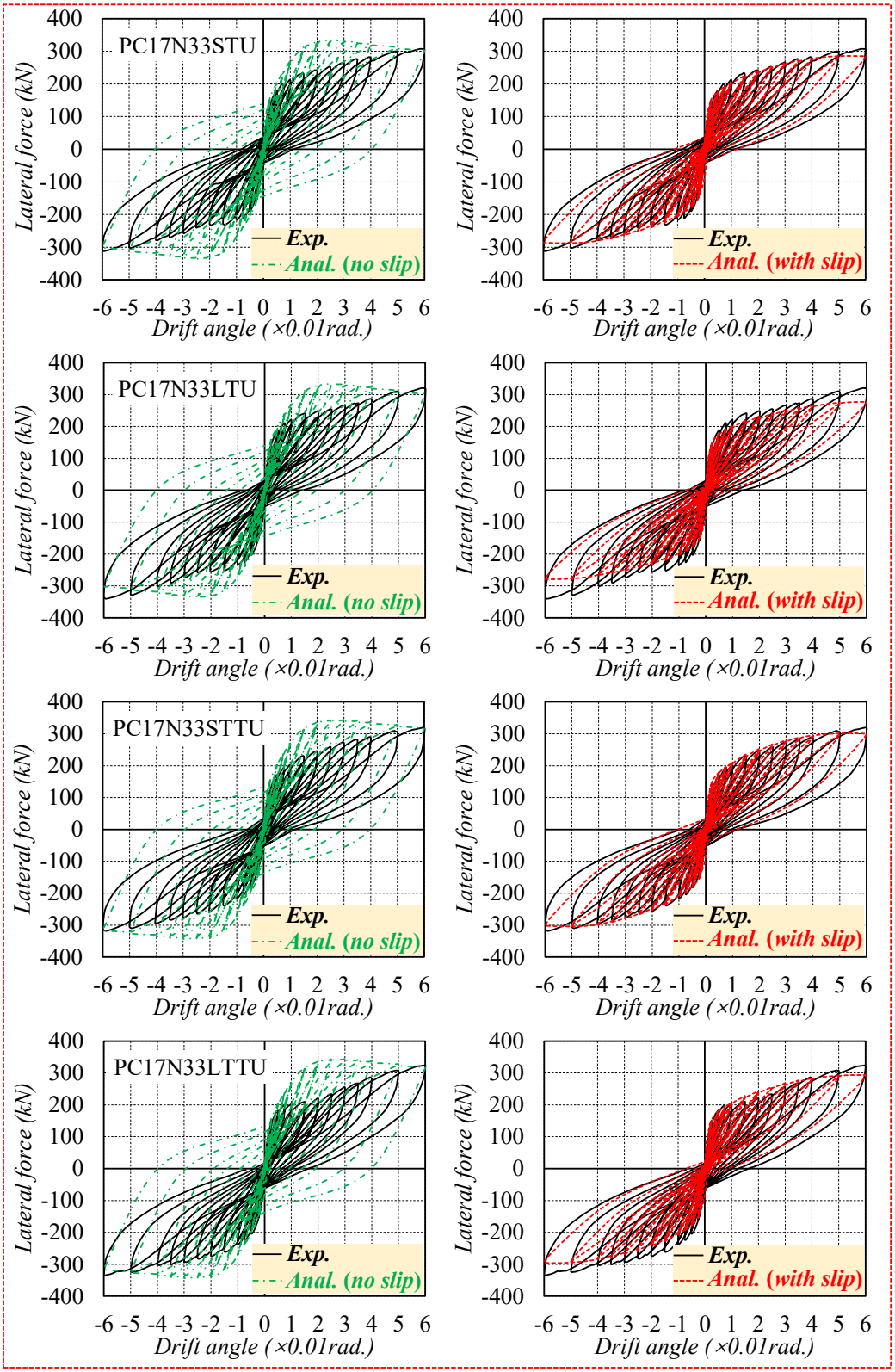

(b) Tubed specimens with a/D=1.7, n=0.33, U12.6 WBUHS rebar

Fig. 5-9 Continued

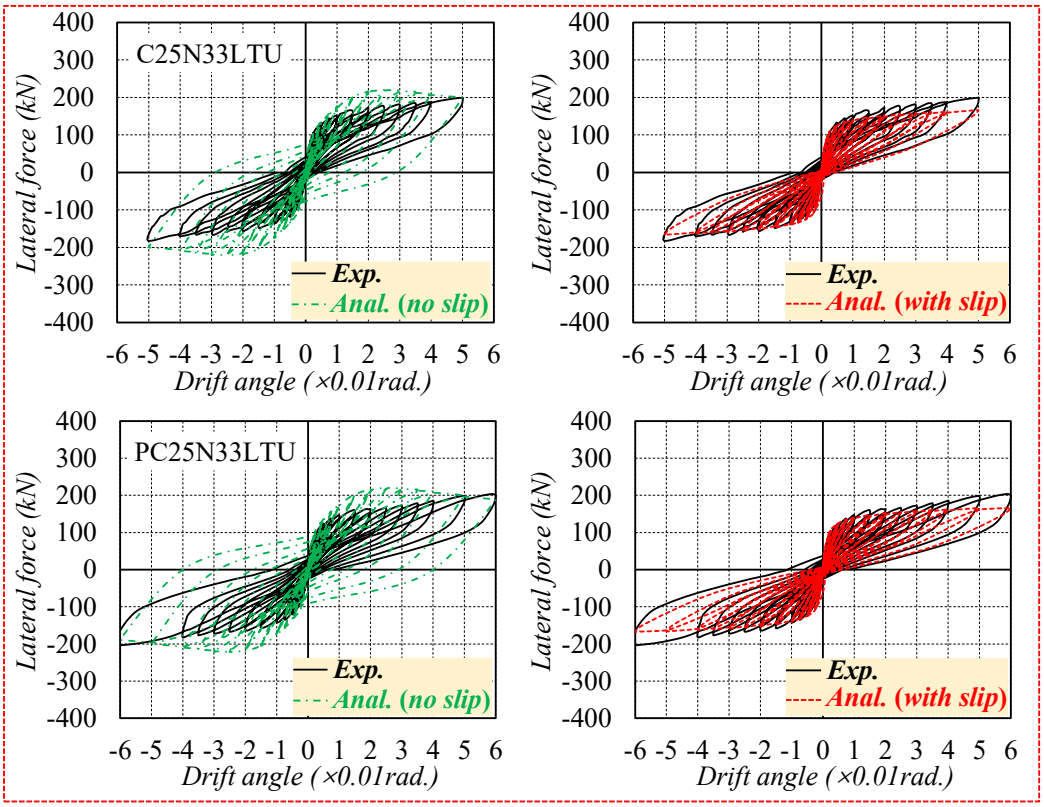

(c) Tubed specimens with a/D=2.5, n=0.33, U12.6 WBUHS rebar

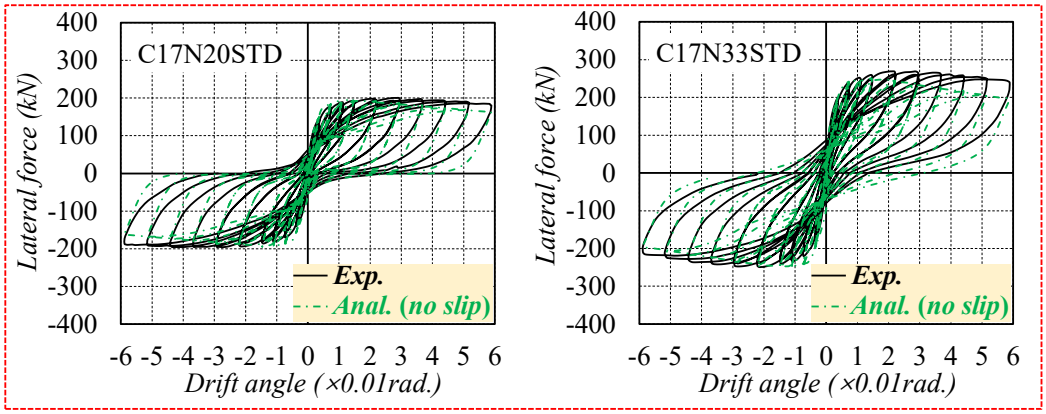

(d) Tubed specimens with a/D=1.7, NS rebar

Fig. 5-9 Continued

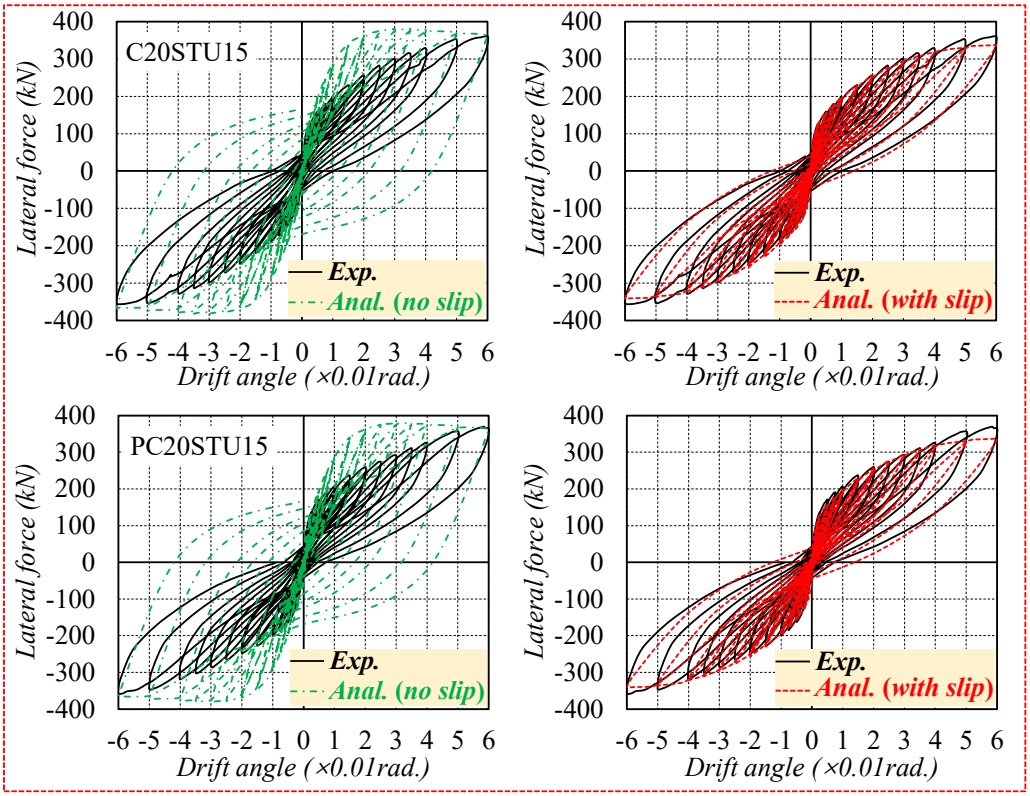

(e) Tubed specimens with a/D=1.7, n=0.20, U15 WBUHS rebar

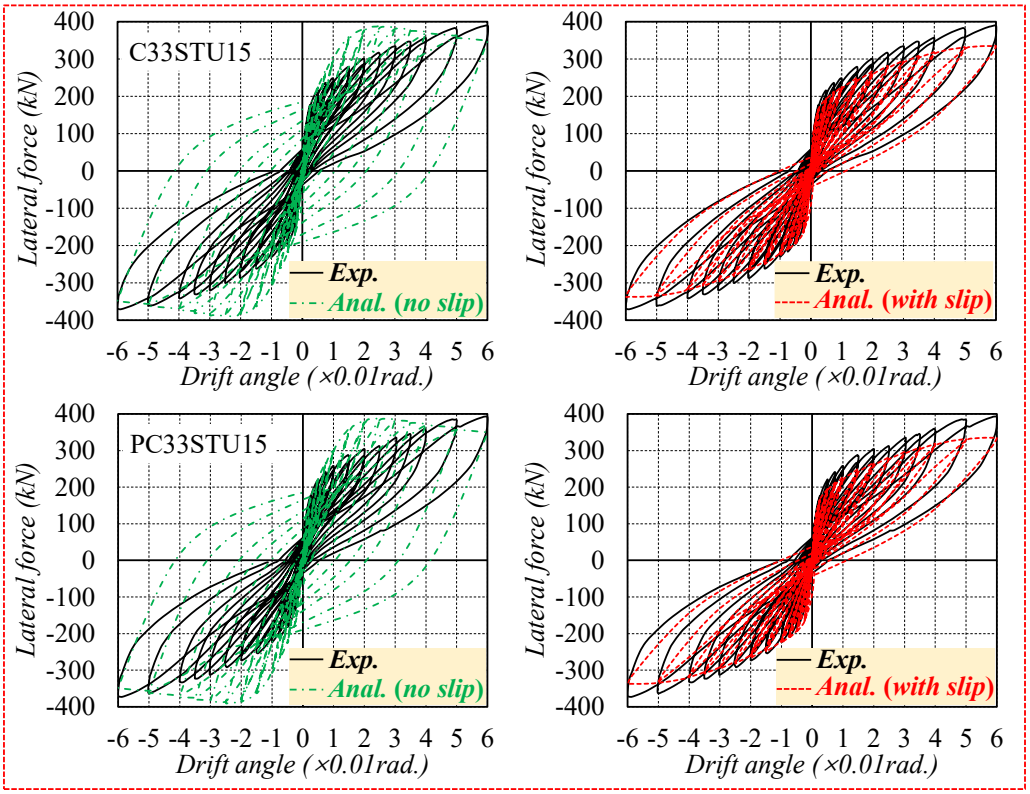

(f) Tubed specimens with a/D=1.7, n=0.33, U15 WBUHS rebar

Fig. 5-9 Continued

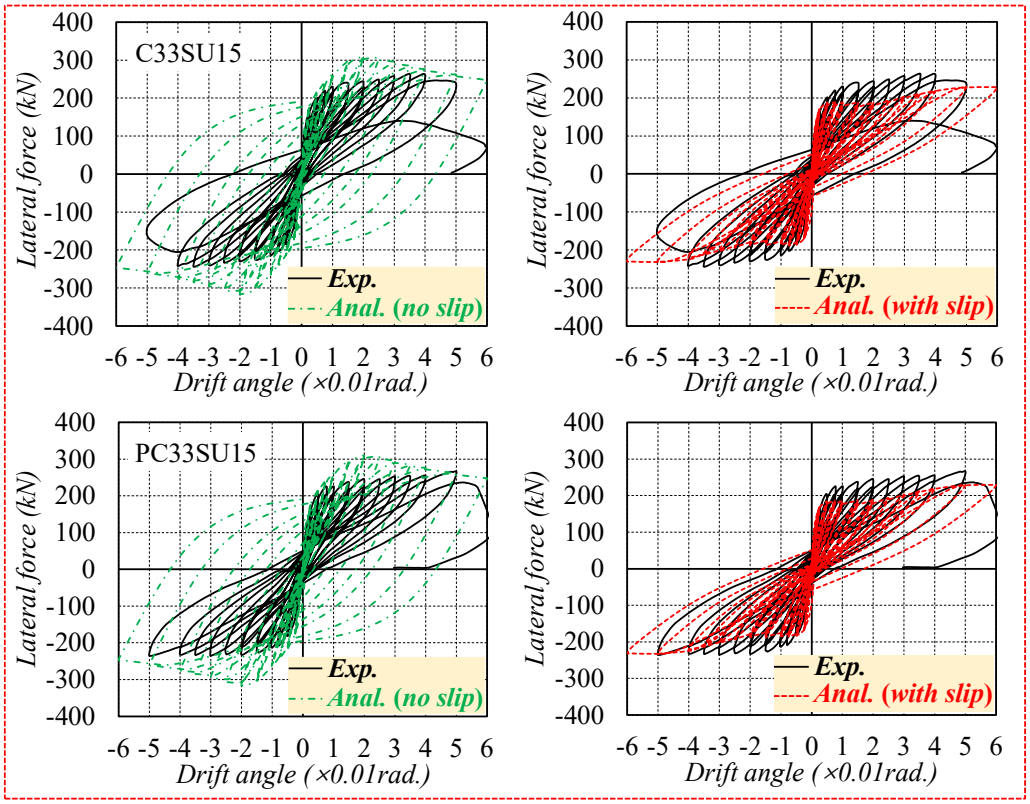

(g) Hooped specimens with a/D=1.7, n=0.33, U15 WBUHS rebar

Fig. 5-9 Continued

5.3.2 Strain of WBUHS Rebar

The hysteretic characteristics of the test columns are closely related to the behavior of the longitudinal rebars. Therefore, in order to better comprehend the accuracy difference resulting from the two analytical methods, it is imperative to conduct an in-depth analysis focusing on the strain of the reinforcements. Fig. 5-10 compared the reinforcement strain between the experimental and analytical results.

On one hand, in the analytical results neglecting the slippage of WBUHS rebars, the WBUHS rebar strain on the tension side increases at an alarming rate, reaching its yield strain well before the drift angle reached 0.02 rad. (0.03rad. for the specimens confined only by hoops). The sharp increase in the WBUHS rebar strain inevitably results in an overestimation of the lateral resistance at the early cyclic loadings by comparison with experimental results. Meanwhile, with the premature yielding of WBUHS rebars, the residual deformation of the resilient columns also increased visibly. As the drift angle increased to 0.025rad., the residual deformation has exceeded 0.005rad, 20% of the experienced peak deformation. While as for the ductile columns reinforced with NS rebars, the development trend of reinforcement strain in the results "*Anal. (no slip)*" agrees well with the experimental value, which explains why the analytical results give an accurate prediction on the hysteretic characteristics of experimental results.

On the other hand, WBUHS rebar strain in the analytical result considering the slippage was apparently controlled at a relatively low level, exhibiting relatively close agreement with the measured value. This relatively close prediction of strain behavior in WBUHS rebars provides a reasonable support for accurate assessment of the hysteretic performance of resilient columns reinforced with WBUHS rebars, characterized by significant drift-hardening capacity as well as self-centering capacity.

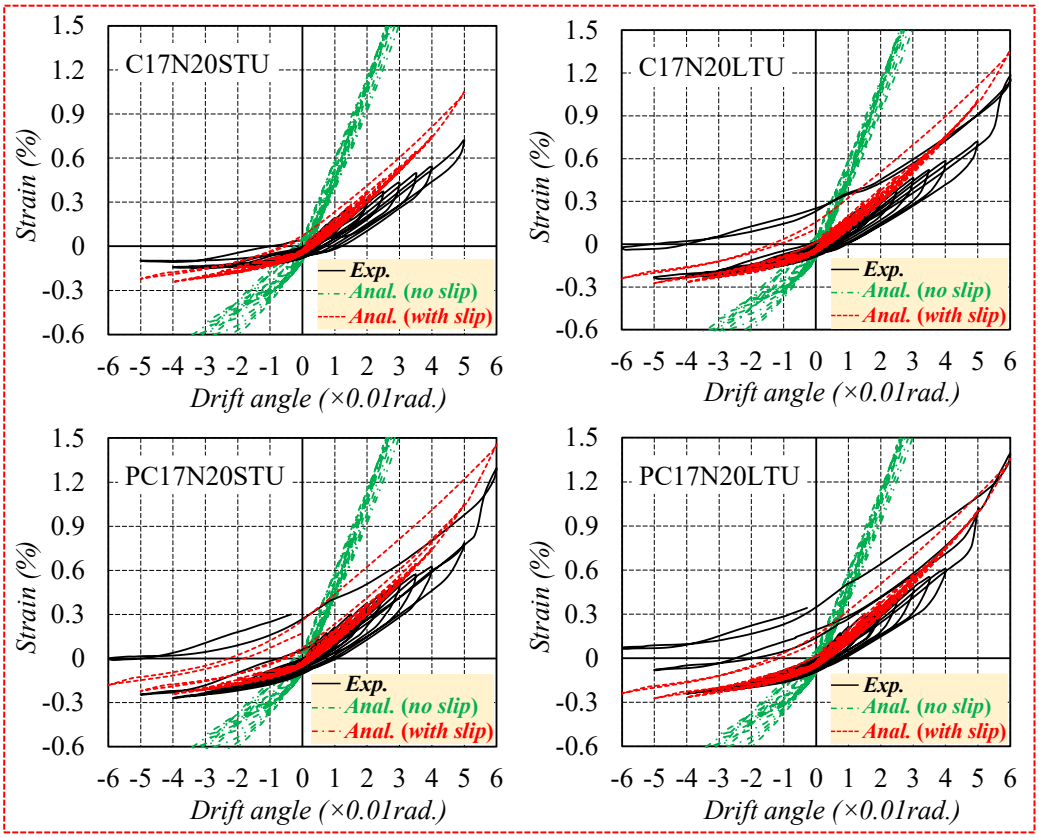

(a) Tubed specimens with a/D=1.7, n=0.20, U12.6 WBUHS rebar

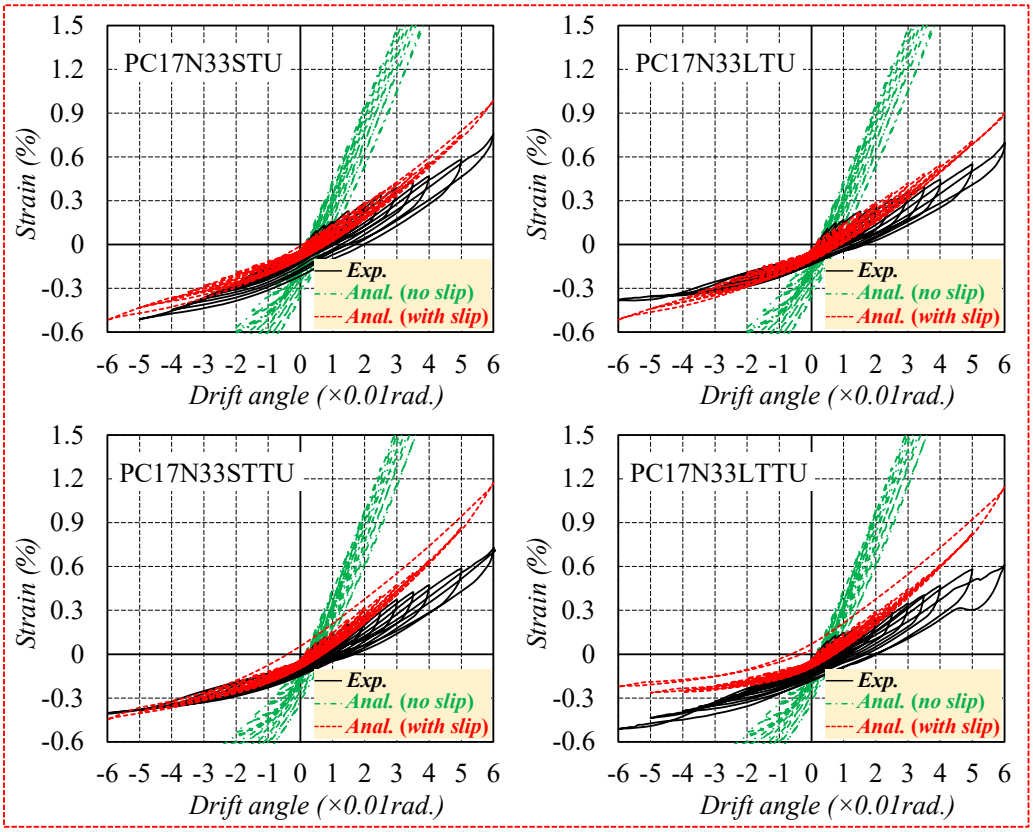

(b) Tubed specimens with a/D=1.7, n=0.33, U12.6 WBUHS rebar

Fig. 5-10 Comparison of reinforcement strain

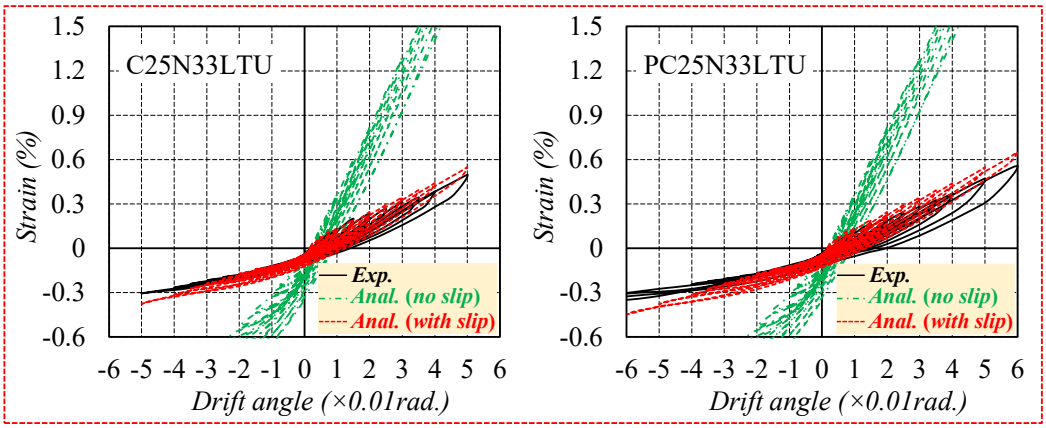

(c) Tubed specimens with a/D=2.5, n=0.33, U12.6 WBUHS rebar

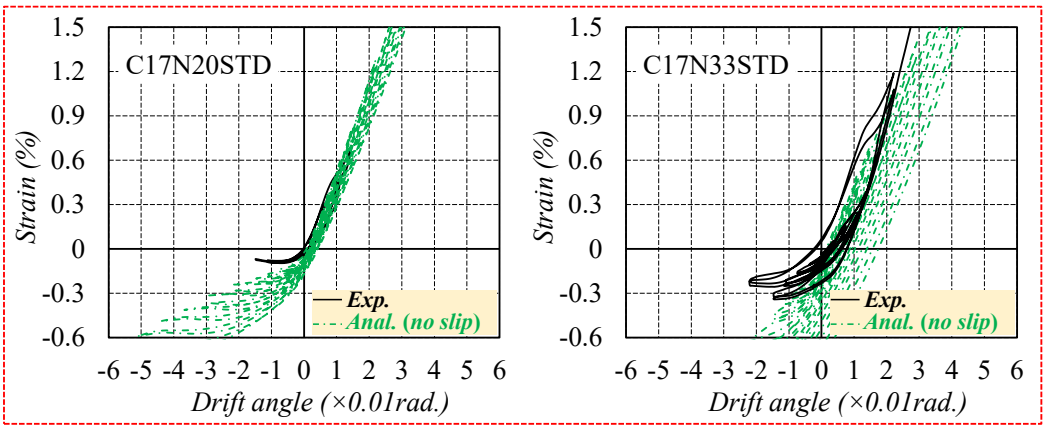

(d) Tubed specimens with a/D=1.7, NS rebar

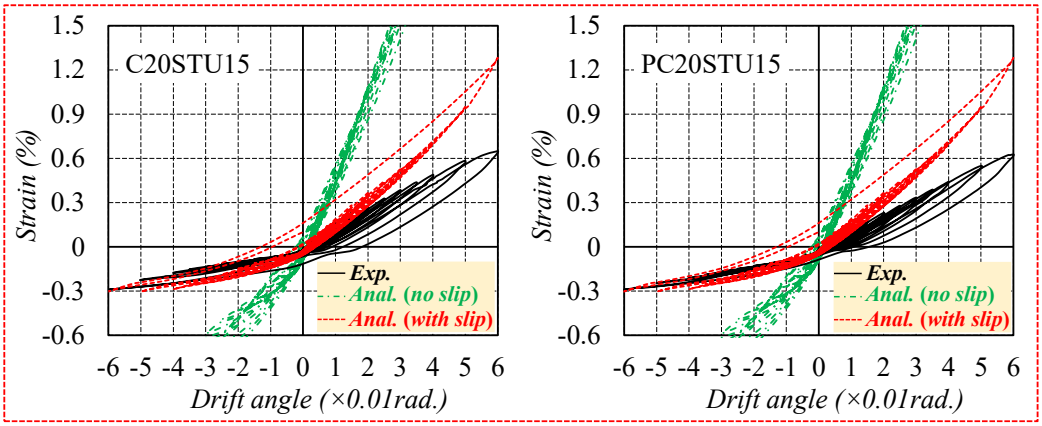

(e) Tubed specimens with a/D=1.7, n=0.20, U15 WBUHS rebar

Fig. 5-10 Continued

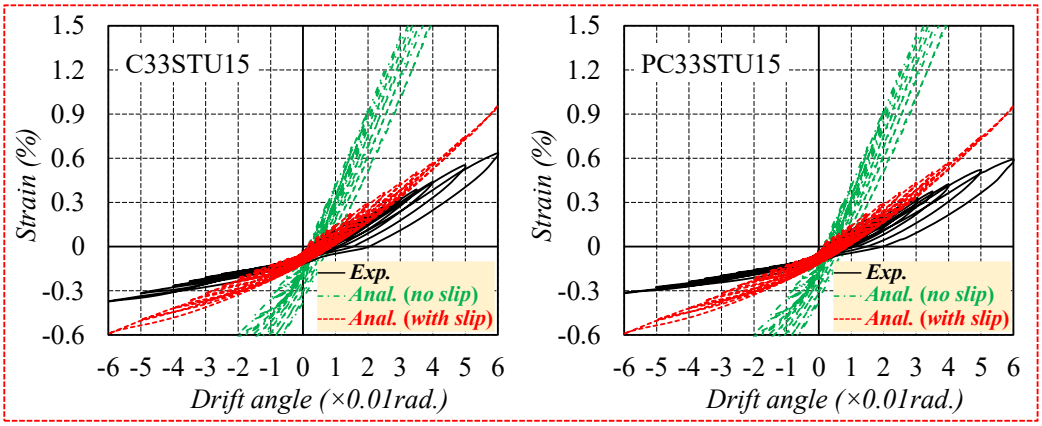

(f) Tubed specimens with a/D=1.7, n=0.33, U15 WBUHS rebar

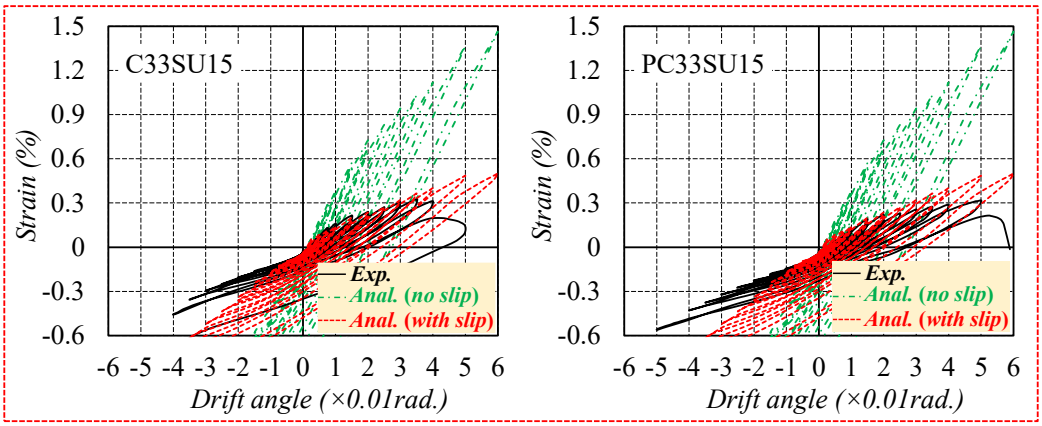

(g) Hooped specimens with a/D=1.7, n=0.33, U15 WBUHS rebar

Fig. 5-10 Continued

5.3.3 Energy Dissipation Capacity

In addition to hysteresis loops and strains, the comparison of energy-dissipating capacity between experimental and analytical values, expressed in terms of equivalent viscous damping coefficient, was presented in Fig. 5-11. The experimental results are represented by solid black line with triangle marks attached, the analytical results taking into account the bond-slip behavior of WBUHS rebar are represented by red dashed line with circles attached, and the analytical results neglecting the slippage are represented by green dot dash line with diamonds attached.

For test specimens reinforced with WBUHS rebars, the equivalent viscous damping coefficient obtained using the analytical method without considering the bond slip "*Anal. (no slip)*" increases from the drift angle of 0.015rad. and becomes much larger than the experimental value from the 0.025rad drift angle (0.03rad for the specimens with n= 0.33). This is because in the cycle from 0.015rad to 0.02rad, the WBUHS bar has yielded, and bar yielding is often accompanied by higher energy dissipation. In contrast, the NS rebars of traditional ductile columns (C17N20STD and C17N33STD) began to yield from 0.75rad. drift angle, consistent with the NS rebar strain confirmed in the experimental result. As a result, the variation in the equivalent viscous damping coefficient along with lateral deformation in the analytical method ("*Anal. (no slip)*") aligns well with the experimental values.

The equivalent viscous damping coefficient in the analytical result "*Anal. (with slip)*" exhibited a relatively stable development trend, agreeing well with the measured values for drift angle lower than 0.01rad., in particular for specimens with large longitudinal steel ratio but tending to present a lower evaluation of the energy-dissipating capacity for the further loading. In spite of this underestimation, the analytical result tends to remain constant as the experimental result for up to a drift angle of 0.04rad., which can reflect the nonlinear elasticity characteristics of the resilient columns reinforced with WBUHS rebars. Starting from a drift angle of 0.04rad., the analytical equivalent viscous damping coefficient denoted as "*Anal. (with slip)*" presented a raising tendency in the subsequent cycles. This is because, from this point onward, the yielding of WBUHS rebars in the analytical result "*Anal. (with slip)*" has been observed, naturally causing an increase in energy dissipation.

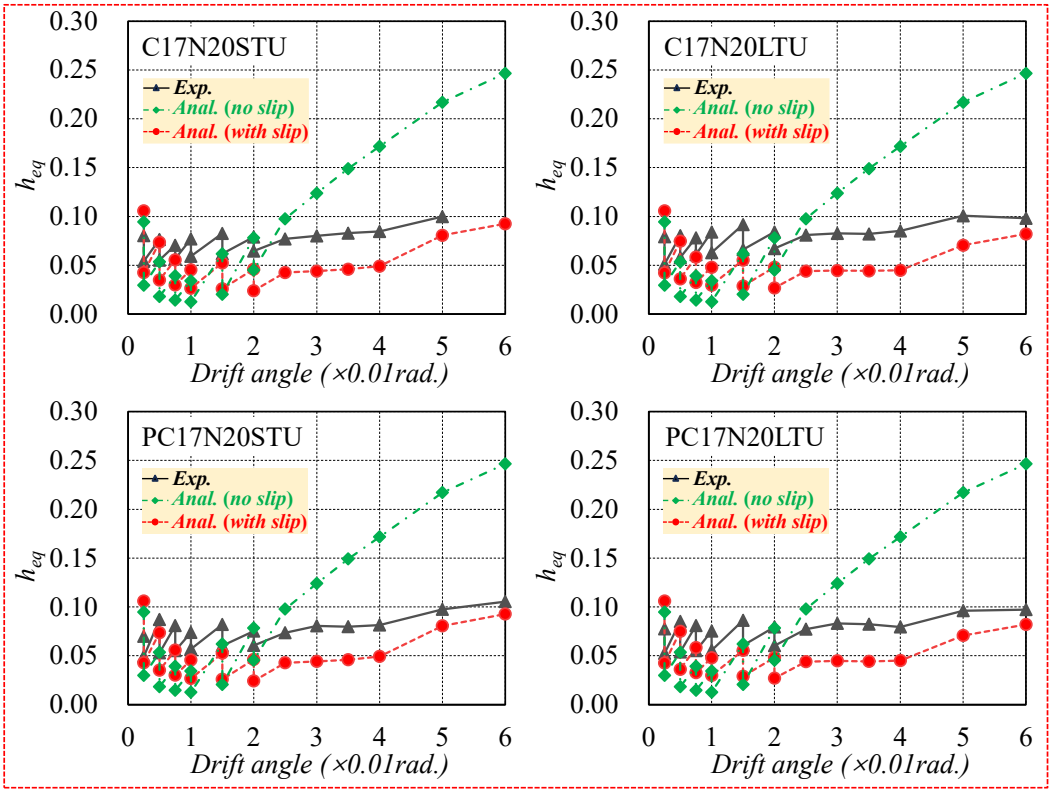

(a) Tubed specimens with a/D=1.7, n=0.20, 12.6 WBUHS rebar

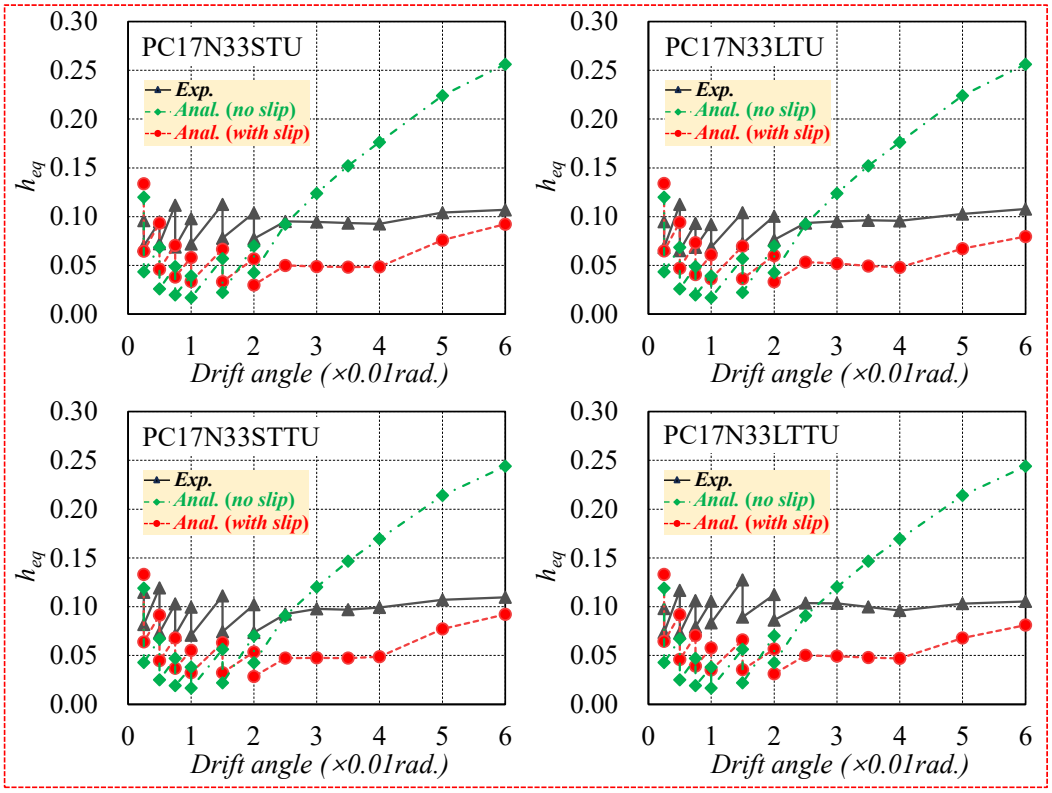

(b) Tubed specimens with a/D=1.7, n=0.33, U12.6 WBUHS rebar

Fig. 5-11 Comparison of equivalent viscous damping ratio

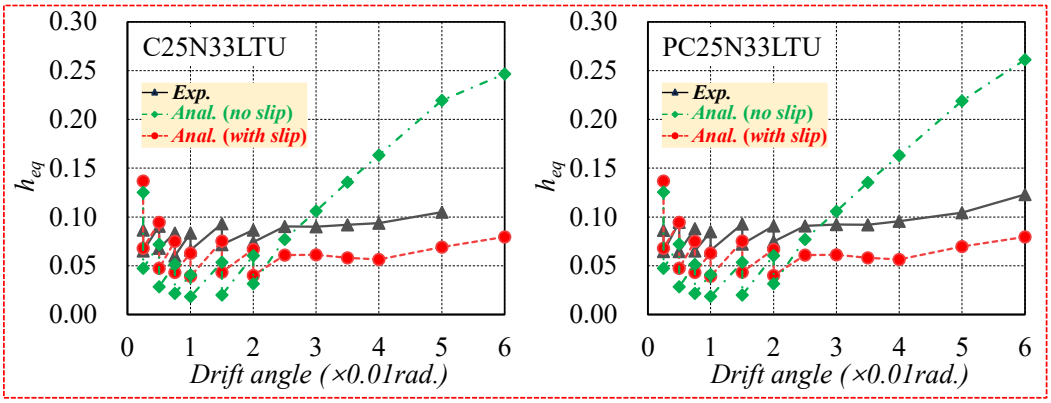

(c) Tubed specimens with a/D=2.5, n=0.33, U12.6 WBUHS rebar

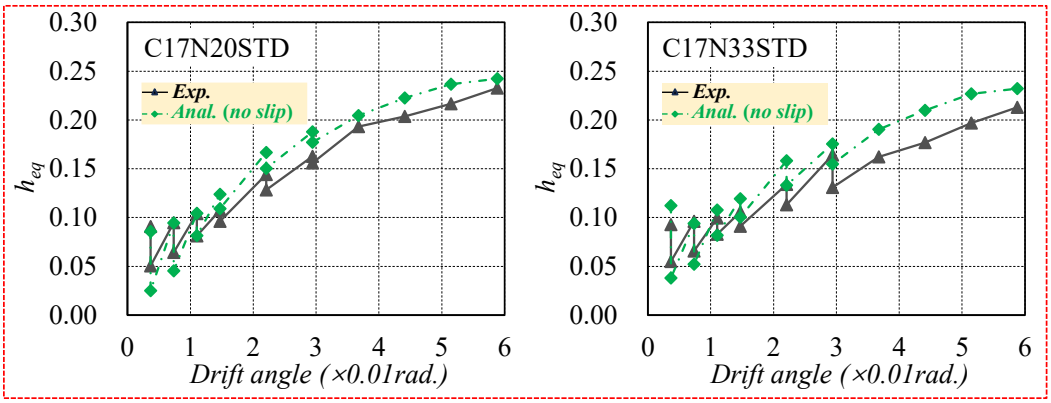

(d) Tubed specimens with a/D=1.7, NS rebar

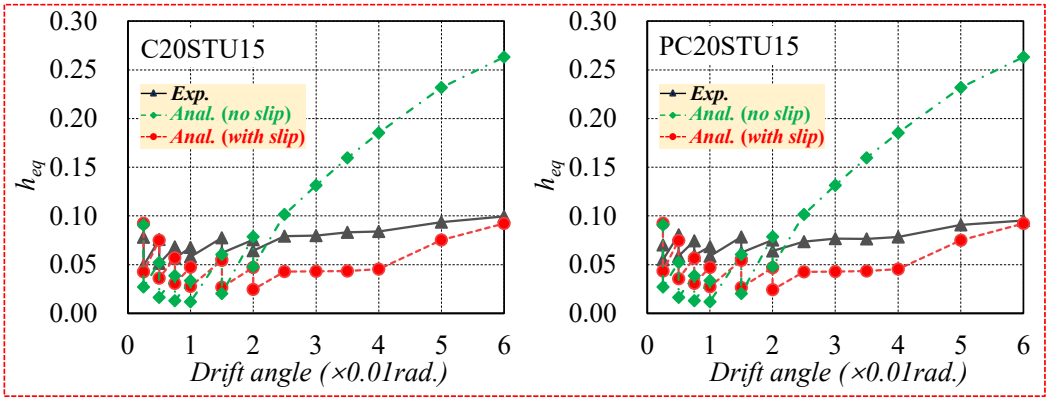

(e) Tubed specimens with a/D=1.7, n=0.20, U15 WBUHS rebar

Fig. 5-11 Continued

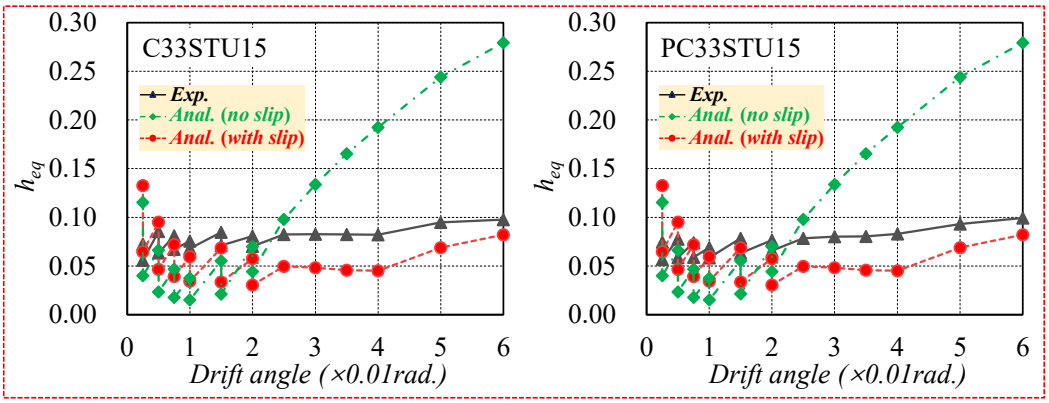

(f) Tubed specimens with a/D=1.7, n=0.33, U15 WBUHS rebar

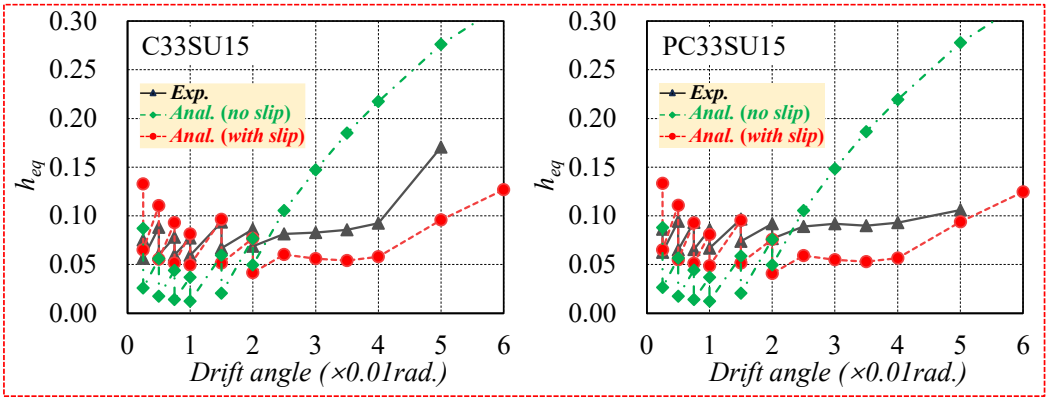

(g) Hooped specimens with a/D=1.7, n=0.33, U15 WBUHS rebar

Fig. 5-11 Continued

5.4 Conclusions

A finite spring element (FSE) method is adopted to predict seismic performance of circular concrete columns reinforced with squarely-arranged WBUHS rebars and externally confined by bolted circular steel tube. Through comparison with experimental results, the validity and accuracy of this method are verified, and the main conclusions are made below.

1) The presented FSE method could predict the hysteresis loops of specimens reinforced by squarely-arranged WBUHS rebars and/or normal-strength rebars with very satisfactory accuracy. When ignoring effect of the slippage of longitudinal rebar, the calculated hysteresis loops exhibited very good agreement with the experimental values of the ductile columns reinforced with NS rebars up to large drift, but overestimated the seismic behavior of the columns reinforced with WBUHS rebars. On the other hand, by taking into consideration the effect of the bond-slip behavior of WBUHS rebars, the calculated results gave an accurate prediction to the hysteretic performance characterized by significant drift-hardening capacity and self-centering capacity.

2) Confinement by bolted circular steel tubes on the seismic performance of both precast and cast-in-site resilient circular concrete columns could be reliably and precisely assessed by assuming their confinement efficiency (the strength raising coefficient of confined concrete) was about half of that provided by welded circular steel tubes.

3) Ignorance of the slippage resulted in a sharp increase in the strain of longitudinal rebar. This was in good agreement with the measured strain of NS rebar, but remarkably overestimated the strain development of WBUHS rebars, thus leading to an overestimation of lateral resistance and residual deformation for the resilient concrete columns. The analytical results obtained by taking into account of the slippage of WBUHS rebars could trace the strain of WBUHS rebars pretty well particularly in tension.

4) Ignoring the bond-slip relationship of longitudinal rebar could predict the energy dissipation capacity of the ductile concrete columns reinforced with NS rebars fairly well up to large drift angles, but gave an overestimation for that of resilient columns with WBUHS rebars. Consideration of slippage of rebars gave a conservative prediction of energy dissipation capacity, but could trace the characteristics of nonlinear elasticity of resilient columns reinforced with WBUHS rebars.

References

[5.1] Funato Y., Sun Y.P. Modeling and application of bond behavior of ultra-high strength bars with spiraled grooves on the surface. Proceedings of Japan Concrete Institute, 34:157–162, 2012. (In Japanese)

[5.2] Wei C., Sun Y., Takeuchi T., et al. Influence of anchorage detailing on seismic behavior of precast concrete walls reinforced with sbpdn rebars. Journal of Structural Engineering, 68: 75-86, 2022.

[5.3] Sun Y., Cai G., Takeshi T. Seismic behavior and performance-based design of resilient concrete columns. Applied Mechanics and Materials, 438: 1453-1460, 2013.

[5.4] Zhang J., Liu J., Li X., et al. Hysteretic behavior of steel fiber-reinforced high-strength concrete columns with high-strength steel bars. Structures, 33: 1833-1852, 2021.

[5.5] Sun Y., Fukuhara T., Kitajima H. Analytical study of cyclic response of concrete members made of high-strength materials. Proceedings of the 8th National Conference on Earthquake Engineering, Paper. No. 1581. 2006.

[5.6] Sun Y., Sakino K. Simplified design method for ultimate capacities of circularly confined high-strength concrete columns. ACI Special Public, 193:571–585, 2000.

[5.7] Fukuhara T., Sun Y., et al. Evaluation method of seismic performance of high-strength RC members and frames, Proceedings of the AIJ Annual Convention 2005; 3:193-198.

[5.8] Menegotto M., Pinto P. Method of Analysis for Cyclic Loaded R. C. Plane Frame Including Changes in Geometry and Non-Elastic Behaviour of Elements under Combined Normal Force and Bending. Proceedings of IABSE Symposium on Resistance and Ultimate Deform ability of Structures Acted on by Well Defined Repeated Loads, 1973, 11,15-22.

CHAPTER SIX

6 Evaluation of Ultimate Flexural Capacity

6.1 Introduction

The assessment of ultimate flexural capacity is crucial for structural design and analysis, as it enables engineers to determine the maximum bending moment that a concrete column section can withstand before failure.

As outlined in the research background, high-strength reinforcements, such as CFRP bars, prestressed concrete (PC) strands, and WBUHS rebars used in this paper, are commonly employed as the primary tensile reinforcement in seismic-resistant concrete members for providing a restoring effect [6.1-6.3]. Their higher tensile strength leads to the enhancement of ultimate flexural capacity, but the contribution to shear capacity is comparatively limited. For the purpose of better understanding the failure mode of the proposed drift-hardening (DH) circular concrete columns reinforced by WBUHS rebars and consequently prevent the potential shear failure that could pose risks to life safety, it is essential to conduct an accurate and reasonable assessment of the ultimate flexural capacity for the DH circular concrete column sections.

The calculation of flexural capacity of concrete sections based on the plane-remain-plane assumption is a commonly employed method in structural engineering. However, as described in chapters three and four, the WBUHS rebars were hard or even fail to yield due to the easily occurred strain penetration along the column height, indicating that conventional theoretical method may overestimate the strain of WBUHS rebar and thus lead to a larger calculation result. This overestimation of WBUHS rebar strain was also confirmed by the numerical analysis described in chapter five. Consequently, developing a method that can take account of the bond-slip behavior of longitudinal rebar for an effective and simple evaluation of ultimate flexural capacity of the resilient columns reinforced by WBUHS rebars is of great significance.

The primary objectives of this chapter are: 1) to propose a simple method for calculating the ultimate flexural capacity of the resilient columns, in which the reinforcement slippage is considered by modifying the elasticity modulus of WBUHS rebar in the tension zone; and 2) to verify the accuracy of the proposed method by comparing the calculated results with experimental values described in chapter three and chapter four.

6.2 Calculation Method

In general, calculating the ultimate flexural capacity of concrete columns with circular sections based on the plane section assumption is more challenging compared to square columns due to the inherent complexities of the circular geometry. Unlike the well-defined edges of a square section, a circular section lacks distinct corners, making it harder to approximate and analyze. Additionally, circular sections involve properties such as the radius and circumference, leading to more complex mathematical expressions in the calculation of bending moments.

Given this complexity, an equivalent stress block originally proposed by Sun et al. [6.4] is utilized to simplify the calculation of the moment resisted by the compressive concrete, in which the confinement effects of hoops and/or steel tubes can also be taken into consideration. The diagram of the equivalent stress block for calculating the ultimate flexural capacity was depicted in Fig. 6-1.

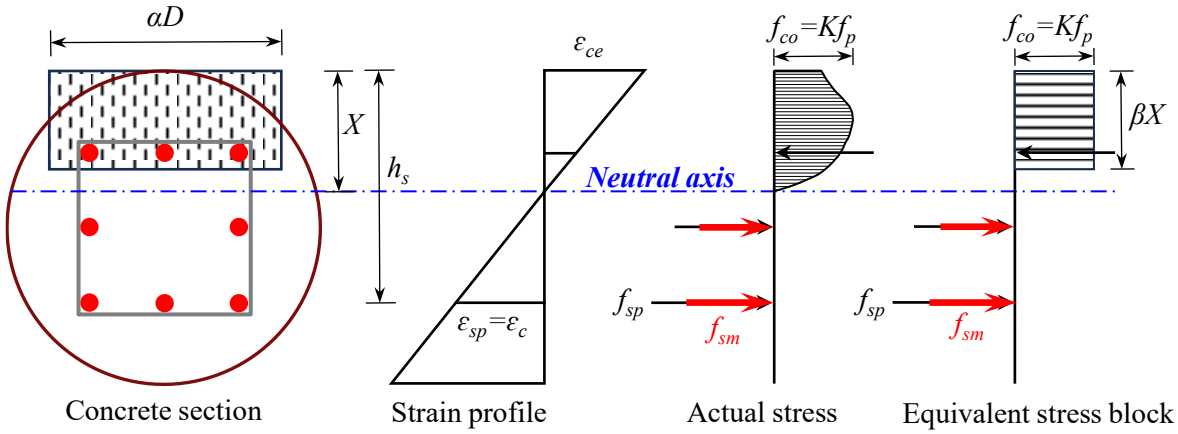

Fig. 6-1 Diagram of equivalent stress block

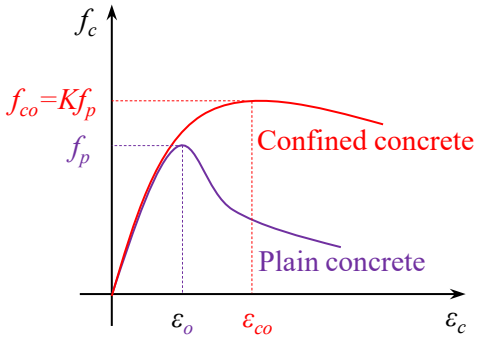

Fig. 6-2 Sakino-Sun model

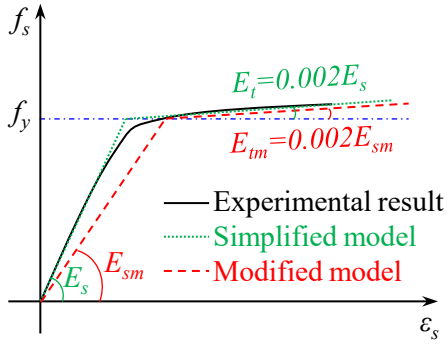

Fig. 6-3 Stress-strain relationship of WBUHS rebar

As presented in Fig. 6-1, the compressive zone can be equivalently represented by a rectangular stress block with a width of αD, a height of βX and a thickness of Kf_p. Therefore, the force sustained by concrete in the compression zone can be obtained using Eq. (6.1).

Where, α and β represent the factor of width of the equivalent stress block and the factor of the neutral axis depth, and can be calculated based on Eqs. (6.2)−(6.8); K represents the strength enhancement coefficient of confined concrete, taken 0.49 times the value calculated based on the Sakino-Sun model [6.5] (see Fig. 6-2); f_p is the compression strength of plain concrete (see Fig. 6-2), D denotes the section diameter of the test column; X represents the neutral axis depth.

$$N_c = \alpha \cdot \beta \cdot K \cdot f_p \cdot D \cdot X \tag{6.1}$$

$$\alpha\beta = A(K, X_n) - B(K, X_n) \cdot \frac{f_p}{42} \tag{6.2}$$

$$\frac{\beta}{2} = C(K, X_n) - D(K, X_n) \cdot \frac{f_p}{42} \tag{6.3}$$

$$A(K, X_n) = \frac{0.723+0.061K}{0.112+X_n} \cdot X_n \tag{6.4}$$

$$B(K, X_n) = \frac{0.048K^{-2}}{0.072K^{-1.5}+X_n} \cdot X_n \tag{6.5}$$

$$C(K, X_n) = (0.476 + 0.051K) \cdot \left(1 - 0.132{X_n}^2\right) \tag{6.6}$$

$$D(K, X_n) = 0.017\left[1 - (0.024 + 0.187K) \cdot {X_n}^2\right] \tag{6.7}$$

$$X_n = \frac{X}{D} \tag{6.8}$$

After obtaining the strain at extreme concrete compression fiber (ε_{ce}) by Eqs. (6.9)−(6.10), the strain of WBUHS rebars (ε_{sp}) at any position could be determined based on the plane-section assumption, as given in Eq. (6.11). As a contrast, a method was proposed to consider the bond-slip behavior of WBUHS rebars. In this method, the strain of WBUHS rebars (ε_{sm}) in tension zone can be divided into the rebar deformation itself and the anchorage slip, which is presumed to be uniformly distributed along the entire member [6.6], and can be calculated by the Eqs. (6.12−6.16). Then, the elasticity modulus in the stress–strain model of WBUHS rebars was modified by Eq. (6.17), as depicted in Fig. 6-3. The strain distribution of WBUHS rebars in the proposed method is illustrated in Fig. 6-4.

$$\frac{\varepsilon_{ce}}{\varepsilon_{co}} = 1.465 + 0.315\mathrm{K} - 0.168\frac{f_p}{42} \tag{6.9}$$

$$\varepsilon_{co} = 0.94 f_p^{0.25} \times 10^{-3} \times [1 + 4.7(K-1)] \tag{6.10}$$

$$\varepsilon_{sp} = \frac{h_s - X}{X} \cdot \varepsilon_{ce} \tag{6.11}$$

$$\varepsilon_{sm} = \varepsilon_y + S_{slip}/L_{apd} \tag{6.12}$$

$$S_{slip} = \int_0^{l_{AL}} \varepsilon_s dx = \begin{cases} \frac{\varepsilon_y}{2} \cdot l_d & l_d \le l_{AL} \\ \frac{\varepsilon_{s0}+\varepsilon_y}{2} \cdot l_{AL} & l_d > l_{AL} \end{cases} \tag{6.13}$$

$$L_{apd} = l_{AL,column} + l_{AL,footing} \tag{6.14}$$

$$l_d = \frac{b \cdot f_y}{4\tau} \tag{6.15}$$

$$\varepsilon_{s0} = \frac{l_d - l_{AL}}{l_d} \cdot \varepsilon_y \tag{6.16}$$

$$E_{sm} = f_y/\varepsilon_{sm} \tag{6.17}$$

Where, ε_{co} represents peak-strength strain of the confined concrete; h_s is the distance between the position of longitudinal rebar and extreme concrete compression fiber; ε_{sm} represents the strain of WBUHS rebars in the proposed method; S_{slip} represents the slip until the yield of WBUHS rebars, which includes the slip within both the column and footing and can be derived from Eq. (6.13) [6.7, 6.8]; L_{apd} is the distance between the anchor plates (see Eq. (6.14)); l_d is the necessary development length until the yielding of WBUHS rebar (see Eq. (6.15)); ε_y and f_y respectively denote the strain and stress of WBUHS rebar when yielding; ε_{s0}

denotes the axial strain at end of WBUHS rebar (see Eq. (6.16)); τ represents the bond strength of WBUHS rebar (τ = 3N/mm^2) [6.9]; b is the diameter of WBUHS rebar; E_{sm} represents the modified elasticity modulus of WBUHS rebar in tensile side, as shown in Eq. (6.17) and given in Table 6-1.

When the strain (ε_{sp} or ε_{sm}) of WBUHS rebar is obtained, the force sustained by WBUHS rebars (N_s) can be calculated using Eq. (6.18) according to the stress-strain relationship shown in Fig. 6-3. Then, the ultimate flexural capacity (V) can be calculated on the basis of the equilibrium of the bending moment, as given in Eq. (6.19).

$$N_s = \sum A_s f_s \tag{6.18}$$

$$V_c = \left\{ N_c \cdot \left(\frac{D}{2} - \frac{\beta X}{2} \right) + \sum N_s \cdot \left(\frac{D}{2} - h_s \right) \right\} / a \tag{6.19}$$

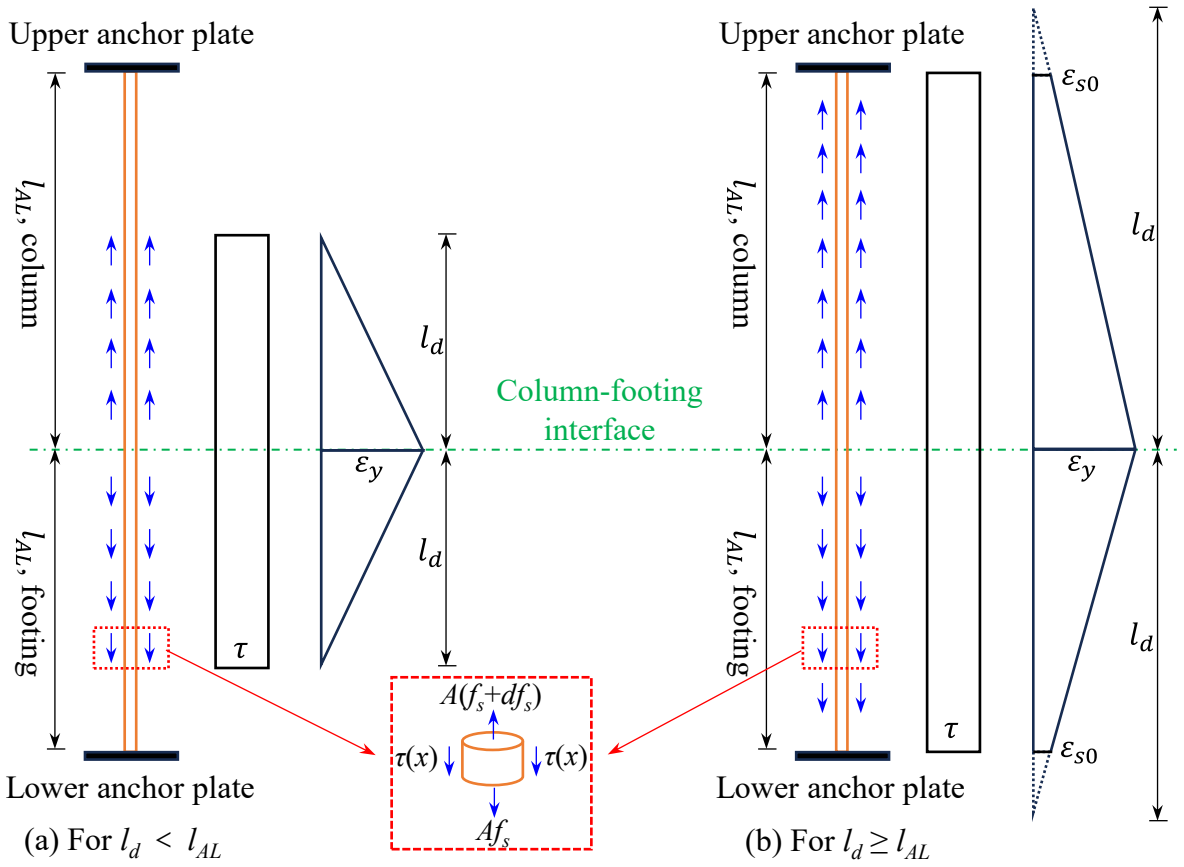

Fig. 6-4 Strain distribution of WBUHS rebars in the proposed method

Table 6-1 Results of the modified elasticity modulus

a/D	Rebar & l_e	f_y (N/mm^2)	ε_y (%)	E_s (kN/mm^2)	l_d (mm)	l_{AL} (mm)		ε_{so} (%)		Slip (mm)		L_{apd} (mm)	ε_{ym} (%)	E_{sm} (kN/mm^2)
						Column	Footing	Column	Footing	Column	Footing			
1.7	U12.6 (20d)	1401	0.66	212	1471	558	252	0.41	0.55	2.98	1.52	810	1.22	115
	U12.6 (30d)	1401	0.66	212	1471	558	378	0.41	0.49	2.98	2.17	936	1.21	116
	U15 (20d)	1356	0.67	202	1695	558	300	0.45	0.55	3.11	1.83	858	1.25	109
2.5	U12.6 (30d)	1401	0.66	212	1471	798	378	0.30	0.49	3.84	2.17	1176	1.17	120

Note: *a/D* denotes the shear span ratio; l_e represents the embedment length of WBUHS rebars; *d* represents the diameter; f_y, ε_y and E_s denote the yield stress, yield strain and elasticity modulus of WBUHS rebar in the simplified model, respectively; l_d is the needed development length until the yielding of WBUHS rebars; l_{AL} represents the anchorage length of WBUHS rebar; ε_{so} denotes the axial strain at ends of WBUHS rebars; S_{slip} represents the slip until the yield of WBUHS rebars; L_{apd} is the distance between the anchor plates; ε_{sm} represents the strain of WBUHS rebars in the proposed method; E_{sm} represents the modified elasticity modulus.

6.3 Assessment of Ultimate Flexural Capacity

The comparison of the ultimate flexural capacity between experimental and calculated values was listed in Table 6-2 and depicted in Fig. 6-5, respectively. Additionally, the analytical values (V_{ca}) obtained from chapter five was also presented in Table 6-2 and Fig. 6-5 for discussion.

One can see from Table 6-2 and Fig. 6-5 that the computed result based on plane-remain-plane assumption (V_{cp}) tends to overestimate the ultimate flexural capacity of resilient concrete columns reinforced with WBUHS rebars, in particular for specimens in groups II (by about 10.4%−13.9%), which were confined by bolted circular steel tube with a diameter-thickness ratio of 96, or for group III specimens with a/D=2.5 (by about 17.7%−23.3%). However, it could predict the ultimate flexural capacity of ductile concrete columns (group IV) with good accuracy. For specimens confined only by hoops (group V), the calculated results were about 5% lower than the experimental values. One of the reasons for this can be explained by the ignorance of confinement effect of hoops on core concrete.

In contrast, the calculated results (V_{cm}) based on the modified elastic modulus of the reinforcement in the tension zone gave relatively conservative prediction to the flexural capacity for specimens in groups I, V and IV. As for specimens in groups II and III, the calculated results were still higher than the measured values, but the difference could be controlled within 8%. In addition, it is noted that the analytical method considering the rebar slippage (V_{ca}) described in chapter five could conservatively evaluate the ultimate flexural capacity of all the resilient specimens reinforced by WBUHS rebars, with a safe margin of 11% in average, compared with the experimental results.

Table 6-2 Comparison of the ultimate flexural capacity

Group	Specimens	Rebar	*a/D*	*n*	Confinement	V_{exp} (kN)	V_{cp} (kN)	V_{cm} (kN)	V_{ca} (kN)	$\frac{V_{exp}}{V_{cp}}$	$\frac{V_{exp}}{V_{cm}}$	$\frac{V_{exp}}{V_{ca}}$
I	C17N20STU	WBUHS rebar (U12.6)	1.7	0.20	PL2.3, D6@100	309.8	315.5	299.7	285.4	0.98	1.03	1.09
	C17N20LTU					305.7	315.5	299.9	278.4	0.97	1.02	1.10
	PC17N20STU					306.0	315.5	299.7	285.4	0.97	1.02	1.07
	PC17N20LTU					314.8	315.5	299.9	278.4	1.00	1.05	1.13
	PC17N33STU			0.33		309.7	341.1	306.5	286.8	0.91	1.01	1.08
	PC17N33LTU					330.2	341.1	307.2	278.3	0.97	1.07	1.19
II	PC17N33STTU				PL3.2, D6@100	319.0	363.4	340.1	303.0	0.88	0.94	1.05
	PC17N33LTTU					329.3	363.4	340.5	294.7	0.91	0.97	1.12
III	PC25N33LTU		2.5		PL2.3, D6@100	199.1	234.3	206.3	165.9	0.85	0.97	1.20
	C25N33LTU					190.1	234.3	206.3	165.9	0.81	0.92	1.15
IV	C17N20STD	NS rebar (D13)	1.7	0.20		193.6	195.8	-	-	0.99	-	-
	C17N33STD			0.33		254.5	241.3	-	-	1.05	-	-
V	C20STU15	WBUHS rebar (U15)	1.7	0.20		358.3	371.7	326.3	338.8	0.96	1.10	1.06
	PC20STU15					363.6	371.7	326.3	338.8	0.98	1.11	1.07
	C33STU15			0.33		375.0	390.9	335.9	336.3	0.96	1.12	1.12
	PC33STU15					382.8	390.9	335.9	336.3	0.98	1.14	1.14
VI	C33SU15				D6@30	254.1	239.8	214.3	230.5	1.06	1.19	1.10
	PC33SU15					250.6	239.8	214.3	230.5	1.05	1.17	1.09

Note: Groups I–IV represent specimens in chapter three; Groups IV and V represent specimens in chapter four; *a/D* denotes shear span ratio; *n* represents axial load ratio; V_{exp} represents the experimental value of ultimate flexural capacity, V_{cp}, V_{cm} and V_{ca} are the calculated based on plane-section assumption, proposed method and analytical method in chapter five, respectively.

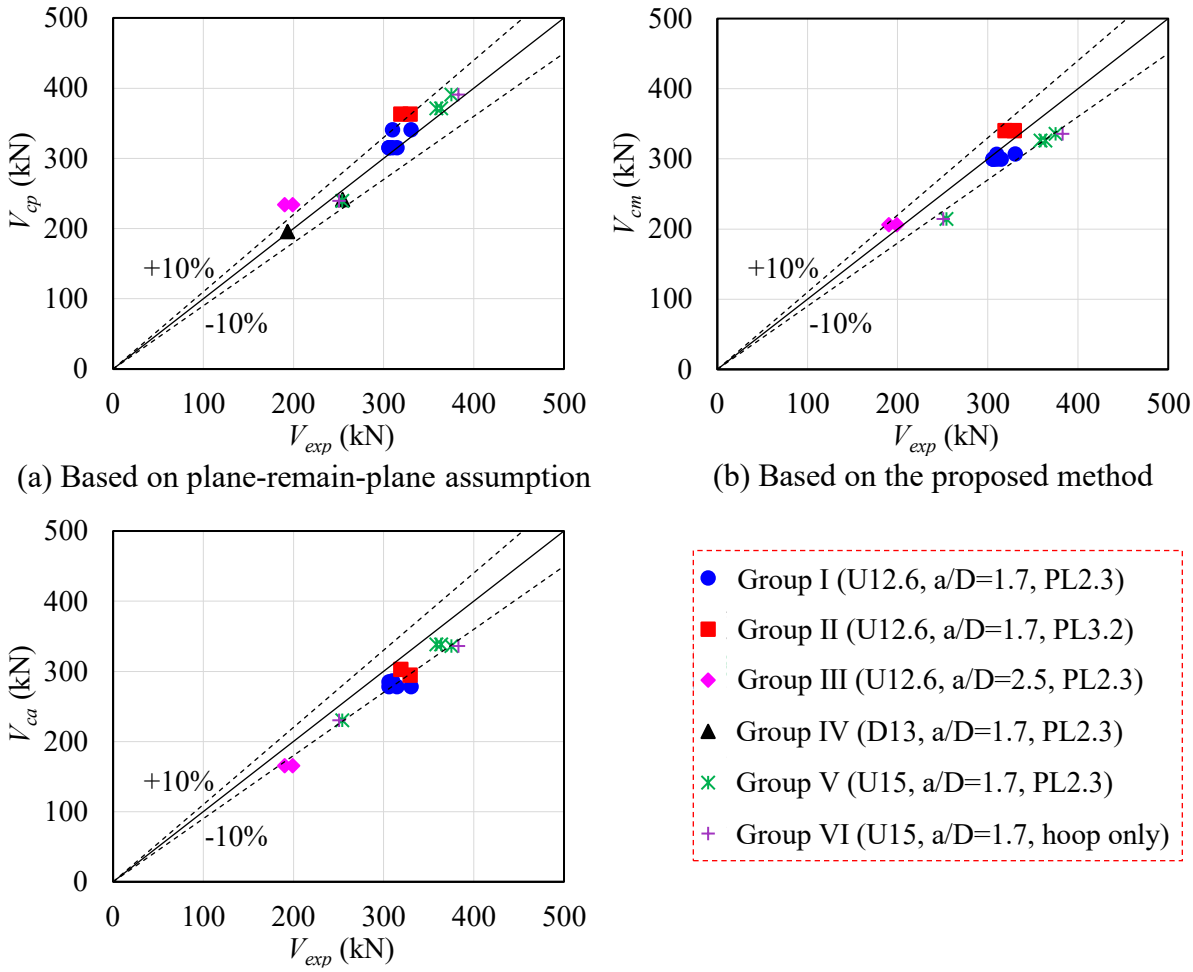

(a) Based on plane-remain-plane assumption

(b) Based on the proposed method

(c) Based on the FSE method in chapter five

Fig. 6-5 Comparison of the ultimate flexural capacity

6.4 Conclusions

Two methods were presented in this chapter with the aim of simplifying calculation the flexural capacity of the proposed circular concrete columns reinforced by squarely-arranged WBUHS rebars: one was on the basis of the plane-remain-plane assumption, and the other involved the modification of elasticity modulus of WBUHS rebars in the tensile region as a consideration of rebar slippage. According to the comparison between the computed results and measured values, the main conclusions are drawn as below:

1) The traditional calculation method following plane-remain-plane assumption was prone to giving an overestimated prediction of the ultimate flexural capacity of concrete specimens reinforced by WBUHS rebars. The overestimation was more remarkable for the specimens with shear span ratio of 2.5 and/or confined by steel tubes with diameter-to-thickness ratio of 96. The ratio between the experimental and calculated capacities varied between 0.81-1.06, having an average value of 0.95 and a standard deviation of 0.07. However, the calculated results using this method agreed fairly well with the measured values for ductile concrete columns reinforced with NS rebars.

2) Combining the equivalent stress block of concrete at the circularly compressed zone with the reduced elasticity modulus for WBUHS rebars could give a very satisfactory prediction of the ultimate flexural capacity of circular concrete columns reinforced by squarely-arranged WBUHS rebars. For the sixteen test columns with WBUHS rebars, the ratio between the experimental and calculated capacities varied between 0.92-1.19, having an average value of 1.05 and a standard deviation of 0.08.

References

[6.1] Zhao J., Luo J., Zhang X., et al. Experimental study on seismic behavior of concrete walls with external magnetorheological dampers. Smart Materials and Structures, 2023, 32(6): 065005.

[6.2] Liu Z., Zhao H., Sun Y., et al. Seismic performance of circular concrete columns reinforced by PC strands. Journal of Advanced Concrete Technology, 2020, 18(5): 256-271.

[6.3] Sun Y., Cai G. Seismic Behavior of Circular Concrete Columns Reinforced by Low Bond Ultrahigh Strength Rebars. Journal of Structural Engineering, 2023, 149(9): 04023126.

[6.4] Sun Y., Sakino K. Simplified design method for ultimate capacities of circularly confined high-strength concrete columns. ACI, Special Publication, 2000, 193: 571-586.

[6.5] Sun Y., Sakino K. Ultimate Strength of RC Columns Retrofitted by Circular Steel Tubes. JCI, Vol. 20, Jun. 1998, pp. 1117-1122. (In Japanese)

[6.6] Feng D., Xu J. An efficient fiber beam-column element considering flexure–shear interaction and anchorage bond-slip effect for cyclic analysis of RC structures. Bulletin of Earthquake Engineering, 2018, 16: 5425-5452.

[6.7] Pan W., Tao M., Nie J. Fiber beam–column element model considering reinforcement anchorage slip in the footing. Bulletin of Earthquake Engineering, 2017, 15: 991-1018.

[6.8] Wang J., Zhao H., He J. Seismic behaviors and resilient capacity of CFRP-confined concrete columns with partially debonded high-strength steel rebars. Composite Structures, 2019, 222: 110912.

[6.9] Funato Y., Sun Y. Modeling and application of bond behavior of ultra-high strength bars with spiraled grooves on the surface. Proceedings of Japan Concrete Institute, 34:157–162, 2012. (In Japanese)

CHAPTER SEVEN

7 Conclusions and Future Works

7.1 Conclusions

Drawing the lessons learnt from recently occurred much more catastrophic earthquakes than anticipated, traditional ductile RC structures may not anymore be deemed the optimal choice for the buildings located in high seismic hazard zone due to the observed severe damage and significant residual deformation after earthquakes. Furthermore, the seismic engineering community has increasingly focused on developing resilient concrete structures in recent years, with emphasis placed on the reduction of repair costs and quick recovery of social activities.

Sun et al. has proposed an innovative method to materialize resilient concrete members, in which a kind of WBUHS rebar (featuring spiral grooves on its surface) is employed as primary tensile reinforcements. Previous studies have proved the simplicity and effectiveness of this approach in providing concrete components with superior earthquake resilience characterized by significant drift-hardening capacity and self-centering capacity. To promote the practical application of precast circular columns reinforced by squarely-arranged WBUHS rebars in construction industry, therefore, experimental and theoretical study were conducted in this doctoral dissertation with focus upon several important aspects, including: 1) effective measures to prevent or delay the buckling of WBUHS rebar due to concrete damage and/or insufficient transverse confinement; 2) solutions to the construction difficulties of rectangular beam-circular column joints caused by the reduced available spacing between the circularly-arranged reinforcements in the horizontal direction; 3) accumulation of information regarding the seismic performance of precast circular concrete columns reinforced by squarely-arranged WBUHS rebars.

This doctoral dissertation consists of seven chapters. Experimental test and theoretical analysis were conducted with objectives to address the issues mentioned above. Based on experimental and analytical results, except for chapter one (introducing the backgrounds and research motivation), the conclusions of this doctoral dissertation will be drawn from the main findings in chapters two through six, as summarized below.

Chapter two is intended to experimentally verify the effectiveness of bolted steel tube in delaying the buckling of WBUHS rebars and in improving the post-buckling behavior of WBUHS rebars through a rational evaluation method for this type of confinements. For this purpose, twenty short concrete columns were made and tested under concentric loading, with primary experimental parameters including hoop spacing (25mm, 50mm, 75mm, 100mm), reinforcement type (WBUHS rebar, NS rebar), confinement of steel tubes, and section type (circular, square). According to the experimental results discussed in this chapter, the main conclusions are made as follows:

1) Confinement by bolted thin steel tubes could reduce concrete damage and simultaneously enhance the strain at peak load of concrete columns with WBUHS rebars significantly. In particular, the bolted circular steel tube could also upgrade the concrete strength, while the confinement effect on concrete strength by square steel tubes was little.

2) The strain ductility of specimens confined by square and circular steel tubes were 36%−89% and 112%−152.9% higher than those of columns confined only by hoops, respectively, suggesting superior deformability for specimens confined by bolted steel tubes.

3) The current method for defining the onset of buckling of longitudinal reinforcements may be not necessarily accurate because buckling of the reinforcements should lead to a decrease in bearing capacity. From this viewpoint and based on the extracted stress-strain behavior of WBUHS rebars, the buckling strain and post-buckling behavior of WBUHS rebars could also be improved by confining the columns with bolted steel tubes. Confinement by bolted square thin steel tube could increase the peak strain beyond 1.0%, which is larger than the yield strain of WBUHS rebar, while the bolted circular thin steel tube enhanced the peak strain close to and/or beyond 2.0% even the slenderness ratio was as large as 12, due to its uniform confinement effect.

In chapter three, to facilitate construction of rectangular beam-circular column joints and offer essential information regarding the seismic performance for precast circular concrete columns, twelve 1/2.5-scale circular concrete columns, reinforced with squarely-arranged longitudinal steels and externally confined by bolt circular steel tubes, were made and tested under reversed cyclic lateral loading while simultaneously subjected to constant axial compression. The main experimental variables included reinforcement type (WBUHS rebar, NS rebar), shear span ratio (1.7, 2.5), diameter-to-thickness ratio (96, 132) of bolted circular steel tubes to confine concrete, axial load ratio (0.20, 0.33), embedment length of reinforcement (20d, 30d) and construction method (cast-in-place, precast). On the basis of the test results discussed in this chapter, the primary conclusions are made as below:

1) All the specimens reinforced by squarely-arranged WBUHS rebars exhibited both excellent drift-hardening capacity and satisfactory self-centering capacity even when deformed to a large drift angle, by comparison with those ductile specimens reinforced with NS rebars. This could be attributed to that the low bond strength of WBUHS rebars makes its strain easily permeate along the column height, allowing the WBUHS rebars to remain in the elastic region up to large deformation, thus contributing to the remarkable drift hardening capacity and self-centering capacity.

2) Providing an embedment length of 20 times its diameter for WBUHS rebars enabled precast concrete columns to exhibit almost identical resilience in terms of drift-hardening and self-centering capacity up to a drift angle of 0.05rad to the cast-in-place columns.

3) Under a higher axial compression with n=0.33, the concrete columns experienced slightly more serious concrete damage and had relatively larger residual deformation but exhibited higher moment resistance and energy dissipation capacity. Moreover, even for the test specimens subjected to higher axial compression, the axial strain gradually increases with the increase in drift angle, but remains below 0.3%. This strain level is much less than the ultimate compressive strain of confined concrete, revealing the favorable axial stability of the proposed precast concrete columns confined by the bolted thin steel tubes.

In chapter four, taking longitudinal steel ratio (1.41%, 1.92%), confinement method (bolted steel tube, hoop), construction methods (cast-in-place, prefabrication) and axial load ratio (0.20, 0.33) as experimental variables, six 1/2.5-scaled circular concrete columns were made and tested under reversed cyclic lateral loading, primarily aimed at studying the effect of longitudinal steel ratio on seismic performance and clarifying the enhancement degree of steel tube confinement on seismic property of circular concrete columns reinforced by squarely-arranged WBUHS rebars. According to the test results discussed in this chapter, the primary conclusions are drawn as follows:

1) Squarely-arranged WBUHS rebars could provide high drift-hardening capacity for circular concrete columns confined by hoops up to the drift level of 0.04 rad. However, after that drift angle, the lateral resisting capacity of the hooped circular column began to decrease due to serious concrete damage. On the other hand, the use of bolted circular steel tubes to confine the column could not only effectively reduce concrete damage but also significantly enhance drift-hardening capacity of the circular columns up to the drift angle of at least 0.06 rad, implying high confinement efficiency of the bolted circular steel tube. Besides, the usage of bolted steel tube was also beneficial to reduce the residual deformation due to the strong confinement of the steel tubes.

2) Providing a 20d anchorage length even for large-diameter WBUHS bars allowed the precast circular columns to demonstrate nearly the same excellent seismic performance as the cast-in-place ones in terms of drift-hardening capability and self-centering capacity. It is particularly noteworthy that increase the steel amount of WBUHS rebars could enhance the lateral resistance of the circular concrete columns without reducing their deformation capacity.

3) Increasing the axial compression level, the steel amount of WBUHS rebar, or utilizing steel tube confinement could effectively improve the lateral bearing capacity. In particular, confinement by the bolted thin steel tubes showed the most significant improvement effect, with lateral force and bending moment resistance increased by up to 48.1% and 40.5% for drift angles within 0.05rad, respectively.

In chapter five, a finite spring element (FSE) method originally proposed by Sun et al. was adopted to evaluate hysteretic performance of the circular concrete columns reinforced by squarely-arranged WBUHS rebars and externally confined by bolted circular steel tubes. In this numerical analysis, effect of the discontinuity of the bolted tube on confinement effect will be considered. By comparing numerical results with experimental values obtained from chapter three and chapter four, the validity and accuracy of this method were assessed in aspects of hysteresis loop, reinforcement strain and energy-dissipating capacity. The primary conclusions can be drawn below:

1) The presented FSE method could predict the hysteresis loops of circular concrete columns reinforced by squarely-arranged WBUHS rebars and/or normal-strength rebars with very satisfactory accuracy. When ignoring the effect of slippage of the longitudinal reinforcement, the analytical hysteresis loops exhibited very good agreement with the experimental results of the ductile columns reinforced with NS rebars up to large drift, but overestimated the seismic behavior of the columns reinforced with WBUHS rebars. On the other hand, by taking into consideration the bond-slip behavior of rebars, the calculated results gave an accurate prediction to the hysteretic performance characterized by significant drift-hardening capacity and self-centering capacity.

2) Confinement effect by bolted circular steel tubes on seismic performance of both precast and cast-in-site resilient circular concrete columns could be reliably and precisely assessed by assuming their confinement efficiency (the strength raising coefficient of confined concrete) was about half of that provided by welded circular steel tubes.

3) Ignorance of the slippage resulted in a sharp increase in the strain of longitudinal rebar. This was in good agreement with the measured strain of NS rebar, but remarkably overestimated the strain development of WBUHS rebars, thus leading to an overestimation of lateral resistance and residual deformation for the resilient concrete columns. The analytical results obtained by taking into account of the slippage effect of WBUHS rebars could trace the strain of WBUHS rebars very well particularly in tension.

4) Ignoring the bond-slip behavior of reinforcements could predict the energy-dissipating capacity of the ductile concrete columns reinforced by NS rebars fairly well up to large drift, but gave an overestimation for that of resilient columns with WBUHS rebars. Consideration of slippage of rebars gave a conservative prediction of energy dissipation capacity, but could trace the characteristics of nonlinear elasticity of resilient concrete columns reinforced with WBUHS rebars.

In chapter six, two methods were presented to simply calculate the ultimate flexural capacity of the proposed circular concrete columns reinforced by squarely-arranged WBUHS rebars: one was on the basis of the plane-remain-plane assumption, and the other involved the modification of elasticity modulus of WBUHS rebars in the tensile region to take consideration the slippage effect of WBUHS rebars. According to the comparison between the computed results and measured values, the main conclusions are drawn below:

1) The conventional method following plane-remain-plane assumption was prone to giving an overestimated prediction of the ultimate flexural capacity of concrete columns reinforced by WBUHS rebars. The overestimation was more remarkable for the specimens with shear span ratio of 2.5 and/or confined by steel tubes with diameter-to-thickness ratio of 96. The ratio between the experimental and calculated capacities varied between 0.81-1.06, having an average value of 0.95 and a standard deviation of 0.07. However, the calculated results using this method agreed fairly well with the measured results for ductile concrete columns reinforced with NS rebars.

2) Combining the equivalent stress block of concrete at the circularly compressed zone with the reduced elasticity modulus for WBUHS rebars could give a very satisfactory prediction of the ultimate flexural capacity of circular concrete columns reinforced by squarely-arranged WBUHS rebars. For the sixteen test columns with WBUHS rebars, the ratio between the experimental and calculated capacities varied between 0.92-1.19, having an average value of 1.05 and a standard deviation of 0.08.

7.2 Future Works

Fundamental aspects related to precast drift-hardening circular concrete columns, reinforced with squarely-arranged WBUHS rebars and externally confined by bolted circular steel tubes, have been addressed in the study described in this doctoral dissertation. However, several vital issues remain to be solved due to time constraints. To further promote the adoption of drift-hardening columns reinforced with WBUHS rebars, research works that needs to be conducted in future are listed as follows:

1) Development of stress-strain model for the buckled WBUHS rebars: although reducing hoop spacing and employing steel tubes confinement have been proven effective in delaying the buckling of WBUHS rebar and enhancing its post-buckling behavior, a comprehensive stress-strain model that can trace the descending caused by the buckling is desirable to accurately predict the seismic performance of precast resilient concrete columns at large deformation.

2) Accumulation of information regarding seismic behavior of drift-hardening circular concrete columns under double curvature deformation: The study conducted in this thesis mainly focused on the cantilever concrete columns deformed under single curvature. Therefore, it is worthwhile to study the seismic behavior of drift-hardening concrete columns confined by bolted circular steel tubes under double curvature deformation, inclusive of both cast-in-site and precast columns.

3) Further improvement in the accuracy of the adopted FSE method: The comparison with experimental results has confirmed the good accuracy of the analytical results, however, it is also observed that the equivalent viscous damping coefficient and reinforcement strain obtained by the FSE method still exhibit some deviation from the experimental values within some specific experimental parameters. Therefore, it is meaningful to analyze and discuss the methods that can further improve the accuracy of FSE method, particularly from the perspectives of the assumed plastic hinge length and the utilized Funato model.

4) Proposition of a simplified hysteresis model for the proposed drift-hardening concrete columns: While the hysteresis performance can be predicted with good accuracy by the FSE method that can consider the rebar slippage, this analytical method involves complex

iterative calculations. Therefore, developing a hysteretic model for the proposed drift-hardening columns with simplified calculation is of great significance.

5) Evaluation of shear capacity of the drift-hardening circular concrete columns: To fully utilize the drift-hardening capacity provided by WBUHS rebars until a large drift, a significant challenge lies in preventing resilient concrete columns from experiencing brittle shear failure in the design of drift-hardening RC structures. Therefore, it is essential to develop reasonable methods to evaluate the complete shear capacity of the resilient concrete columns reinforced with squarely-arranged WBUHS rebars, both precast and cast-in-site.

List of Publications

[1] **Jing LUO**, Takashi TAKEUCHI, Jun ZHAO, Yuping SUN: Experimental study on axial behavior of confined concrete columns with SBPDN rebars. *Proceedings of the Japan Concrete Institute*, 2022, 44(2):397-402.

[2] **Jing LUO**, Shiyu YUAN, Takashi TAKEUCHI, Yuping SUN: Seismic behavior of circular precast concrete columns with square-arranged SBPDN rebars. *Proceedings of the Japan Concrete Institute*, 2023, 45(2):343-348. (in Japanese)

[3] **Jing LUO**, Shiyu YUAN, Jun ZHAO, Yuping SUN: Seismic behavior of concrete columns reinforced with weakly bonded ultra-high strength rebars and confined by steel tubes. *Materials*, 2023, 16(21):6868.

[4] Jun ZHAO, **Jing LUO**, Xiangcheng ZHANG, Xiaohui RUAN, Yuping SUN: Experimental study on seismic behavior of concrete walls with external magnetorheological dampers. *Smart Materials and Structures*, 2023, 32(6): 065005.

[5] **Jing LUO**, Mitsuru ASHIDA, Shiyu YUAN, Jun ZHAO, Yuping SUN: Seismic behavior of precast circular concrete columns reinforced with WBUHS rebars. *18th World Conference on Earthquake Engineering*, 2024. (accepted for publication)

Doctoral Dissertation, Kobe University

"Study on Seismic Behavior of Precast Drift-hardening Concrete Columns Confined by Bolted Circular Steel Tube", 150 pages

Submitted on January, 15, 2024

When published on the Kobe University institutional repository /Kernel/, the publication date shall appear on the cover of the repository version.